

CZECH TECHNICAL UNIVERSITY IN PRAGUE
Faculty of Electrical Engineering

MICHAELA POPLOVÁ ~ *Doctoral Thesis*

January 2024



CZECH TECHNICAL UNIVERSITY IN PRAGUE
Faculty of Electrical Engineering ~ Department of Circuit Theory



PHOTOCOUNT STATISTICS AND SPECTRAL ANALYSIS OF ULTRAWEAK PHOTON EMISSION FROM BIOLOGICAL SYSTEMS

Doctoral Thesis

ING. **MICHAELA POPLOVÁ**

PRAGUE, JANUARY 2024

PH.D. PROGRAMME: ELECTRICAL ENGINEERING AND INFORMATION TECHNOLOGY - P2612
BRANCH OF STUDY: ELECTRICAL ENGINEERING THEORY - 2602V013

SUPERVISOR: PROF. ING. **PAVEL SOVKA**, CSc.
SUPERVISOR SPECIALIST: ING. **MICHAL CIFRA**, Ph.D.

Thesis Supervisor:

PROF. ING. PAVEL SOVKA, CSc.
Department of Circuit theory
Faculty of Electrical Engineering
Czech Technical University in Prague
Technická 2
160 00, Prague 6
Czech Republic

Thesis Supervisor Specialist:

ING. MICHAL CIFRA, PH.D.
Bioelectrodynamics research team
Institute of Photonics and Electronics
The Czech Academy of Sciences
Chaberská 1014/57
182 00, Praha 8 - Kobylisy
Czech Republic

ACKNOWLEDGEMENTS

First of all, I would like to express my deepest gratitude to my supervisor, Dr. Michal Cifra, for his amazing guidance, considerate support, overall insights into the topic, and enthusiastic assistance during my research project. Further, I would like to thank my supervisor, Prof. Pavel Sovka, for his valuable experience and advice on signal analysis and the thoughtful recommendations for this dissertation. I am also thankful to the Faculty of Electrical Engineering at the Czech Technical University in Prague and all members of the staff for providing knowledge. Many thanks to colleagues from the Institute of Photonics and Electronics of the Czech Academy of Sciences for their scientific and personal support. And my biggest thanks to my husband and parents for all the unconditional support in these very intense academic years. Finally, I cannot forget to thank my kids for bringing a different view to the world and adding worry but also fun and laughter to my daily life.

This dissertation has been financially supported by the Czech Grant Agency under grants No. P102/11/0649, GP13-29294S, and GX20-06873X. Further, the Czech Technical University in Prague under grants No. SGS13/138/OHK3/32T/13 and SGS15/198/OHK3/3T/13.

DECLARATION OF ORIGINALITY

I, the undersigned, hereby declare that this doctoral thesis is the result of my research in our research team and my contribution corresponds to that specified at the beginning of each research chapter. The thesis was written under the professional supervision of Dr. Michal Cifra and Prof. Pavel Sovka, using the literature and resources listed in the Bibliography and References. I used AI technologies in proofreading and correcting the grammar of this thesis.

In Prague, 31. January 2024

.....

ING. MICHAELA POPLOVÁ

ABSTRACT

Biological autoluminescence (BAL), also known as ultra-weak photon emission (UPE), is an endogenous bioluminescent phenomenon present in all biological samples with an active oxidative metabolism caused by the chemical formation of electronically excited species. BAL can reflect changes in oxidative metabolism due to differences in the surrounding environment or the presence of biological agents. The main aims of this dissertation include (I) developing a methodology for BAL measurement; (II) examining the statistical and spectral properties of measured BAL signals; (III) devising a new method for improving BAL signal analysis and (IV) designing a new type of experiment demonstrating the practical usability of BAL.

At the outset, a light-tight chamber was designed to ensure a dark environment. Biological samples and detectors were selected, and a measuring methodology for BAL was developed. Preliminary BAL results from human leukemia (HL-60) cells and yeast cells were presented, demonstrating oxidative changes under different measurement conditions or using an antioxidant. In the subsequent part, mung bean seedlings were investigated during growth in two different media: pure water or 1% sucrose. Their photocount distributions of BAL time series followed the negative binomial distribution with mean BAL values increasing during seedling growth, while Fano factor values showed a decreasing trend through the days. Optical spectral analyses of BAL from differentiated HL-60 cells and yeast cells revealed clear differences between them. Additionally, an optical model of BAL propagation through the human skin at selected wavelengths was created to estimate the initial intensity generated inside the skin. A preprocessing method for non-stationary signals with dependence between the mean and variance, typical for a Poisson-like process, was developed, preserving the type of photocount distribution and phase-space structure of the signal. The importance of the suggested pre-processing method was demonstrated by Fano factor and Hurst exponent analysis. In the final part, an experiment was conducted, demonstrating the capability of quantitative differentiation between several degrees of oxidation level on human skin *in vivo* induced by the application of H_2O_2 and the possibility of monitoring the protective effect of antioxidants. The imaging of BAL identified spatial inhomogeneity and local differences in oxidative stress under controlled conditions.

Overall, the results of this dissertation demonstrate that BAL is a label-free, real-time, non-contact, non-invasive, and likely the only technique that requires no additional acute external energy input to the biosystem to observe endogenously or exogenously triggered oxidation processes.

KEYWORDS

biological autoluminescence, ultra-weak photon emission, reactive oxygen species, PMT, EMCCD camera, photocount statistics, pre-processing, time series, imaging, spectral analysis

ABSTRAKT

Biologická autoluminiscence (BAL), známá také pod pojmem ultraslaba fotonová emise (UPE), je endogenní bioluminiscenční fenomén, vlastní všem organismům s aktivním oxidativním metabolismem, vznikající díky chemickým reakcím vedoucím k elektronově excitovaným stavům. BAL zrcadlí změny oxidativního metabolismu vzniklé například změnou okolního prostředí či přítomnosti biologických činitelů. Hlavní cíle dizertační práce jsou: (I) vytvořit metodiku měření BAL; (II) zhodnotit statistické a spektrální vlastnosti naměřených BAL signálů; (III) navrhnout metodu pro zlepšení analýzy BAL signálů; (IV) vymyslet nový typ experimentu demonstrující využitelnost BAL v praxi.

V první části dizertační práce jsem navrhla světlotěsnou komoru pro měření BAL a určila vhodné biologické vzorky a detektory. Dále jsem vypracovala metodiku pro BAL měření. Výsledky z diferencovaných buněk HL-60 a kvasinkových buněk ukazují oxidativní změnu v BAL signálech při změnách podmínek měření či použití antioxidantu. V následující části jsem se zabývala fotopulzní statistikou BAL signálů z klíčících semínek munga ve vodě nebo roztoku 1% sacharózy. Distribuce obou skupin byla ve shodě s negativní binomickou distribucí po dobu 6 dnů, kdy střední hodnota postupně narůstala a Fano faktor klesal. Porovnáním optické spektrální analýzy BAL z diferencovaných buněk HL-60 a kvasinkových buněk jsem demonstrovala rozdílná spektra v závislosti na daném biologickém systému. Dále jsem navrhla model odhadující množství generovaných fotonů uvnitř lidské kůže na jednotlivých vlnových délkách, který zahrnuje jejich útlum v jednotlivých vrstvách při průchodu k povrchu kůže. Nakonec jsem navrhla metodu předzpracování pro nestacionární signály, pro které platí rovnost střední hodnoty a rozptylu jako jsou například Poissonovské procesy. Tato metoda zachovává typ distribuce a strukturu dat signálů ve fázovém prostoru. Důležitost navrhovaného předzpracování byla demonstrována na analýze Fano faktoru a Hurstově exponentu. V závěrečné části jsem provedla experiment demonstrující využití BAL k zobrazení prostorových nehomogenit tedy lokálních rozdílů oxidativního stresu v předem definovaných podmínkách. Experiment byl proveden na lidské kůži, ukazující schopnost kvantitativně rozlišit několik stupňů oxidace vyvolané peroxidem vodíku H_2O_2 a možnost pozorovat ochranné účinky antioxidantu.

Z dizertační práce vyplývá, že BAL je neinvazivní, nepřímá metoda měření oxidativním procesů v biologických vzorcích v reálném čase bez použití externích zdrojů a markerů a je využitelná v praxi.

KEYWORDS

biologická autoluminiscence, ultra-slabá emise fotonů, reaktivní formy kyslíku, PMT, EMCCD kamera, fotopulzní statistika, předzpracování, časová řada, spektrální analýza

CHEMICAL ABBREVIATIONS

Cd	Cadmium
CO₂	carbon dioxide
Fe²⁺	iron (II)
Fe³⁺	iron (III)
H₂O₂	hydrogen peroxide
Hg	Mercury
HO•	hydroxyl radical
¹O₂	singlet oxygen
³O₂	molecular oxygen
O₂^{•-}	superoxide anion radical
¹P*	singlet excited chromophore
³P*	triplet excited chromophore
P	chromophores
Pb	Lead
³R = O*	triplet excited carbonyl
R•	alkyl radical
RH	bio-molecule
RO•	alkoxyl radical
ROO•	peroxyl radical
ROOH	hydroperoxide
ROOR	dioxetane
ROOOOR	tetraoxide

ABBREVIATIONS

A/D	analog/digital
BAL	biological autoluminescence
CCD	charge-coupled device
DFA	detrended fluctuation analysis
DMEM	Dulbecco's modified eagle medium
DNA	deoxyribonucleic acid
EDTA	ethylenediaminetetraacetic acid
EMCCD	electron multiplying charge-coupled device
FBS	fetal bovine serum
HEPA	high-efficiency particulate air filter
HL-60	human promyelocytic leukemia
HMVECad	human microvascular endothelial cells, adult dermis
IR	infrared
NADPH	nicotinamide adenine dinucleotide phosphate hydrogen
NIH 3T3	mouse fibroblast cells NIH/Swiss embryo
PBS	phosphate buffered saline
PMA	phorbol 12-myristate 13-acetate
PMT	photomultiplier
RONS	reactive oxygen and nitrogen species
ROS	reactive oxygen species
RPMI	medium developed at Roswell Park Memorial Institute
SNR	signal to noise ration
TTL	transistor-transistor-logic
UPE	ultra-weak photon emission
UV	ultra-violet
VIS	visible
YPD	Yeast extract-Peptone-Dextrose

CONTENTS

Acknowledgments	i
Declaration of originality	i
Abstract	ii
Abstrakt	iii
Chemical abbreviations	iv
Abbreviations	v
1 INTRODUCTION	1
2 STATE OF THE ART	3
2.1 Historical perspective on the natural light phenomenon	3
2.2 From ultra-weak photon emission to Biological auto-luminescence	4
2.3 Biological auto-luminescence	4
2.3.1 Generation mechanism of photons	5
2.3.2 Application of BAL	9
2.3.3 BAL from human body	11
2.4 Measurements of BAL	11
2.4.1 Photomultipliers	11
2.4.2 CCD cameras	14
2.5 Analysis of BAL signals	15
2.5.1 Photocount statistics	15
2.5.2 Advanced signal analysis	17
2.5.3 Spectral analysis	18
3 AIMS OF THE DOCTORAL THESIS	19
4 DESIGN OF LIGHT-TIGHT CHAMBERS FOR BAL MEASUREMENT	21
5 METHODOLOGY OF BAL MEASUREMENTS	23
5.1 Configuration of measuring systems	23
5.2 Preparation of biological samples	24
5.3 Preliminary results	26
5.3.1 Adherent tissue cultures	26
5.3.2 HL-60 cells	27
5.3.3 Yeast cells	28
6 PHOTOCOUNT STATISTICS AND ANALYSIS	29
7 INVESTIGATION OF NON-STATIONARY SIGNALS	37
8 OPTICAL SPECTRAL ANALYSIS OF BAL FROM BIOLOGICAL SYSTEMS	55
9 OPTICAL MODEL OF BAL PROPAGATION AT HUMAN SKIN FOR DIFFERENT WAVELENGTHS	63
10 INVESTIGATION OF BAL FROM HUMAN SKIN	69
11 RESULTS	97

12 CONCLUSIONS	99
12.1 Contribution of the dissertation	99
12.2 Future directions	99
BIBLIOGRAPHY	100
LIST OF PUBLICATIONS RELATED TO THE DOCTORAL THESIS	115
CURRICULUM VITAE	119
APPENDIX	121

1 | INTRODUCTION

At the beginning of the 20th century, researchers observed **natural light** emission in **living organisms**, which occurred **without** the involvement of **specialized enzymes**, such as luciferase [1,2]. Technological limitations hindered its exploration, and it was often dismissed as a secondary product of metabolism [3]. This phenomenon is being reevaluated with advancements in sensitive detectors like photomultiplier tubes and CCD cameras [3,4]. Recent studies connect luminescence to **cellular oxidation processes**, offering new insights into fundamental biology and applications in various fields [5–8].

Cellular oxidation processes are essential for functions such as cell signaling and pathophysiology [9–11]. The accepted mechanism of generating natural luminescence is the chemical production of **electron excited states** within organisms, hinging on the presence of **reactive oxygen and nitrogen species (RONS)** [4,6,7]. RONS are vital signaling molecules, that contribute to cell regulation, energy conversion, and immune defense [5,12]. RONS arise from **endogenous metabolic** processes such as respiration in mitochondria [13], non-enzymatic peroxidation of lipids in membranes, or are **induced** by abiotic (chemical [14] or physical stimuli [15]) or biotic (virus [16], bacteria [17] or fungi [18]) factors. Within these processes, transient **intermediates** form, emitting **photons** as they return to their ground energy state [7,19].

At its core principle, **biological auto-luminescence (BAL)** offers a way to assess oxidative processes within living organisms. The advantage of BAL monitoring is a **non-invasive, label-free method without perturbing the organism using any external source of energy** [8].

2 | STATE OF THE ART

2.1 HISTORICAL PERSPECTIVE ON THE NATURAL LIGHT PHENOMENON

The terminology for **natural light** phenomenon, originating from all living system **without any specific pigments or enzymes**, historically varies by research field. In the early 20th century, A. Gurwitsch suggested that this light was produced during cell mitosis in the ultraviolet wavelength range of 200 to 400 nm and naming it as **mitogenetic radiation** [1, 20]. Nevertheless, its existence was challenged by other authors [21].

In the mid-1970s, German professor F.A.Popp introduced the term **biophoton emission** [22] and proposed that light originates from DNA (deoxyribonucleic acid). According to this theory, the DNA double helix was considered as a quantum electrodynamics structure [23] that is continuously stimulated by the metabolic activity leading to the creation of a coherent electromagnetic field [22]. DNA serving as an energy reservoir, can emit accumulated energy as photon quanta in the wavelength range of 100 to 300 nm [23]. However, these hypotheses have not been adequately experimentally validated [24].

Concurrently, a large biochemistry group was formed in Brazil around G. Cilento, W. Adam, H. Sies, and E.J.H. Bechara. This scientific community, specializing in excited electronic states during biological processes, termed this phenomenon as **biological chemiluminescence** or simply chemiluminescence [25–27].

Currently, spiritual alternative medicine speculates about the link between biophoton emission or **biophotons** [2] and the aura. However, scientists are progressively shifting away from this terminology and aiming for a more precise description.

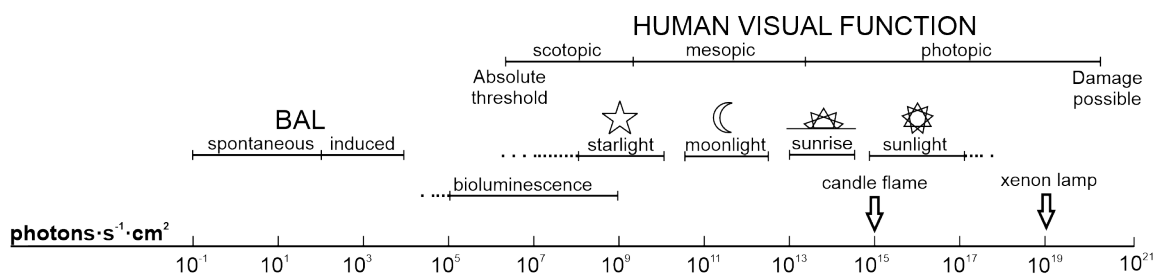


Figure 2.1: BAL intensities vs other light phenomena.

2.2 FROM ULTRA-WEAK PHOTON EMISSION TO BIOLOGICAL AUTO-LUMINESCENCE

Recently, the term **ultra-weak photon emission(UPE)** [19] has been commonly used. UPE describes this light phenomenon from the perspective of detected particles-photons with very low intensity, without providing information about the generation mechanism. **Biological auto-luminescence (BAL)** appears to be a more informative term. "Biological" indicates that the light originates from living systems or organic samples. "Auto" signifies that the generation mechanism is endogenous within cells and occurs spontaneously without external inputs, maintaining a basic luminescence level. "Luminescence" refers to the non-thermal essence of light emission.

2.3 BIOLOGICAL AUTO-LUMINESCENCE

BAL is a product of oxidative processes [28–31], especially involving reactive oxygen species (ROS) that react with biomolecules to create electronic excited states and emit photons without external photoexcitation [32]. Photons are emitted in the spectral range of at least **350 to 1300 nm** [19]; further details are described in Chapter:2.3.1. Two types of BAL are distinguished. **Spontaneous BAL**, occurring naturally, is characterized by low intensity emission, typically around **100 or less photons·s⁻¹·cm⁻²** [2, 7], depending on the organism type. **Induced BAL** is a term used for endogenous luminescence that increases due to **stress factors** originating from changes in the **surrounding environments** such as temperature [15], chemical treatments (H₂O₂ [14], PMA (phorbol 12-myristate 13-acetate) [33]), variations in gas concentration [15] or the presence of **biotic factors** like viruses [16], bacteria [17] or fungi [18] in the organism. The intensity of induced BAL is around **100 - 1000 photons·s⁻¹·cm⁻²** [19]. BAL is **not visible** directly **by human eyes** due to their limited sensitivity, and because the surrounding daylight intensity is higher than BAL, as depicted in Fig.2.1. It can **not be attributed to thermal radiation from a black body** [19], as shown in Fig.2.2 **or bioluminescence**. Bioluminescence is a different type of light generation process because its main principle involves electron excited states of special complex (luciferin-luciferase) or photoproteins (green fluorescent protein GFP, Aequorin), which not all organisms possess, making it highly specific [19].

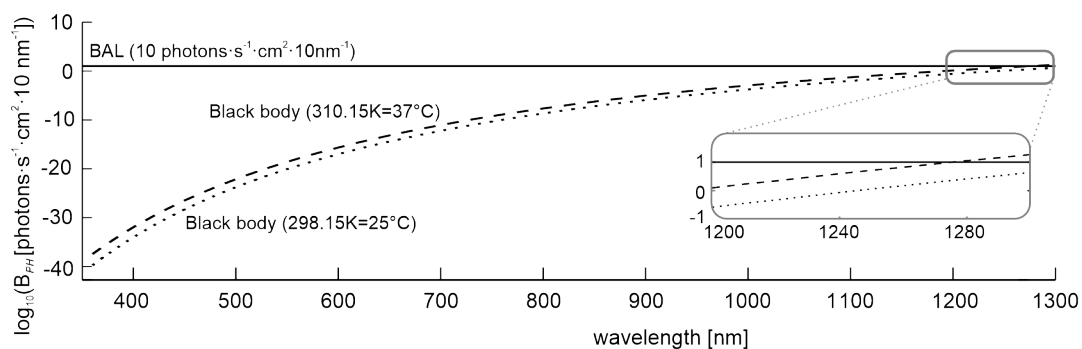


Figure 2.2: Spectral radiance of black body with temperature 25°C (dotted line) and 37°C (dashed line) is compared with BAL flux approximation of $10 \text{ photons}\cdot\text{s}^{-1}\cdot\text{cm}^{-2}$ per 10 nm (solid line). The BAL may be influenced by thermal radiation in the near infra-red region of the spectrum.

2.3.1 Generation mechanism of photons

Reactive oxygen species (ROS) are crucial for BAL generation, examples are provided in Tab. 2.1 [23, 34, 35]. **Mitochondria or chloroplasts** primarily produce ROS during aerobic metabolism in the presence of oxygen [13, 36]. One-electron reduction of **molecular oxygen** ($^3\text{O}_2$) **creates superoxide anion** ($\text{O}_2^{\bullet-}$). The dismutation of $\text{O}_2^{\bullet-}$ **generates hydrogen peroxide** (H_2O_2). Consequently, one-electron reduction of H_2O_2 could **lead to the formation of hydroxyl radical** (HO^\bullet). HO^\bullet is a **highly reactive radical** due to the presence of unpaired electrons and high positive redox potential [7]. Other cellular components capable of generating ROS include **peroxisomes, cytosol, the plasma membrane** [13,37], the **endoplasmatic reticulum** [38] and the **extracellular space** [39]. ROS can also form during various **cellular enzymatic reactions** involving NADPH oxidase and nitric oxidase synthase [5, 40]. They may arise during a **respiratory burst** as part of the defense against pathogens [10, 12] or as a product of **cellular signaling** pathways [10, 12, 35], contributing to the **maintenance of the surroundings environment** [9, 10, 40] and the **regulation of the cell cycle** including processes like differentiation, proliferation, growth and apoptosis [9]). **Exogenous conditions** such as heat, drought, UV exposure, or the presence of heavy metals cations (Hg, Cd, Pb) [11] can also **increase ROS** production.

Table 2.1: Examples of reactive oxygen species

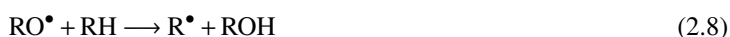
free radicals	non-radical species
superoxide anion $\text{O}_2^{\bullet-}$	hydrogen peroxide H_2O_2
hydroxyl HO^\bullet	hydroperoxides ROOH
alkoxyl RO^\bullet	singlet oxygen $^1\text{O}_2$
nitric oxide NO^\bullet	singlet ozone O_3
nitrogen dioxide NOO^\bullet	hydrochlorous acid -HOCl

A long-term **imbalance of ROS** inside cells can lead to **pathological states** such as cell death, fibrogenesis, or tumor growth [35]. The **antioxidant** defense system **protects the organism** against oxidative stress, characterized by increased ROS production. Disruption of the ROS balance can result in **i) an adaptive response by organism** to increase antioxidant production, **ii) cell damage** or **iii) cell death** [10, 36]. **Too little ROS** can also **disrupt the cell's redox homeostasis** due to errors in signaling pathways [41]. Two types of **antioxidants** are distinguished: **enzymatic** (catalases, superoxide dismutases, glutathione reductase and peroxidase, etc.), and **non-enzymatic** (ferritin, albumin, NADPH, ascorbic acid, carotenoids, etc.) [42–45].

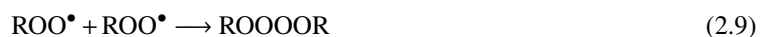
The **hydroxyl radical (HO•)**, a reactive oxygen species, can **react** with various **biomolecules (RH)** like **lipids, proteins** or **DNA**, and **leading** to the formation of **alkyl organic radical (R•)**, Eq. 2.1 [7, 46].



One-electron **oxidation of R•**(alkyl radical) can lead to the **formation** of a **peroxyl radical (ROO•)**, Eq. 2.2 [7, 46, 47]. The peroxyl radical (**ROO•**) can **abstract a hydrogen** atom **from** another biomolecule (**RH**), **forming hydroperoxide (ROOH)** and regenerating **R•**(alkyl radical), Eq. 2.3 [7, 46]. **ROOH** (hydroperoxide) **can also be created**, by the ene reaction of **RH** (biomolecule) **with ¹O₂** (singlet oxygen), Eq. 2.4 [7, 46]. The **one-electron reduction of ROOH** (hydroperoxide) can result in the **formation** of **alkoxyl (RO•)**, Eq. 2.5 [7]. **Alkoxyl (RO•)** could react **with hydroperoxide (ROOH)** resulting back in **peroxyl radical (ROO•)**, Eq. 2.6 [46]. **Alkyl radical (R•)** can be also formed by **β-fragmentation from alkoxyl (RO•)**, Eq. 2.7 or **reaction alkoxyl (RO•) with biomolecule (RH)**, Eq. 2.8 [46, 47].



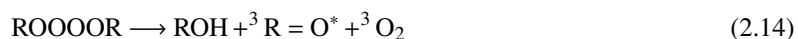
Very unstable, high energy **intermediate** called **tetraoxide (ROOOOR)** is **created** by the **recombination of two peroxy (ROO[•])**, Eq. 2.9, and its decomposition results to two **alkoxyls (RO[•])**, Eq. 2.10 [7, 46]. **Dioxetane (ROOR)**, **second intermediate**, can be formed by **cyclization of ROO[•]**(peroxy), Eq. 2.11 [7] or the **cycloaddition of ¹O₂(singlet oxygen) to RH**(biomolecule), Eq. 2.12 [7].



Decomposition of dioxetanes (ROOR) and tetraoxides (ROOOOR) can result in **electron excited states** [48]. These electron excited species **return to ground states** through several possibilities, including vibrational decay, releasing energy as **heat**, or engagement in further **chemical reaction** [8]. The emission of energy in the form of **photons** is often the least probable outcome, and this phenomenon is referred to as **BAL**.

Triplet excited carbonyls

Decomposition of dioxetanes (ROOR), Eq. 2.13 or **tetraoxides (ROOOOR)**, Eq. 2.14 leads to production of **triplet excited carbonyls (³R = O^{*})** [7, 47, 49].



Triplet excited carbonyl returns to its ground state through **photon emission**, Eq. 2.15 [4, 7, 49, 50].

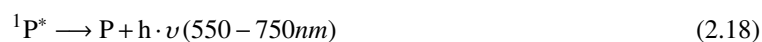


Chromophores

Energy from triplet excited carbonyls (³R = O^{*}) can be **transferred to chromophores (P)** leading to the generation of singlet (¹P^{*}), Eq. 2.16 or triplet (³P^{*}), Eq. 2.17 excited chromophores [7].

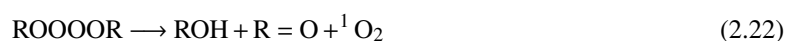


These excited singlet ($^1\mathbf{P}^*$), Eq. 2.18 and triplet ($^3\mathbf{P}^*$), Eq. 2.19 chromophores return to their ground state by emitting photons [7, 51–53]. While photon emission from excited triplet chromophores ($^3\mathbf{P}^*$) has not been experimentally verified, it is assumed to occur in the infrared (IR) wavelength range [7]. Typical examples of chromophores include chlorophyll, melanin, bilirubin.



Singlet oxygen $^1\mathbf{O}_2$

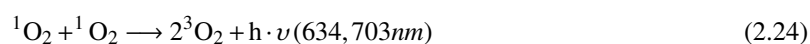
Singlet oxygen ($^1\mathbf{O}_2$) can be generated from triplet oxygen ($^3\mathbf{O}_2$) its basic state when it receives energy from excited triplet carbonyl ($^3\mathbf{R} = \mathbf{O}^*$), Eq. 2.20 or excited chromophores ($^3\mathbf{P}^*$), Eq. 2.21 [7]. Additionally, the decomposition of tetraoxide (ROOOOR) can also lead to the formation of singlet oxygen ($^1\mathbf{O}_2$) due to the Russel-type mechanism, Eq. 2.22 [7].



While monomolar emission from singlet oxygen ($^1\mathbf{O}_2$), Eq. 2.23, within biological organisms has not been experimentally confirmed, it is assumed that it may contribute to BAL in the IR wavelength range [7,47].



The recombination of two singlet oxygen molecules ($^1\mathbf{O}_2$) may result in dimol emission, Eq. 2.24, characterized by the emission of a photon of double the energy (half the wavelength of monomolar emission) a photon leaving the two triplet oxygen molecules ($^3\mathbf{O}_2$) in ground state [2, 7, 47, 54]. A simplified diagram illustrating the complex chemical reactions that result in photon emission is depicted in Fig.2.3.



A simplified diagram illustrating the complex chemical reactions that result in photon emission is depicted in Fig.2.3.

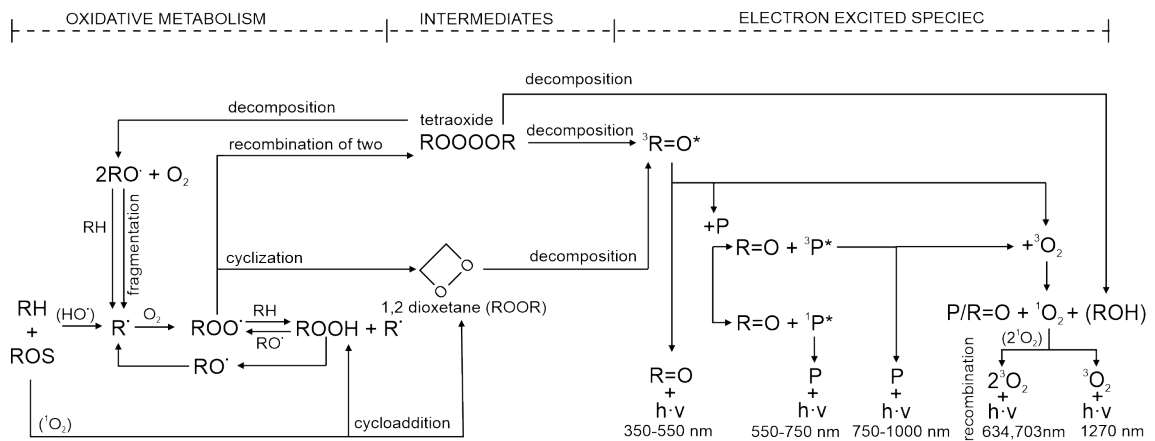


Figure 2.3: Approximate reaction scheme leading from oxidation of biomolecules to BAL.

2.3.2 Application of BAL

BAL holds a potential for evaluating oxidative processes in bio-samples within the **food industry, agriculture, and medicine**. **Intensity and spectra** are key **parameters**, there is a perspective that time series data can contain more information based on fractal theory [55]. The primary **advantage** of monitoring BAL is its **label-free, non-invasive real-time approach without** the need for **external energy input**. Representative BAL experiments are shown in Tab.2.2. Germany's SUPER lab company (<https://super-lab.de/liana.html>, Germany) has developed LIANA (LIght ANALaser), a device that assesses food quality covering aspects like freshness, chemical composition, and biological contamination through a combination of BAL and auto-fluorescence. BAL has also been applied in **plant studies**, examining their responses to pathogens [16, 17, 56], herbicides [57, 58], and environmental stress [59, 60]. Additionally, **animal studies** [61–63] have served as a precursor to human experiments in biomedicine, indicating BAL's potential as a **diagnostic tool for various diseases** [64–68].

Table 2.2: Representative BAL experiments, demonstrating key findings and results

Authors	Measurements of BAL in biological samples and others experiments
W. Adam and W. J. Baader	dioxetanes [27], peroxidase [69], cyclic peroxides [70]
R.C. Allen	phagocyte [71], leukocyte and bacteria [72]
R.P. Bajpai	lichen (<i>Parmelina wallichiana</i> [73], <i>Parmelia tinctorum</i> [74])
E.J.H. Bechara	dioxetane [25], proteins [75], lipid peroxidation [76]
L.V. Belousov, I.V. Volodyaev and A. B. Burlakov	fish [61, 77–79] and amphibian [80] eggs and embryos
A.V. Budagovski	apple with fungi spores [81] and plant leaves with chlorosis [82]
E. Cadenas, A. Boveris	bovine heart mitochondria [54], hepatocytes [83] and liver of rat [30]
G. Cilento	electronic excited states from free radicals [84] and triplet carbonyls [49]
Ch.M. Galleg	wheat seedlings [85, 86], coffee seeds [87], toxicology of seedlings [88] and planktonic crustaceans [89]
A.A. Gurvich	glycine [90], liver cells [91] and muscles [92]
A.G. Gurwitsch	cell division of root-tip [1], yeasts [93], red blood cells [1] and amino acid [94]
E. Hideg	spinach leaf and plant organelles [95–97]
H. Inaba	human body [98], human blood [66] and soybeans [99]
H. Inagaki	rice [58] herbicide [57]
M. Kobayashi	human body [100, 101], HeLa cancer cell line [67], rat's brain [102] cucumber mosaic virus [16], soybean seedlings [103]
S. Miyamoto and P. Di Mascio	peroxyl radical [104] and singlet molecular oxygen [105, 106]
F.A. Popp	DNA structure [22, 23], cucumber [107] and human body [108]
P. Pospíšil, A. Prasad and A. Rastogi	plants [14, 109–111], heat stress [60] human body [112] and porcine skin [113, 114]
T.I. Quickenden and R.M. Tilbury	<i>Saccharomyces cerevisiae</i> [115, 116] and <i>Candida utilis</i> [117]
H. Siess	oxidative stress [118, 119]
J. Slawinski	yeasts [120], plants [59], cereal grains [121, 122] humic acids [123, 124]
J. Stauff	triplet states [125]
R. F. Vasil'ev, G.F. Ferodova and A.V. Trofimov	molecular oxygen [126], tetraoxides [127] indol [128] and vegetable lipids [129]
Y. A. Vladimirov and I.P.Ivanova	free radicals [6, 130] and Fenton reaction [131]
R. van Wijk and E. van Wijk	mouse [132], blood of diabetics [68], human [133–135] and Chinese medicine [136–138]

2.3.3 BAL from human body

BAL from **human** subjects **in vivo** has only been **detected** from the outer surface of the human body, specifically the **skin** [139–142]. The BAL intensity **depends on** various factors [141], including the particular **body site** [133] and **physical activity** [143, 144], displays **anatomic asymmetry** [134, 145], undergoing **diurnal, monthly and annual cycles** [100, 146–148]. It tends to **increase with age** [149] and, when combined with spectral analysis, has the **potential** to be used to **monitor disease processes**, such as diabetes, hemiparesis, protoporphyria, or a typical cold [150]. However, research on BAL from humans is often related to skin research and **dermatology**, reporting the capability of using BAL to detect oxidation processes in the skin [113, 151, 152]. The skin protects humans against continuous oxidative damage by ROS coming from environmental stresses (physical and chemical factors) [28, 112, 139]. BAL measurements on the skin have also been performed **ex vivo** in **biopsies** [113, 153, 154], **in vivo**, and **in vitro** conditions (e.g., keratinocytes, fibroblast, homogenate) under **diseased conditions** such as malignancy and/or externally applied stresses (such as ultraviolet irradiation, exogenously applied chemicals) [113, 155–157]. The studies mentioned above concluded that BAL can be used to evaluate the physiology of the skin and help to understand how skin tissue reacts to different exogenous stresses. It is necessary to mention that the **measuring BAL in the skin is challenging**, primarily due to the **low intensity** of BAL.

2.4 MEASUREMENTS OF BAL

BAL is measured using highly sensitive light detectors. The most commonly used detectors are **photomultipliers (PMT)** and **CCD (Charge-Coupled Device) cameras**, which operate in completely **dark conditions** due to very low intensity of BAL (Fig. 2.1), as mentioned in Chapter:2.3. **PMTs** offers very **high time resolution**, ranging from seconds to nanoseconds, but they **lack spatial resolution**. To measure very low light, PMTs require the detection system to operate in the **photon counting mode**. In contrast, **CCD cameras** provide **high spatial resolution**, but capturing a single BAL image can take **15-60 minutes**. To **reduce noise**, both types of detectors can be equipped with air or water **cooling systems**. The **physical principle** underlying these detectors is the **photoelectric effect**, where photons strike the surface of a special material, leading to the ejection of electrons. The entire process is facilitated by the transfer of energy from the photons to the material. This Chapter 2.4 and its sub-sessions are based on handbooks of Hamamatsu [158–160], Stanford research systems [161], Oxford Instruments [162, 163], and Teledyne technologies companies [164, 165] producing light detectors.

2.4.1 Photomultipliers

The PMT (Photomultiplier tube) is a photosensitive device that **converts light into an electrical signal**. Photons enter through **entrance window** and interact with the **photo-cathode**, typically composed of highly reactive alkali metals such as sodium (Na), potassium (K), rubidium (Rb), and cesium (Cs). As a result, emitted

photo-electrons are accelerated by a **focusing electrode** toward the first **dynode**, where secondary emission occurs. This secondary emission process is repeated on each subsequent dynode, leading to **electron multiplication**. The degree of electron gain typically ranges from 10^3 to 10^8 , depending on the number of dynodes and the applied **high voltage**, ranging from 1000 to 2500V. The final emission of electrons is collected by the **anode**, resulting in a current output signal. All of these processes take place in a **vacuum** at a pressure of approximately 10^{-4} Pa.

The **photon counting method** involves converting the current output into voltage pulses **using** a wide-band **pre-amplifier**. These **voltage pulses** are either **accepted or rejected** by the **comparator** based on the discriminator level. Finally, the accepted pulses are **shaped** and **counted**.

PMTs can be **categorized** based on their **geometry** into **side-on** and **head-on types**. Most **side-on** detectors feature an **opaque, reflective photo-cathode** and typically have a **circular arrangement of dynodes**. In contrast, **head-on** types include a **semitransparent photocathode** on the top and typically feature a **linear array of dynodes**. The head-on type often provides better spatial uniformity of the photo-cathode compared to the side-on type.

Construction of PMT

PMT detectors typically consist of **two detachable parts**: a **vacuum glass tube** with electrodes, and a **socket** containing electronic components and input/output connectors for high-voltage, signal, and supporting devices. The **current gain** at each **dynode** typically ranges from **2 to 6 electrons**. To **stabilize the output** signal, the **first two dynodes** of the voltage-divider circuit use **higher resistors** to increase electron gain. Replacing the last few resistors with a combination of Zener diodes and capacitors resolves the issue of voltage drop as the output current increases. However, this combination can cause high-frequency ringing in the anode output signal, so it is recommended to add a small resistor between the dynode and capacitor. **Snubber networks** on the anode consist of a short piece of 50 Ω coaxial cable terminated into a resistor (less than 50 Ω). These networks serve several purposes, including (i) protecting the PMT from the dark current of the anode, (ii) improving pulse-pair resolution, (iii) canceling ringing in the output caused by multiple counts from a single photon, and (iv) terminating reflections from the input to the pre-amplifier.

The **spectral response** of a PMT **depends** on the material of the **photo-cathode** and **entrance window**. It is **expressed** by two physical quantities: **Radiant Sensitivity** S_λ [mA/W] and **Quantum Efficiency** QE_λ [%] as a functions of wavelength. The relationship between these quantities is described by the equation:

$$QE_\lambda = S_\lambda \cdot \frac{h \cdot \nu}{e} = S_\lambda \cdot \frac{h \cdot c}{\lambda \cdot e} = 124 \cdot \frac{S_\lambda}{\lambda} \quad (2.25)$$

Here, λ [nm] represents the wavelength, e [J] is the electron charge, h is Planck's constant, and c is the speed of light in a vacuum. **Radiant sensitivity** is the **ratio** of the **current I [A]** transmitted by the photo-cathode **to** the

incident **radiant power** ϕ [W] at a specific wavelength. **Quantum efficiency** is the **ratio** of **photo-electrons emitted from the photo-cathode** n_k to the number of **incident photons** n_p . The type of **window material determines the short wavelengths cutoff** of the PMT's spectral response. Borosilicate glass is suitable for measurements in the VIS spectrum ($\lambda > 300$ nm). For UV measurements, materials like UV glass ($\lambda > 185$ nm), synthetic silica ($\lambda > 160$ nm), or MgF_2 ($\lambda > 115$ nm) are used. The choice of **photo-cathode material affects the long wavelength cutoff** of the spectral response, as shown in Tab. 2.3.

Dark current refers to the low-level current that persists in a detector in the absence of any external light source, establishing the lower limit of light detection. It depends on the supply voltage and can have various **sources**, including: (i) **Thermionic emission** from the photo-cathode, which is a primary source of dark current but can be reduced by cooling the photo-cathode. (ii) **Residual gas ions** inside the PMT that may interact with electrons and strike the photo-cathode or first dynodes, resulting in larger output noise pulses, often observed after the primary signal pulse. (iii) **Glass scintillation**, caused by the collision of glass and electrons due to deviation in their trajectories. (iv) **Leakage current**, resulting from imperfect connections between the glass tube and the socket of the PMT or contamination from dirt and moisture. (v) **Field emission**, arising from high operating voltages near the maximum rate. It is recommended to work with 70-80 % of the maximum voltage. (vi) **Electrical devices**, which can be a source of noise. (vii) **Cosmic radiation** from the surrounding environment. PMTs are typically designed with electric and magnetic shields.

Table 2.3: Photocathode materials

materials	spectral range [nm]	specification
Ag-O-Cs	300-1200	near IR with cooled photocathode, transmission mode
GaAs(Cs)	160-930	wider range than multialkali (300-850 nm flat)
InGaAs(Cs)	300-1000	extended IR than GaAs; higher S/N ratio than Ag-O-Cs
Sb-Cs	185-650	reflection mode only
Bialkali (Sb-Rb-Cs/Sb-K-Cs)	185-650	higher sensitivity and lower noise than Sb-Cs
Bialkali(Na-K-Sb)	185-680	higher operating temperature (175°C) or very low dark current
Multialkali(Na-K-Sb-Cs)	185-900	high, wide spectral response (spectrophotometers)
Cs-Te/Cs-I	115-320/115-200	sensitive only for UV

2.4.2 CCD cameras

A **charge-coupled device** (CCD) is an **image sensor** that converts **light into electric charge**. The CCD chip is **composed of** small elements known as **pixels**. In each pixel, incoming **photons are absorbed** by the semiconductor material, **releasing electrons** that are then **accumulated under electrodes**. Subsequently, these electrons are **transferred to the output** node, where they are **amplified** and **converted into voltage**. The electric charge is directly proportional to the intensity of light captured by the pixel. For measuring very weak light emission, it is recommended to use a back-illuminated **EMCCD** (Electron multiplying) **camera** with a **pre-amplifier directly on the chip**. The **binning method**, which combines 2x2, 3x3, 4x4, or 8x8 pixels, is a valuable technique for **improving the signal to noise ratio** (SNR). However, this method comes with the disadvantage of **decreasing the resolution** in the final image.

Construction of CCD cameras

A **CCD is composed of silicon matrix** in the photo-active region and a **shift register** in the transmission region. The semiconductor is grounded on the lower side, and **covered with** a thin layer of **silicon dioxide**, which acts as an insulator, on the other side. Electrodes are deposited on this dioxide layer. **Each pixel** consists of **three electrodes**, with **only one** electrode being **activated** at a time. The first electrode creates the potential well, while other are responsible for transferring the charge to the output of the CCD through their gradual activation. The CCD chip features both a **vertical** shift register and an output **horizontal shift register**. Described schematic structure of EMCCD chip is shown in Fig.2.4. Ultimately, the current pulse corresponds to the incoming brightness at the pixel. Silicon-based CCDs are optimized for the visible wavelength range (400-700 nm). Lower wavelengths are blocked by the insulator and higher wavelengths are penetrating into the deep-depletion layer.

The noise in a CCD **degrades the image quality** and arises randomly, depending on surrounding temperature, pixel size, manufacturing, and structural technology. There are three main types of noise: (i) **Dark current**, which is a thermally generated charge expressed in electrons per pixel at a defined temperature. It can be reduced through cooling systems and image processing. (ii) **Photon noise**, which is associated with the fluctuating speed of incident photons on the CCD camera. This deviation follows a Poisson distribution and is defined as plus or minus the square root of the measured signal intensity. (iii) The last type is **reading noise**, which occurs during the recording of the measured signal. It can originate in an A/D converter or pre-amplifier on the chip.

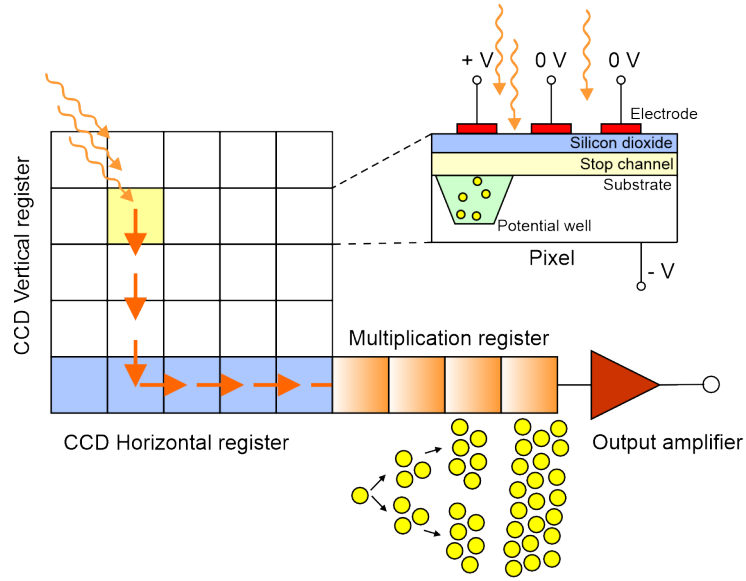


Figure 2.4: Principal structure of the EMCCD sensor

2.5 ANALYSIS OF BAL SIGNALS

The most common **parameter** analyzed from **BAL** measurements is the **BAL intensity** (number of photo-counts). However, further BAL can be assessed from **time series**, **image**, or **spectra**. The **time series**, measured by PMT, comprises the number of detected **photons in each bin**, with the bin size representing the time **sampling step**. The size of the bin depends on the type of investigation phenomenon. BAL signals may manifest as **stationary**, **nonstationary**, or **quasistationary** depending on the generation mechanism. **Images** depict detected **photons in a pixel matrix** offering **spatial information**. Emission **spectra** of BAL, measured in the visible range, provide information on the quantity of detected **photons within** the selected **wavelength band**.

2.5.1 Photocount statistics

This section is written according to The Oxford Master Series in Physics [166]. In **classical physics**, **light** is considered as an **electromagnetic wave**, simplified as a coherent light beam with a constant angular frequency ω , phase Φ , and amplitude ε_0 :

$$\varepsilon(x, t) = \varepsilon_0 \sin(kx - \omega t + \Phi). \quad (2.26)$$

Here, $\varepsilon(x, t)$ represents the electric field, and the propagation constant k is expressed as $\frac{\omega}{c}$, where c is the velocity of light. Equation 2.26 assumes a **constant light flux** without changing intensity. For **BAL**, **quantum theory** describes light as a **stream of photon** particles. The photon is a basic particle of light with zero mass, where energy or momentum depends only on frequency. **Photocount statistics** are expressed as a probability

$p(n, \Delta t)$ of detecting n photons in a defined time interval Δt (bin), following the **Poisson distribution** p_p :

$$p_p(n, \Delta t) = \frac{\langle n \rangle^n}{n!} \cdot e^{-\langle n \rangle}, \quad n = 0, 1, 2, 3, \dots \quad (2.27)$$

Here, $\langle n \rangle$ is the mean value of detected photons, and σ^2 is the variance. The Poisson distribution is **derived from the Binomial distribution** for a coherent light wave with constant intensity. The Poisson distribution has a typical characteristics of $\sigma^2 = \langle n \rangle$.

In quantum optics, the **photon statistics** can be categorized to **three types**, as shown in Fig. 2.5. (i) **Poisson statistic** describes a perfectly stable type of light with standard deviation $\sigma = \sqrt{\langle n \rangle}$. (ii) **Super-Poisson statistics** describe classical light beams with time-varying light intensities, such as thermal light of a black body, incoherent or partially coherent (chaotic) light with $\sigma > \sqrt{\langle n \rangle}$. Super-Poisson distributions could be the most common case in nature, and an example is the Negative binomial distribution [167]. (iii) **Sub-Poisson statistics** are theoretically described for light with narrower distribution than Poisson with $\sigma < \sqrt{\langle n \rangle}$, indicating even lower fluctuation in the intensity than the coherent beam of constant intensity, which does not exist in classical electromagnetic theory. An example is the Binomial distribution [168] or squeezed states (quantum optics).

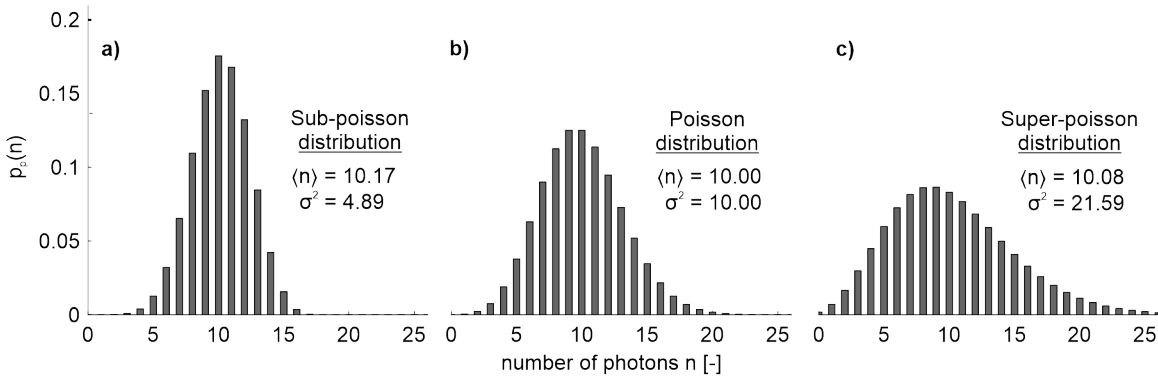


Figure 2.5: Light according to quantum optics could have a) Sub-Poisson, b) Poisson, or c) Super-Poisson distribution.

Chaotic light sources are characterized by a **short coherence time**. **Thermal light** is a common chaotic field source, and it can be filtered or polarized for measurements. For a **single mode of chaotic field**, photo-counts statistics follow the **Bose-Einstein distribution**:

$$p_g(n, \Delta t) = \frac{\langle n \rangle^n}{(1 + \langle n \rangle)^{n+1}} \quad \text{with} \quad \sigma^2 = \langle n \rangle(1 + \langle n \rangle). \quad (2.28)$$

The **Multi-mode chaotic field** ($\Delta t \gg \tau$, τ is the coherence time of the field) follows the **distribution by**

Mandel (1995):

$$p_{ch}(n, \Delta t) = \frac{(n+M-1)!}{n!(M-1)!} \left(1 + \frac{M}{\langle n \rangle}\right)^{-n} \left(1 + \frac{\langle n \rangle}{M}\right)^{-M} \quad \text{with } \sigma^2 = \langle n \rangle \left(1 + \frac{\langle n \rangle}{M}\right), \quad (2.29)$$

where M is a number of sources. In the case of a **large number of sources M** , the multi-mode chaotic distribution **converges** to the **Poisson distribution**, as illustrated in Fig. 2.6.

Photocount distribution can be also described by the **first four statistical moments** (mean eq.2.30, variance eq.2.31, skewness eq.2.32, and kurtosis eq.2.33), or parameters called **Fano factor F** eq.2.34 or **Mandel parameter Q** eq.2.35:

$$\langle n \rangle = \frac{1}{N} \sum_{n=1}^N x[n] \quad (2.30)$$

$$\sigma^2 = \frac{1}{N} \sum_{n=1}^N (x[n] - \langle n \rangle)^2; \quad (2.31)$$

$$s = \sqrt{N} \frac{\sum_{n=1}^N (x[n] - \langle n \rangle)^3}{(\sum_{n=1}^N (x[n] - \langle n \rangle)^2)^{\frac{3}{2}}} \quad (2.32)$$

$$k = N \frac{\sum_{n=1}^N (x[n] - \langle n \rangle)^4}{(\sum_{n=1}^N (x[n] - \langle n \rangle)^2)^2} \quad (2.33)$$

$$F = \frac{\sigma^2}{\langle n \rangle} \quad (2.34)$$

$$Q = F - 1. \quad (2.35)$$

Signals demonstrate super-Poisson statistics if $F > 1$ and $Q > 0$ or sub-Poisson statistics if $F < 1$ and $Q < 0$.

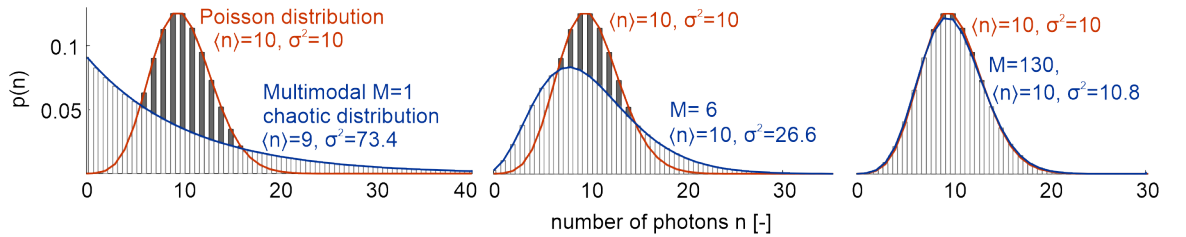


Figure 2.6: Comparison of the approximation of the Multi-mode chaotic distribution with a different number of modes (blue line) and the Poisson distribution (red line)

2.5.2 Advanced signal analysis

BAL assumes **fractal** and **chaotic behavior** due to its inherent properties, including the **physical property of light** (Chapter 2.5.1) and its origin in **biochemical processes** (Chapter 2.3.1). **Biochemical reactions** can display **nonlinear chemical dynamics**, such as **periodic oscillations** [169] indicating **chaotic behavior** [170]. Oscillation during respiration and cell division is slower than metabolic cycles inside cells [171]. **Exciton-**

fusion reactions, where two triplet excitations fuse to form a singlet excitation or chemical reactions in pores of membranes can exhibit **fractal-like kinetics** [172, 173]. The **Fano factor** $F(T)$ can be used for the **evaluation fractality**, where T is the measurement window [174]. For a **random Poisson process**, $F(T)$ is **approximately 1**, and for a **fractal process**, $F(T)$ can be **greater than 1** (Teich, 1989).

Van Wijk employed the Fano factor and statistical moments to characterize BAL signals from human subjects [135, 175, 176]. Additional parameters include the **slope of the doubly logarithmic plot** of $F(T)$ (referred to as the scaling exponent α), which is related to long-time correlations and was used by Stanley [177]. Stanley also analyzed **Fractal dimension** $D(h)$, **Hurst exponent** h and **multifractal spectrum** $\tau(q)$. BAL researchers also utilized **correlation or autocorrelation methods** [61, 178] and **amplitude spectral analysis** [77]. Some sophisticated analyses involved detrending processes, such as **Detrended fluctuation analysis** *DFA* [177], or **Multifractal detrending moving average** *MFDMA* method applied by Scholkmann [55].

2.5.3 Spectral analysis

From the beginning of BAL discovery, researchers required **spectral analysis** to elucidate the **mechanisms which generate BAL**. The complication arose from the technical limitation of BAL spectral measurements, as commercial spectroscopic tools with diffraction grating were unsuitable for BAL. Although **filter-type spectroscopy** with **color filters** was an available method [66, 179–182], its limitation was inaccuracy caused by the **low sharpness** of cut-of wavelength of filters, their **lower transmittance**, and **optical density**. With the **development of filters** improving described parameters, this type of spectroscopy is **commonly used for BAL** in plants [110, 183, 184], cells [155, 185], or human [134, 186]. While this method is suitable for **stationary BAL signals** [157, 187], its **disadvantage** lies in **lower spectral resolution** and the **angular dependence of filters**.

Polychromatic spectroscopy, designed by Scott [188] used a multichannel plate and a position-sensitive detector and addressed the problem of low spectral resolution resulting from filter-type spectroscopy. The **advantages** of polychromatic spectroscopy are **high spectral resolution in real-time** and suitability for **non-stationary** or **temporal variate signals** [189]. Nowadays, the polychromatic spectral system for BAL comprises an input slit, collimator lens, diffractive grating, collecting lens, and highly sensitive imaging device [101]. Nagoshi was the first to use a simplified system described earlier [190]. The **challenge** of this method is **choosing** the suitable **optical parts** of the spectrometer and **slit size** [101].

Spectral analyses can also be used for **diagnostics** of the **state** of the **biological systems** because changes in spectra have been observed in certain diseases such as Alzheimer's and vascular dementia [191], cold [186], breast cancer [185], melanoma cells [155] or plant defense response [56].

The goal of this thesis is to provide an overview of the BAL phenomenon, covering its generation mechanism, spectral and signal analyses, and identifying potential areas for deeper investigation. Furthermore, the thesis aims to measure BAL in the laboratory, identifying suitable measuring equipment, environments, and biological systems. Ultimately, our experiments should either verify or discover potentially useful aspects of BAL.

THE SPECIFIC AIMS OF THE DOCTORAL THESIS ARE AS FOLLOWS:

- 1) Designing light-tight chambers for BAL measurement to enable measurements with different types of detectors.
- 2) Creating a methodology for BAL measurements and select suitable PMT and biological samples.
- 3) Summarizing and investigating photocounts statistics of BAL from biological samples.
- 4) Exploring non-stationary BAL signals to design a suitable preprocessing method.
- 5) Examining the spectral analysis of BAL from biological systems using optical filters.
- 6) Estimating BAL propagation through human skin for different wavelengths and comparing the model with measured data.
- 7) Investigating BAL from human skin to distinguish different levels of oxidation.

4 | DESIGN OF LIGHT-TIGHT CHAMBERS FOR BAL MEASUREMENT

In 2012, a light-tight chamber for BAL measurement was not available from commercial producers according to our requirements for the variability of measurements using different types of PMTs and EMCCD cameras. BAL signals have a very specific property of low intensity ($10 - 1000 \text{ photons} \cdot \text{s}^{-1} \cdot \text{cm}^{-2}$), which is not detectable by the naked eye, mentioned in Chapter. 2.3. It is necessary to provide an absolutely dark environment that enables measurement with very sensitive detectors, such as PMTs or EMCCD cameras.

SOLUTION:

I designed 3D models in Pro/ENGINEER program version Wildfire 4.0, coordinated the procurement of materials and surface treatment, and assembled the chambers. The first type of chamber was designed for measurement with one detector, allowing for the use of different types of detectors. The design was based on previous work [192]. In comparison to the original proposal, I modified the interlocking systems of joints to simplify production in the mechanical workshop, designed flanges compatible with various detector types, and addressed their light-resistant attachment. The chamber was enhanced with direct access to a light-tight chamber through a flange with a two-layer black sleeve secured by three rubber bands, as depicted in Fig.4.1. This chamber is suitable for measuring BAL from hands and enables real-time sample manipulation.

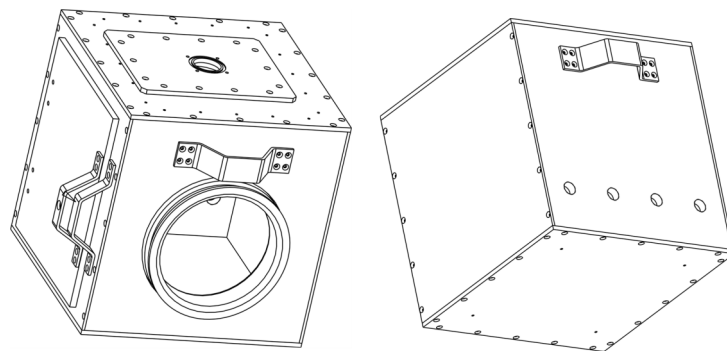


Figure 4.1: Light-tight chamber for measuring BAL with direct access inside, according to utility model 26119.

The second chamber was designed for parallel measurement, offering the flexibility to change its position based on the type of sample. The chamber facilitates horizontal or vertical measurements, depending on the suitability of the sample for measurement in Petri dishes or cuvettes. The advantage of this geometry is the same distance of detectors from the sample. This chamber is composed of three main parts: (i) a positioned chamber, (ii) a stand, and (iii) a holder with a delineation system, as depicted in Fig.4.2.

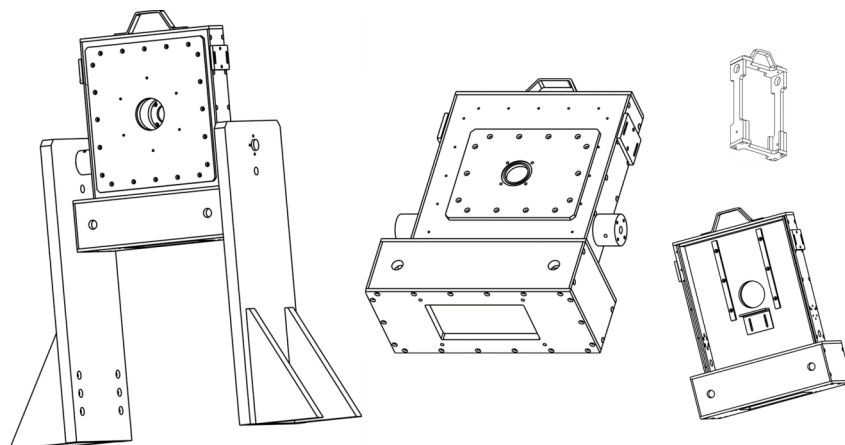


Figure 4.2: Light tight chamber with holder and its delineation system

This chapter includes two utility models in Appendix:

- | 26119: Light-tight chamber for measuring photon emission from biological samples
- | 26574: Positioning light-tight chamber for parallel measurement of photon emission samples

5 | METHODOLOGY OF BAL MEASUREMENTS

This chapter deals with the BAL measurement systems, mainly deals with a selection of suitable detectors, creation of sample preparation protocols, and selection of suitable biological systems. Some results of the preliminary studies were presented in the form of conference papers [C2-C5], Chapter 10. The primary objective of BAL investigation is to analyze signal and statistical parameters and find a connection between them and the states of organisms, both natural and pathological. This indirect method for assessing the levels of free radicals and RONS (Chapter 2.3.1) appears to be a valuable tool in the fields of biology, chemistry, and medicine (Chapter 2.3.2). The main advantages of BAL are that it is a non-invasive, affordable, label-free method without the need for any external illumination of the biosample under test (Chapter 2.3.2.4).

5.1 CONFIGURATION OF MEASURING SYSTEMS

Our BAL measuring system consists of a light-tight chamber (Chapter 4), a detector, and its accessories depending on its type. In total, there are two chambers sized 50x50x50 cm, one chamber with 25x25x25 cm size, and one chamber for parallel measurement. The temperature inside the chamber can be regulated using thermoregulation, which consists of a Peltier air-to-air unit (UEPK-A2AH-24V-100W or UEPK-A2AH-24V-50W, UWE electronic) and temperature sensor PT 100 (UE-Y15-M2163-4O, UWE electronic) included in the chamber. The source box, manufactured and assembled at IPE, includes a switching power supply (S8VS-12024, Omron), an electrical reverser unit for Peltier modules (LSTW5.1.2, UWE Electronic), and a digital temperature controller (E5CN-Q2MT-500, Omron) with option units (E53-CNQBN2, Omron). A PMT or EMCCD camera is mechanically and optically connected to the chamber via a flange, designed and manufactured at

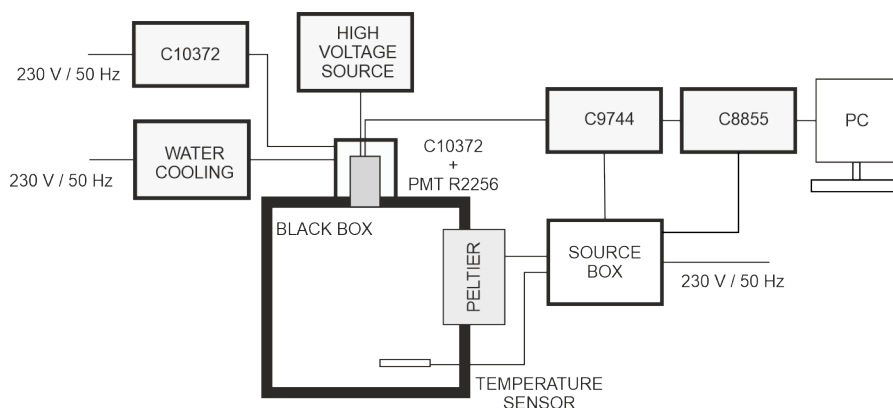


Figure 5.1: Configuration of measuring system with PMT R2256-02.

Table 5.1: Tested PMTs with their basic parameters [194]

type	geometry	cathode [mm]	spectral range [nm]	peak sensitivity [nm]
H7360-01	head on	∅ 22	300-650	420
R4220	side on	8 x 24	185-710	410
R3896	side on	8 x 24	185-900	450
R7515	side on	8 x 24	185-730	410
R4632	side on	8 x 24	185-850	430
R2256-02	head on	∅ 46	160-650	420

Institute of Photonics and Electronics, The Czech Academy of Sciences. In total, 6 PMTs from Hamamatsu Photonics. K. K. company were tested, see Tab. 5.1.

The **H7360-01** is a PMT module with an integrated high-voltage source, preamplifier, discriminator, and shaper of pulses. Its outputs are 5 V TTL pulses processed by count unit C8855-01 (Hamamatsu Photonics K. K.). This type of PMT module cannot be cooled but displays rather low noise due to low red sensitivity and integration of all electronic parts inside the shielded module.

The **R2256-02** is a head-on photomultiplier with a water cooling unit C10372 (Hamamatsu Photonics K. K.) that consists of a control panel and housing. External water cooling is used to achieve lower cooling temperatures -30°C. The high voltage power supply PS350 (Stanford Research Systems) was experimentally set to -1550V with a discriminator level of -500V, based on the SNR parameter obtained from signals of background, mungs, and oil [193]. C9744 unit consists of a pre-amplifier, discriminator, and shaping circuit, forming 5V TTL pulses. The counts are processed by the counting unit C8855. The entire configuration can be seen in Fig.5.1

Side-on PMTs, namely **R4220, R3896, R4632, and R7518** were used with the air-to-air cooling unit C9144-02 (Hamamatsu Photonics K. K.), operating in the temperature range from -30°C to -5°C. The high power supply PS350 (Stanford Research Systems) was set to -1150V. Both C9744 and C8855 units were utilized.

A **back-illuminated EMCCD camera (Andor iXon ULTRA 888)** with Xenon 0.95-25 mm objective (Jos. Schneider Optische) was cooled using a water chiller (Oasis™ 160LT, Solid State Cooling Systems) to -100°C. The spectral response of the EMCCD covers the wavelength range from 300 to 1100 nm, with a peak quantum efficiency of 97.5% at 575 nm.

5.2 PREPARATION OF BIOLOGICAL SAMPLES

Several types of biological samples were investigated, as shown in Tab. 5.2. The preparation of **Mung bean seeds** (*Vigna radiata*, BIO Mung, CZ-BIO-001) involved surface sterilization with 70% ethanol (1 min) and a 50% disinfecting agent (SAVO, CZ) treatment (10 min), followed by rinsing with distilled water (6 times). The

Mungs were soaked for 6 hours, with regular shaking every half an hour, and germinated in dark conditions. Before measurements, the green covers of the seeds were removed. Mung beans exhibit a long-term stationary and high-intensity BAL signal, and the results are presented in Chapters 6 and 7.

Yeast cells (*Saccharomyces cerevisiae*, Euroscarf collection; genetic background BY4741, MATa) used in Chapter 8 were stored on an agar plate in the fridge at 4°C and inoculated to a new plate once a month. The agar medium was prepared from 1% yeast extract (Chemos Cz, 212750, CZ), 2% peptone (Chemos Cz, 211677, CZ), 2% agar (Chemos CZ, 214050, CZ), and 2% D-glucose (Ing. Petr Šulc Penta, 70470-31000, CZ) in distilled water. Before the BAL measurement, yeast cells were inoculated to YPD medium (1% yeast extract, 2% peptone, 2% D-glucose in distilled water) on an orbital shaker incubator (LM420D, Yihder technology Co., CN) at 180 rpm at 30°C for 16 hours.

The **neutrophil** suspension investigated in Chapter 7 was isolated from the venous blood of healthy donors. 12 mL of blood was taken from each donor and delivered in vacuum tubes with lithium heparin from the Institute of Hematology and Blood Transfusion in Prague (Czechia). The density gradient method was used for the isolation of neutrophils. Three different layers of liquids were placed in a 15 mL plastic test tube (P-Lab, type K081151, Prague, Czechia). The bottom layer was 3 mL of histopaque solution 1119 (Sigma-Aldrich), the middle was 3 mL of histopaque solution 1007 (Sigma-Aldrich) and the upper was 6 mL of whole blood. The tube was centrifuged at 890 G for 30 min at 20°C. Then, the neutrophils were removed and doubled in volume using PBS (Phosphate buffered saline). The neutrophil suspension was centrifuged at 870 g for 5 min at 4°C. The supernatant was removed. 3 mL of lysis solution (composed of 154.4 mM ammonium chloride, 7.2 mM potassium carbonate, 126 µM EDTA (Ethylenediaminetetraacetic acid), pH 7.2–7.4) was added into the neutrophil pellet, and the tube was kept for 15 min in the dark at room temperature for red blood cells' lysing process. After that, 3 mL of PBS was added to the tube, and another centrifugation at 870 g for 5 min at 4°C took place. The supernatant was removed. The final cell suspension was neutrophils in 2 mL of PBS with Ca²⁺ and Mg²⁺. Luminol at the final concentration of 5.6 µM was used as a chemiluminescent probe. Phorbol 12-myristate 13-acetate (PMA, Sigma-Aldrich, USA) was used to stimulate oxidative burst at the final concentration of 8 µM, simulating the defense process against pathogens.

The human promyelocytic leukemia **HL-60 cell** line examined in Chapter 8 was maintained in 89% RPMI 1640 medium (Biotech, E15-048, CZ) supplemented with 10% thermally inactivated fetal bovine serum (FBS, Biotech, A15-101, CZ), 1% L-glutamine - penicillin - streptomycin solution (Sigma-Aldrich, G6784, CZ) in a CO₂ incubator (model CCL-170B-8, ESCO, Biotech, CZ) with 5% CO₂ atmosphere at 37°C. To mature HL-60 cells to a neutrophil-like model, they were exposed to all-trans-retinoic acid (Sigma Aldrich, CZ) with a final concentration of 1 µM and incubated for 6 days. The respiratory burst was initiated by phorbol 12-myristate, 13-acetate PMA (Sigma Aldrich, CZ) dissolved in 96% ethanol, the final concentration of PMA in a cell suspension was 54 nM.

Endothelial cells from human **HMVECad** (Human microvascular endothelial cells, adult dermis) and

Table 5.2: Tested biological samples

category	type	medium
yeast cells	mitochondrial mutant <i>ptc5Δ</i> [195]	YPD
	mitochondrial mutant <i>pkp1Δ</i> [195]	(1% yeast extract + 2% peptone
	wild type BY4741, MATa [196–198]	+ 1% dextrose + Q water)
tissue culture	HMVECad	89% DMEM + 10% PBS + 1% antibiotics
	NIH 3T3	-"-
	human neutrophils	PBS
	HL-60 [197]	89% RPMI 1640 + 10% inactivated FBS + 1% antibiotics
germinating seeds	mungs wheat	Q water
human	skin of hand	-

mouse embryonic fibroblast **NIH 3T3** were used for experiments. Cells were maintained in a plastic cultivation flask with DMEM medium (Dulbecco's modified eagle medium) with 10% FBS (Biotech, A15-101, CZ) and 1% L-glutamine-penicillin-streptomycin solution (Sigma-Aldrich, G6784, CZ) in the incubator with 5% CO₂ at 37°C.

The **human skin** of the hands mentioned in Chapter 10 was washed with unscented antibacterial soap and water before measurements. It is also important to ensure that no cream or lotion is applied to the hands that day.

5.3 PRELIMINARY RESULTS

Measurement of BAL in biological samples can be affected by several factors, including delayed luminescence from Petri dishes, Erlenmeyer flasks, media, or buffers important for the cell viability. For statistical analysis, the background was subtracted from the signals.

5.3.1 Adherent tissue cultures

The cells were transferred into glass Petri dishes using trypsin, and 2 mL of DMEM was added. BAL measurements with the R4220 PMT started second day from seeding and it took 15 minutes. Before each measurement, the DMEM medium was replaced with a fresh one. Results from human HMVECad cells show that the intensity of BAL decreases with the number of days of cultivation, as seen in Fig. 5.2. Initially, the fresh seeded cells were highly metabolically active due to sufficient space and nutrients from the medium. However, as the population grew, metabolic activity slowed down. On the last day, the cells' response to oxidative stress was measured with 150 μM and 300 μM hydrogen peroxide (H₂O₂). The results indicate that the increase in BAL is not directly proportional to the amount of H₂O₂. In contrast, the BAL signals from NIH 3T3 cells were of very low intensity, close to the background. Neither the oxidative treatments (50 μM and 200 μM H₂O₂) nor

osmotic treatment (60 mM, 160 mM, 310 mM NaCl) had a measurable effect on the BAL signal.

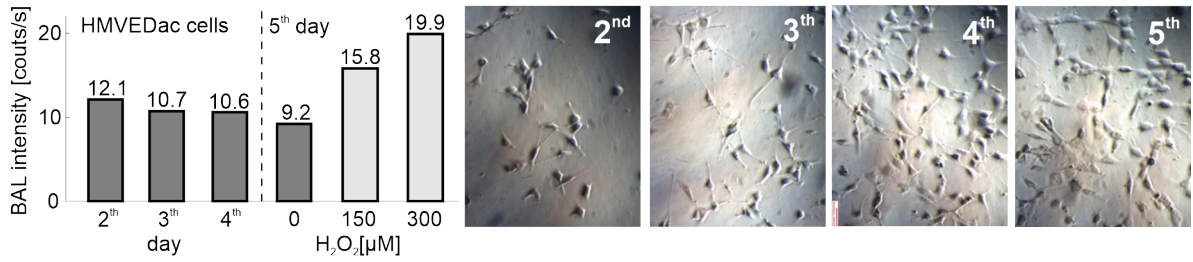


Figure 5.2: Intensity evolution of BAL and cell population from HMVECad during 5 days and BAL intensity after oxidative stress

5.3.2 HL-60 cells

HL-60 cells can be used in immunology research due to their phagocytic activity. We measured BAL from 3 mL of differentiated HL-60 cells in RPMI 1640 in glass Petri dishes with a 4 cm diameter. The signals were recorded using the H7360-01 PMT module. Preliminary results indicate that the intensity of BAL increases with a higher concentration of HL-60 cells, as shown in Fig. 5.3:a. We also investigate respiratory burst induced by different concentrations of PMA. The lowest final concentration of 0.054 nM PMA did not have any effect on HL-60 cells. However, the final concentrations of 5.4 nM and 0.54 nM PMA induce similar kinetics with different time scales, as seen in Fig. 5.3:b. We performed a chemical modulation test using ascorbic acid antioxidant. Ascorbic acid immediately suppressed the signal after application. The effect for two lower concentrations is not permanent, as the signal started to increase, as shown in Fig. 5.3:c.

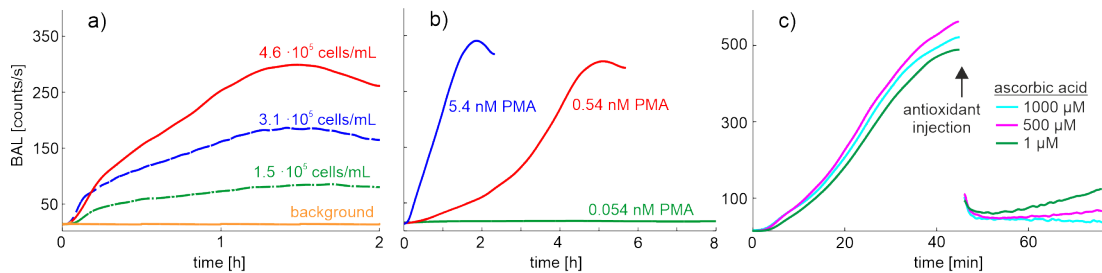


Figure 5.3: BAL signal from differentiated HL-60 cells: (a) of three different concentrations of cells; (b) of three different concentrations of PMA; (c) with three different concentrations of ascorbic acid [197].

5.3.3 Yeast cells

Yeast cells are commonly used as model organism due to general knowledge of their metabolic pathways. BAL from the yeasts were measured in an Erlenmeyer flask with 200 mL of fresh liquid YPD medium at 30°C, with an initial concentration of $5 \cdot 10^6$ cells/mL. Our experiments observed that the BAL phenomenon is highly sensitive to cell sedimentation and the composition of air within the cell suspension. We tested two methods to prevent sedimentation and two air compositions. Stirring the suspension with a magnetic stirrer resulted in lower BAL intensity compared to stirring with a peristaltic pump equipped with a HEPA 13 filter, as shown in Fig. 5.4:a. We achieved two different air compositions by placing the HEPA filter either outside or inside the measuring box. Spontaneous BAL under normal atmospheric air conditions had a lower intensity, while increasing CO₂ inside the chamber as a stress factor caused an increase in the BAL signal. When comparing two different types of PMTs, the H7360-01 detected higher signal than the R7518, as shown in Fig. 5.4:b. We performed a chemical modulation test using ascorbic acid at three different concentrations, as illustrated in Fig. 5.4:c. All three selected concentrations suppressed the BAL signal. Sample preparation and experiments with yeasts are time-consuming, as the entire procedure takes more than 30 hours.

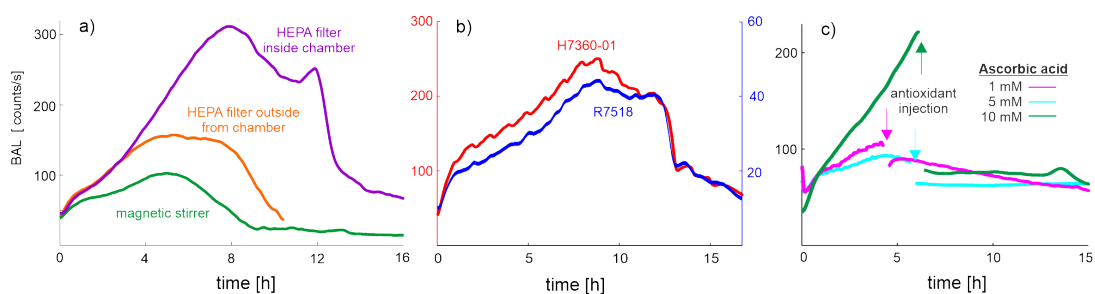


Figure 5.4: BAL Signal from *Saccharomyces cerevisiae*: (a) Using different stirring methods [196]; (b) detected by H7360 PMT module and R7518 PMT [198] (c) with three different concentrations of ascorbic acid [197].

Photocount statistics is useful in assessing light properties. In Chapter 2.5.1, the classical photocount theory was introduced concerning BAL. However, nontrivial statistical properties of BAL, such as coherence and squeezed states of light, were not mentioned, based on the conclusion drawn from our critical review [A5] [199]. Currently, there is no reliable evidence supporting the existence of optical coherence or non-classicality in BAL. The interpretation of BAL distributions is challenging when deciding on their generation mechanism or state of light. In paper [A5], it is demonstrated that classical and thermal light can generate non-Poisson distributions. Trivial manifestation of non-Poisson distributions could be caused by the non-stationarity of the light source, such as modulation of the intensity of the photon signal due to the (i) slow drifting or (ii) periodic trends resulting in Super-Poisson statistics, or (ii) random small bursts caused, for example, by electronic noise. Alternatively, BAL stochastic generation processes could result in sub-Poisson statistics. In Chapter 2.5.1, it is also shown, that photocount statistics of thermal multimodal (with a large number of modes M), converges to a Poisson distribution, which describes a coherent state of light. The photocount statistics of the BAL time series serve as a valuable tool for comparing samples measured by one type of detector, as is shown in our paper [A3] below. We explored BAL statistical properties to monitor the metabolism of germinating mung bean seedlings (*Vigna radiata*) under two different water conditions: pure water and 1% sucrose imbibition.

This chapter is a version of:

| N. Rafieiolhosseini, **M. Poplová**, P. Sasanpour, H. Rafii-Tabar, M. R. Alhossaini, Cifra, Photocount statistics of ultra-weak photon emission from germinating mung bean, *Journal of Photochemistry and Photobiology B: Biology*, vol. 162, pages 50-55, 2016. DOI: 10.1016/j.jphotobiol.2016.06.001.

Journal: Journal of Photochemistry and Photobiology B: Biology, 2016

| Impact factor (2016): 2.673
| Category: Biochemistry & molecular biology
| Quartile in category (2016): Q3

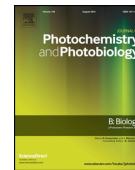
Author contributions:

| **N. Rafieiolhosseini** (contribution 30 %)
| **M. Poplová** (contribution 30 %) Investigation, Methodology, Data curation, Software, Visualization, Writing - original draft
| **P. Sasanpour** (contribution 5 %)
| **H. Rafii-Tabar** (contribution 5 %)
| **M. R. Alhossain** (contribution 10 %)
| **Michal Cifra** (contribution 20 %)



Contents lists available at ScienceDirect

Journal of Photochemistry & Photobiology, B: Biology

journal homepage: www.elsevier.com/locate/jphotobiol

Photocount statistics of ultra-weak photon emission from germinating mung bean



Neda Rafieiolhosseini^{a,1}, Michaela Poplová^{b,c,1}, Pezhman Sasanpour^{d,e}, Hashem Rafii-Tabar^{d,*}, Mahsa Rafiee Alhossaini^f, Michal Cifra^{b,**}

^a Computational Physical Sciences Research Laboratory, School of Nano-Science, Institute for Research in Fundamental Sciences (IPM), 19395-5531 Tehran, Iran

^b Institute of Photonics and Electronics, The Czech Academy of Sciences, Chaberská 57, 18251, Praha 8 - Kobylisy, Prague, Czech Republic

^c Department of Circuit Theory, Faculty of Electrical Engineering, Czech Technical University in Prague, Technická 2, 16627, Praha 6, Prague, Czech Republic

^d Department of Medical Physics and Biomedical Engineering, Faculty of Medicine, Shahid Beheshti University of Medical Sciences, 1985717443 Tehran, Iran

^e Computational Nano-Bioelectromagnetics Research Group, School of Nano-Science, Institute for Research in Fundamental Sciences (IPM), 19395-5531 Tehran, Iran

^f Department of Biostatistics, Faculty of Medical Sciences, Tarbiat Modares University, Jalal Ale Ahmad Highway, 14115-111 Tehran, Iran

ARTICLE INFO

Article history:

Received 22 June 2015

Received in revised form 30 May 2016

Accepted 2 June 2016

Available online 03 June 2016

Keywords:

Ultra-weak photon emission

Mung bean

Photocount statistics

ABSTRACT

Ultra-weak photon emission (UPE) is an endogenous bioluminescence phenomenon present in all biological samples with an active oxidative metabolism, even without an external pre-illumination. To verify the potential of UPE for non-invasive monitoring of metabolism and growth in germinating plants, the aim of this study was to investigate the UPE from a model system – germinating mung bean seedlings (*Vigna radiata*) – and analyze the statistical properties of UPE during the growth in two different conditions of imbibition (pure water and 1% sucrose). We found that in all days and in both conditions, photocount distributions of UPE time series follow the negative binomial distribution whose parameters changed during the growth due to the increasing ratio of signal-to-detector dark count. Correspondingly for both groups, the mean values of UPE increased during the seedlings growth, while the values of Fano factor show a decreasing trend towards 1 during the 6 day period. While our results do not show any significant difference in hypocotyl length and weight gain between the two groups of mung seedlings, there is an indication of a tiny suppressing effect of sucrose on UPE intensity. We believe that UPE can be exploited for a sensitive non-invasive analysis of oxidative metabolism during the plant development and growth with potential applications in agricultural research.

© 2016 Elsevier B.V. All rights reserved.

1. Introduction

UPE can be considered a new type of biological signal, i.e., a photonic biosignal. It is generally accepted that the UPE from biological samples arises from excited electron species formed during the oxidative metabolism and oxidative stress processes [1]. There is also an alternative hypothesis about the origin of UPE which refers to the DNA-based generation of UPE [2,3]. However, unambiguous experimental evidence for this alternative hypothesis is missing. While it is mostly believed that the UPE is a byproduct of cellular metabolism, there are several

scientists who propose that UPE may possibly play a regulatory role in biological systems [4,5].

UPE also holds the promise as a diagnostic method in several biomedical and biological research fields [1]. In plant biology, UPE could form a useful method for monitoring plant responses to some agents such as pathogens or herbicides [1]. For instance, it was shown that pathogens increase the number of emitted photons from plants. Also, the intensity of the UPE from weeds susceptible to herbicides has been shown to be different from the resistant ones [6]. It has been demonstrated that oxidative stress increases UPE intensity from plants suggesting that the balance between oxidants and antioxidants plays an important role in UPE parameters [7]. Simple sugars such as sucrose play an important role in the protection of plants against oxidative damage and induces a tolerance towards oxidative stress [8,9], yet it is not clear whether the protective effects of sucrose in plants are detectable by UPE measurement.

While the intensity and spectra of UPE have been studied most extensively [1], the statistical properties of UPE time series which could also be exploited to act as fingerprints have been poorly investigated [10–15]. In general, the photocount statistics of any photon signal are

Abbreviations: UPE, ultra-weak photon emission; PMT, photomultiplier tube; ANOVA, analysis of variance.

* Correspondence to: H. R. Tabar, Department of Medical Physics and Biomedical Engineering, School of Medicine, Shahid Beheshti University of Medical Sciences, 1985717443 Tehran, Iran.

** Correspondence to: M. Cifra, Institute of Photonics and Electronics, The Czech Academy of Sciences, Chaberská 57, 18251, Praha 8 - Kobylisy, Czech Republic.

E-mail addresses: rafii-tabar@nano.ipm.ac.ir (H. Rafii-Tabar), cifra@ufe.cz (M. Cifra).

¹ Authors contributed equally.

<http://dx.doi.org/10.1016/j.jphotobiol.2016.06.001>

1011-1344/© 2016 Elsevier B.V. All rights reserved.

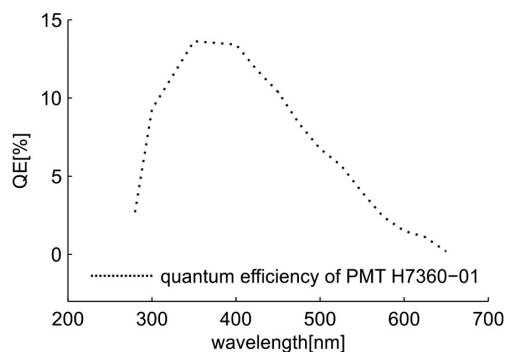


Fig. 1. Quantum efficiency of the photomultiplier detector used in our study. Photomultiplier module H7360-01 used in this study has a peak quantum efficiency at about 400 nm (according to the manufacturer datasheet [19]).

related to the physical state of the light field from which the photons originate. There has been a wide-ranging debate as to whether these states can be characterized as coherent, squeezed, or thermal states. Some researchers proposed that UPE emanates from an endogenous biological coherent electromagnetic field [3,16] while others have attempted to find the parameters associated with a squeezed state representing this radiation [11,12]. However, thermal states with high number of modes seem to be the most reasonable working model for UPE [10].

Instrumental and methodological challenges still pose questions on the exact nature of UPE photocount statistics which are fundamental to elucidate the quantum optical state of UPE. For instance, the coherent optical state is characterized by a Poisson distribution of the photocounts [17], but different light states can have similar statistical distributions, too. It is known that a single mode coherent state and a thermal state with high number of modes have similar photocount distributions [10], close to a Poissonian. Kobayashi and co-workers [18] have indicated that the emission from an LED displays either a Poisson or a super-Poisson distribution. In another work, the statistical distribution of photons from three different areas of a human body was obtained [12]. By comparing these distributions with the theoretical photocount distribution of a squeezed state, the parameters associated with a squeezed state were obtained. It was also shown that the size of the bins affects the form of the photocount distribution of UPE. In some other studies, the Fano factor has been employed to quantitatively determine the agreement with or the departure from a Poisson distribution [10,13,17]. Apart from a squeezed state of light, which does not seem to be justified for UPE, no other reasonable analytical

approximations of UPE photocount distributions have been used to model super-Poisson distributions.

To contribute more data on UPE photocount statistics, in this paper, we have studied the UPE from samples of mung bean seedlings during the germination over a period of 6 days. Furthermore, we tested the hypothesis whether the intensity and statistical parameters of UPE from the seedlings will be affected by the addition of sucrose.

2. Experimental Materials and Methods

2.1. Preparation of Samples

Mung bean seeds (*Vigna radiata*, BIO Mung, CZ-BIO-001) were used as a biological material. Mung seeds were surface-sterilized with 70% ethanol for 1 min. Then, the ethanol was removed and 50% disinfecting agent (SAVO, CZ) was added. After 10 min, the seeds were washed with distilled water 6 times and soaked for 6 h (shaken every half an hour). After the preparation, the green covers of the seeds were removed. Then, they were germinated in dark condition on large Petri dishes with ultra-pure water.

2.2. UPE Detection System

A selected low-noise photomultiplier tube (PMT) module H7360-01 (Hamamatsu Photonics Deutschland, DE) was used in this study (Dark count typ. 15 s^{-1} and photocathode diameter 2.2 cm); see its quantum efficiency in Fig. 1. PMT module was mounted from the top outer side of the black light-tight chamber (standard black box, Institute of Photonics and Electronics, CZ). The distance between PMT module input window and the inner side of the bottom of Petri dish was 2 cm.

2.3. Measurement Protocol

Following the preparation day, 72 similar mung beans were chosen for the study. Seeds were distributed into 6 Petri dishes (5 cm in diameter), each containing 12 seeds. Three Petri dishes (A, B, C) contained seeds in ultra-pure water and the other three Petri dishes (D, E, F) contained seeds in 1% sucrose solution. For 6 days, each day, we measured UPE of each sample, dark count of the PMT (empty black light-tight chamber) and background, specifically the Petri dish with water and the Petri dish with 1% sucrose solution. Although the entire measurement procedure (6 dishes) lasted only 2 h, to avoid any effect due to the different ages of samples, we measured them in a random sequence every day. Since we treated the seeds at the same time, if the samples were measured in the same sequence every day, any difference between them could then be assumed to be due to the different ages of



Fig. 2. Photographs of the mung bean seedlings in dish A during 6 days.

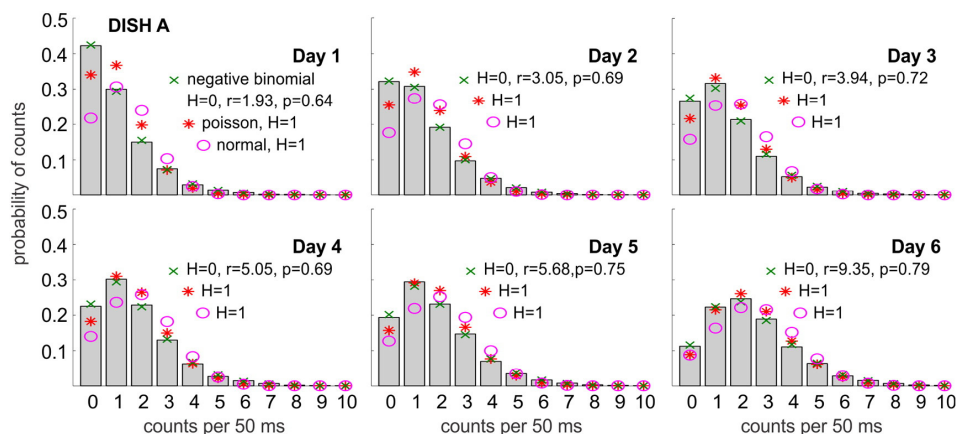


Fig. 3. The evolution of experimental photocount distributions from mung seeds (grey bars) and their fitting with three theoretical distributions (cross, asterisk, circle) over time. The hypothesis H was tested whether the experimental distribution originates from the theoretical distribution ($H = 0$ – hypothesis is accepted; $H = 1$ – hypothesis is rejected). r and p are parameters of the fitted negative binomial distribution.

samples. Each raw data set contained time series of photocounts with the bin size of 50 ms and the length of 10,000 bins.

Furthermore, in order to exclude any effect due to delayed luminescence on the data, the seedlings were kept in dark between measurements and white filter papers were not used since they produce long delayed luminescence. Seeds were grown and measured at room temperature. Photographs were taken after measurements each day and it was the only time that the seeds were exposed to the visible light. The seedling weight was measured in the first and last day and the hypocotyl length was measured on the last day.

2.4. Signal Analysis and Statistical Methods

In order to find out whether photocount statistics could be used for signal analysis or not, all the UPE signals as well as PMT dark counts must be tested for stationarity. A signal is said to be stationary if its distribution does not change over time. To verify this, we segmented each signal into 10 short signals, each consisting of 1000 data points. Then, photocount distributions of different segments were compared using Chi square two sample test [20]. After that, we computed photocount distributions of all the measured UPE signals. To find the best theoretical fit for the measured photocount distributions, we tried several forms (Poisson, Gaussian, negative binomial, exponential, lognormal, gamma and two-parameter Weibull) and used MATLAB software [21] for fitting

the data. Fitting was done for all the UPE signals (i.e. signals from all the dishes in different days) and for different bin sizes (50 ms up to 500 ms with 50 ms step). Goodness of fit was assessed using Chi square two sample test [20]. Another test, Kruskal-Wallis, was also used. It is a one-way analysis of variance which is used as a replacement for ANOVA when the distribution of the data is not normal. It is a non-parametric test to determine whether the samples originate from the same distribution or not. In these tests, H is a test decision for the null hypothesis that the data come from a chosen distribution, using the two-sample chi-squared test. The result $H = 0$ confirms the null hypothesis at the 0.05 significance level, and 1 otherwise.

To investigate the effect of time and sucrose on the intensity of UPE, we utilized the negative binomial regression employing the generalized linear models [22]. We used R v3.2.1 free software for this analysis. Negative binomial regression can be used for over-dispersed count data (when the conditional variance exceeds the conditional mean). It has the same mean structure as Poisson regression and can be considered as its generalized form. Also, it has an additional parameter which enables modeling of the over-dispersion. Eq. (1) in the appendix describes the negative binomial probability distribution. From the mathematical point of view, p is the probability of success, $(1-p)$ is the probability of failure, r is the number of successes, and x indicates the number of failures before reaching the r th success. Furthermore, $r + x$ is the total number of trials. In this model, the photocount of UPE was considered

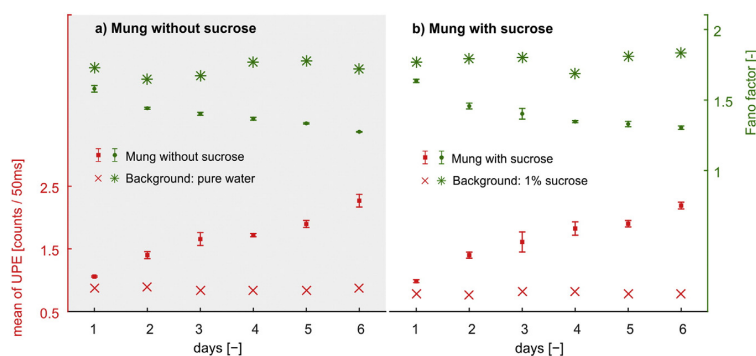


Fig. 4. The estimation of mean and the computed Fano factor of UPE signals from mung seeds and background (water and water with 1% sucrose) are illustrated during 6 days for both water (a) and sucrose group (b). Error bars represent standard error of mean (SE).

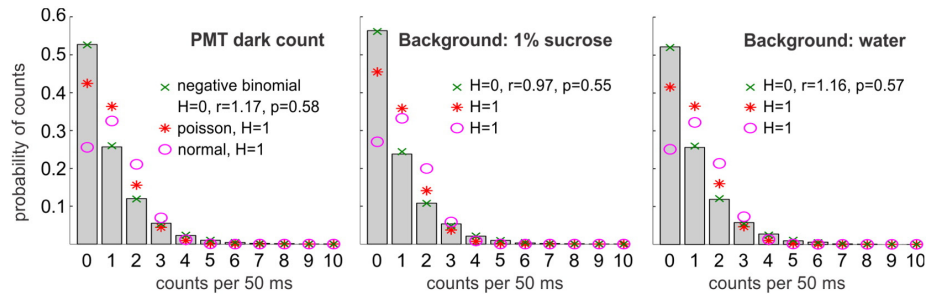


Fig. 5. Example of experimental photocount distributions of the PMT dark count and background (water and water with 1% sucrose) (grey bars) and their fitting with three theoretical distributions (cross, asterisk, circle). The hypothesis H was tested whether the experimental distribution originates from the theoretical distribution (H = 0 – hypothesis is accepted; H = 1 – hypothesis is rejected). r and p are fitted parameters of negative binomial distribution.

as a discrete response variable with a negative binomial distribution and the effect of time (a continuous variable) and sucrose (a binary factor) as independent variables influencing photocounts were tested. We considered all the measured photocount time series each contained 10,000 data points for our analysis. Since we had 3 water dishes and 3 other dishes containing 1% sucrose solution, data from 6 dishes on each day were entered to the model.

Furthermore, we calculated the values of mean and the Fano factor of the UPE signals from all the dishes in different days. The Fano factor, a measure of dispersion or variability, is defined as $F = \frac{\sigma_w^2}{\mu_w}$, where σ_w^2 and μ_w are the variance and the mean of a signal in some time window W, respectively.

3. Results and Discussion

We measured UPE from germinating mung beans in two groups during 6 days. The overall growth process is illustrated on a selected dish A in the sequence of images displayed in Fig. 2. According to the results of Chi square two sample test, all the measured signals (UPE time series as well as PMT dark counts) from both groups were stationary. Therefore, we used photocount statistics for our signal analysis. As stated previously, our sucrose group contained 1% sucrose solution, since we wanted to test whether this small concentration can affect oxidative metabolism which is underlying the UPE generation. We evaluated both the signal parameters of UPE such as the mean value and Fano factor as well as length of hypocotyls and weight of the seedlings.

We found the photocount distributions of all the UPE signals for each day; the typical daily development is shown in Fig. 3. Since photocounts are data of a discrete nature, the measured photocount distributions

often have a shape rather similar to a Poisson distribution, but still certain deviations from Poisson distribution are apparent towards super-Poisson distribution as can be seen from the Fano factor > 1 (Fig. 4). Therefore, it is reasonable to use a more general distribution, capable of modeling a Poisson-like distribution with over dispersion [22], to describe the UPE photocount distribution. We have found that the negative binomial distribution, which was used in other photon statistics research fields [23,24], can be used to appropriately fit the UPE photocount distributions. Although the initially super-Poisson distribution gradually evolved and seemed to approach a Poisson distribution, Chi-square two sample test results indicated that in all cases only the negative binomial distribution appropriately fitted the experimentally obtained distributions; results from dish A through all days are shown in Fig. 3.

The obtained values of Fano factors of UPE signals were always greater than one for both groups. Fig. 4 shows the values of Fano factors for UPE signals and background (water and water with 1% sucrose) during 6 days for both water and sucrose group. In both groups, the values of the Fano factor display a decreasing trend approaching unity. It indicates that during the growth period, UPE photocount distribution gets closer and closer to a Poisson process, for which the Fano factor is equal to unity. For the background, the Fano factor values do not show any specific trend. The observed signal is a sum of the background (PMT dark count) with ultra-weak photon emission. Consequently, the shape of the measured photocount distribution is due to a convolution of the background distribution with a pure UPE photocount distribution. Fig. 5 shows that also the measurement system's noise obeys a negative binomial distribution with the parameters close to those of the UPE from the mung beans in the first day, when the UPE signal intensity was low and very close to the PMT dark count. When the UPE

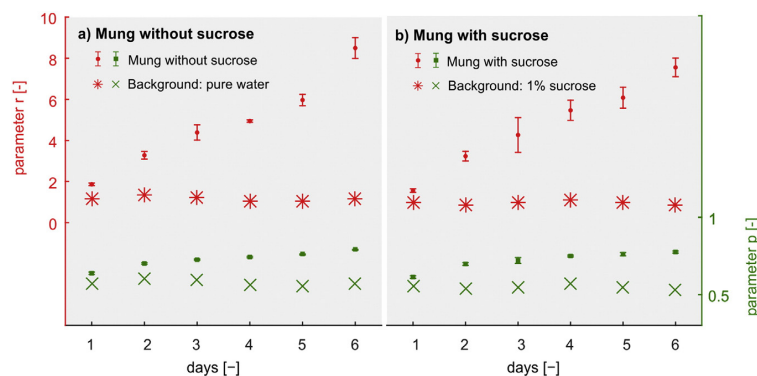


Fig. 6. Estimation of parameters of the negative binomial distribution for the water group (a) and the sucrose group (b). Error bars are \pm standard errors of means.

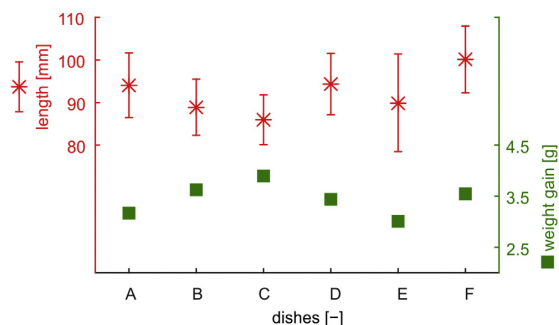


Fig. 7. Seedling weight gain (difference between seedling weights in the first and the last day of experiment) and their hypocotyls length (measured in the last day) are depicted by their means and standard error (SE) for each dish.

intensity from samples dominated the noise, its photocount distribution approached a Poisson distribution. The evolution of the negative binomial distribution parameters of UPE is shown in Fig. 6.

In both groups, the mean values of the UPE signals increased within the period of 6 days (Fig. 4). This behavior is consistent with the findings from other studies focused on UPE during the plant seedling germination such as wheat [25]. We attribute the increase in the mean value of the UPE signal during the growth to the increase in the total volume or mass of metabolizing mung bean tissue as well as the intensity of the metabolism. However, the mean values of the background almost remained constant over this period. Therefore, we used a model in which the mean values of the observed signals were compared.

In our model, called negative binomial regression, the effect of time and sucrose (independent variables) on the mean values of photocounts (response variable) was tested. The results of the regression are summarized in Table 1. In this table, β is regression coefficient and is interpreted differently for each of the variables. For time - our quantitative continuous variable - it shows that by one level change in time (one day for example), how much our response variable (UPE) changes, while for sucrose - our qualitative discrete variable - β shows that how much our response variable (UPE) changes in one group (sucrose), in comparison with another group (water). Wald Z is the test statistic in negative binomial regression. In this case, if the p-value, representing the significance of each factor, is much less than the standard significance level (0.05), it indicates that the factor significantly affects the response variable (mean value of photons). The first line of the Table 1 confirms that the UPE intensity increases over time (positive $\beta = 0.137$) - this can be seen also from the UPE intensity data over the six days (Fig. 4). The second line in Table 1 indicates a finding which is much more subtle and which cannot be easily seen from the Fig. 4: the sucrose group tends to have lower UPE than the water group (negative $\beta = -0.020$). While the effect is very weak in absolute numbers, it is highly statistically significant ($p < 0.001$). The indication that the UPE intensity from mung seedlings in the 1% sucrose is lower compared to water group is corroborated by the fact that the sucrose is involved in the regulation of levels of ascorbic acid, a major antioxidant, in plants. The mechanism likely involves upregulation of genes related to ascorbic acid biosynthesis and recycling pathway by the sucrose [26]. Ascorbic acid is known to suppress UPE intensity in various biological systems [27] including plants [7] through scavenging ROS [28] thus preventing oxidation of biomolecules which leads to generation of electron excited states and subsequent photon emission [29]. Therefore we suggest that sucrose slightly increased the levels of ascorbic acid and cause a slight decrease of UPE. In contrast to our expectation, we found that the presence of sucrose had no statistically significant effect on either the hypocotyl length or the total weight gain in the sucrose group (Fig. 7), (t-test: alpha = 0.05, p-value = 0.4). Comparing the results from Fig. 7 and Table 1 we just discussed, one may suggest that 1%

sucrose did not have any effect on the macroscopic features of the seedling, but it could affect them at the subtle microscopic/biochemical level which underlies generation of ultra-weak photon emission.

We also investigated time series with bin sizes up to 500 ms with 50 ms time steps created from measured signals with bin size 50 ms. Example of the time series with three different bin sizes is shown in Fig. 8 first row. Fitting was also done for different bin sizes, the example for three different bin sizes from dish A is shown in Fig. 8 second row. According to the results for both groups, although the shape of UPE photocount distributions changes depending on the bin size, it is perfectly fitted solely by the negative binomial distribution, and not by the other distributions such as Poisson, normal and exponential. Log-normal, Gamma and two-parameter Weibull distribution are not defined for signals with 0 values.² So, it seems more logical that UPE data follows a Poisson-type distribution (including Neg. Binomial).

4. Conclusion

We investigated the ultra-weak photon emission from germinating mung beans with the aim to elucidate dependence of UPE parameters for the potential applications of monitoring and diagnostics in biotechnology and biomedicine. It has been discovered that the UPE intensity increases with growth over the analyzed period of 6 days. We focused on the photocount statistics of the UPE and we found that solely the negative binomial distribution out of several other tested distribution can fit the data in all cases. Due to the low intensity of UPE and signal-to-noise ratio, statistical properties of the detector dark count contribute significantly to the overall measured statistical properties of UPE. We also found that as the signal-to-noise (noise = dark count) ratio increases, the UPE photocount statistics approaches Poisson distribution. It can be inferred from the Fano factor values showing a decreasing trend towards 1 and also from the shape of the distribution.

Furthermore, within a minor secondary aim we also tested the hypothesis whether the presence of 1% sucrose, a common sugar involved in signaling pathway regulating antioxidants in plants, can affect the UPE parameters. Interestingly, while total length and weight gain of mung seedlings has been unaffected by the sucrose, the UPE displayed a tiny yet statistically significant decrease compared to the control (water only) group.

Our results and the framework we established should aid future analysis of the UPE parameters and statistical properties taking into account the intensity dependent (due to the unavoidable detector noise) photocount distribution. When the proper methods for its signal analysis are embraced, we believe that the UPE can be exploited for a non-invasive, real-time and low-operation cost analysis of oxidative metabolism in many fields including biology and biomedicine beyond the agricultural research application demonstrated here.

Acknowledgements

The authors would like to thank Mohammad Rafeielhosseini (Ph.D, Assistant Prof., Agronomist, Department of Agronomy and Plant Breeding, College of Agriculture, Shahrekord University, Shahrekord, P.O. Box 115, Chaharmahal-Va-Bakhtiari Province, Iran) for helping us in the design of the experiment. Michal Cifra and Michaela Poplová acknowledge support from Czech Science Foundation, grant no. GP13-29294S and from the Czech Technical University in Prague, grant no. SGS15/198/OHK3/3T/13. Michal Cifra and Michaela Poplová also participate in COST Action BM1309 and bilateral exchange project between Czech and Slovak Academies of Sciences, no. SAV-15-22.

² The reason is that a random variable with lognormal, Gamma or two-parameter Weibull distribution shows the time required for reaching to the first event (and this time is always nonzero), while a random variable with Poisson-type distribution shows the number of events within a specific time interval

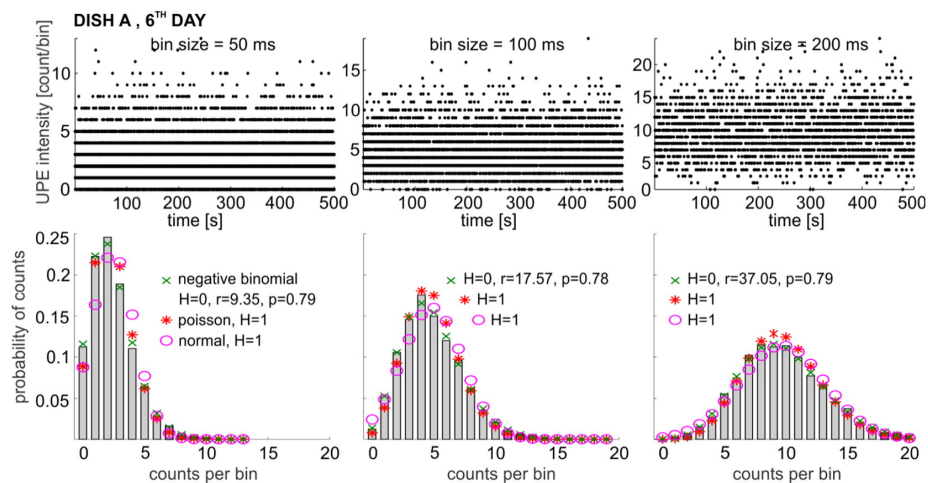


Fig. 8. UPE intensity of mung seeds as a function of time for different bin sizes (first row) and their photocount distribution (second row) of measured signal (left) and its integration into greater bin sizes (middle, right) (grey bars) and their fitting with three theoretical distributions (cross, asterisk, circle). The hypothesis H was tested whether the experimental distribution originates from the theoretical distribution (H = 0 – hypothesis is accepted; H = 1 – hypothesis is rejected).

Appendix A

$$F(x) = \binom{r+x-1}{x} p^r (1-p)^x = \frac{\Gamma(r+x)}{\Gamma(r)\Gamma(x+1)} p^r (1-p)^x \quad (1)$$

Table 1

Results of negative binomial regression representing the effect of time (first row) and sucrose (second row) on the mean values of photocounts. β is regression coefficient, Wald Z is the test statistic and p-value is used to show the significance of each factor on the mean values of photocounts.

Source	β	Wald Z	p-Value
Time	0.137	151.42	<0.001
Sucrose	-0.020	-6.40	<0.001

References

- [1] M. Cifra, P. Pospíšil, Ultra-weak photon emission from biological samples: definition, mechanisms, properties, detection and applications, *J. Photochem. Photobiol. B Biol.* 139 (2014) 2–10.
- [2] F.A. Popp, W. Nagl, K. Li, W. Scholz, O. Weingärtner, R. Wolf, Biophoton emission, *Cell Biophys.* 6 (1984) 33–52.
- [3] K. Li, F. Popp, Dynamics of DNA excited states, in: Springer (Ed.), *Molecular and Biological Physics of Living Systems* 1990, pp. 31–52.
- [4] F. Laager, Light based cellular interactions: hypotheses and perspectives, *Front. Phys.* 3 (2015) 0055.
- [5] F. Schollmann, D. Fels, M. Cifra, Non-chemical and non-contact cell-to-cell communication: a short review, *Am. J. Transl. Res.* 5 (2013) 586–593.
- [6] K. Kato, H. Iyozumi, C. Kageyama, H. Inagaki, A. Yamaguchi, H. Nukui, Application of ultra-weak photon emission measurements in agriculture, *J. Photochem. Photobiol. B Biol.* 139 (2014) 54–62.
- [7] A. Rastogi, P. Pospíšil, Effect of exogenous hydrogen peroxide on biophoton emission from radish root cells, *Plant Physiol. Biochem.* 48 (2010) 117–123.
- [8] W. Van den Ende, R. Valluru, Sucrose, sucrosyl oligosaccharides, and oxidative stress: scavenging and salvaging? *J. Exp. Bot.* 60 (2009) 9–18.
- [9] F. Ramel, C. Sulmon, M. Bogard, I. Couée, G. Gouesbet, Differential patterns of reactive oxygen species and antioxidative mechanisms during atrazine injury and sucrose-induced tolerance in *Arabidopsis thaliana* plantlets, *BMC Plant Biol.* 9 (2009) 1.
- [10] M. Cifra, C. Brouder, M. Nerudová, O. Kučera, Biophotons, coherence and photocount statistics: a critical review, *J. Lumin.* 164 (2015) 38–51.
- [11] R. Bajpai, Biophoton emission in a squeezed state from a sample of *Parmelia tinctorum*, *Phys. Lett. A* 322 (2004) 131–136.
- [12] R. Van Wijk, E. Van Wijk, R.P. Bajpai, Photocount distribution of photons emitted from three sites of a human body, *J. Photochem. Photobiol. B Biol.* 84 (2006) 46–55.
- [13] R.P. Bajpai, E.P. Van Wijk, R. Van Wijk, J. van der Greef, Attributes characterizing spontaneous ultra-weak photon signals of human subjects, *J. Photochem. Photobiol. B Biol.* 129 (2013) 6–16.
- [14] E. van Wijk, J. van der Greef, R. van Wijk, Photon counts statistics in leukocyte cell dynamics, *Journal of Physics: Conference Series* 2011, p. 012021.
- [15] M. Kobayashi, H. Inaba, Photon statistics and correlation analysis of ultraweak light originating from living organisms for extraction of biological information, *Appl. Opt.* 39 (2000) 183–192.
- [16] Q. Gu, On coherence theory of biophoton emission, *J. GCPD eV* 5 (1999).
- [17] X. Shen, F. Liu, X. Li, Experimental study on photocount statistics of the ultraweak photon emission from some living organisms, *Experientia* 49 (1993) 291–295.
- [18] M. Kobayashi, B. Devaraj, H. Inaba, Observation of super-Poisson statistics of bacterial (*Photobacterium phosphoreum*) bioluminescence during the early stage of cell proliferation, *Phys. Rev. E* 57 (1998) 2129.
- [19] H. Corporation, Photon counting head H7360 series(Online). Available: <http://www.alldatasheet.com/datasheet-pdf/pdf/62583/HAMAMATSU/H7360-02.html>.
- [20] W.H. Press, B.P. Flannery, S.A. Teukolsky, W.T. Vetterling, *Numerical recipes in C: the art of scientific programming*, Section 10 (1992) 408–412.
- [21] I. MathWorks, MATLAB: the language of technical computing, Desktop Tools and Development Environment, Version 7, vol. 9, MathWorks, 2005.
- [22] A. Agresti, *An Introduction to Categorical Data Analysis*, vol. 135, Wiley, New York, 1996.
- [23] M.C. Teich, Role of the doubly stochastic Neyman type-A and Thomas counting distributions in photon detection, *Appl. Opt.* 20 (1981) 2457–2467.
- [24] C. Beenakker, H. Schomerus, Counting statistics of photons produced by electronic shot noise, *Phys. Rev. Lett.* 86 (2001) 700.
- [25] C. Mello Gallep, Ultraweak, spontaneous photon emission in seedlings: toxicological and chronobiological applications, *Luminescence* 29 (2014) 963–968.
- [26] F. Nishikawa, M. Kato, H. Hyodo, Y. Ikoma, M. Sugiura, M. Yano, Effect of sucrose on ascorbate level and expression of genes involved in the ascorbate biosynthesis and recycling pathway in harvested broccoli florets, *J. Exp. Bot.* 56 (2005) 65–72.
- [27] A. Rastogi, P. Pospíšil, Spontaneous ultraweak photon emission imaging of oxidative metabolic processes in human skin: effect of molecular oxygen and antioxidant defense system, *J. Biomed. Opt.* 16 (2011) 096005–096005-7.
- [28] M.G. Traber, J.F. Stevens, Vitamins C and E: beneficial effects from a mechanistic perspective, *Free Radic. Biol. Med.* 51 (2011) 1000–1013.
- [29] P. Pospíšil, A. Prasad, M. Rác, Role of reactive oxygen species in ultra-weak photon emission in biological systems, *J. Photochem. Photobiol. B Biol.* 139 (2014) 11–23.

BAL can be characterized by photocounts parameters (Chapter 2.5.1) or analyzed using signal analysis discussed in Chapter 2.5.2. Understanding the data origins is crucial for both approaches. Signals typically consist of BAL signal and detector noise. In scenarios with a low signal-to-noise ratio, detector noise, fluctuation in the signal, or the addition of different types of noise can distort the results. Non-stationary signals require sophisticated analysis with the detrending processes (Chapter 2.5.2) or preprocessing. We have developed the preprocessing method for non-negative integer signals with specific characterization where the mean equals the variance. This method transforms a non-stationary Poisson signal into a stationary signal with a Poisson distribution while preserving the photocount distribution type and the phase-space structure of the signal, as explained below.

This chapter is a version of:

| **M. Poplová**, P. Sovka and M. Cifra

Poisson pre-processing of nonstationary photonic signals: Signals with equality between mean and variance, *Plos one*, vol. 12, issue 12, pages e0188622, 2017. DOI: 10.1371/journal.pone.0188622.

Journal: PloS One, 2017

| Impact factor (2017): 2.766

| Category: Multidisciplinary sciences

| Quartile in category (2017): Q1

Author contributions:

| **M. Poplová (contribution: 50 %)**

Data curation, Formal analysis, Investigation (equal), Methodology(equal), Software Visualization, Writing - original draft

| **P. Sovka (contribution: 20 %)**

Methodology (equal), Supervision (supporting), Writing - review & editing (equal)

| **M. Cifra (contribution: 30 %)**

Conceptualization, Funding acquisition, Investigation (equal), Methodology (equal) Project administration, Resources. Supervision (lead), Writing - review & editing

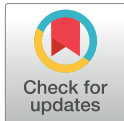
RESEARCH ARTICLE

Poisson pre-processing of nonstationary photonic signals: Signals with equality between mean and variance

Michaela Poplová^{1,2}, Pavel Sovka², Michal Cifra^{1*}

1 Institute of Photonics and Electronics, the Czech Academy of Sciences, Chaberská 57, 182 51, Prague 8, Czechia, **2** Faculty of Electrical Engineering, Czech Technical University in Prague, Technická 2, 166 27, Prague 6, Czechia

* cifra@ufe.cz



OPEN ACCESS

Citation: Poplová M, Sovka P, Cifra M (2017) Poisson pre-processing of nonstationary photonic signals: Signals with equality between mean and variance. PLoS ONE 12(12): e0188622. <https://doi.org/10.1371/journal.pone.0188622>

Editor: Joseph Najbauer, University of Pécs Medical School, HUNGARY

Received: June 28, 2017

Accepted: November 10, 2017

Published: December 7, 2017

Copyright: © 2017 Poplová et al. This is an open access article distributed under the terms of the [Creative Commons Attribution License](https://creativecommons.org/licenses/by/4.0/), which permits unrestricted use, distribution, and reproduction in any medium, provided the original author and source are credited.

Data Availability Statement: All relevant data are within the paper and its Supporting Information files.

Funding: The authors acknowledge the support from the Czech Science Foundation (grant no. GA13-29294S) to M.C. and a grant from the Czech Technical University in Prague (grant no. SGS15/198/OHK3/3T/13). M.C. and M.P. participate in COST Actions BM1309, CA15211 and project no. SAV-15-22 between Czech and Slovak Academies of Sciences. The funders had no role in study

Abstract

Photonic signals are broadly exploited in communication and sensing and they typically exhibit Poisson-like statistics. In a common scenario where the intensity of the photonic signals is low and one needs to remove a nonstationary trend of the signals for any further analysis, one faces an obstacle: due to the dependence between the mean and variance typical for a Poisson-like process, information about the trend remains in the variance even after the trend has been subtracted, possibly yielding artifactual results in further analyses. Commonly available detrending or normalizing methods cannot cope with this issue. To alleviate this issue we developed a suitable pre-processing method for the signals that originate from a Poisson-like process. In this paper, a Poisson pre-processing method for nonstationary time series with Poisson distribution is developed and tested on computer-generated model data and experimental data of chemiluminescence from human neutrophils and mung seeds. The presented method transforms a nonstationary Poisson signal into a stationary signal with a Poisson distribution while preserving the type of photocount distribution and phase-space structure of the signal. The importance of the suggested pre-processing method is shown in Fano factor and Hurst exponent analysis of both computer-generated model signals and experimental photonic signals. It is demonstrated that our pre-processing method is superior to standard detrending-based methods whenever further signal analysis is sensitive to variance of the signal.

Introduction

Photonic signals lie at the heart of modern sensing methods used for environmental protection [1], food safety [2], and early detection of biomarkers of diseases such as cancer [3] and neurodegenerative diseases [4]. Analysis and processing of photonic signals and their statistical properties are also crucial in quantum optics and communication technologies [5]. Hence, robust signal analysis and processing of photonic signals and their statistical properties are essential for exploiting photonic technologies to their limits.

design, data collection and analysis, decision to publish, or preparation of the manuscript.

Competing interests: The authors have declared that no competing interests exist.

Advanced analysis of photonic signals extends well beyond mere detection of the mean intensities or optical wavelength spectra of photon signals; photocount distributions [6, 7], correlation analyses [8], and fractal/chaos-based signal analysis techniques [9] are required to fully exploit the information carried by the photonic signals under study. Most of these methods of signal analysis inherently assume stationary signals. If the signal contains an unwanted trend that is unrelated to the analyzed process, detrending methods exploiting the trend removal estimated by smoothing (moving average, exponential or Gaussian approximation) or robust smoothing [10] have to be applied to make a signal stationary in order to prevent artificial findings. While the detrending is typically a straightforward task for many types of common non-photonic signals, the story is far more complicated for photonic signals. Due to their intrinsic quantum nature they are naturally non-negative integer signals and typically exhibit a Poisson-like photocount statistics [11], which brings a coupling between the mean and variance of the signal [12]. This coupling poses a problem for the currently available signal pre-processing and detrending methods that find and subtract the mean of the signal: the information about the mean still remains in the variance of the signal. These issues are especially pronounced for the signals of low intensity that occur when one strives for high optical spectral resolution or when the generation process itself is very weak, which is the case for the signals from advanced photonics methods such as those employing Raman-scattering [13] or electro/bio/chemiluminescence analysis [14–17]. While most pre-processing methods applied on Poisson and Poisson-like signals perform variance stabilization, e.g. Anscombe or Bartlett transforms [18–21], which is employed in signal denoising, there are no methods for proper detrending and stationarization of Poisson signals up to our knowledge.

In this paper, we develop a method for proper pre-processing of nonstationary signals originating from any process with a Poisson distribution. We demonstrate the superiority of our method compared to the detrending methods on both computer-generated model signals and experimental luminescence signals.

Poisson signals

Photonic signals are non-negative integers with Poisson-like distribution. In such distribution, the signal mean and variance are interconnected. Therefore we first summarize the statistical properties of signals with Poisson distribution

$$f(k; \lambda) = Pr(X = k) = \frac{\lambda^k}{k!} \cdot e^{-\lambda}, \quad k = 0, 1, 2, \dots \tag{1}$$

which is a discrete probability distribution, where λ is the average number of events in a specified interval such as time, distance, area or volume. The random variable $X = 0, 1, 2, \dots$ is a non-negative integer number. The cumulative probability function is

$$F_p(k; \lambda) = \sum_{i=0}^k \frac{\lambda^i \cdot e^{-\lambda}}{i!}. \tag{2}$$

When λ is sufficiently high, the Poisson distribution can be approximated by a normal distribution [22]:

$$\hat{F}_p(k; \lambda) = \frac{1}{\sqrt{2\lambda\pi}} \int_{-\infty}^k e^{-\frac{(k-\lambda)^2}{2\lambda}} du. \tag{3}$$

For example when $\lambda = 40$, the maximum of the absolute error,

$$\epsilon = \max_k |F_p(k; \lambda) - \hat{F}_p(k; \lambda)| \tag{4}$$

will be approximately 0.01.

The Poisson distribution has a special property:

$$\lambda = E(X) = \text{Var}(X); \tag{5}$$

that is, the mean is equal to its variance. This property is corrupted if common pre-processing methods are used such as detrending procedures (which find the trend using smoothing or robust smoothing methods), data normalization such as min-max [23] or decimal scaling [23], or both detrending and normalization procedures together. Alternatively, the method based on the Z-score [22, 23],

$$Z = \frac{X - \mu}{\sigma}, \tag{6}$$

where μ is the mean and σ is the standard deviation of the value of a random variable X , is often used. In the next text we will use a simplified notation for random processes (signals). Typically the symbol $X(\epsilon_i, n)$ is used where ϵ_i represents i -th realization of the random signal and n is the time instant of the discrete-time random signal. Instead of this symbol we are going to use a simplified notation $x[n]$. Then expected value $E[x[n]] = \sum_i p_i x_i[n]$ represents the ensemble average of the discrete-time random signal at the time instant n . Similarly, $\text{Var}[x[n]] = \sum_i p_i x_i^2[n]$ represents the variance of the random process at the time instant n evaluated over the ensemble of realizations.

Experimental photonic data are naturally discrete in time, and therefore we use a discrete-time approach to describe our method and signals. Fig 1 illustrates the problems of detrending and normalization (6) of the signal with a Poisson distribution. Fig 1a depicts the original nonstationary signal with a Poisson distribution. Each sample of the signal can be considered as one realization of a random process with a Poisson distribution with its parameter λ evolving in time such that $\lambda = \lambda[n]$. One can see that the variance and mean are closely interconnected. An increasing time-varying mean value (trend, $t[n] = \lambda[n] = E(x[n])$) causes increasing variance, as suggested in (5). The detrended signal $x_d[n] = x[n] - t[n]$ still has a growing variance that contains information about the increasing trend of the original signal (Fig 1b). Z-score normalization ensures both signal detrending and normalization by the average variance

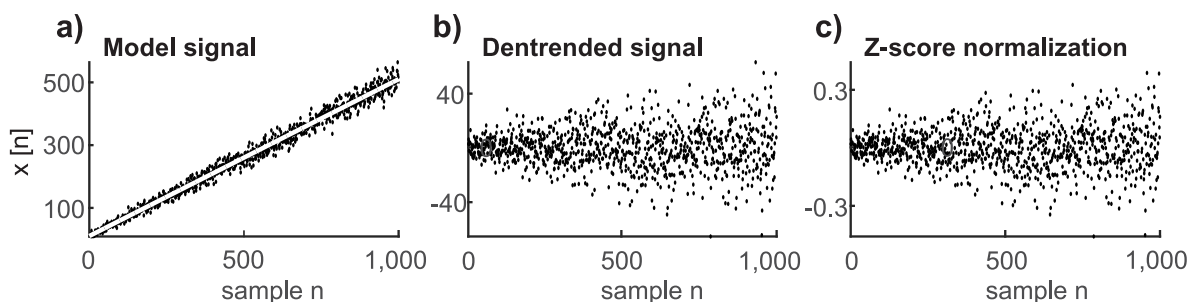


Fig 1. Nonstationary poisson signal preserves its variance after detrending. a) A model signal with Poisson distribution, linearly increasing trend $t[n]$ (white line) according to equation $t[n] = 0.5 \cdot n + 10$ for each sample of signal $n = 1, 2, \dots, 1000$; b) the detrended signal is created by subtraction of the trend from the model signal; c) the pre-processed model signal after Z-score normalization.

<https://doi.org/10.1371/journal.pone.0188622.g001>

(scale change), but information about the time-varying mean value is still preserved in the form of nonstationary growing variance (see Fig 1c). Thus the relation between the mean and variance after detrending or Z-score normalization is corrupted:

$$t[n] = \lambda[n] = 0 \neq \text{Var}(x[n]) = \sigma^2[n]. \tag{7}$$

Moreover, the samples of the resulting signal $t[n]$ are not integers anymore. The other two normalization methods (min-max transformation and decimal scaling) mentioned earlier give the same results as the Z-score normalization.

The second inherent property of a random process (signal) with Poisson distribution is a rectangular grid in the phase space $(x[n], x[n + 1])$ depicted as a close-up view in Fig 2b. This property follows from the fact that the Poisson distribution allows only integer numbers while most of the random processes, for example signals with a normal distribution, form an irregular random grid in this phase space (Fig 2d, close-up). This grid irregularity is caused by the lack of real numbers in the respective realization of the random signal. It is worth emphasizing that it is necessary to use the zoomed-in view of the cluster because the shapes of the whole clusters of the two random processes (Fig 2b: Poisson distribution; Fig 2d: normal distribution) as well as the time signal wave-forms are similar (Fig 2a and 2c).

Materials and methods

Poisson pre-processing

The suggested Poisson pre-processing (PP) method is based on Z-score normalization (6). Z-score transformation is originally applied in order to normalize a random variable with normal distribution [24] and is frequently used for the signal detrending and signal variance

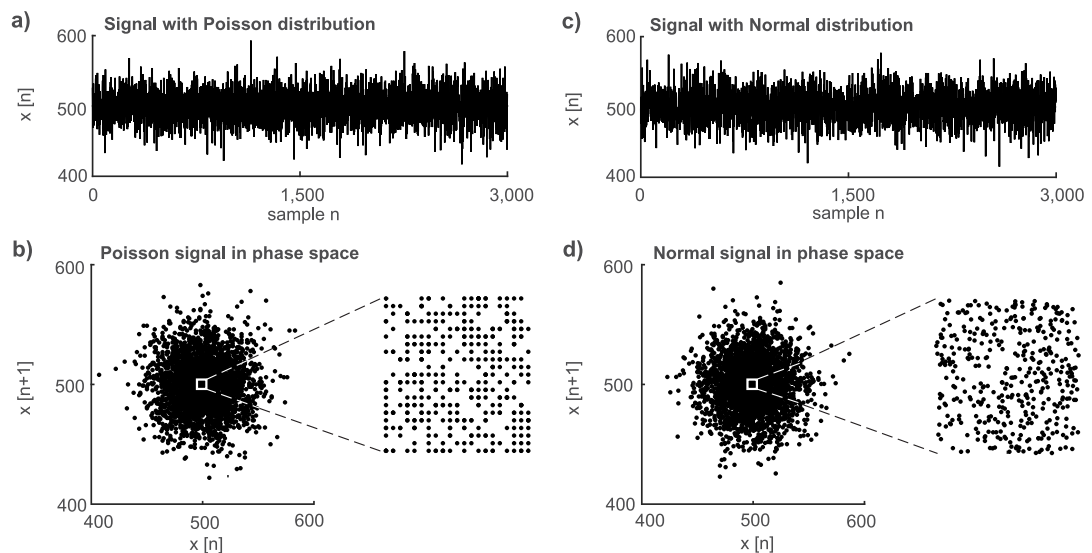


Fig 2. Phase space plot shows a marked difference of signals originating from poisson vs. normal distribution. a) Time waveform of a model signal with Poisson distribution ($\lambda = 500, n = 3000$); b) its depiction in the phase space and a close-up view of its central part. c) Time waveform of a model signal with normal distribution ($\mu = 500; \sigma = \sqrt{500}, n = 3000$); d) its depiction in the phase space and a close-up view of its central part.

<https://doi.org/10.1371/journal.pone.0188622.g002>

normalization [22]. The Z-score method standardizes the signal into a signal with zero mean and a standard deviation equal to one. This type of transformation of a random variable with normal distribution preserves the type of distribution [22]. It changes only its mean and variance. Eq (6) can be modified for Poisson random variable

$$S = \frac{X - \lambda}{\sqrt{\lambda}}. \tag{8}$$

For a discrete-time nonstationary signal with a Poisson distribution Eq (8) can be rewritten into

$$s[n] = \frac{x[n] - t[n]}{\sqrt{t[n]}}, \tag{9}$$

where $x[n] \geq 0$ represents signal integer samples, and $t[n]$ is the trend of the signal for each time instant (instead of μ in (6)). The assumption is that one sample $x[n]$ can be thought as one realization of an integer random variable with Poisson distribution (1) for each time instant, with $\lambda = t[n]$. Therefore, according to (5), the trend $t[n]$ is also equal to the variance $\text{Var}(x[n])$, and the standard deviation σ from (6) is replaced by the square root of the variance $\sqrt{t[n]}$. Consequently, (9) standardizes the detrended signal $(x[n] - t[n])$ according to its dynamically changing standard deviation. The standardized signal $s[n]$ has zero mean $E[s[n]] = \mu_s[n] = 0$ and unity variance $E[s^2[n]] = \sigma_s[n] = 1$ for all time instants. Our goal is to detrend the signal $x[n]$ while preserving the relation between mean and variance which is typical for Poisson distribution. To reach this goal it is necessary to recover a positive integer samples of the signal $p[n]$ with a Poisson distribution, the following transformation has to be used:

$$p[n] = \lfloor (\sqrt{t'} \cdot s[n] + t') \rfloor, \tag{10}$$

where

$$t' \geq \max_n |x[n] - t[n]| \tag{11}$$

for all $n = 1, 2, \dots, N$, where N is equal to the number of signal samples. The symbol \hat{X} represents the integer part of a variable X and the symbol $|X|$ represents the absolute value of a variable X . The whole algorithm consists of a detrending and normalizing part (9) and a restoring part (10). The numerator of (9) provides a detrending signal $x[n]$ so that the trend of the signal $x'[n] = x[n] - t[n]$ is zero. The denominator of (9) decreases (normalizes) the variance of the signal $x'[n] = \frac{x'[n]}{\sqrt{t[n]}}$ to the value of $\text{Var}(x') = 1$. Operations in both the numerator and denominator clearly break the relation between the signal mean and variance, $\mu_s[n] \neq \sigma_s^2[n]$. To restore the relation between the signal mean and the variance, (10) has to be realized. The second term of the right side of this equation ensures that the signal mean is non-zero, $\mu_p[n] > 0$, so that all samples are non-negative $p[n] \geq 0$. The first term of the right side of this equation ensures that the signal variance is equal to the signal mean $\mu_p[n] = \sigma_p^2[n]$. The last operation yields the integer part of the result. Converting numbers to non-negative integers performed by Eq (9) ensures that resulting signal samples represent a Poisson signal, that is they are non-negative numbers with $\mu_p[n] = \sigma_p^2[n]$, $n = 0, 1, \dots$

As described above, the suggested pre-processing procedure should change only the mean and variance of the measured signals but not their type of distribution. Moreover this procedure ensures that the mean of the signal equals the variance and that samples of the signal are non-negative integers. Both features are connected with a Poisson distribution.

Estimation of trend

The trend $t[n]$ has to be estimated from $x[n]$ using a suitable method. Two types of frequently used detrending methods are investigated, specifically smoothing and robust smoothing approximation. Smoothing approximation exploits one or more Gaussian or exponential functions; their number or type depends on the shape of the time series. A method exploiting two Gaussian fittings is chosen according to the character of the experimental nonstationary neutrophil signals used in this paper; the robust smoothing method is based on the cosine transform and weighting of outliers designed by Damien Garcia [10]. Both detrending methods are also used for stationary signals to assess their suitability for usage on stationary Poisson data. The difference between trends estimated by the two Gaussian fitting method (solid black line) and the robust smoothing method (dashed grey line) is illustrated on the experimental nonstationary signal from neutrophils in Fig 3.

Data

Experimental time series and model data are used for the evaluation of the suggested PP method. Three types of experimental data are investigated in total: i) nonstationary luminol-chemiluminescence signals of human neutrophils induced by Phorbol 12 myristate 13-acetate (PMA, Sigma-Aldrich, USA) [25], ii) stationary signals of endogenous biological chemiluminescence from mung seeds [26], and iii) noise (dark count) from a photomultiplier tube (PMT) detector module. The experimental data were obtained using a selected low-noise PMT module H7360-01 (Hamamatsu Photonics K.K.) operated in a photon-counting mode (dark count with stable value of cca. 13 counts per second) in a light-tight chamber (custom-made by the Bioelectrodynamics research team, Institute of Photonics and Electronics of the Czech Academy of Sciences). These discrete-time data are obtained by accumulation of photocounts (detected photons + detector generated dark counts) in each selected time step (bin size). The bins size was 1 s and 50 ms for mung signals and neutrophil signals respectively. In order to statistically evaluate and verify the suggested PP method, the model data are used. The computer-generated model signals (denoted as model neutrophil signals hereafter) matched to the experimental neutrophil signals are generated as random signals with Poisson distribution with $\lambda[n] = \hat{t}[n]$, which is estimated from 10 realizations of experimental nonstationary neutrophil signals using the two fitting methods. Model signals of mungs are generated as random signals with a Poisson distribution with $\lambda = \hat{\mu}$ estimated from 10 realization of the

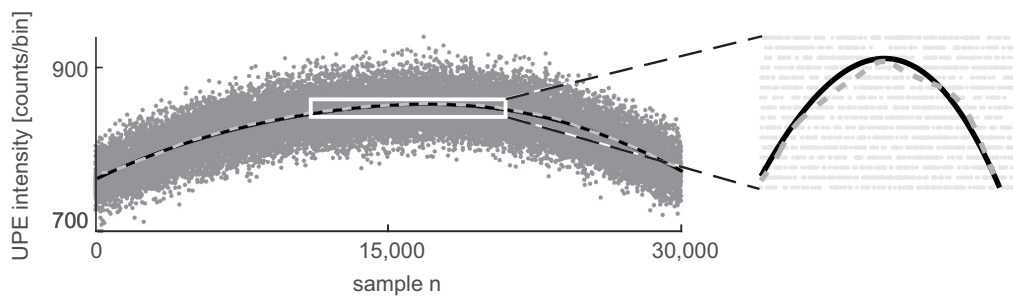


Fig 3. Estimation of trend. Experimental nonstationary signal from neutrophils (grey dots) and their trend obtained by the two-Gaussian-fitting method (solid black line) or the robust smoothing (dashed grey line) method. The length of the signal $T_0[s] = N \cdot T$, where $T = 1$ sample step (bin size) and N is the number of signal samples.

<https://doi.org/10.1371/journal.pone.0188622.g003>

experimental signals of mungs, respectively. One hundred realizations of the model signals are generated from one estimation of the trend $\hat{t}[n]$ from the neutrophil signal for each type of detrending method or mean value $\hat{\mu}$ from mungs. This means that 1000 Poisson model signals of one data type are used for evaluation of the PP method.

Biological sample preparation

Mung seeds (*Vigna radiata*, BIO Mungs, CZ-BIO-001) were surface-sterilized with 70% ethanol (1 min) and 50% disinfecting agent (SAVO, CZ) (10 min). After sterilization the seeds were washed with distilled water 6 times and soaked for 6 h (shaken every half an hour). Then, the seeds were germinated in dark conditions on large Petri dishes with ultra-pure water. Before measurement the green covers of the seeds were removed. Totally twelve seeds were measured on the Petri dishes (5 cm in diameter).

The neutrophils suspension was isolated from venous blood of healthy donors. 12 mL of blood was taken from each donor and delivered in vacuum tubes with lithium heparin from the Institute of Hematology and Blood Transfusion in Prague (Czechia). The density gradient method [27] [28] [29] was used for isolation of neutrophils. Three different layers of liquids were placed to 15 mL plastic test tube (P-Lab, type K081151, Prague, Czechia). The bottom layer was 3 mL of histopaque solution 1119 (Sigma-Aldrich), the middle was 3 mL of histopaque solution 1007 (Sigma-Aldrich) and upper was 6 mL of whole blood. The tube was centrifuged at 890 g for 30 min at 20°C. Then, the neutrophils were removed and doubled in volume using PBS (Phosphate buffered saline). The neutrophils suspension was centrifuged at 870 g for 5 min at 4°C. The supernatant was taken off. 3 mL of lysis solution (composed of 154.4 mM ammonium chloride, 7.2 mM potassium carbonate, 126 μ M EDTA (Ethylenediaminetetraacetic acid), pH 7.2–7.4 [30] [31]) was added and the tube was kept for 15 min in the dark at room temperature for red blood cells lysing process. After that, 3 mL of PBS was added to the tube and another centrifugation at 870g for 5 min at 4°C took place. The supernatant was taken off. The final cell suspension were neutrophils in 2 mL of PBS with Ca^{2+} and Mg^{2+} . The luminol at the final concentration of 5.6 μ M was used added as a chemiluminescent probe. Phorbol 12-myristate 13-acetate (PMA, Sigma-Aldrich, USA) was used to stimulate oxidative burst at the final concentration of 8 μ M.

Evaluation of pre-processing method

Time domain parameters and phase space ($x[n]$, $x[n + 1]$) are used for verification of the PP method. To demonstrate the effect of the PP method on the parameters used for the analysis of experimental luminescence signals, we chose the Fano factor [32], the Hurst exponent [33] computed by Rescaled Range Analysis (RRA [34, 35]) and Detrended Fluctuation Analysis (DFA [36–39]). Fano factor theory states that a Poisson process should have a value of 1 [32]. The Hurst exponent varies within the range from 0 to 1. A Hurst exponent close to 0.5 indicates a random (i.e. a stochastic) process. If it is higher than 0.5, the increments of the process are positively correlated (persistent), or conversely if it is lower than 0.5, the increments of the process are negatively correlated (anti-persistent). All analyzes and generation of model data was performed in Matlab (version R2015a, MathWorks). Below, we compare the raw, detrended, and pre-processed signals. Two types of detrending methods are used: detrending ($x[n] - t[n]$) and detrending+DC ($x[n] - t[n] + t'$), where DC is constant value t' . The use of the detrending+DC method is necessary for calculation and comparison of the results of the distribution and Fano factor analysis or for illustration of the results in segmentation analysis. For a clear graphical interpretation, in the current paper we chose $t' = \min(t)$, which obeys the condition (11).

Let us summarize the original moments of the Poisson distribution of the signal $x[n]$. The mean at the time instant n is $\mu[n] = t[n]$, the variance $\text{Var}[x[n]] = t[n]$, the skewness $\tilde{\mu}_3 = \frac{1}{\sqrt{t[n]}}$, and the kurtosis $e_4 = \frac{1}{t[n]}$. Eq (9) gives the following moments of Poisson distribution of the signal $s[n]$: $\mu[n] = 0$, the variance $\text{Var}[s[n]] = 1$, while the skewness and the kurtosis are unchanged. But Eq (10), which involves both the signal trend shift and the quantization, introduces some changes and errors we analyze in the following text. First, Eq (10) without the quantization gives following moments: $\mu[n] = t'[n]$ which is constant, the variance is also equal to $t'[n]$, the skewness $\tilde{\mu}_3 = \frac{1}{\sqrt{t'[n]}}$, and the kurtosis $e_4 = \frac{1}{t'[n]}$. Eq (11) suggests that the stationary trend $t'[n]$ might be less than the original nonstationary trend $t[n]$. Second, the nonlinear operation represented by the quantization clearly introduces a certain bias and variance into the transformed data and into their statistical moments. As a result, the moments of the signal $p[n]$ including the skewness or kurtosis are not reproduced faithfully to a full extent. To quantitatively assess the influence of the suggested signal transformation and quantization given by Eqs (9)–(11) on the final result the signal-to-noise ratio (SNR) using the mean square value [40] can be used as a measure

$$SNR = 10 \log \frac{P_{sig}}{P_{noise}}. \tag{12}$$

P_{sig} and P_{noise} are the signal power (mean square value) and the noise power, respectively. The Poisson distribution implies that the signal power is $P_{sig} = t' + (t')^2$ (we omit the index n for simplicity). The same holds for the measurement noise power P_{noise} . Both, the original and transformed signal (and the noise) samples are the integer numbers thus the quantization step size Δ is equal to 1. Then the quantization noise with the uniform distribution has the power $P_{noiseQ} = 1/12$ [40]. The resulting signal-to-noise ratio caused by the quantization is then

$$SNR_Q = 10 \log \frac{P_{sig}}{P_{noiseQ}} = 10 \log \frac{t' + (t')^2}{\frac{1}{12}} = 10 \log(12) + 10 \log(t' + (t')^2). \tag{13}$$

This equation enables us to estimate a range of possible values t' using the information about the measured SNR of the respective experiment. The admissible minimum value of t'_{min} can be obtained as the number for which the level of the quantization noise is less than the level of noise of the photomultiplier tube. In other words the SNR_Q given by (13) and caused by the quantization process has to be greater than the measured SNR of a respective experiment. For example, the typical value of the t' for the mung seeds experiment is $t'_{sig} = 50$ giving the signal power $P_{sig} = 2550$ while $t'_{noise} = 13$ gives the noise power $P_{noise} = 3.5$. Eq (12) returns the measured SNR = 12 dB while the SNR_Q caused by the quantization and given by Eq (13) is $SNR_Q = 45$ dB. This result clearly shows that the error caused by the quantization is much lower than the error (noise due to dark count) introduced by the PMT detector module. When one admits $SNR \leq SNR_Q$ then the suggested transformation (9)–(11) can be used for $t'_{min} \approx 0.7$. The results of the neutrophil experiment are: $t'_{sig} = 700$ and $t'_{noise} = 0.65$ yields SNR = 60 dB, $SNR_Q = 67$ dB, and $t'_{min} \approx 315$. On the other hand, the maximum value of t' is determined by the number of samples N available in a respective experiment. A reasonable choice seems to be $t' \leq N/10$. In this case the quick check of data transformation (9)–(11) can be performed by the inspection of the phase space grid to see if it still has a lattice structure. For example, the maximum value of t' is about 3000 for the neutrophil experiment with $N = 30000$ samples. Another problem is the bias $b(\hat{\Phi}) = E[\hat{\Phi}] - \Phi$ [40] of the skewness and kurtosis caused by the quantization process. Symbol Φ stands for the true but unknown parameter (here skewness or kurtosis) and

$\hat{\Phi}$ is the respective estimate. The rough estimate of the maximum bias error can be performed as follows. As mentioned before the quantization step size Δ is equal to 1 therefore the resulting maximum error is also 1 (more precisely (-1) because rounding to the floor is used). Thus the bias can be approximately expressed as $b(\tilde{\mu}_3) = \frac{1}{\sqrt{t'-1}} - \frac{1}{\sqrt{t}}$ for the skewness or $b(e_4) = \frac{1}{t'-1} - \frac{1}{t}$ for the kurtosis. The mung beans experiment with $t' = 50$ yields $b(\tilde{\mu}_3) = 0.0014$ and $b(e_4) = 4.10^{-4}$. Therefore the bias error is negligible for our experiments. But the admissible minimum value of t' is not so low as reported above. First, t' must be greater than 1 as suggested by equations for the bias error. Second, the bias error is large for the low values of t' . For example, for $t' = 10$ is 2% which is greater than 0.14% for the mung bean experiment with $t' = 50$.

Results and discussion

Quality of poisson pre-processing

The goal of the PP method is to render the data mean and variance stationary while simultaneously preserving the original Poisson distribution. Because the mean and variance of the preprocessed signal $p[n]$ do not change over time (they are constant), the signal $p[n]$ can be considered as a wide-sense stationary (wss) one. In fact, wss requires that the first moment (mean) and the second moment (covariance) do not vary with respect to time. Thus to be more precise, the suggested PP ensures only trend and variance stationarity. This part is focused on the evaluation of the PP method in a time domain and in a phase space. The PP method requires trend estimation. Both types of fitting methods used give the same results, as described below. The results of the detrending and PP methods obtained by using the robust smooth fitting method are given in Fig 4.

Fig 4 compares the time and statistical parameters of the a) raw (measured), b) detrended +DC, and c) pre-processed experimental signal of neutrophils. To illustrate the differences between the detrended and pre-processed signal, the DC component is added into the

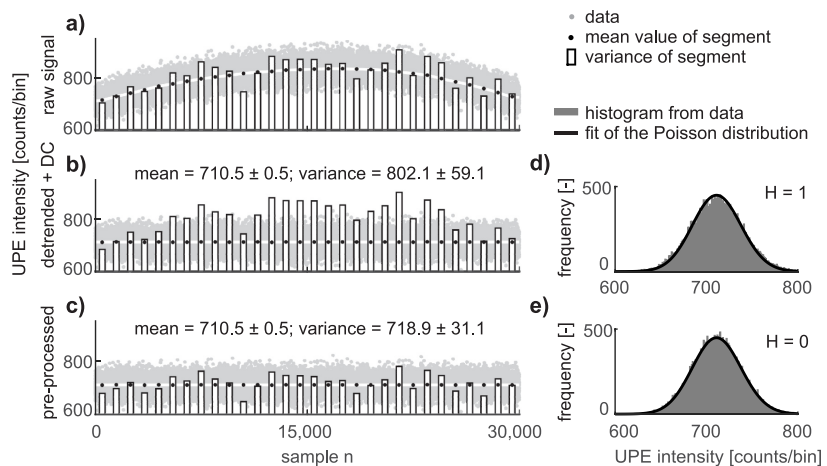


Fig 4. Our poisson preprocessing method recovers poisson distribution. a) The experimental signal from neutrophils, where grey dots are the number of counts per 50 ms, the white line is a trend determined by the robust smoothing method, black dots are mean values in segments, and the bars are the variance in segments. b) Detrended (DC component $\min(t[n])$ added) and c) the pre-processed signal from neutrophils. On the graphs d) and e) are histograms from the data (gray bars), and the black line is the computed Poisson distribution with the parameter λ estimated from the experimental data.

<https://doi.org/10.1371/journal.pone.0188622.g004>

detrended signal corresponding to the minimum value of the trend $\min(t[n])$. The differences in signal shape between the detrended (Fig 4b, gray dots) and the pre-processed signal (Fig 4c, gray dots) cannot be seen by the naked eye. For the purpose of illustrative visualization of the difference between the detrending and PP methods, the following approach is applied. The signal is divided into 30 segments, each containing 1000 samples. The mean value $\hat{\mu}_i$ (black points) and variance $\hat{\sigma}_i^2$ (bar graph) in the i -th segment are calculated. The length of segments is selected as a compromise between the errors in the estimated trend $\hat{t}[n]$ (white line) and the values of the mean $\hat{\mu}_i$ (black dots), as seen in Fig 4a. The results of segment analysis show that the variance of the detrended signal is still almost the same as the variance of the raw signal (compare the bar graphs in Fig 4a and 4b), whereas the variance of the pre-processed signal corresponds to its mean value (Fig 4c, bar graphs versus black points). Our PP method ensures that the variance of the pre-processed signal is equal to its mean, in contrast to the detrended signal, whose variance differs from its mean. The deviation from equality between the parameters μ_i and σ_i (according to the equation $t_i[n] = \text{Var}(x_i[n])$) in segments of experimental or model neutrophils data (raw, pre-processed) is mainly caused by the stochastic character of the signals. Imperfect estimation of the trend, the final length of the intervals, or additive composition of the photonic signal and noise could also contribute to this deviation.

Preservation of the Poisson distribution is verified by the chi-square two-sample test [41]. The null hypothesis stating that the data come from a Poisson distribution is rejected for the detrended signal from the experimental data of neutrophils (Fig 4d) and not rejected for the pre-processed data (Fig 4e, p-values higher than 0.9). This conclusion is still valid for the model data of neutrophils (p-values typically higher than 0.9). The null hypothesis is not rejected for the stationary luminescence experimental data and model data from mung seeds before and after application of the PP method (p-values typically higher than 0.8). The null hypothesis is rejected for detector noise (which is known to be super-Poissonian [26]) before and after application of the PP method.

Another view of the property of the PP method is obtained from the phase space ($x[n]$, $x[n+1]$). Fig 5 demonstrates the behavior of nonstationary experimental Poisson signals from neutrophils in the phase space. The almost elliptic shape of data from neutrophils in the phase space (Fig 5a) is caused by the existence of a nonstationary trend. This statement is also verified on model Poisson data of neutrophils. After detrending the experimental neutrophils data or pre-processing same data by the suggested PP method, rendering the data mean in both cases, the cluster shape in the phase space is changed from an ellipse to a circle (Fig 5c and 5e). However, on zooming in the central part of the data in the phase space, it is clearly seen that the structure of the data is different. After detrending, the dependence between adjacent samples is removed, causing changes in the structure of the lattice (compare Fig 5a and 5c). The PP method defined by (9) and (10) preserves the structure of the lattice in the phase space (see Fig 5e). The data waveform in the time domain remains almost the same, as can be seen by comparing details of the raw (Fig 5b), detrended+DC (Fig 5d), and pre-processed (Fig 5f) signals. Detrending and the PP method change the scale (energy) of the signal but the pattern of the time series is preserved. It can be concluded that while the details of the phase space representation is a very sensitive descriptor, the signal waveform itself is not a good descriptor for revealing differences between results achieved by detrending or by the PP method. Preservation of the phase space lattice by the PP method is closely connected with the fact that the PP method does not change the Poisson distribution of the data.

We also tested our PP method on stationary data with and without a Poisson distribution and nonstationary non-Poisson data. Stationary Poisson data remained unchanged, as verified on real photonic data of mungs and model data of mungs. If stationary non-Poisson data are

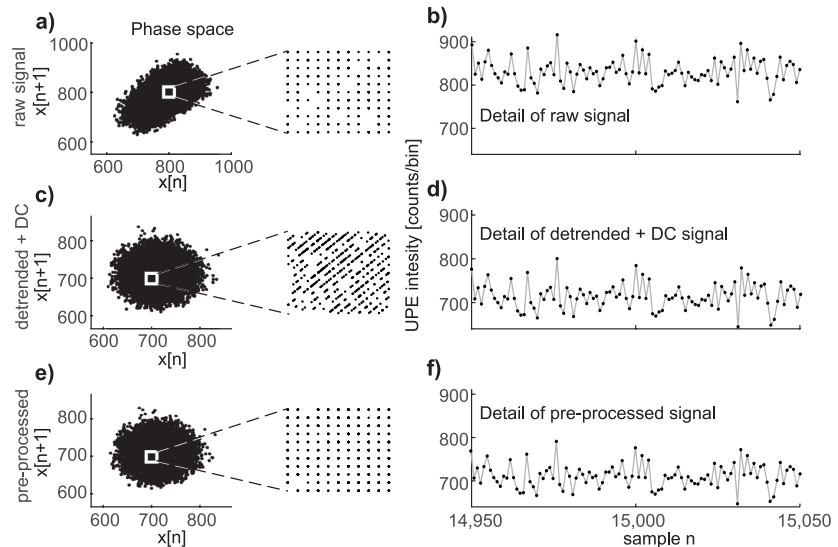


Fig 5. Phase space provides better assessment of the pre-processing than the time domain. a) Experimental neutrophil chemiluminescence data in the phase space and a close-up view of the raw neutrophils data in phase space, b) detail of the time series of raw experimental data from neutrophils luminescence. c) Detrended+DC data in phase space and a close-up view, d) a detail of the time series of the detrended+DC data. e) The pre-processed data in phase space and a close-up view, f) detail of the time series of the pre-processed data.

<https://doi.org/10.1371/journal.pone.0188622.g005>

non-integer, the PP method takes only the integer part of the data; we showed this on model data with a normal distribution (both types: $\mu = \sigma$, $\mu \neq \sigma$). In the case of stationary non-Poisson integer data, the PP method does not change the data; this was verified on detector noise data. Nonstationary non-Poisson data are radically changed after using the PP method (verified on model data with a normal distribution). This conclusion is consistent with the theoretical assumption based on (9) and (10).

Influence of poisson pre-processing method on the result of further signal analysis

Fractal analysis of photonic signals arising, for example, from chemiluminescence and fluorescence is one of several possible ways to obtain further information from photonic signal time series, offering the promise of new fingerprints and markers beyond mere intensity, optical wavelength, and simple correlation analyzes. Signals from certain luminescent systems require fractal/chaos based approaches for their analysis [42, 43]. Several authors used the Fano factor [44–46], Hurst exponent [9, 47, 48] or further advanced methods such as description in terms of quantum squeezed states [49–51] to analyze photonic data and found correlations with biological parameters. However, most of these earlier works either did not use any detrending or used just a simple subtraction of the mean value of the signals so the interpretation of their results is ambiguous [52].

Here we demonstrate that our PP method removes artifactual findings from Fano factor (Fig 6) or Hurst exponent (Fig 7) analysis of photonic signals and performs better than just detrending with an added DC component in the case of Fano factor analysis. The Fano factor

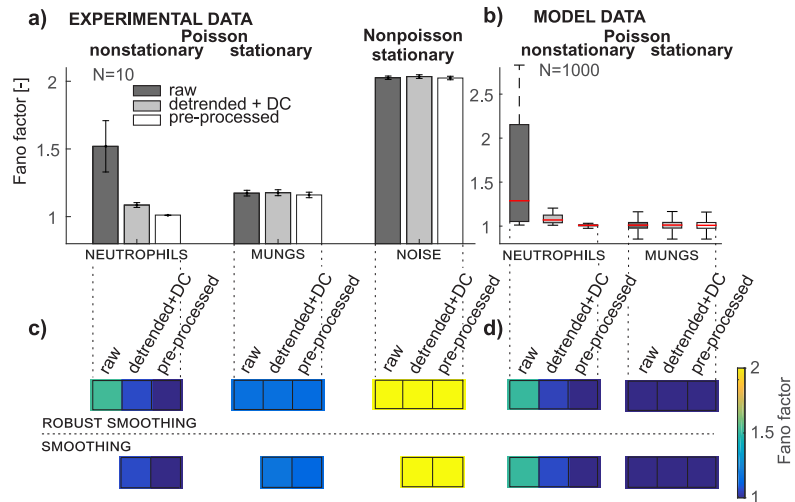


Fig 6. Pre-processing removes artificial findings in fano factor analysis. Preprocessing removes artificial findings in Fano factor analysis. a) Bar graphs depict mean values and the 95% confidence interval of the Fano factor of experimental data from neutrophils, mungs, and detector noise for all three data types (raw, detrended+DC, and pre-processed); b) the box plot depicts the distribution of the Fano factor of model data of neutrophils and mungs for all three data types (raw, detrended+DC, and pre-processed); c) the color bar represents the mean value of the Fano factor from experimental data for both types of detrending methods (smoothing, robust smoothing); d) the color bar represents the mean value of the Fano factor from model data for both types of detrending methods.

<https://doi.org/10.1371/journal.pone.0188622.g006>

and Hurst exponent estimated by RRA are sensitive to the trend in nonstationary data and thus detrending and the PP method radically change their values, as illustrated in Figs 6c, 6d, 7c and 7d for both types of neutrophils data (experimental and model). Comparison of the Fano factor from experimental and model data of neutrophils gives almost the same results (Fig 6c and 6d). This conclusion corresponds to the assumption that the nonstationary raw neutrophils data come from a Poisson distribution, which is confirmed by a chi-square two-sample test of pre-processed data with a 0.05 level of significance. The hypothesis of the Poisson distribution is rejected for experimental and model neutrophils data after detrending. The Fano factor of both types of model data (Fig 6b) after using the PP method for mungs and also for raw and detrended data is equal to the expected value of 1. The difference between the Fano factor in model and experimental data from mungs (Fig 6c and 6d) is caused by the fact that the experimental data are composed from the chemiluminescence signal and non-Poisson detector noise while the model data are not. If the SNR is low, the non-Poisson detector noise depreciates the final signal and its distribution, as we recently demonstrated [26]. Although the Fano factor of experimental mungs data after detrending and the PP method is slightly higher than 1 (specifically, it is 1.17), the chi-square two-sample test confirms the hypothesis of a Poisson distribution (summarized in the section Quality of Poisson pre-processing). The detector noise is found to be non-Poissonian since its Fano factor equals 2.02 (Fig 6a) and also chi-square two-sample test rejected the hypotheses of the Poisson distribution. Both types of detrending (smoothing and robust smoothing) leads to very similar values of the Fano factor for all data considered (Fig 6c and 6d).

RRA and DFA yield an estimate of the Hurst exponent but the principle of its calculation is different. The Hurst exponent from RRA responds to the trend (Fig 7a and 7b, neutrophils)

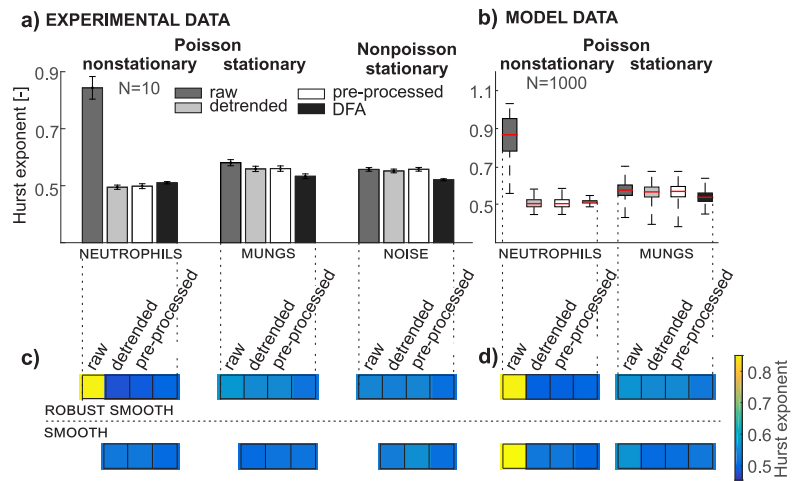


Fig 7. Pre-processing removes artificial findings in Hurst exponent analysis. Preprocessing removes artificial findings in Hurst exponent analysis. a) Bar graphs depict mean values and the 95% confidence interval of the Hurst exponent of signals estimated from Rescaled range analysis and Detrended Fluctuation Analysis from experimental data of neutrophils, mungs, and detector noise for all three data types (raw, detrended and pre-processed); b) the box plot depicts the distribution of Hurst exponent of signals from model data of neutrophils and mungs for all three data types (raw, detrended, and pre-processed); c) the color bar represents the mean value of the Hurst exponent from experimental data for both types of detrending methods (smoothing, robust smoothing); d) the color bar represents the mean value of the Hurst exponent from model data for both types of detrending methods.

<https://doi.org/10.1371/journal.pone.0188622.g007>

whereas DFA is designed for nonstationary data since the detrending procedure is applied within the DFA method. However, the disadvantage of the DFA is in its subjective setting of the scale parameter for the segmentation. Thus the DFA, when applied to a nonstationary signal, could yield incorrect results for an inappropriate selection of the scale parameter.

The output from DFA shows that the results from raw, detrended, and pre-processed data are almost identical (Fig 7c and 7d, black bar). Application of the RRA to detrended or pre-processed signals provides a very similar value, which means that it is not sensitive to small changes in the variance of data applied in the PP method. This conclusion holds for both types of the model signals (Fig 7b) as well as for all three types of experimental signals (Fig 7a). The RRA of stationary signals should give the same result for the Hurst exponent estimated for raw, detrended, and pre-processed data. The noticeable exception is the Hurst exponent from the raw data of experimental and model mungs (Fig 7a and 7b) caused by detrending in the PP method, although the stationarity of the signals from mungs is verified by the Lilliefors test (level of significance = 0.05, p-values higher than 0.4). We also tested the influence of signal length (1000, 10000, and 30000 samples) on the results of RRA from raw, detrended, and pre-processed model data of mungs. The differences between the results are smaller if the length of the signal is greater. The differences in results between the raw and detrended signals of model mungs are larger than those for the raw and pre-processed signal. The Hurst exponent (RRA) from nonstationary neutrophils data shows artificial findings of a positive correlation while the Hurst exponent from detrended, preprocessed neutrophils data, and DFA reveals the actual uncorrelated character of the data.

According to the results of the Fano factor and the Hurst exponent estimated from neutrophils data (Figs 6c, 6d, 7c and 7d) the type of detrending method (smoothing and robust smoothing) is not a crucial part of the PP method. A suitable method for trend estimation should yield a smoothed curve following slow changes in the signal.

Conclusion

We present a new pre-processing method for nonstationary Poisson signals in this paper. The assumption of the input signal properties is that its mean is equal to its variance ($E[x[n]] = \text{Var}[x[n]]$) and signal samples are nonnegative integers ($x[n] \geq 0 \wedge x[n] \in \mathbb{Z}$). Our Poisson pre-processing method renders the signal stationary and preserves the relation between the mean and variance of the random signal composed of non-negative integer samples. This property is illustrated by the segmentation analysis and verified by statistical testing. Moreover, the pre-processed signal keeps its original rectangular structure in the phase space, making our pre-processing method potentially useful for preparing the signals for further complexity and chaos-theory-based analyzes. Application of the pre-processing method to nonstationary signals that are non-Poisson never recovers a Poisson distribution, and hence a *a posteriori* check of whether the analyzed signal originated from a Poisson distribution is possible. Moreover the Poisson pre-processing method does not change the distribution of stationary integer data and causes only minor changes due to rounding when applied to non-integer data such as those originating from a normal distribution.

While our primary motivation was to focus on the pre-processing and analysis of photonic signals such as bio/chemiluminescence and fluorescence, the method we developed is completely general and can be applied to any signal originating from a Poisson process. Furthermore, our method can be generalized to any mean-variance-coupled signals of non-Poisson distribution provided that the analytic formula for the dependence of the mean and the variance is known.

We believe that the application of our method can prevent artifactual findings and enable the analysis of nonstationary photonic signals that might otherwise have been unusable and discarded due to the baseline drifts.

Supporting information

S1 Dataset. Dataset contains all raw experimental and computer generated photocount signals used in this paper.
(ZIP)

Acknowledgments

The authors acknowledge the support from the Czech Science Foundation (grant no. GA13-29294S) and a grant from the Czech Technical University in Prague (grant no. SGS15/198/OHK3/3T/13). M.C. and M.P. participate in COST Actions BM1309, CA15211 and project no. SAV-15-22 between Czech and Slovak Academies of Sciences. Honorata Nawrocka-Bogusz is acknowledged for introducing the neutrophil isolation method to us.

Author Contributions

Conceptualization: Michal Cifra.

Data curation: Michaela Poplová.

Formal analysis: Michaela Poplová.

Funding acquisition: Michal Cifra.

Investigation: Michaela Poplová, Michal Cifra.

Methodology: Michaela Poplová, Pavel Sovka, Michal Cifra.

Project administration: Michal Cifra.

Resources: Michal Cifra.

Software: Michaela Poplová.

Supervision: Michal Cifra.

Visualization: Michaela Poplová.

Writing – original draft: Michaela Poplová.

Writing – review & editing: Pavel Sovka, Michal Cifra.

References

1. Kim HN, Ren WX, Kim JS, Yoon J. Fluorescent and colorimetric sensors for detection of lead, cadmium, and mercury ions. *Chemical Society Reviews*. 2012; 41(8):3210–3244. <https://doi.org/10.1039/C1CS15245A> PMID: 22184584
2. Piliarik M, Párová L, Homola J. High-throughput SPR sensor for food safety. *Biosensors and Bioelectronics*. 2009; 24(5):1399–1404. <https://doi.org/10.1016/j.bios.2008.08.012> PMID: 18809310
3. Im H, Shao H, Park YI, Peterson VM, Castro CM, Weissleder R, et al. Label-free detection and molecular profiling of exosomes with a nano-plasmonic sensor. *Nature Biotechnology*. 2014; 32(5):490. <https://doi.org/10.1038/nbt.2886> PMID: 24752081
4. Neely A, Perry C, Varisli B, Singh AK, Arbneshi T, Senapati D, et al. Ultrasensitive and highly selective detection of Alzheimer's disease biomarker using two-photon Rayleigh scattering properties of gold nanoparticle. *ACS Nano*. 2009; 3(9):2834–2840. <https://doi.org/10.1021/nn900813b> PMID: 19691350
5. O'Brien JL, Furusawa A, Vučković J. Photonic quantum technologies. *Nature Photonics*. 2009; 3(12):687–695. <https://doi.org/10.1038/nphoton.2009.229>
6. Malchus N, Weiss M. Elucidating anomalous protein diffusion in living cells with fluorescence correlation spectroscopy: facts and pitfalls. *Journal of Fluorescence*. 2010; 20(1):19–26. <https://doi.org/10.1007/s10895-009-0517-4> PMID: 19582558
7. Sperling J, Vogel W, Agarwal G. True photocounting statistics of multiple on-off detectors. *Physical Review A*. 2012; 85(2):023820. <https://doi.org/10.1103/PhysRevA.85.023820>
8. Rigler R, Elson ES. *Fluorescence correlation spectroscopy: theory and applications*. vol. 65. Springer Science & Business Media; 2012.
9. Ramanujan VK, Herman BA. Nonlinear scaling analysis of glucose metabolism in normal and cancer cells. *Journal of Biomedical Optics*. 2008; 13(3). <https://doi.org/10.1117/1.2928154> PMID: 18601543
10. Garcia D. Robust smoothing of gridded data in one and higher dimensions with missing values. *Computational Statistics & Data Analysis*. 2010; 54(4):1167–1178. <https://doi.org/10.1016/j.csda.2009.09.020>
11. Walls DF, Milburn GJ. *Quantum optics*. Springer; 2008.
12. Teich MC, Saleh BE. Squeezed state of light. *Quantum Optics: Journal of the European Optical Society Part B*. 1989; 1(2):153. <https://doi.org/10.1088/0954-8998/1/2/006>
13. Halvorson RA, Vikesland PJ. Surface-enhanced Raman spectroscopy (SERS) for environmental analyses. *Environmental Science & Technology*. 2010; 44(20):7749–7755. <https://doi.org/10.1021/es101228z>
14. Kobayashi M, Inaba H. Photon statistics and correlation analysis of ultraweak light originating from living organisms for extraction of biological information. *Applied Optics*. 2000; 39:183–92. <https://doi.org/10.1364/AO.39.000183> PMID: 18337887
15. Kobayashi M, Deveraj B, Inaba H. Observation of super-Poisson statistics of bacterial (*Photobacterium phosphoreum*) bioluminescence during the early stage of cell proliferation. *Physical Review E*. 1998; 57:2129–33. <https://doi.org/10.1103/PhysRevE.57.2129>
16. Miao W. Electrogenenerated chemiluminescence and its biorelated applications. *Chemical Reviews*. 2008; 108(7):2506–2553. <https://doi.org/10.1021/cr068083a> PMID: 18505298

17. Cifra M, Pospíšil P. Ultra-weak photon emission from biological samples: definition, mechanisms, properties, detection and applications. *Journal of Photochemistry and Photobiology B: Biology*. 2014; 139:2–10. <https://doi.org/10.1016/j.jphotobiol.2014.02.009>
18. Bartlett MS. The Square Root Transformation in Analysis of Variance. *Supplement to the Journal of the Royal Statistical Society*. 1936; 3(1):68. <https://doi.org/10.2307/2983678>
19. Anscombe FJ. The Transformation of Poisson, Binomial and Negative-Binomial Data. *Biometrika*. 1948; 35(3/4):246. <https://doi.org/10.1093/biomet/35.3-4.246>
20. Yu G. Variance stabilizing transformations of Poisson, binomial and negative binomial distributions. *Statistics & Probability Letters*. 2009; 79(14):1621–1629. <https://doi.org/10.1016/j.spl.2009.04.010>
21. Azzari L, Foi A. Variance Stabilization for Noisy+Estimate Combination in Iterative Poisson Denoising. *IEEE Signal Processing Letters*. 2016; 23(8):1086–1090. <https://doi.org/10.1109/LSP.2016.2580600>
22. King MR, Mody NA. *Numerical and statistical methods for bioengineering: applications in MATLAB*. Cambridge University Press; 2010.
23. Larose DT, Larose CD. *Data mining and predictive analytics*. John Wiley & Sons; 2015.
24. Manolakis DG, Ingle VK, Kogon SM. *Statistical and adaptive signal processing: spectral estimation, signal modeling, adaptive filtering, and array processing*. vol. 46. Artech House Norwood; 2005.
25. Samuni A, Krishna CM, Cook J, Black CD, Russo A. On radical production by PMA-stimulated neutrophils as monitored by luminol-amplified chemiluminescence. *Free Radical Biology and Medicine*. 1991; 10(5):305–313. [https://doi.org/10.1016/0891-5849\(91\)90037-4](https://doi.org/10.1016/0891-5849(91)90037-4) PMID: 1649785
26. Rafieiolhosseini N, Poplová M, Sasanpour P, Rafii-Tabar H, Alhossaini MR, Cifra M. Photocount statistics of ultra-weak photon emission from germinating mung bean. *Journal of Photochemistry and Photobiology B: Biology*. 2016; 162:50–55. <https://doi.org/10.1016/j.jphotobiol.2016.06.001>
27. Bland E, Keshavarz T, Bucke C. Using 2, 7-dichlorodihydrofluorescein-diacetate to assess polysaccharides as immunomodulating agents. *Molecular biotechnology*. 2001; 19(2):125–131. PMID: 11725482
28. Freitas M, Porto G, Lima JL, Fernandes E. Isolation and activation of human neutrophils in vitro. The importance of the anticoagulant used during blood collection. *Clinical biochemistry*. 2008; 41(7):570–575. <https://doi.org/10.1016/j.clinbiochem.2007.12.021> PMID: 18226596
29. Costa D, Marques AP, Reis RL, Lima JL, Fernandes E. Inhibition of human neutrophil oxidative burst by pyrazolone derivatives. *Free Radical Biology and Medicine*. 2006; 40(4):632–640. <https://doi.org/10.1016/j.freeradbiomed.2005.09.017> PMID: 16458194
30. Poniedzialek B, Rzymiski P, Nawrocka-Bogusz H, Jaroszyk F, Wiktorowicz K. The effect of electromagnetic field on reactive oxygen species production in human neutrophils in vitro. *Electromagnetic biology and medicine*. 2013; 32(3):333–341. <https://doi.org/10.3109/15368378.2012.721845> PMID: 23137127
31. Nawrocka-Bogusz H, Jaroszyk F. May the variable magnetic field and pulse red light induce synergy effects in respiratory burst of neutrophils in vitro? In: *Journal of Physics: Conference Series*. vol. 329. IOP Publishing; 2011. p. 012023.
32. Fano U. Ionization yield of radiations. II. The fluctuations of the number of ions. *Physical Review*. 1947; 72(1):26. <https://doi.org/10.1103/PhysRev.72.26>
33. Hurst HE. Long-term storage capacity of reservoirs. *Trans Amer Soc Civil Eng*. 1951; 116:770–808.
34. Feder J. *Fractals*. Springer Science & Business Media; 2013.
35. Mandelbrot BB, Wallis JR. Robustness of the rescaled range R/S in the measurement of noncyclic long run statistical dependence. *Water Resources Research*. 1969; 5(5):967–988. <https://doi.org/10.1029/WR005i005p00967>
36. Peng CK, Buldyrev SV, Havlin S, Simons M, Stanley HE, Goldberger AL. Mosaic organization of DNA nucleotides. *Physical Review E*. 1994; 49(2):1685. <https://doi.org/10.1103/PhysRevE.49.1685>
37. Bunde A, Havlin S, Kantelhardt JW, Penzel T, Peter JH, Voigt K. Correlated and uncorrelated regions in heart-rate fluctuations during sleep. *Physical Review Letters*. 2000; 85(17):3736. <https://doi.org/10.1103/PhysRevLett.85.3736> PMID: 11030994
38. Bryce R, Sprague K. Revisiting detrended fluctuation analysis. *Scientific reports*. 2012; 2. <https://doi.org/10.1038/srep00315> PMID: 22419991
39. Shao YH, Gu GF, Jiang ZQ, Zhou WX, Sornette D. Comparing the performance of FA, DFA and DMA using different synthetic long-range correlated time series. *Scientific reports*. 2012; 2. <https://doi.org/10.1038/srep00835>
40. Bendat J. S., Piersol G. A. *Measurement and Analysis of Binomial and Random Data*. John Wiley & Sons, New York 1966.
41. Press WH. *Numerical Recipes Third Edition: The Art of Scientific Computing*. Cambridge University Press; 2007.

42. Guderian A, Münster A, Jinguji M, Kraus M, Schneider F. Resonant chaos control by light in a chemiluminescent reaction. *Chemical Physics Letters*. 1999; 312(5):440–446. [https://doi.org/10.1016/S0009-2614\(99\)00931-8](https://doi.org/10.1016/S0009-2614(99)00931-8)
43. Iranifam M, Segundo MA, Santos JL, Lima JL, Sorouraddin MH. Oscillating chemiluminescence systems: state of the art. *Luminescence*. 2010; 25(6):409–418. <https://doi.org/10.1002/bio.1275> PMID: 20354969
44. Van Wijk E, Wijk RV, Bajpai RP, van der Greef J. Statistical analysis of the spontaneously emitted photon signals from palm and dorsal sides of both hands in human subjects. *Journal of Photochemistry and Photobiology B: Biology*. 2010; 99(3):133–143. <https://doi.org/10.1016/j.jphotobiol.2010.03.008>
45. van Wijk E, van der Greef J, van Wijk R. Photon counts statistics in leukocyte cell dynamics. In: *Journal of Physics: Conference Series*. vol. 329. IOP Publishing; 2011. p. 012021.
46. Bajpai RP, Van Wijk E, Van Wijk R, van der Greef J. Attributes characterizing spontaneous ultra-weak photon signals of human subjects. *Journal of Photochemistry and Photobiology B: Biology*. 2013; 129:6–16. <https://doi.org/10.1016/j.jphotobiol.2013.09.002>
47. Ramanujan VK, Biener G, Herman BA. Scaling behavior in mitochondrial redox fluctuations. *Biophysical Journal*. 2006; 90(10):L70–L72. <https://doi.org/10.1529/biophysj.106.083501> PMID: 16565066
48. Ramanujan VK. Metabolic imaging in multiple time scales. *Methods*. 2014; 66(2):222–229. <https://doi.org/10.1016/j.ymeth.2013.08.027> PMID: 24013043
49. Van Wijk R, Van Wijk E, Bajpai RP. Photocount distribution of photons emitted from three sites of a human body. *Journal of Photochemistry and Photobiology B, Biology*. 2006; 84(1):46. <https://doi.org/10.1016/j.jphotobiol.2006.01.010> PMID: 16520060
50. van Wijk EPA, van Wijk R, Bajpai RP. Quantum squeezed state analysis of spontaneous ultra weak light photon emission of practitioners of meditation and control subjects. *Indian J Exp Biol*. 2008; 46:345–52. PMID: 18697618
51. Bajpai RP. Quantum nature of photon signal emitted by *Xanthoria parietina* and its implications to biology. *Indian J Exp Biol*. 2008; 46:420–32. PMID: 18697628
52. Cifra M, Brouder C, Nerudová M, Kučera O. Biophotons, coherence and photocount statistics: A critical review. *Journal of Luminescence*. 2015; 164:38–51. <https://doi.org/10.1016/j.jlumin.2015.03.020>

8 | OPTICAL SPECTRAL ANALYSIS OF BAL FROM BIOLOGICAL SYSTEMS

BAL is emitted on different wavelengths depending on its generation mechanism, as described in Chapter.2.3.1. Spectral analysis of BAL could be utilized for non-invasive diagnostics of the state of the biological system and elucidation of underlying mechanisms of BAL generation. In previous work, colored filters with imperfect characteristics were used, mentioned in Chapter 2.5.3. This work aims to improve spectral analysis by using the most suitable optical filters with high optical density (rejection band $OD > 4$) and a sharp transition between the rejection and pass band (cut-off slope $< 1\%$). The investigation of the sensitivity of spectral analysis was conducted on two biological organisms: HL-60 cells and yeast cells (*Saccharomyces cerevisiae*). The respiratory burst of neutrophil-like HL-60 cells was induced with the PMA (phorbol 12-myristate, 13-acetate). PMA activates an assembly of NADPH oxidase, which induces a rapid formation of reactive oxygen species (ROS). The yeast cells were investigated during natural metabolism without stress factors. Propagation of error of indirect measurements and standard deviation were used to assess the reliability of the measured spectra. Results indicate a clear difference in the BAL spectra between two organisms using rigorous methodology and error analysis.

This chapter is a version of:

- | **M. Nerudová**, K. Červinková, J. Hašek and M. Cifra,
Optical spectral analysis of ultra-weak photon emission from tissue culture and yeast cells,

Conference and proceedings:

- | Proceedings of SPIE-The International Society for Optical Engineering, 2015
- | Impact factor (2015): 0.53

Author contributions:

- | **M. Poplová (contribution: 60 %)**
Data curation, Formal analysis, Investigation (lead), Methodology (lead)
Software, Visualization, Writing - original draft
- | **K. Červinková (contribution: 15 %)**
Investigation (supporting), Methodology (supporting)
- | **J. Hašek (contribution: 5 %)**
Methodology (supporting - yeast cells handling)
- | **Michal Cifra (contribution: 20 %)**
Conceptualization, Funding acquisition, Project administration
Resources, Supervision, Writing - review & editing

Optical spectral analysis of ultra-weak photon emission from tissue culture and yeast cells

Michaela Nerudová*^{a, b}, Kateřina Červinková^{a, b}, Jiří Hašek^c, Michal Cifra^b

^aFaculty of Electrical Engineering, Czech Technical University in Prague, Czech Republic

^bInstitute of Photonics and Electronics, Academy of Sciences of the Czech Republic, Czech Republic

^cInstitute of Microbiology, Academy of Sciences of the Czech Republic, Czech Republic

ABSTRACT

Optical spectral analysis of the ultra-weak photon emission (UPE) could be utilized for non-invasive diagnostic of state of biological systems and for elucidation of underlying mechanisms of UPE generation. Optical spectra of UPE from differentiated HL-60 cells and yeast cells (*Saccharomyces cerevisiae*) were investigated. Induced photon emission of neutrophil-like cells and spontaneous photon emission of yeast cells were measured using highly sensitive photomultiplier module Hamamatsu H7360-01 in a thermally regulated light-tight chamber. The respiratory burst of neutrophil-like HL-60 cells was induced with the PMA (phorbol 12-myristate, 13-acetate). PMA activates an assembly of NADPH oxidase, which induces a rapid formation of reactive oxygen species (ROS). Long-pass edge filters (wavelength 350, from 400 to 600 with 25 nm resolution and 650 nm) were used for optical spectral analysis. Propagation of error of indirect measurements and standard deviation were used to assess reliability of the measured spectra. Results indicate that the photon emission from both cell cultures is detectable in the six from eight examined wavelength ranges with different percentage distribution of cell suspensions, particularly 450-475, 475-500, 500-525, 525-550, 550-575 and 575-600 nm. The wavelength range of spectra from 450 to 550 nm coincides with the range of photon emission from triplet excited carbonyls (350-550 nm). The both cells cultures emitted photons in wavelength range from 550 to 600 nm but this range does not correspond with any known emitter. To summarize, we have demonstrated a clear difference in the UPE spectra between two organisms using rigorous methodology and error analysis.

Keywords: ultra-weak photon emission, optical spectrum, HL60 cells, yeast cells photomultiplier

1 INTRODUCTION

Ultra-weak photon emission (UPE) is phenomenon of light generated by all living systems, from unicellular organisms to humans. UPE is created in the course of oxidative chemical reactions inside cells without external photo-excitation¹. Emitted photons have wavelength ranging at least from 350 to 750 nm². In this paper, we provide an experimental analysis of the spectral properties of UPE from HL-60 cells as a representative of animal tissue cultures (biomedical applications) and from yeast cells (biotechnological and food industry applications).

There exist two types of UPE, the spontaneous emission described above and induced photon emission. Induced photon emission is invoked by stress factors such as temperature³, chemical substances (H₂O₂⁴, PMA (phorbol 12-myristate 13-acetate)⁵), changes in atmospheric gas composition³ and other simulating ambient factors that can affect the cells in a natural environment. Intensity of the spontaneous emission is approximately 100 photons·s⁻¹·cm⁻² or less and that of the induced emission is around 100 to 1 000 photons·s⁻¹·cm⁻².

UPE is solely a product of oxidative metabolic and oxidative stress processes and it is not related to thermal blackbody-like radiation² or photoluminescence such as fluorescence or phosphorescence². It is generally recognized that generating mechanism of UPE are chemical reactions of reactive oxygen and nitrogen species (RONS), namely free radicals (O₂[·], HO₂[·], HO[·], RO₂[·], NO[·], NO₂[·]...) and non-radical substances (H₂O₂, O₃, NO⁺, NO⁻, HNO₂...) with biomolecules such as lipids and proteins. These reactions lead to the lipid peroxidation or protein carbonylation whose products are electron excited states which subsequently can lead to photon emission⁷. UPE has a potential to be prospectively used in biomedicine for diagnostic purposes, however, knowledge this phenomenon is not understood enough for direct applications yet.

*nerudova@ufe.cz; phone +420 266 773 444

It could give information about the oxidative state of the cells and tissues and underlying regulatory processes^{8, 9, 10}. However, reliable detection of UPE currently requires customized experimental setup-us and evaluation methods. The optical spectral analysis of UPE, on which we focus in our current work, is crucial for verification of the UPE generating mechanisms. It may be used as well as for providing potential diagnostic fingerprint of a first choice. In this paper we focused on the corrections of spectra due to quantum efficiency of detectors, due to spectral transmittance of filters, measurement errors, etc., there are only few experimental works which provided assessment of UPE spectral properties using rigorous methodology.

2 MATERIALS AND METHODS

2.1 Biological material

The human promyelocytic leukemia HL-60 cell line and yeast cells (*Saccharomyces cerevisiae*) type BY4741, MATa were used as biological materials in this experiment. The HL-60 cells were maintained in RPMI 1640 medium (Biotech, E15-048, CZ) supplemented with 10% thermally inactivated fetal bovine serum (Biotech, A15-101, CZ), 1% L-glutamine - penicillin - streptomycin solution (Sigma-Aldrich, G6784, CZ) in an CO₂ incubator (model CCL-170B-8, ESCO, Biotech, CZ) with 5% CO₂ atmosphere at 37°C. The HL-60 cells were differentiated into neutrophil-like cells by incubation with 1 µM all-trans-retinoic acid (Sigma, R2500, CZ) for 6 days.

The yeasts cells were stored on agar plate in the fridge at 4 °C. Agar was prepared from 1% yeast extract (Chemos Cz, 212750, CZ), 2% peptone (Chemos Cz, 211677, CZ), 2% agar (Chemos Cz, 214050, CZ), 2% D-glucose (Ing. Petr Šulc Penta, 70470-31000, CZ) in distilled water. Before the UPE measurement, yeast cells were inoculated to YPD medium (1% yeast extract, 2% peptone, 2% D-glucose in distilled water) on an orbital shaker incubator (LM420D, YIHDER TECHNOLOGY CO., CN) at 180 rpm at 30°C for 16 hours.

2.2 Measurement equipment

Experimental data were obtained utilizing high-sensitive photomultiplier module H7360-01 (Hamamatsu Photonics Deutschland, DE), selected type for low dark count, which was mounted from the top outer side of the black light-tight chamber (HL-60 cells) or was mounted on the side of the light tight chamber (yeast cells). This head-on type detector is sensitive to wavelength range from 300 to 650 nm with peak of sensitivity at 375 nm. Temperature inside the chamber was set to 37°C for HL-60 cells or 30°C for yeast cells by thermo-regulating unit (UEPK-A2AH-24V-100W-LN, UWE Electronic, DE). The distance between detector and biological sample was 3.5 cm for HL60 cells and from 4 to 4.5 cm for yeast cells. An electrical filter wheel (ATIK USB Filter Wheel EFW2, UK) was placed between the biological sample and detector as close as possible. The filter wheel contained nine long pass edge filters with cut-off wavelengths of 400, 425, 450, 475, 500, 525, 550, 575 and 600 nm (Edmund optics). Another long pass filters were used (350 nm (Chroma technology corporation) and 650 nm (Edmund optics)) but they haven't been used for continual measurement. The setup of measurement of yeast cells did not allow used the filter with cut-off wavelength 350 nm and low value of quantum efficiency for 650 nm do not allowed used the filter with this cut-off wavelength. These types of filters have optical density greater than 4 in the rejection band and slope factor less than 1 %. The setup of both measurement equipment for HL-60 cells (a) and yeast cells (b) is shown in Fig. 1.

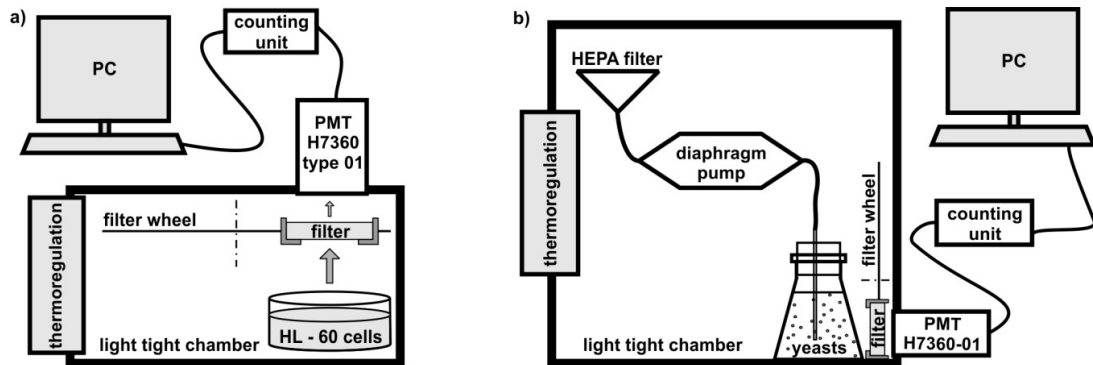


Fig. 1: Setup of the measurement equipment for HL-60 cell in a) and yeast cells in b)

PMT works as follows. Photons from the biological sample incident on the photomultiplier tube's (PMT) photocathode were converted to photo-electrons. Further they were amplified to electron current in the dynode cascade in the PMT. H7360-01 PMT module contains integrated high voltage power supply, PMT preamplifier, discriminator and pulse shaper. Output from H7360 are 5V TTL pulses detected by separate Hamamatsu C8855-01 counting unit, which also serves as an interface with PC. Photo-counts were displayed and recorded using Control Software program (Hamamatsu Photonics Deutschland, DE) in the computer.

2.3 Measurement protocol

Each measurement with a filter took 60 s and then we switched to another filter and so on. A Coulter counter (Z2 Coulter, BECKMAN COULTER, CZ) was used to evaluate cell concentration. After differentiation (six days) the UPE from neutrophil-like cells was measured in the same medium as maintained for differentiation (RPMI 1640). Cell suspension sample had volume of 3ml and was pipetted to the 4 cm diameter glass Petri dish. Following values of cell concentration were set for three experiments: $1 \cdot 10^6$, $1.5 \cdot 10^6$ and $2 \cdot 10^6$ cells/ml. Respiratory burst has been induced by PMA (Sigma, P8139-1MG, CZ, dissolved in 96% ethanol) with final 54 nM concentration in cell suspension, which was applied just before the UPE measurement. HL-60 cells from a single cultivation flask were split into three samples of different cell concentration. Each sample was measured to obtain one set of UPE spectra using filters. The sequence of filters was from lowest cut-off wavelength to the highest (400, 425, ..., 600 nm).

After inoculation (16 hours) the yeast cells were placed to Erlenmeyer flask (250 ml size). 200 ml of cell suspension (cells + YPD medium) with initial concentration $5 \cdot 10^6$ cells/ml was used for UPE measurement. The cell suspension was bubbled with the air cleaned by a HEPA filter (Philips FC8031/00 HEPA12, Alza.cz, CZ). The air within the chamber was pumped by diaphragm pump (M2K3, SCHEGO, airflow 97.2 ml/s, DE) through a glass tube, which passed the stopper in neck of the bottle. This bubbling procedure should ensure the homogeneity of the suspension and their oxygenation. Three sets of signals from yeast cell were recorded from one sample. In the first signal set the sequence of filters was random, in the second set from the lowest to the highest cut-off wavelength and in the third set conversely from the highest to the lowest cut-off wavelength.

2.4 Data

Raw data (see Fig.2 for an example) were time series of photon counts with bin size of 1 sec. Measured signals from cell suspensions were non-stationary but only quasi-stationary parts were used for optical spectral analysis. The trend (red line) was calculated by Robust smooth function¹¹ based on the cosine transform and weighting outliers. For conversion of detected photo-counts to the number of photons coming from cell suspension average values of measured signals without average value of PMT noise (dark count) were used. Dark count of PMT was 15 cps (counts per second). All the signal processing and visualization was performed in Matlab (The MathWorks, version 2011b).

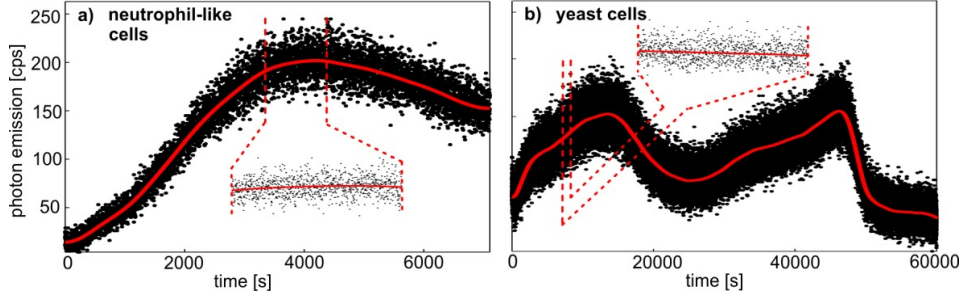


Fig. 2: Example of measured signals without filters and their quasi-stationary part, which was used for optical spectral analysis. a) neutrophil-like HL-60 cells, b) yeast cells

2.4 Optical spectral analysis

The spectral transmittance curves of the filters were measured on spectrometer (Lambda EZ 210, Perkin Elmer, USA) with bandwidth 1 nm. The finer curve (step 1 nm) of quantum efficiency was obtained by interpolation (cubic method) of values of quantum efficiency from datasheet of detector with step 10 nm from 270 to 670 nm. Spectra of photon emission from biological samples were calculated from the raw data as follows.

The signals of photon emission passing through a given filters had to be normalized, because of variability in signal intensity from biological sample (the intensities from various cell suspensions or one cell suspension during one day are different). The normalized signals of photon emission were taken to be the ratio of counts passing through a given filter divided by the average of the counts of signal passing through a given filter with the lowest wavelength, in this case 400 nm. This filter was used as a reference because the entire spectrum of the interest is covered by this filter. The filter wheel with nine filter slots has ensured continuous measurement in the shortest possible time. The normalized luminescence through a given filter (L_i) is given by¹²

$$L_i = k \int T_i(\lambda) S(\lambda) Q(\lambda) d\lambda, \quad (1)$$

where $T_i(\lambda)$ is the transmission spectrum of i^{th} filter, $S(\lambda)$ is the spectrum of photon emission, $QE(\lambda)$ is the quantum efficiency of the detector, λ is wavelength and k is constant which contain parameters as losses of intensity caused by distance, interaction with environment (dispersion, refraction, absorption, etc.) and direction of photon propagation. Because the aim of this work was to obtain relative spectra, constant k could be neglected. The value obtained by subtracting of two normalized signals provides information about spectrum in the wavelength region given by difference of cut-off wavelength used filters. This value of the relative spectrum corresponds to the total optical intensity in the given wavelength band. The average spectral intensity between λ_i and λ_j $S(\lambda_i, \lambda_j)$ is given by quantum efficiency and transmission spectrum of filters in the same interval¹²

$$S(\lambda_i, \lambda_j) = (L_i - L_j) / Q(\lambda_i, \lambda_j) \int (T_i - T_j) d\lambda, \quad (2)$$

where L_i and L_j are average values of the normalized signals of the measured UPE, $Q(\lambda_i, \lambda_j)$ is the average value of quantum efficiency in the interval of wavelength λ_i and λ_j . To evaluate the data, standard deviation σ for raw spectra and two methods for corrected spectra were used, specifically standard deviation σ and propagation of error of indirect measurement

$$\sigma_{(Y)} \approx \sqrt{\left(\frac{\partial f}{\partial x_1} \sigma_{x_1}\right)^2 + \left(\frac{\partial f}{\partial x_2} \sigma_{x_2}\right)^2 + \dots + \left(\frac{\partial f}{\partial x_n} \sigma_{x_n}\right)^2}. \quad (3)$$

Standard deviation of the mean for variable L and standard deviation for variables T and QE was used to evaluate the data. The standard deviation indicates the variability of measured values. Propagation of error of indirect measurement indicates the error of measurement method.

3 RESULTS

The result of optical spectral analysis of ultra-weak photon emission from differentiated HL-60 cells and yeast cells are spectra, shown in Fig. 3. Bars of corrected spectrum indicate percentage contribution to the total sum of photon emission of biological sample coming from the region from 400 to 600 nm. The blue error bars were calculated as a standard deviation of measurements. The red error bars were calculated as propagation of error of indirect measurements. Eight regions from 400 to 600 nm with 25 nm resolution were observed in total. The raw normalized spectra of both cell cultures have different shape than corrected spectra which is caused by the different sensitivity of the measurements apparatus to different wavelength.

The photon emission from cell suspension of neutrophil-like HL-60 cells originates from the range of 450 to 600 nm. The main part comes from 500 to 575 nm, the second highest range is from 575 to 600 nm and range of lower intensity is from 450 to 500nm. The photon emission from cell suspension of yeast cells originates from the range of 450 to 600 nm too, but the spectral distribution is different. The main part comes from 550 to 600 nm, the range with second highest intensity is from 500 to 550 nm and range of lower intensity is the same from 450 to 500nm. Two other spectral ranges, specifically from 350 to 400 nm only for neutrophil-like cells and from 600 to 650 nm for both cell suspensions have been measured. No photon emission from neutrophil-like cells was detected in the 350 to 400 nm region (data not shown in the figures). No UPE measurement of the yeast cell was performed in this region, because the Erlenmeyer flask used (standard laboratory glass) attenuates transmission of light at wavelengths under 400 nm. The second region from 600 to 650 nm wasn't evaluated because of the large error coming from low intensity of signal due to the low quantum efficiency of the detector used.

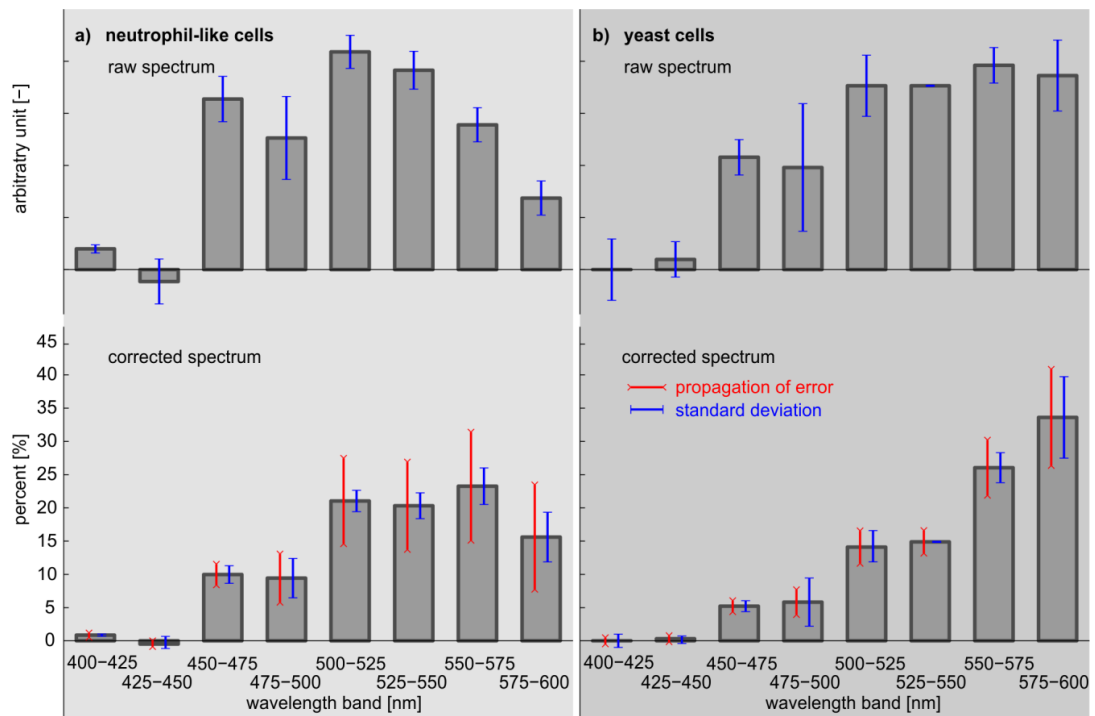


Fig. 3: Spectra of ultra-weak photon emission from cell suspension of a) neutrophil-like cells and b) yeast cells. Raw spectrum from the measured data is shown on the top and the corrected spectrum is shown in the bottom of the figure. The blue error bars show standard deviation of spectra and red error bars show propagation of error of indirect measurement.

4 DISCUSSION AND CONCLUSION

The photons emitted from the cell suspension of neutrophil-like and yeast cells have originated from the wavelength range of 450 to 600 nm (explored range was from 400 to 600nm). These spectra are in accordance with known mechanism underlying generation of UPE. They correspond to the radiative transition from triplet excited level to ground singlet levels of carbonyls², which are emitting near UVA-blue-green region of the spectrum (350-550 nm). The range of 550 nm to 600 nm is usually attributed to chlorophylls and other pigments². However, these are not known to be present in the biological systems (HL60 and yeast cells) under our current study.

The neutrophil-like cells were measured three times with another cell's sample with different final concentration ($1 \cdot 10^6$, $1.5 \cdot 10^6$ and $2 \cdot 10^6$ cells/ml). It was experimentally found that the variation between the maximum values of the intensity of UPE in one type of experiment under our conditions during one day is about 10-15%, but the fluctuation in quasi-stationary part of the signal is lower than 2%. The corrected spectra of neutrophil-like HL-60 cells are very similar; see the standard deviation in Fig. 3 a) bottom, blue line. The propagation of error of indirect measurements from method (Fig. 3 a) bottom, red line) is larger than the standard deviation but it doesn't change the conclusion from corrected spectra.

The yeast cells were measured three times from one cell sample with different sequence of filters (either random or from the lowest to the highest cut-off wavelength or conversely from highest to the lowest cut-off wavelength). The fluctuation in quasi-stationary part is very similar about 1.5 %. The corrected spectra of yeast cells are more similar than corrected spectra of neutrophil-like cells showing both error bars in Fig. 3 b). Spectra of yeast cells are more accurate the reason for this is different treatment of the samples. The highest difference between corrected spectra of neutrophil-like cells could be caused by different initial concentration of cells in suspension because the number of cells is connected with intensity of signals of photon emission (higher number of cells caused the higher intensity).

This model does not include losses of intensity caused by distance, interaction of light with environment and due to angular and spatial dependence of filter transmittance and the detector quantum efficiency. This information could be important in the case of searching for absolute spectra. It should be noted that the distance of samples from PMT and viewing angle of the detector defined by the aperture are very important factors. For instance, when the distance from the sample is increased by 5 cm and the filter wheel is used, even without any filter, the intensity of signal is decreased by 50 % or more.

Our research shows (i) a possibility of UPE optical spectrum measurement from living systems which is not trivial due to low intensity, (ii) a reproducibility of the measurement, even if using different initial concentrations of cells and (iii) a stability of measurement from one biological sample which is not related to sequences of used filters. The importance of our results resides in clear demonstration of a difference between optical spectra of UPE from two distinct types of cell cultures.

The UPE spectral analysis in combination with antioxidant tests can be used for elucidation of mechanism of UPE generation which is not fully described yet. Already some work on spectral analysis of UPE was done in the past using filters with low edge steepness at cut-off wavelength (color filters) that distorted the spectra due to overlaps. Therefore, it is necessary to perform the experiments using more accurate and rigorous tools. For correct representation, spectra must be recalculated according to the optical elements used in the measurement path. The average spectrum must be accompanied by information about the error or uncertainty of measurement. We analyzed propagation of error of indirect measurements which confirm reliability of the results from both spectra described above. The standard deviation is the most commonly used for evaluation of data but it only reflects variability of resulting values.

Impact of our measurement is towards diagnostics of oxidative processes in biological systems. For instance, increased intensity of oxidative processes accompanies and causes many types of diseases and is prominent also in the senescence of organism. Since UPE spectral analysis is completely label-free, noninvasive and almost real-time, it could be developed into diagnostic screening method in multiple fields of biomedicine.

ACKNOWLEDGEMENTS

This research was supported by the Czech Science Foundation, grant no. GP13-29294S, and the Grant agency of the Czech Technical University in Prague, grant no. SGS13/138/OHK3/2T/13 and SGS14/189/OHK3/3T/13.

REFERENCES

- [1] Cifra, M., "Electromagnetic cellular interactions", *Progress in Biophysics and Molecular Biology* 105(3), 223-246 (2011).

- [2] Cifra, M., Pospíšil, P., “Ultra-weak photon emission from biological samples: definition, mechanisms, properties, detection and applications”, *Journal of Photochemistry and Photobiology B: Biology*, (2014).
- [3] Nakamura, K., Hiramatsu, M., “Ultra-weak photon emission from human hand: Influence of temperature and oxygen concentration on emission”, *J. Photochem. Photobiol. B* 80 (2), 156-160 (2005).
- [4] Rastogi, A., Pospíšil, P., “Effect of exogenous hydrogen peroxide on biophoton emission from radish root cells”, *Plant Physiology and Biochemistry* 48 (2), 117-123 (2010).
- [5] Freitas, M., Porto, G., Lima, J.L., Fernandes, E., “Optimization of experimental settings for the analysis of human neutrophils oxidative burst in vitro”, *Talanta* 78 (4), 1476-1483(2009).
- [6] Van Wijk, R., Kobayashi, M., Van Wijk, E., “Anatomic characterization of human ultra-weak photon emission with a moveable photomultiplier and CCD imaging”, *Journal of Photochemistry and Photobiology B: Biology* 83 (1), 69-76 (2006).
- [7] Prasad, A., Pospíšil, P., “Linoleic acid-induced ultra-weak photon emission from *Chlamydomonas reinhardtii* as a tool for monitoring of lipid peroxidation in the cell membranes”, *PLOS ONE* 6 (7), e22345 (2011).
- [8] Fels, D., “Cellular communication through light”, *PLOS ONE* 4 (4), e5086 (2009).
- [9] Van Wijk, R., Schamhart, D.H.J., “Regulatory aspects of low intensity photon emission”, *Experientia* 44 (7), 586-593 (1988).
- [10] Cadenas, E., “Biological chemiluminescence”, *Photochemistry and photobiology* 40 (6), 823-830 (1984).
- [11] Garcia, D., “Robust smoothing of gridded data in one and higher dimensions with missing values”, *Computational Statistics and Data Analysis* 54 (4), 1167-1178 (2010).
- [12] Cheson, B. D., Christensen, R. L., Sperling, R., Kohler, B.E., Babior, B. M., “The origin of the chemiluminescence of phagocytosing Granulocytes”, *The Journal of Clinical Investigation* 58 (4), 789-796 (1976).

9 | OPTICAL MODEL OF BAL PROPAGATION AT HUMAN SKIN FOR DIFFERENT WAVELENGTHS

Spectral analysis is one of the methods that can be used to evaluate BAL signals (Chapter 2.5). This model focuses on the propagation of BAL through the human skin at a selected wavelength. The optical model represents the photon flux attenuation in various skin layers. The initial intensity is evenly distributed into each layer. This model was used to estimate the initial intensity based on skin measurements using PMT R2256-02. It has been enhanced by parameters such as the quantum efficiency of the PMT and losses of intensity caused by photons passing through different environments on their way to the detector. This model was developed during a one-month internship at Aachen, Germany.

PARAMETERS OF SKIN:

This model was developed based on the Meglinski-Matcher model of skin layers [200]. It consists of six layers defined by their thickness and blood volume, as detailed in Tab. 9.1. The model was enhanced by incorporating the melanin parameter, which significantly affects the degree of scattering within the epidermis [201]. Melanin is a black pigment that serves to protect the skin from Ultraviolet (UV) radiation, with the volume percentage depending on the individual's skin type. This model was specifically designed for the Europoid race, with 3% melanin [202]. The model was created using the Matlab program (version 2011b, The Math Works).

DISCRETE MODEL:

Table 9.1: Parameters of skin [200]:

layer of skin	thickness [μm]	blood volume [%]	melanin volume [%]
epidermis	100	0	3
capillary layer	150	4	0
upper vessel plexus	80	30	0
supply layer cutis	1500	4	0
deeper vessel plexus	100	10	0
supply layer subcutis	3000	5	0

The model is based on the Beer-lambert law, which describes the dependence of light attenuation through a homogeneous material with thickness d [cm] using a formula:

$$I = I_0 \cdot e^{-[\beta \cdot d]}. \quad (9.1)$$

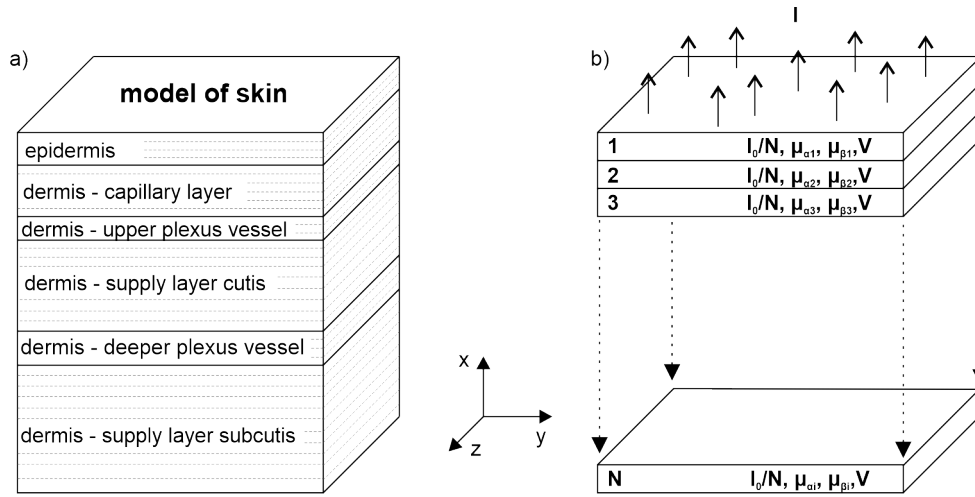


Figure 9.1: Schema of skin model (a) discretization of skin model; (b) principle of calculation.

In this formula, I [$\text{photons} \cdot \text{s}^{-1} \cdot \text{cm}^{-2}$] represents the final intensity of light, I_0 [$\text{photons} \cdot \text{s}^{-1}$] is the initial intensity of light, and β [cm^{-1}] is the linear absorption coefficient. The model is discretized for N -layers, and β [cm^{-1}] is replaced by the sum of the absorption coefficient μ_α [cm^{-1}] and scattering coefficient μ_s [cm^{-1}], in the equation:

$$I = \sum_j^N \frac{I_0}{N} \cdot e^{-[\sum_i^j (\mu_{\alpha i} + \mu_{s i}) \cdot \frac{d}{N}]}, \quad (9.2)$$

The discretization process involves subdividing homogeneous layers into sub-layers, as depicted in Fig. 9.1:a. The outcome of this procedure is the simulation of a continuous model of skin, as illustrated in Fig. 9.1:b.

PARAMETERS OF ABSORPTION AND SCATTERING:

Absorption and scattering parameters of individual layers depend on wavelength λ [nm]. For blood, the scattering coefficient μ_s is equal to 2000 cm^{-1} for all wavelength [203], while the absorption coefficient is calculated based on the molar extinction coefficient e_λ [$\text{cm}^{-1} \cdot \text{M}^{-1}$] for hemoglobin in water, as provided according to calculation by Scott Prahl at <https://omlc.org/spectra/hemoglobin>. The absorption and scattering coefficients for the individual layers of the skin were calculated using the following equations, which were derived as approximations from measured data by Huelsbusch [204]:

Epidermis:

$$\mu_a(\lambda) = 0.244 + 85.3 \cdot e^{-\frac{\lambda-154}{66.2}} \quad (9.3)$$

$$\mu_s(\lambda) = (2 \cdot 10^5 \cdot \lambda^{-1.5} + 2 \cdot 10^{12} \cdot \lambda^{-4}) \cdot (1 - g(\lambda)) \quad (9.4)$$

$$g(\lambda) = 0.5861 + 3.5289 \cdot 10^{-4} \cdot \lambda \quad (9.5)$$

Melanin:

$$\mu_a(\lambda) = 6.6 \cdot 10^{11} \cdot \lambda^{-3.33} \quad (9.6)$$

$$\mu_s(\lambda) = (2 \cdot 10^5 \cdot \lambda^{-1.5} + 2 \cdot 10^{12} \cdot \lambda^{-4}) \cdot (1 - g(\lambda)) \quad (9.7)$$

$$g(\lambda) = 0.5861 + 3.5289 \cdot 10^{-4} \cdot \lambda \quad (9.8)$$

Dermis:

$$\mu_a(\lambda) = 0.244 + 85.3 \cdot e^{\left(-\frac{\lambda-154}{66.2}\right)} \quad (9.9)$$

$$\mu_s(\lambda) = (2 \cdot 10^5 \cdot \lambda^{-1.5} + 2 \cdot 10^{12} \cdot \lambda^{-4}) \cdot (1 - g(\lambda)) \quad (9.10)$$

$$g(\lambda) = 0.6012 + 3.3726 \cdot 10^{-4} \cdot \lambda \quad (9.11)$$

Blood:

$$\mu_a(\lambda) = 0.0054 \cdot e_{\lambda} \quad (9.12)$$

$$\mu_s(\lambda) = 2000 \quad (9.13)$$

DESIGNED MODEL:

The result obtained from the optical model of BAL propagation is an estimation of the light intensity generated by the skin's surface at selected wavelength. In this model, it is possible to set initial intensity (I_0), thickness of one layer (d/N) and wavelength (λ). In Fig. 9.2:a, solid lines represents the number of photons emitted at the skin's surface from each layer. The initial intensity was $1000 \text{ photons} \cdot \text{s}^{-1} \cdot \text{cm}^{-3} \cdot \text{nm}^{-1}$, and thickness of layer 0.0001 cm . Most photons are emitted from skin layer with depths up to 0.03 cm . The dash-dotted lines in Fig. 9.2:a illustrate the attenuation of the signal at different skin depths and wavelengths. The effect of attenuation in the graph is defined as $1 - \text{Attenuation}$. Fig. 9.2:b shows the sum of BAL throughout the entire depth of the skin. The graph was created for four initial intensities (I_0) of 10, 100, 1000 and 5000 $\text{photons} \cdot \text{s}^{-1} \cdot \text{cm}^{-3} \cdot \text{nm}^{-1}$, and six various of wavelengths ranging from 400 to 650 nm. At longer wavelengths, more photons reach the surface, as evident when comparing the red line (400 nm) and turquoise line (650 nm) for reference.

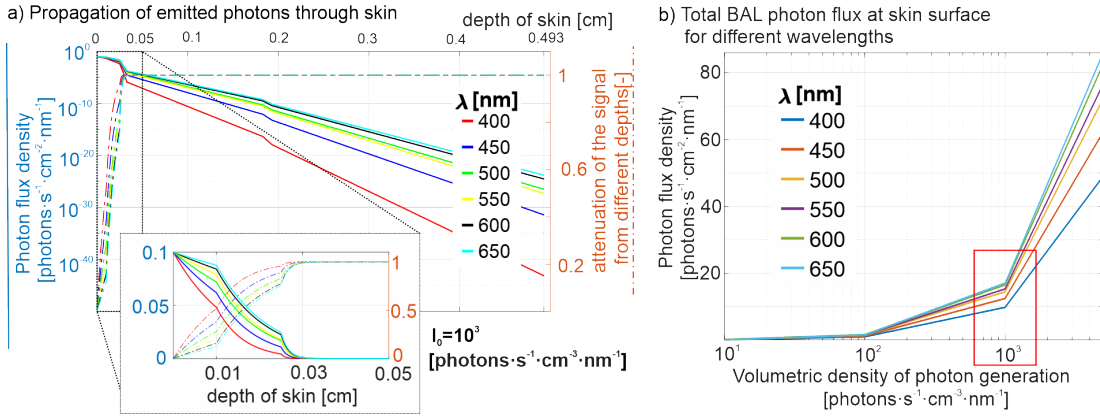


Figure 9.2: Results calculated by optical model of BAL propagation. (a) Solid lines represents photon flux at the skin's surface generated at various depths, while dash-dotted lines shows relationship (1-attenuation) calculated for each depth. (b) Total BAL photon flux throughout the entire depth of the skin resulting from four different initial intensities, calculated for six different wavelengths.

COMPARISON OF MEASURED AND CALCULATED DATA:

BAL from human skin was measured using the head-on type R2256-02 PMT, which featured a circular bialkali photocathode of diameter 46 mm. Measurements were conducted on both the palmar and dorsal sides of the right hand from five subjects. The mean values of BAL, after subtracting the background, was 14.8 photons/s. This mean value was then recalculated based on photocathode's detection area, resulting in $0.89 \text{ photons}\cdot\text{s}^{-1}\cdot\text{cm}^{-2}$, as depicted in Fig. 9.3:a. The optical model for BAL propagation was enhanced by considering a parameter quantum efficiency of R2256-02 across all wavelengths from 400 to 650 nm, with a step of 1 nm. The model is expressed by the following equation:

$$I = \sum_j^N \frac{I_0}{N} \cdot e^{-[(\sum_i^j (\mu_{ai} + \mu_{si})) \cdot \frac{d}{N}]} \cdot \text{QE}(\lambda). \quad (9.14)$$

Subsequently, the photons on the skin's surface were recalculated considering reflectivity (RF) at the interface of the neighboring layers.

$$I_{\text{detected}} = I \cdot \text{RF}. \quad (9.15)$$

A total of eight interfaces were included into optical model, as illustrated in Fig. 9.3:c, each with its refractive index n_k . Assuming the normal incidence of light to interfaces, the reflectivity (RF) is calculated using the following equation:

$$\text{RF} = \prod_k^{P-1} \left| \frac{n_k - n_{k+1}}{n_k + n_{k+1}} \right|^2. \quad (9.16)$$

The mean BAL intensity measured from the human hand of five subjects was $0.89 \text{ photons}\cdot\text{s}^{-1}\cdot\text{cm}^{-2}$ in the spectral wavelength range of 400 to 650 nm. Our model estimated a total of $913 \text{ photons}\cdot\text{s}^{-1}\cdot\text{cm}^{-3}$ generated within human skin in the spectral wavelength range of 400 to 650 nm, with only 13.1 reaching the surface, as

shown in Fig. 9.3:a.

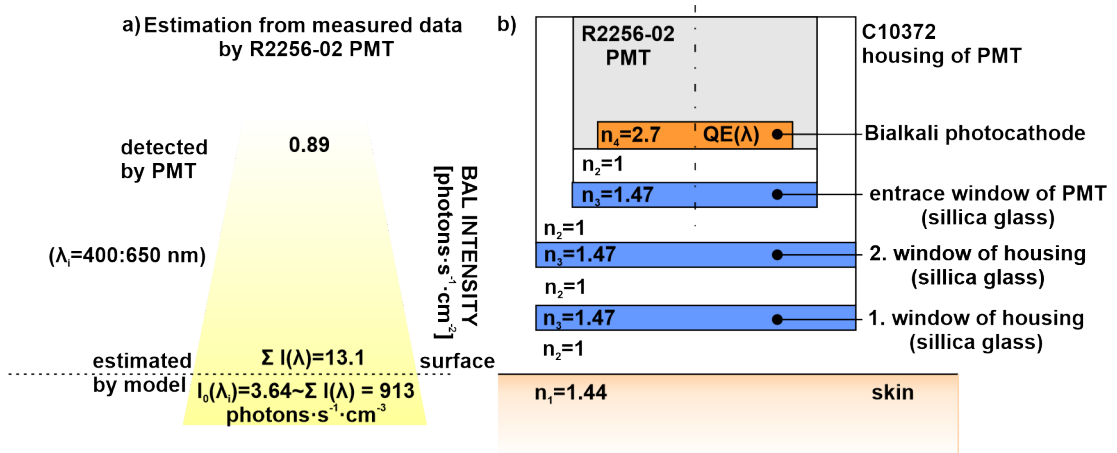


Figure 9.3: (a) The mean BAL intensity recalculated to 1 cm² from measured data by R2256-02 PMT, and estimation of 913 photons·s⁻¹·cm⁻³ generated within human skin, with only 13.1 photons·s⁻¹·cm⁻² reaching the surface of human skin in spectral wavelength range of 400 to 650 nm. (b) A total of eight interfaces and refractive index n_k of individual layers used in this model.

BAL from human subjects was investigated in various studies under different conditions, as described in Chapter 2.3.3. Imaging this luminescence phenomenon using ultra-sensitive devices could potentially enable monitoring of oxidative stress in optically accessible areas of the human body, such as skin. While oxidative stress induced by UV light has been explored, there is no in vivo quantified imaging of chemically induced stress processes in human skin using BAL under controlled oxidative stress conditions. Furthermore, the mechanisms and dynamics of BAL from the skin have not been fully explored. Designed experiments demonstrate that different degrees of chemically-induced oxidative stress on the skin can be spatially resolved quantitatively through non-invasive, label-free BAL imaging. Additionally, to gain insight into the underlying mechanisms, a minimal chemical model of skin was developed based on a mixture of lipid, melanin, and water. This model was used to show that it can reproduce essential features of the response of a real skin to oxidative stress.

This chapter is a version of:

| **M. Poplová**, A. Prasad, E. V. Wijk, P. Pospíšil and M. Cifra,
Biological Auto(chemi)luminescence Imaging of Oxidative Processes in Human Skin
Analytical Chemistry, vol. 95, issue 40, pages 14853–14860, 2023. DOI:10.1021/acs.analchem.3c01566

Journal: *Analytical chemistry*, 2023

| Impact factor (2022): 7.4
| Category: Chemistry, Analytical
| Quartile in category(2022): Q1*

Author contributions:

| **M. Poplová (contribution: 55 %)**
Investigation, Methodology, Data curation, Formal analysis, Validation, Visualization
Software, Writing – original draft (equal), Writing – review and editing (supporting)

| **A. Prasad (contribution: 10 %)**
Methodology, Data curation (supporting), Formal analysis (supporting)
Writing – review and editing (supporting)

| **E. Van Wijk (contribution: 5 %)**
Investigation (supporting), Methodology, (supporting) Writing - review and editing

| **P. Pospíšil (contribution: 10 %)**
Methodology, Data curation (supporting), Investigation (supporting)
Formal analysis (supporting), Writing - review and editing (supporting)

| **M. Cifra (contribution: 20 %)**
Conceptualization, Formal analysis (supporting), Funding acquisition, Investigation (supporting)
Methodology, Project administration, Resources, Supervision
Validation (supporting), Writing – original draft (equal), Writing – review and editing

Biological Auto(chemi)luminescence Imaging of Oxidative Processes in Human Skin

Michaela Poplová, Ankush Prasad, Eduard Van Wijk, Pavel Pospíšil, and Michal Cifra*

Cite This: *Anal. Chem.* 2023, 95, 14853–14860

Read Online

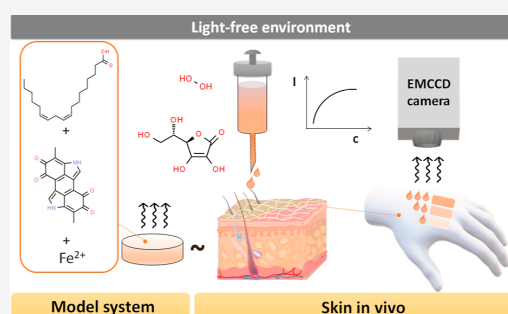
ACCESS |

Metrics & More

Article Recommendations

Supporting Information

ABSTRACT: Oxidative processes in all types of organisms cause the chemical formation of electronically excited species, with subsequent ultraweak photon emission termed biological auto(chemi)luminescence (BAL). Imaging this luminescence phenomenon using ultrasensitive devices could potentially enable monitoring of oxidative stress in optically accessible areas of the human body, such as skin. Although oxidative stress induced by UV light has been explored, for chemically induced stress, there is no *in vivo*-quantified imaging of oxidative processes in human skin using BAL under the controlled extent of oxidative stress conditions. Furthermore, the mechanisms and dynamics of BAL from the skin have not been fully explored. Here, we demonstrate that different degrees of chemically induced oxidative stress on the skin can be spatially resolved quantitatively through noninvasive label-free BAL imaging. Additionally, to gain insight into the underlying mechanisms, a minimal chemical model of skin based on a mixture of lipid, melanin, and water was developed and used to show that it can be used to reproduce essential features of the response of real skin to oxidative stress. Our results contribute to novel, noninvasive photonic label-free methods for quantitative sensing of oxidative processes and oxidative stress.



INTRODUCTION

The mere fact that biological tissue generates endogenously electron-excited molecular species that lead to ultraweak luminescence, even without any prior light stimulation,¹ is fascinating and exciting. The accepted mechanism for generating electron-excited states is chemiexcitation; that is, the excitation by energy from chemical reactions—here, initiated by reactive oxygen species (ROS).^{2,3} Hence, this ultraweak photon emission phenomenon is considered to be a biological auto(chemi)luminescence (BAL). The term “auto” refers to the fact that the biomolecular reactants responsible for light generation are inherent to the system itself and also to the fact that no external physical stimuli are required to produce the light. The emission spectrum of this luminescence lies in the wavelength range of at least 350–750 nm, the integral intensity across this band is from 10 to 1000 photons·s⁻¹·cm⁻² and is present at all levels of living species ranging from the simplest organisms, such as bacteria, to humans.^{1,4,5} Various stress factors can lead to an increase in ROS production^{6,7} and consequently an increase in BAL intensity.⁸ In this paper, we examine the use of imaging BAL as a means of sensing varying degrees of oxidative stress induced in human skin and chemical model systems.

The general underlying mechanism of generating BAL involves the chemical reaction of free radicals and reactive nonradical species with biomolecules, such as lipids, proteins, and DNA.³ These reactions lead to the formation of unstable

intermediates such as dioxetanes^{9,10} and tetraoxides,¹¹ which in turn can decompose into electronically excited species, such as excited triplet carbonyls¹² or singlet oxygen (¹O₂).^{13,14} The excited states can radiatively decay to generate a photon of BAL. Some molecules influence this reaction chain at the very beginning by either suppressing or promoting oxidation and, hence, the generation of BAL. One of the molecules that are often present in the initial part of the reaction chain is the hydrogen peroxide (H₂O₂) molecule. H₂O₂ is generated endogenously in cells¹⁵ and is also commonly used to induce oxidation and BAL when added to biological samples.^{5,16–18} Although H₂O₂ has a relatively low redox potential to be able to directly oxidize most biomolecules (apart from a few selected groups such as sulfhydryls¹⁹), it can participate in Fenton or Haber–Weiss reactions²⁰ to produce the hydroxyl radical (HO•), which is the most potent biologically relevant radical able to oxidize virtually any biomolecule. Typically, only trace amounts of reduced transition metal cations (Cu⁺ or Fe²⁺) are sufficient to generate hydroxyl radicals from H₂O₂.

Received: April 11, 2023

Accepted: September 4, 2023

Published: September 27, 2023



Hydroxyl radicals or other primary radicals produced can then initiate a chain reaction, which is manifested as autooxidation.²¹ See the [Supporting Information](#) for a brief review of antioxidants in the skin.

What are the typical characteristics of BAL from humans? BAL from human subjects *in vivo* has only been detected from the outer surface of the human body,^{22–25} which is mostly covered by skin. The BAL intensity depends on a variety of factors,²⁴ including the particular site of the body²⁶ and physical activity,^{27,28} displays anatomic asymmetry,^{29,30} undergoes diurnal, monthly, and annual cycles,^{31–34} tends to increase with age³⁵ and together with spectral analysis has the potential to be used to monitor disease processes, such as diabetes, hemiparesis, protoporphyria, or a typical cold.⁴ The systemic and internal states of the human body can exert influence on the processes in the skin. However, there is evidence that BAL signals which are detected from outside the human body originate from the skin.³⁶ For this reason, research on BAL from humans is often related to skin research and dermatology, reporting the capability of using BAL to detect oxidation processes in the skin.^{37,38} Currently, there are two methods used for the measurement of BAL. Temporal pattern detection of BAL by a highly sensitive photomultiplier tube (PMT) and imaging of the spatial distribution of BAL by a cooled charge-coupled device (CCD) camera were used in this study. For both methods, it is necessary to ensure measuring conditions without the presence of external light and to take measures against delayed luminescence.^{1,23,39} Although most of the BAL research employs single-channel photomultipliers as the main workhorse for BAL detection,¹ the imaging of BAL provides a substantial advantage for the BAL research of spatially structured systems such as skin.

Imaging naturally provides spatial information on BAL from the skin.^{30,40} The skin protects humans against continuous oxidative damage by ROS coming from environmental stresses (physical and chemical factors).^{22,41} Imaging BAL from different parts of the human body²⁶ has been employed in the past and has uncovered temporal variations of BAL,³² the influence of oxygen content in the environment⁴² or the effect of scavengers.^{41,42}

Although sensitive CCD cameras have been used to demonstrate that H₂O₂^{22,41} or other oxidizing treatments such as UVA⁴¹ elicit increased BAL from human skin, the possibility to spatially discern oxidative stress of various defined degrees within a single image *in vivo* has not been demonstrated yet.

The relation of BAL to oxidative stress was previously reported in several studies. The main benefit of this direct measurement of BAL from the skin is that it can also be measured *in vivo* under physiologically relevant conditions. During the past few decades, BAL (also called low-level chemiluminescence, ultraweak photon emission, and biophotons) measurements have been performed on skin in biopsies (*ex vivo* skin models),^{36,43,44} under *in vivo* and *in vitro* conditions (e.g., keratinocytes and fibroblast homogenates), and under diseased conditions such as malignancy and/or externally applied stresses (such as ultraviolet irradiation, exogenously applied chemicals).^{36,45–47} The studies mentioned above concluded that BAL can be used as a method for evaluating the physiology of the skin and helping us to understand how skin tissue reacts to different exogenous stresses. Therefore, it has been claimed that BAL can be used as a signature for oxidative radical reactions in the skin and can

serve as a tool for understanding skin conditions related to free radicals, such as wound healing, skin aging (which occurs principally by breaking down skin collagen), and skin cancer, among others. There are often challenges related to the measurement of BAL in the skin, the primary reason being the low intensity of BAL. However, the intensity of BAL has been shown to increase by several folds in the case of the application of various (oxidative) stimuli.^{36,48} In most studies, the increase in BAL emission is claimed to be related to free radical generation and reactions; however, the understanding of the mechanism of how these phenomena are linked is incomplete.

In this work, we use an ultrasensitive electron-multiplying (EM) CCD-camera-based system to image the spatial distribution and a photomultiplier system to detect the kinetics of BAL from human skin *in vivo* and from the chemical model system. We designed the chemical model system to contain a representative of lipids, pigments, water, and transition metal cations to mimic basic components in the skin relevant to BAL. Using both detection techniques (CCD and photomultiplier), we test the capability to quantitatively differentiate between several different degrees of oxidation induced by the application of H₂O₂ and the possibility of monitoring the protective effect of antioxidants *in vivo*. Our study also addresses the underlying mechanisms of BAL generation on a chemical model system by validating the ROS-based mechanism of BAL generation using electron paramagnetic resonance (EPR) spin-trapping spectroscopy and high-performance liquid chromatography (HPLC), where the chemical skin content was mimicked with a pigment (melanin), lipids (linoleic acid), and water.

■ EXPERIMENT AND METHODS

BAL Measurement Equipment. Luminescence measurements were performed in light-tight black chambers (custom-made by the Bioelectrodynamics research team, Institute of Photonics and Electronics of the Czech Academy of Sciences), which have a light-proof sleeve designed for direct access to the interior chamber without any light leakage. Both setups (electron-multiplying charge-coupled device-based camera imaging in the 300–900 nm wavelength range and photomultiplier-based photon counting in the 300–600 nm wavelength range) are depicted in [Figure S1](#). See more details in the [Supporting Information](#).

Chemical Model System of the Skin. We designed a chemical model system of the skin consisting of lipid (linoleic acid), pigment (melanin), water, and transition metal cations (iron) to mimic basic components in the skin relevant to BAL based on the following rationale. Linoleic acid is present in skin sebum⁴⁹ and cell membranes⁵⁰ and provides moisture to the skin.⁵¹ Linoleic acid, as a polyunsaturated fatty acid, plays a role as a substrate for chain lipid peroxidation, which is known to generate BAL.⁵⁰ Melanin is a major pigment of human skin and also has a role in chemiexcitation.⁵² Micromolar to millimolar concentrations of iron cations are present in biological systems.^{53,54} Iron plays an important role both in the physiology and pathophysiology of the skin.⁵⁵ The reactions of Fe²⁺ and other transition metals with hydrogen peroxide (H₂O₂) lead to the Fenton and Fenton-like reactions, which initiate radical oxidation of organic molecules either via the generated hydroxyl radicals or other pathways.²⁰ Fenton reaction is known to lead to the oxidation of organic compounds and the generation of BAL.⁵ See more details in the [Supporting Information](#).

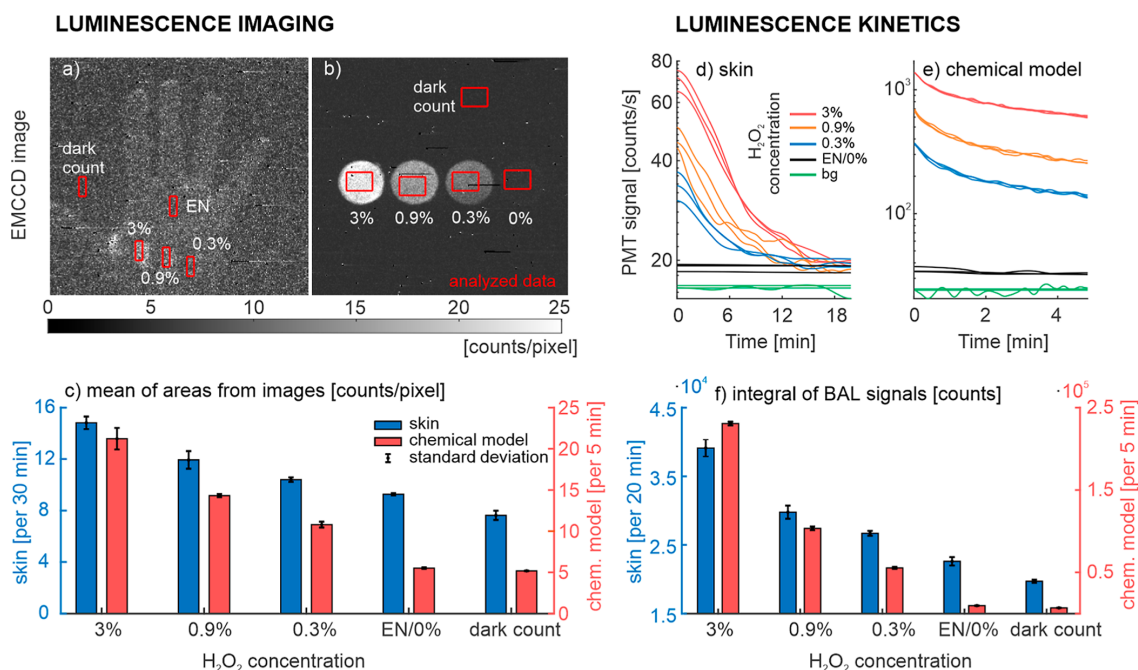


Figure 1. Different degrees of H₂O₂ oxidation-induced BAL of skin and the chemical model system in the temporal and spatial distribution. Mean values and standard deviations are from $N = 3$ independent experiments. In the BAL image of the hand, (a) red rectangular analyzed areas with identical areas were used for the analysis across all hand BAL measurements. Three different concentrations of H₂O₂ were applied on the skin (3, 0.9, and 0.3%), and endogenous (EN) BAL signals as well as a dark count of the detector were captured. (b) The same approach was used in BAL images of the chemical model system; the label 0% corresponds to the vehicle (Q-water) only application. (c) Mean values of analyzed areas from the hand (left axis: blue bars) and chemical model system (right axis: red bars). The smoothed kinetic BAL signals from the skin (d) and the chemical model system (e) are evaluated in (f) as the integral sum of BAL from the skin (left y-axis: blue bars) and the chemical model system (right y-axis: red bars).

Chemical Treatment. Two studies were conducted: one involving varying concentrations of H₂O₂ to induce oxidative stress and another examining the antioxidant effects using ascorbic acid. For the first study, H₂O₂ concentrations of 3, 0.9, and 0.3% were used with a 0.3 mL injection of the stock solution. In the antioxidant experiment, a 5 mM stock solution of ascorbic acid was applied. Imaging experiments utilized a tape mask to define three rectangular spots, with each substance (5 μ L) evenly distributed within the spots. The tape mask was removed prior to measurement. In the skin BAL kinetics experiments, substances (10 μ L) were applied to the entire dorsal hand area, while in imaging experiments, only smaller areas were treated. For the liquid chemical model system, there was one type of treatment per Petri dish. See more details in the [Supporting Information](#).

RESULTS AND DISCUSSION

Biological Autoluminescence: Imaging and Kinetics.

In this work, we focused on the BAL signals from the sites of topical H₂O₂ treatment of skin (Figure 1a) and quantified the imaging data. The data are from a volunteer (female, age 29, Fitzpatrick skin type III); see the [Supporting Information](#) on ethical aspects of the study. Our quantified results in Figure 1c (left y-axis: blue bars) display mean values from the three skin areas treated with different concentrations of H₂O₂ as well as from nontreated skin areas, all from three experimental replicates. The BAL signal intensity increases with an

increasing H₂O₂ concentration. The endogenous BAL signal (0% H₂O₂) from the skin was approximately 1.5 counts/pixel, which increases to approximately 6.5 counts/pixel for 3% H₂O₂, above the mean of the dark count (approximately 8 counts/pixel). These results demonstrate that BAL imaging can discern different levels and spatial distributions of oxidative treatments and stress on the skin.

We developed a well-defined minimal chemical model system of the skin: water emulsion of linoleic acid and melanin (see methods for details), inspired by Kobayashi et al.⁵⁶ We selected linoleic acid⁵⁷ as a representative of the 16 and 18 carbon-free fatty acids which, together with triglycerides, constitute the major (57.5%) component of skin surface lipids,⁴⁹ and melanin as a pigment important in skin photophysical and photochemical processes. Linoleic acid is also a suitable model in oxidation experiments as it is a polyunsaturated fatty acid containing two double bonds, which make it prone to oxidation attack, see Chapter One in de Paulet et al.⁵⁸ To induce the oxidation in the chemical model (Figure 1b—3 mL final volume of the sample in a Petri dish), we used the same H₂O₂ concentrations (0.3, 0.9, and 3%) as in the skin. There was one treatment condition per each Petri dish. The image clearly shows that the BAL signals were much higher than the background and depended on the H₂O₂ concentration. The quantified results in Figure 1c (right y-axis: red bars) display mean values from specific areas from two replicate measurements. They show that H₂O₂ elicits

increased BAL intensity in the chemical model in a concentration-dependent manner with a behavior qualitatively similar to the response of BAL from the hand, albeit with higher intensities. For a comparison of the quantitative data in a representation as ratios of treated vs nontreated area, see Figure S7.

There are at least four major differences in the chemical model in contrast to the skin, which contribute to the higher overall BAL signal from the chemical model:

- Higher volume of H₂O₂ added to the chemical model than on the skin sample: 300 vs 5 μ L on the whole dorsal side of the hand
- Faster diffusion in a liquid compared with a solid skin surface
- The exact chemical composition of the skin is different from the chemical model, which contains just representative molecules of lipids and pigments
- There is no antioxidative system in the chemical model

To analyze the kinetics of BAL from the skin, we used our sensitive PMT system. Three concentrations (0.3, 0.9, and 3%) of H₂O₂ were applied consecutively on the whole dorsal side of the right hand of the test subject. The results are presented in Figure 1d. The endogenous BAL signal was approximately 3 counts/s. The background (PMT dark count) was approximately 16 counts/s. H₂O₂ treatment induced a substantial increase of BAL intensity in a concentration-dependent manner, with 3% treatment causing more than a 15-fold increase of net BAL at time = 0 of the measurement. Using the PMT detection technique, we were also able to follow the kinetics of BAL after H₂O₂ treatment in both the hand (Figure 1d) and the chemical model (Figure 1e). After H₂O₂ treatment, the BAL intensity from the skin decayed to the level of endogenous BAL within 12–19 min (Figure 1d) depending on the concentration of H₂O₂. In the case of the chemical model, the BAL intensity drops to approximately 38–44% of the H₂O₂ induced value within 5 min, yet still being almost 1 order of magnitude higher than the spontaneous BAL. We suggest the following explanation for the differences between the kinetics of the decay of BAL between the skin and the chemical model: the skin possesses an antioxidative system that is activated after oxidative stress to remove excessive ROS, as known in other tissues.⁵⁹ However, the chemical model treated with H₂O₂ experiences an initiation of chain lipid peroxidation,⁶⁰ which can persist for an extended period of time with no antioxidants to terminate the propagation. In general, the integral value of H₂O₂ concentration-dependent BAL signals scales similarly for both imaging (Figure 1c) and kinetics data (Figure 1f), confirming the validity of the data. How does the intensity of BAL induced due to oxidative stimulus relate to endogenous BAL? This question boils down to the rate of the processes that lead to electron-excited states and photon emission and the effective volume where these processes take place. The processes leading to photon emission in the skin are likely more complex than just the assumed Fenton-reaction-based generation of ROS, which is dependent on H₂O₂ and iron cation concentration. Nevertheless, for simplicity, let us discuss endogenous versus stimulated BAL intensity values and H₂O₂ concentrations. The integral BAL intensity from imaging data has mean values of 1.6 and 7.2 counts/pixel for the endogenous and 3% H₂O₂ stimulated cases, respectively, above the dark count, which had a mean value of 7.6 counts/pixel (Figure 1c). The concentrations of

H₂O₂ used were 880, 264, and 88 mM. It is known from liquid chemical models from our earlier work that for fixed Fe²⁺, decreasing the concentration of H₂O₂ by an order of magnitude causes only a 1.1–2-fold decrease of the integral BAL intensity, depending on the specific iron and H₂O₂ concentrations.⁶¹ In our case of BAL skin data, there was a 2.6-fold decrease of integral BAL intensity per 1 order of magnitude decrease of H₂O₂ concentration (from 7.2 counts at 3% H₂O₂ to 2.8 counts at 0.3% H₂O₂). If we extrapolated this value and decreased the BAL intensity (at 0.3% H₂O₂) 2.6-fold to correspond to 0.03% (88 mM) we would obtain the value of 1.07 counts per pixel, which is lower than the BAL value of 1.6 counts per pixel for nontreated skin (0% H₂O₂). However, the endogenous and biologically relevant steady-state values for intratissue H₂O₂ concentration lie in the nM– μ M range.^{15,62}

How can we explain this seeming discrepancy? First, the exogenously added H₂O₂ of the given concentrations was not applied to the whole optically accessible volume of the skin tissue but only on the surface of the skin, and the concentrations were only transient to simulate oxidative stress. The excess H₂O₂ is then rapidly depleted (see Figure 1d). Another possible reason is that the BAL due to topically applied H₂O₂ is likely emitted only from a very thin layer (few microns) of the upper layers of the skin, while the endogenous BAL is generated by a volumetric source, skin tissue. All other things being the same, the larger the volume, the higher the BAL intensity. The quantitative answer to the question “What is the thickness of this volumetric source?” is roughly bounded by the depth of the light penetration from/to the tissue. This very much depends on the wavelength of the light. The BAL spectrum from the skin is rather broad, with a peak at approximately 600 nm.⁵⁶ The models of light penetration into the skin predict that light fluence decreases to approximately 50% of its original value at the surface of the skin at a few tens of 10 μ m depth (stratum corneum—epidermis) and approximately 1 mm depth (dermis) in the skin for 400 and 600 nm wavelength, respectively, for a diffuse light source,⁶³ which is a good approximation of BAL. The reciprocity of light propagation suggests that these (10 μ m–1 mm) are the depths in the skin from which we can expect the BAL to reach the surface and then also the photodetector.

Which cells can actively generate the ROS in the epidermis leading to BAL? The skin epidermis consists mainly of keratinocytes, melanocytes, Langerhans cells, and Merkel cells.⁶⁴ They work closely together and contribute to skin health. Epidermal cells, especially keratinocytes, express nicotinamide adenine dinucleotide phosphate hydrogen (NADPH) oxidase (NOX), an enzyme that generates ROS normally.⁶⁵ NOX enzymes transfer electrons from NADPH to molecular oxygen, producing superoxide anion radicals (O₂^{•-}), which eventually can lead to the formation of hydrogen peroxide (H₂O₂) and hydroxyl radicals (HO[•]). Expression of NOX1, NOX2, NOX4, and NOX5 has been reported in keratinocytes.⁶⁶ In addition to NOX, keratinocytes express several cytochrome P450 enzymes.⁶⁷ Some of the cytochrome P450 enzymes, such as CYP1A1 and CYP1B1, have been shown to generate ROS as byproducts of their enzymatic reactions. Additionally, inflammatory cells, such as neutrophils and macrophages, can infiltrate the epidermis during an immune response, producing ROS as part of their defense mechanisms against pathogens. Although not precisely within epidermal cells, the ROS generated by inflammatory cells can influence epidermal cell function and contribute to oxidative

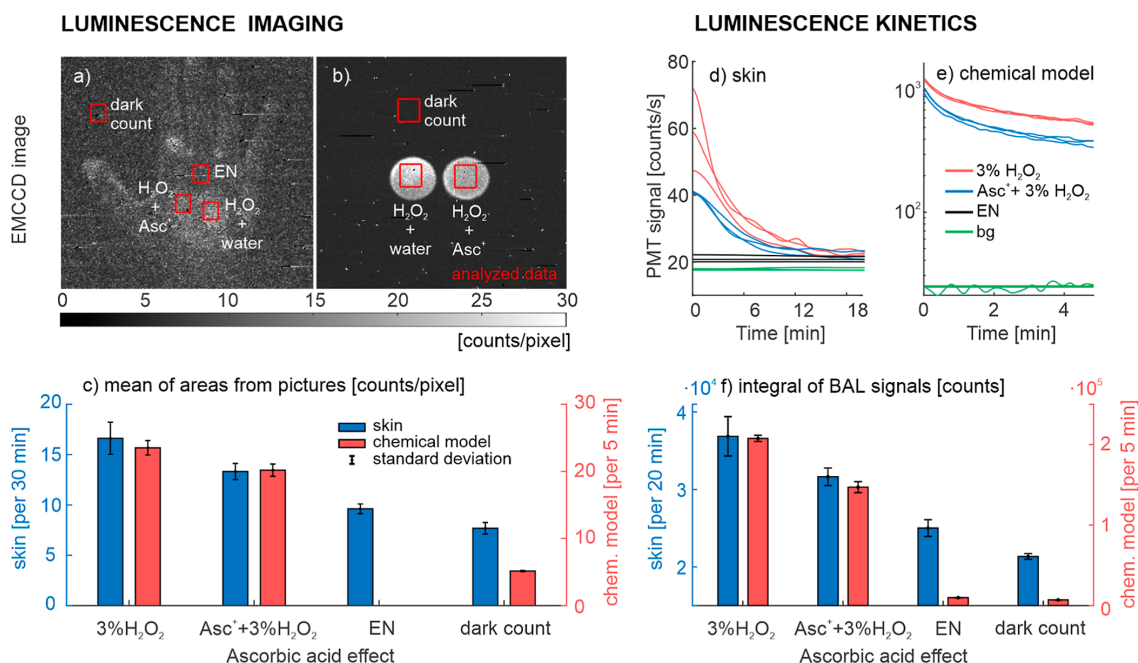


Figure 2. Antioxidant (ascorbic acid) suppresses the BAL signal induced by H₂O₂ treatment. In imaging of hand (a) and the chemical model system (b), areas enclosed by the red rectangles are investigated: with ascorbic acid (+Asc), without ascorbic acid (+water), endogenous BAL (EN), and dark count, which are analyzed in (c) as mean values of skin (left y-axis: blue bars) and the chemical model system (right y-axis: red bars). Smoothed kinetic signals from the skin (d) and the chemical model system (e) are analyzed as an integral sum of BAL (f) of the skin (left y-axis: blue bars) and the chemical model system (right y-axis: red bars).

stress. While oxygen is consumed during melanogenesis, ROS levels generated by melanocytes are generally relatively low.

After we showed that the BAL signal responds to oxidative treatment in a dose-dependent manner, we investigated whether our technique can monitor the protective effect of antioxidants. Antioxidant ascorbic acid was applied in the hand/model system as a prevention against oxidative effects of H₂O₂, which was added thereafter. As in the previous section, both EMCCD and PMT systems were used for BAL detection. Analysis of EMCCD images for both the hand and model system (Figure 2a,b) supports the fact that the antioxidant suppressed the oxidative effect of H₂O₂, see in Figure 2c: blue (skin) and red (model system) bars. Although it was possible to distinguish the differences in BAL intensity in the previous experiment with various concentrations of H₂O₂ even by visual observation, as shown in Figure 1a, the differences were more subtle in the case of antioxidant action (Figure 2a). The quantitative analysis showed that the BAL signal induced by 3% H₂O₂ was only partially suppressed by ascorbic acid (Figure 2d). For a comparison of the quantitative data in a representation as ratios of treated vs nontreated area, see Figure S8. In the skin, after subtraction of the background, one can see that the presence of the antioxidant decreased the BAL signal to ca. 60% (Figure S8a). The BAL kinetics measurement using PMT uncovers the subtlety of this effect (Figure 2d: blue lines); the suppressing effect of ascorbic acid is only temporary, acting up to approximately 15 min. After this period, the signals with and without the antioxidant are almost identical; see Figure 2d: red lines. The consumption of the applied antioxidant could cause this. The ascorbic acid effect in the

chemical model system (Figure 2e: blue lines) mirrored the trend of the PMT signal without the antioxidant (Figure 2e: red lines) but was approximately 200 counts lower all of the time. The analysis of the integral BAL of both systems (skin and chemical model) supports the assumption that ascorbic acid scavenges ROS, hence causing a decrease in BAL intensity [Figure 2f: blue (skin) and red (chemical model) bars].

These results are corroborated by earlier studies in which the application of a variety of antioxidants, including ascorbic acid, decreased BAL signal to a different extent.^{36,42,48,68} Ascorbate, glutathione, α -tocopherol, and coenzyme-Q were able to suppress the intensity of endogenous BAL signals from human skin in vivo,⁴² and ascorbate also suppressed H₂O₂-induced signals from porcine skin in vitro.³⁶ Ascorbate, glutathione, and δ -tocopherol also mildly suppressed BAL increased by UV-induced reactive oxygen in human skin in vitro.⁴⁸

Next, we aimed to dissect the lipid (linoleic acid) and pigment (melanin) contribution to the observed BAL signals. To do this, we varied the concentration of either linoleic acid or melanin in the chemical model system and induced oxidation by treatment with Fe²⁺ and H₂O₂. The strategy was to start with a mixture of lipid (linoleic acid) and pigment (melanin), keep the concentration of one component fixed, and test the systems with gradually decreased concentration of the other component. See the details of concentrations in Table 1 and the results in Figure 3a,b. We found that the changes in the BAL signal intensity caused by the different concentrations of linoleic acid (LA) (10 mM and lower, fixed 0.15 mM melanin) were minimal (Figure 3a). However,

Table 1. Final Concentration of Chemicals in the Tests with Variable Concentrations of Substrates

variable concentration of	linoleic acid	melanin
linoleic acid	0/0.1/10 mM	10 mM
melanin	0.15 mM	0.0325/0.075/0.15 mM
Fe ²⁺	2 mM	2 mM
H ₂ O ₂	3% ~ 880 mM	3% ~ 880 mM

decreasing melanin concentration (0.15 mM and lower, fixed 10 mM LA and lower) had a substantial effect on BAL intensity. Hence, we conclude that the most important modulating parameter of BAL signals for our chemical model system was melanin (Figure 3b).

What could be some of the underlying ROS and electron-excited species leading to BAL? Earlier studies suggest that the triplet excited carbonyl and ¹O₂ are considered the main primary electron-excited species leading to BAL³ in the visible band (300–700 nm). To understand this better in a controlled way, we focused on a model chemical model system. Due to the multiple roles of ¹O₂, being both an ROS and a potential emitter, we decided to focus on this species. We used EPR spectroscopy to confirm the presence of ¹O₂ emerging in our chemical model system using hydrophilic diamagnetic spin label TMPD (2,2,6,6-tetramethyl-4-piperidone). TMPD produces paramagnetic 2,2,6,6-tetramethyl-4-piperidone-1-oxyl (TEMPONE) in the presence of ¹O₂ to give an EPR signal. One data set of TEMPONE EPR spectra (10 min incubation and measurement) is shown in Figure 4a: color lines. The bar graph result shows that the (max–min) value from the first peak in the EPR signals (three replicates) (Figure 4a: bars) decreases with decreasing the concentration of H₂O₂ (0.3, 0.09, 0.03, and 0%). For this experiment, we used a 10-fold lower concentration of H₂O₂ than in BAL experiments, considering the sensitivity of the EPR spectrometer.

Characterizing the relative EPR signal is more than sufficient for the analysis and using higher concentration may lead to oversaturation of signal intensity. We also performed a control experiment, where the effect of Fenton's reagent containing 0.3% H₂O₂ was tested on a sample without melanin according to previous sensitivity analysis of a model system (Figure 3a,b). Removal of melanin led to partial suppression of the EPR signal (data not shown). The application of antioxidant ascorbic acid into the chemical model system led to a

significant reduction of ¹O₂ (Figure 4b: bars) and the formation of a monodehydroascorbate radical (Asc[•]).

Further, HPLC was used to confirm the presence of MDA as a product of lipid peroxidation of linoleic acid in our model system. A chromatogram of Fenton-reagent-treated linoleic acid, with the peak of MDA-DNPH derivated at a retention time of 25.2 min, is shown in Figure 4c. The absorption spectrum of the MDA-DNPH derivate showed a maximum at 315.2 nm (data not shown). A model system without melanin was used for the HPLC method (Table S1). The proposed mechanism of linoleic acid oxidation leading to MDA production is as follows.⁶⁹ A hydroxyl radical produced in the Fenton reaction abstracts hydrogen from linoleic acid to form an alkyl radical, which is oxygenated to produce a peroxy radical. The peroxy radical can cyclize to form radical endoperoxide and subsequently bicyclic endoperoxide. Those endoperoxides then decompose to MDA.⁷⁰

CONCLUSIONS

The detection and analysis of BAL were used to demonstrate the capability of quantitative differentiation between several degrees of oxidation level on human skin in vivo induced by the application of H₂O₂ and the possibility of monitoring the protective effect of antioxidants. In our work, for the first time, we quantitatively demonstrated topical differences due to chemically induced oxidative stress within one image and within one human subject in vivo using BAL. This is an important step toward the potential biomedical application because the earlier BAL imaging studies are not mutually quantitatively comparable due to the variability between subjects, their physiological states, skin types and conditions, and different imaging systems and settings. The imaging of BAL was used to demonstrate not only quantitative differences but also the capability of identifying spatial inhomogeneity and local differences of oxidative stress under controlled conditions. The data from BAL correlated well with the minimal chemical model of skin. In this experimental model, we showed that the content of the pigment (melanin) has a strong role in the overall BAL signal. Using EPR spectroscopy, we detected the presence of ¹O₂, which is both a potential emitter of BAL and an ROS itself. The oxidation in the samples was confirmed by detecting MDA as a lipid peroxidation product. Overall, our results demonstrate that BAL is a label-free, real-time, in situ, noncontact, noninvasive, and probably the only technique that

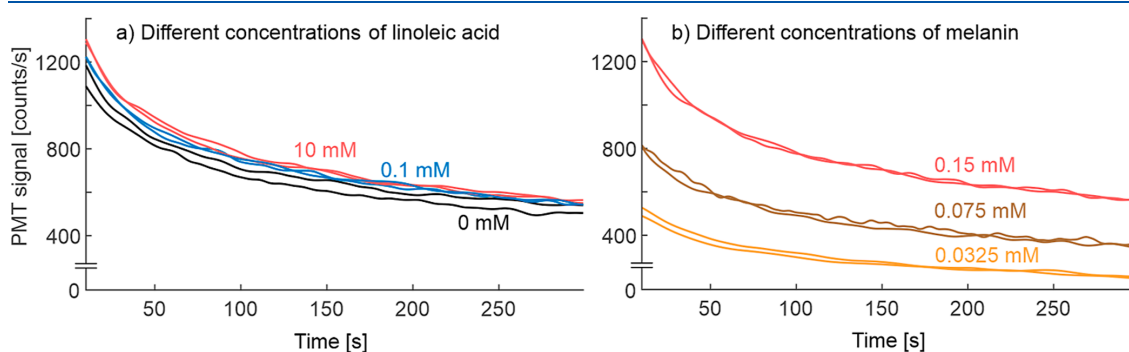


Figure 3. BAL kinetic data from a chemical model system for different concentrations of linoleic acid and melanin. Part (a) shows data with varied linoleic acid concentrations (10, 0.1, and 0 mM) for a fixed melanin concentration (0.15 mM) and (b) data for varied concentrations of melanin (0.15, 0.075, and 0.0325 mM) for a fixed linoleic acid concentration (10 mM).

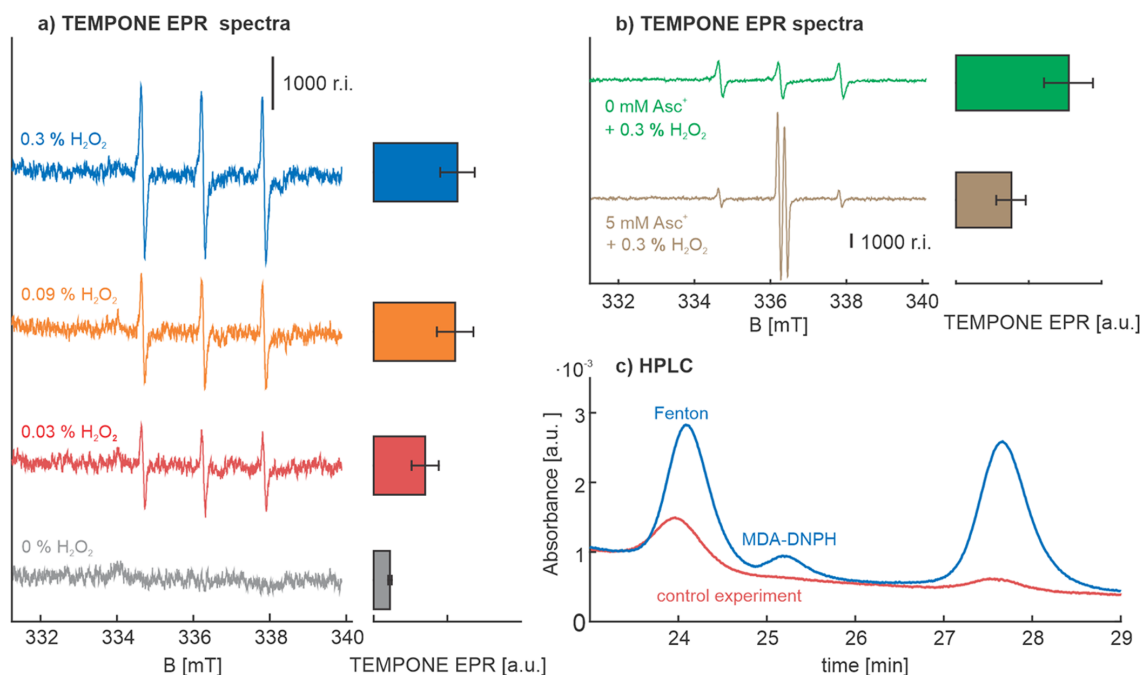


Figure 4. (a) TEMPONE EPR signals from the chemical model system with different H_2O_2 concentrations (left side: lines) and mean values from max–min value of the first peak (right side: bar graphs); (b) TEMPONE EPR signals from the chemical model system of 0.3% H_2O_2 with and without ascorbic acid (left side: lines) and their mean values from max–min value of first peak (right side: bar graph); (c) chromatograms of the malondialdehyde-2,4-dinitrophenylhydrazine (MDA-DNPH) derivate detected by HPLC in the control experiment (10 mM linoleic acid) is represented by a red line and chemical model system without melanin is represented by a blue line. Details of the concentrations are given in Table S1.

requires no additional acute external energy input (e.g., light excitation) to the biosystem to observe endogenously or exogenously triggered oxidation processes.

■ ASSOCIATED CONTENT

Supporting Information

The Supporting Information is available free of charge at <https://pubs.acs.org/doi/10.1021/acs.analchem.3c01566>.

Details of experiments and methods, additional imaging and kinetics data for additional concentrations of chemical components, and a brief review of antioxidants in skin (PDF)

■ AUTHOR INFORMATION

Corresponding Author

Michal Cifra – Institute of Photonics and Electronics, The Czech Academy of Sciences, Prague 182 00, Czechia; orcid.org/0000-0002-8853-9523; Phone: +420 266 773 454; Email: cifra@ufe.cz

Authors

Michaela Poplová – Institute of Photonics and Electronics, The Czech Academy of Sciences, Prague 182 00, Czechia; Faculty of Electrical Engineering, Czech Technical University in Prague, Prague 166 27, Czechia

Ankush Prasad – Department of Biophysics, Faculty of Science, Palacký University, 783 71 Olomouc, Czechia; orcid.org/0000-0002-2009-8987

Eduard Van Wijk – Meluna Research Business & Science Park Wageningen, 10 6708 PW Wageningen, Netherlands

Pavel Pospíšil – Department of Biophysics, Faculty of Science, Palacký University, 783 71 Olomouc, Czechia; orcid.org/0000-0001-9126-2011

Complete contact information is available at: <https://pubs.acs.org/10.1021/acs.analchem.3c01566>

Notes

The authors declare no competing financial interest.

■ ACKNOWLEDGMENTS

M.C. and M.P. acknowledge the Czech Science Foundation project no. 20-06873X. A.P. and P.P. were supported by the European Regional Development Fund project “Plants as a tool for sustainable global development” (CZ.02.1.01/0.0/0.0/16_019/0000827). Small fractions of the text were modified using ChatGPT3.

■ REFERENCES

- (1) Cifra, M.; Pospíšil, P. *J. Photochem. Photobiol., B* **2014**, *139*, 2–10.
- (2) Pospíšil, P.; Prasad, A.; Rác, M. *J. Photochem. Photobiol., B* **2014**, *139*, 11–23.
- (3) Pospíšil, P.; Prasad, A.; Rác, M. *Biomolecules* **2019**, *9*, 258.
- (4) Zapata, F.; Pastor-Ruiz, V.; Ortega-Ojeda, F.; Montalvo, G.; Ruiz-Zolle, A. V.; García-Ruiz, C. *J. Photochem. Photobiol., B* **2021**, *216*, 112141.

- (5) Vahalová, P.; Cifra, M. *Prog. Biophys. Mol. Biol.* **2023**, *177*, 80–108.
- (6) Halliwell, B.; Cross, C. E. *Environ. Health Perspect.* **1994**, *102*, 5.
- (7) Ghaemi Kerahrodi, J.; Michal, M. *Redox Biol.* **2020**, *37*, 101588.
- (8) Van Wijk, R.; Van Wijk, E. P. *Indian J. Exp. Biol.* **2008**, *46*, 273.
- (9) Cilento, G. *Pure Appl. Chem.* **1984**, *56*, 1179–1190.
- (10) Cilento, G.; Adam, W. *Photochem. Photobiol.* **1988**, *48*, 361–368.
- (11) Di Mascio, P.; Martinez, G. R.; Miyamoto, S.; Ronsein, G. E.; Medeiros, M. H. G.; Cadet, J. *Arch. Biochem. Biophys.* **2016**, *595*, 161–175.
- (12) Vacher, M.; Fdez Galván, I.; Ding, B.-W.; Schramm, S.; Berraud-Pache, R.; Naumov, P.; Ferré, N.; Liu, Y.-J.; Navizet, I.; Rocca-Sanjuán, D.; Baader, W. J.; Lindh, R. *Chem. Rev.* **2018**, *118*, 6927–6974.
- (13) Miyamoto, S.; Martinez, G. R.; Medeiros, M. H.; Di Mascio, P. *J. Photochem. Photobiol., B* **2014**, *139*, 24–33.
- (14) Di Mascio, P.; Martinez, G. R.; Miyamoto, S.; Ronsein, G. E.; Medeiros, M. H. G.; Cadet, J. *Chem. Rev.* **2019**, *119*, 2043–2086.
- (15) Cadenas, E.; Davies, K. J. *Free Radical Biol. Med.* **2000**, *29*, 222–230.
- (16) Rác, M.; Krupka, M.; Binder, S.; Sedlářová, M.; Matusšková, Z.; Raška, M.; Pospíšil, P. *PLoS One* **2015**, *10*, No. e0116958.
- (17) Bereta, M.; Teplan, M.; Chafai, D. E.; Cifra, M. *Biological Autoluminescence as a Non-invasive Monitoring Tool for Pulsed Electric Field Effects on Yeast Cells*; URSI GASS: Rome, Italy, 2020; pp 1–3.
- (18) Vahalová, P.; Červinková, K.; Cifra, M. *Sci. Rep.* **2021**, *11*, 10852.
- (19) García-Santamarina, S.; Boronat, S.; Hidalgo, E. *Biochemistry* **2014**, *53*, 2560–2580.
- (20) Meyerstein, D. *Antioxidants* **2022**, *11*, 1368.
- (21) Buettner, G. R.; Czapski, P. G. *Free Radical Res. Commun.* **1986**, *1*, 349–353.
- (22) Rastogi, A.; Pospíšil, P. *Sking Res. Technol.* **2010**, *16*, 365–370.
- (23) Van Wijk, R.; Van Wijk, E. P.; van Wietmarschen, H. A.; Greef, J. v. d. *J. Photochem. Photobiol., B* **2014**, *139*, 39–46.
- (24) Calcerrada, M.; Garcia-Ruiz, C. *Crit. Rev. Anal. Chem.* **2019**, *49*, 368–381.
- (25) He, M.; Sun, M.; van Wijk, E.; van Wietmarschen, H.; van Wijk, R.; Wang, Z.; Wang, M.; Hankemeier, T.; van der Greef, J. *Complement Ther Med.* **2016**, *25*, 20–26.
- (26) Wijk, E. P. V.; Koch, H.; Bosman, S.; Wijk, R. V. J. *Altern. Complementary Med.* **2006**, *12*, 31–38.
- (27) Seo, D.-I.; M Laager, F.; Young, K.; Chang, H.; So, W.-Y.; Kim, H.-T.; Soh, K.-S.; Song, W. *Electromagn. Biol. Med.* **2012**, *31*, 122–131.
- (28) Laager, F.; Park, S.-H.; Yang, J.-M.; Song, W.; Soh, K.-S. *Eur. J. Appl. Physiol.* **2008**, *102*, 463–469.
- (29) Wijk, R. V.; Wijk, E. P. J. *Complementary Med. Res.* **2005**, *12*, 77–83.
- (30) Wijk, E. P. V.; Wijk, R. V. J. *Complementary Med. Res.* **2005**, *12*, 96–106.
- (31) Cifra, M.; Van Wijk, E.; Koch, H.; Bosman, S.; Van Wijk, R. *Radioengineering* **2007**, *16*, 15.
- (32) Kobayashi, M.; Kikuchi, D.; Okamura, H. *PLoS One* **2009**, *4*, No. e6256.
- (33) Cohen, S.; Popp, F. *Sking Res. Technol.* **1997**, *3*, 177–180.
- (34) Scholkmann, F.; van de Kraats, E.; van Wijk, R.; van Wijk, E.; van der Greef, J. *Matters* **2018**, *4*, 1.
- (35) Zhao, X.; van Wijk, E.; Yan, Y.; van Wijk, R.; Yang, H.; Zhang, Y.; Wang, J. *J. Photochem. Photobiol., B* **2016**, *162*, 529–534.
- (36) Prasad, A.; Balukova, A.; Pospíšil, P. *Front. Physiol.* **2018**, *9*, 1109.
- (37) Ou-Yang, H. *J. Photochem. Photobiol., B* **2014**, *139*, 63–70.
- (38) Gabe, Y.; Takeda, K.; Tobiishi, M.; Kikuchi, S.; Tsuda, K.; Haryuu, Y.; Nakajima, Y.; Inomata, Y.; Nakamura, S.; Murase, D.; Tokunaga, S.; Miyaki, M.; Takahashi, Y. *Sking Res. Technol.* **2021**, *27*, 1064–1071.
- (39) Inaba, H. *J. Int. Soc. Life Inf. Sci.* **2000**, *18*, 448–452.
- (40) Prasad, A.; Pospíšil, P. *Sci. Rep.* **2013**, *3*, 1211.
- (41) Prasad, A.; Pospíšil, P. *J. Biophotonics* **2011**, *4*, 840–849.
- (42) Rastogi, A.; Pospíšil, P. *J. Biomed. Opt.* **2011**, *16*, 096005.
- (43) Tsuchida, K.; Kobayashi, M. *Sci. Rep.* **2020**, *10*, 21667.
- (44) Tsuchida, K.; Sakiyama, N.; Ogura, Y.; Kobayashi, M. *Exp. Dermatol.* **2023**, *32*, 146–153.
- (45) Musumeci, F.; Applegate, L. A.; Privitera, G.; Scordino, A.; Tudisco, S.; Niggli, H. J. *J. Photochem. Photobiol., B* **2005**, *79*, 93–99.
- (46) Hagens, R.; Khabiri, F.; Schreiner, V.; Wenck, H.; Wittern, K.-P.; Duchstein, H.-J.; Mei, W. *Sking Res. Technol.* **2008**, *14*, 112–120.
- (47) Kobayashi, M. *J. Photochem. Photobiol., B* **2014**, *139*, 34–38.
- (48) Tsuchida, K.; Iwasa, T.; Kobayashi, M. *J. Photochem. Photobiol., B* **2019**, *198*, 111562.
- (49) Picardo, M.; Ottaviani, M.; Camera, E.; Mastrofrancesco, A. *Derm.-Endocrinol.* **2009**, *1*, 68–71.
- (50) Prasad, A.; Pospíšil, P. *PLoS One* **2011**, *6*, No. e22345.
- (51) Spencer, T. S. *Clin. Dermatol.* **1988**, *6*, 24–28.
- (52) Premi, S.; Wallisch, S.; Mano, C. M.; Weiner, A. B.; Bacchiocchi, A.; Wakamatsu, K.; Bechara, E. J. H.; Halaban, R.; Douki, T.; Brash, D. E. *Science* **2015**, *347*, 842–847.
- (53) Martínez-Garay, C. A.; de Llanos, R.; Romero, A. M.; Martínez-Pastor, M. T.; Puig, S. *Appl. Environ. Microbiol.* **2016**, *82*, 1906–1916.
- (54) Olivieri, N. F. *Semin. Hematol.* **2001**, *38*, 57–62.
- (55) Wright, J. A.; Richards, T.; Strai, S. K. S. *Front. Pharmacol.* **2014**, *5*, 156.
- (56) Kobayashi, M.; Iwasa, T.; Tada, M. *J. Photochem. Photobiol., B* **2016**, *159*, 186–190.
- (57) Pappas, A.; Johnsen, S.; Liu, J.-C.; Eisinger, M. *Derm.-Endocrinol.* **2009**, *1*, 157–161.
- (58) *Free Radicals, Lipoproteins, and Membrane Lipids*; de Paulet, A. C., Douste-Blazy, L., Paoletti, R., Eds.; Springer US: Boston, MA, 1991.
- (59) Banerjee, A. K.; Mandal, A.; Chanda, D.; Chakraborti, S. *Mol. Cell. Biochem.* **2003**, *253*, 307–312.
- (60) Repetto, M.; Semprine, J.; Boveris, A. *Lipid Peroxidation: Chemical Mechanism, Biological Implications and Analytical Determination*; Catala, A., Ed.; InTech, 2012.
- (61) Vahalová, P.; Havelka, D.; Vaněčková, E.; Zakar, T.; Kolivoška, V.; Cifra, M. *Sens. Actuators, B* **2023**, *385*, 133676.
- (62) Loo, A. E. K.; Ho, R.; Halliwell, B. *Free Radical Biol. Med.* **2011**, *51*, 884–892.
- (63) Finlayson, L.; Barnard, I. R. M.; McMillan, L.; Ibbotson, S. H.; Brown, C. T. A.; Eadie, E.; Wood, K. *Photochem. Photobiol.* **2022**, *98*, 974–981.
- (64) Prost-Squarcioni, C. *Med. Sci.* **2006**, *22*, 131–137.
- (65) Raad, H.; Serrano-Sanchez, M.; Harfouche, G.; Mahfouf, W.; Bortolotto, D.; Bergeron, V.; Kasraian, Z.; Dousset, L.; Hosseini, M.; Taieb, A.; Rezvani, H. R. *J. Invest. Dermatol.* **2017**, *137*, 1311–1321.
- (66) Bedard, K.; Krause, K.-H. *Physiol. Rev.* **2007**, *87*, 245–313.
- (67) Baron, J. M.; Höller, D.; Schiffer, R.; Frankenberg, S.; Neis, M.; Merk, H. F.; Jugert, F. K. *J. Invest. Dermatol.* **2001**, *116*, 541–548.
- (68) Tsuchida, K.; Sakiyama, N. *Photochem. Photobiol. Sci.* **2023**, *22*, 345–356.
- (69) Frankel, E. N. *Lipid Oxidation*, 2nd ed.; *Oily Press lipid library 18*; Oily Press: Bridgewater, 2005, OCLC: 254484796.
- (70) Pryor, W. A.; Stanley, J. P.; Blair, E. *Lipids* **1976**, *11*, 370–379.

Supporting Information ” Biological auto(chemi)luminescence imaging of oxidative processes in human skin”

Michaela Poplová,^{†,‡} Ankush Prasad,[¶] Eduard Van Wijk,[§] Pavel Pospíšil,^{||} and
Michal Cifra^{*,†}

[†]*Institute of Photonics and Electronics, The Czech Academy of Sciences, Prague, 182 00,
Czechia*

[‡]*Faculty of Electrical Engineering, Czech Technical University in Prague, Prague 166 27,
Czechia*

[¶]*Department of Biophysics, Faculty of Science, Palacký University, Šlechtitelů 27, 783 71
Olomouc, Czech Republic*

[§]*Meluna Research, Business & Science Park Wageningen, Agro Business Park 10, 6708
PW Wageningen, Netherlands*

^{||}*Department of Biophysics, Faculty of Science, Palacký University, Šlechtitelů 27, 783 71
Olomouc, Czechia*

E-mail: cifra@ufe.cz

Phone: +420 266 773 454

Abstract

The supporting information details of experiments and methods, additional imaging and kinetics data for additional concentrations of chemical components, and a brief review of antioxidants in skin.

Contents

1 Experiment and methods	S2
1.1 Luminescence measurement equipment	S2
1.2 EPR and HPLC methods	S5
1.3 Subject	S6
1.4 Chemical model system of skin	S6
1.5 Chemical treatment	S7
1.6 Data processing	S9
2 Additional data	S10
3 Antioxidants in skin	S14

1 Experiment and methods

1.1 Luminescence measurement equipment

Luminescence measurements were performed in light-tight black chambers (custom-made by the Bioelectrodynamics research team, Institute of Photonics and Electronics of the Czech Academy of Sciences), which have a light-proof sleeve designed for direct access to the interior chamber without any light leakage. Both setups are depicted in Figure S1.

For the luminescence imaging, the highly sensitive Andor iXon ULTRA 888 back-illuminated electron-multiplying charge-couple device camera (EMCCD, Andor Technology Ltd, 118 Belfast, Northern Ireland) with a Xenon 0.95/25 mm objective (Jos. Schneider Optische Werke GmbH, Bad 131 Kreuznach, Germany) was mounted on the top of the black chamber (Figure S1a). The spectral response of the EMCCD is in the range 300–1100 nm with a peak quantum efficiency of 97.5 % at 575 nm (Figure S1b). The objective with a maximum

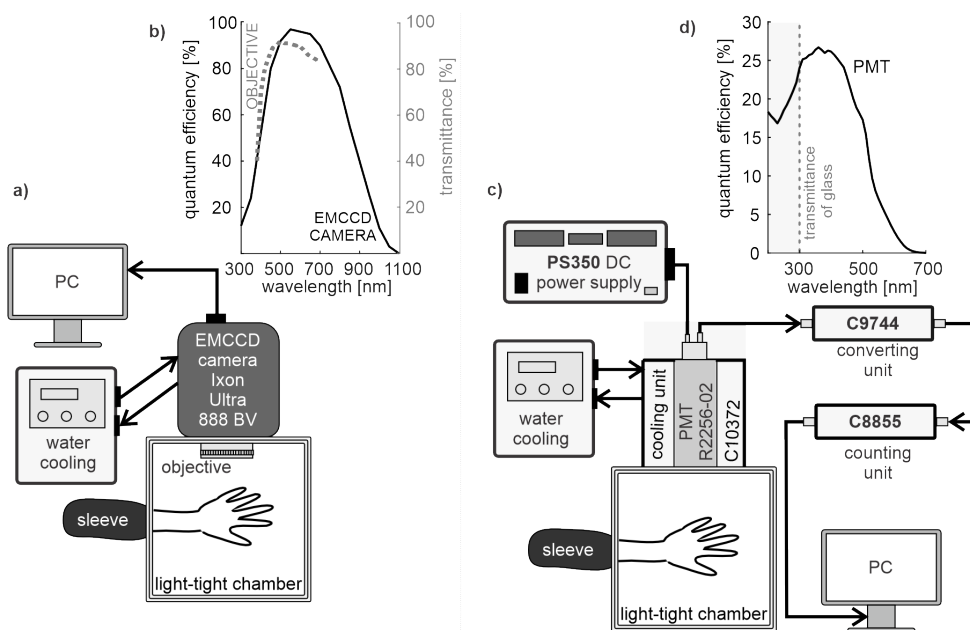


Figure S1: Schematic diagram of the measurements for a) spatial distribution (imaging) and c) temporal distribution (kinetics) of BAL. The same setups were used both for experiments with skin on a dorsal side of a hand in vivo and chemical model system (Petri dish) b) shows QE of EMCCD camera and transmittance of objective lenses. d) shows the QE of the PMT detector, where the transmittance limit of the PMT input window (borosilicate glass) is also shown.

relative aperture 0.95 is perfectly suitable for low light conditions and its transmittance is designed for the visible spectrum from 400 to 700 nm (Figure S1b). The EMCCD detector was cooled to $-100\text{ }^{\circ}\text{C}$ using a thermoelectric cooling system supplemented with an extra water cooling chiller (OasisTM 160LT, Solid State Cooling Systems, 126 NY, USA) for dark current reduction. Each luminescence image was obtained by using the following settings: 4×4 binning, 16 bits at 1 MHz readout rate, 1024×1024 pixel format, 1.7 s vertical shift speed, ‘normal’ clock amplitude, electron multiplying gain level 300, pre-amplifier gain 5.2. The distance between the detector and sample was approximately 30 cm.

Luminescence kinetics were measured with the photomultiplier R2256-02 (PMT, Hamamatsu Photonics Deutschland, DE; see in Figure S1c). This head-on type PMT has a circular photocathode with a 46 mm diameter and its sensitivity is in the wavelength range from 160 to 650 nm with a peak of sensitivity at 420 nm (Figure S1d). The PMT was cooled to $-30\text{ }^{\circ}\text{C}$ inside the housing unit C10372 (Hamamatsu Photonics Deutschland, DE) with the support of water cooling and powered at -1550 V with a high voltage power supply PS350 (Stanford Research System, USA). The pulses from PMT were amplified and converted to TTL pulses by the unit C9744 (Hamamatsu Photonics Deutschland, DE) (discriminator set to -500 mV) and processed with a counting unit C8855 (Hamamatsu Photonics Deutschland, DE) connected to a computer (PC). The high voltage settings and the discriminator were set according to the recommendation of the photomultiplier producer and based on the signal-to-noise optimization, see the thesis.¹

The effective cut-off in terms of detected BAL wavelengths is determined by the transparency of the optical elements and the wavelength sensitivity of the optical detector, see Figure S1. We know that the sensitivity range of wavelengths of our detectors is appropriate based on our prior work as well as others who measured BAL spectrum from skin.^{2,3}

1.2 EPR and HPLC methods

The following methods were used to analyze the oxidative processes in the chemical model system. We used electron paramagnetic resonance (EPR) spectroscopy for the sensitive detection of substances with unpaired electrons. In our case, we focused on the formation of $^1\text{O}_2$ in a chemical model system. EPR signals were measured with a spectrometer (MiniScope MS4001 Magnettech GmbH, Berlin, Germany). As a spin label, we used a hydrophilic diamagnetic TMPD (2,2,6,6-tetramethyl-4-piperidone, Sigma Aldrich GmbH, USA), which produced paramagnetic 2,2,6,6-tetramethyl-4-piperidone-1-oxyl (TEMPONE) in the presence of $^1\text{O}_2$ to give the EPR signal. TMPD was purified twice by vacuum distillation to reduce impurity. The reaction mixture was treated and transferred into a glass capillary tube and EPR spectra were collected at room temperature. The incubation time was 10 min. Signal intensity (*r.u.*) was calculated from the first peak of the EPR spectrum. EPR spectrometer settings were as follows: microwave power 10 mW; modulation amplitude 1 G; modulation frequency 100 kHz; sweep width 100 G; scan rate $1.62 \text{ G}\cdot\text{s}^{-1}$.

We used high-performance liquid chromatography (HPLC) to separate and identify oxidative products. In our model system, we monitored the amount of malondialdehyde (MDA), which is an indicator of oxidative stress as a product of lipid peroxidation. MDA reacted with 2,4-dinitrophenylhydrazine (DNPH) forming an MDA-DNPH derivate. Detection of the MDA-DNPH derivate was performed by a reverse-phase HPLC using an Alliance e 2695 HPLC System (Waters, Milford, MA, USA) equipped with 2998 Photodiode Array detectors. The isocratic separation was carried out using a LiChrosper 100 RP-18 ($5 \mu\text{m}$) LiChroCART 250-4 (Merck, Darmstadt, Germany) with acetonitrile:water (50:50 v/v) as a solvent system and a flow rate of 0.25 mL min^{-1} .

1.3 Subject

A volunteer (female, age 29, Fitzpatrick skin type III) participated in this study. The case study was conducted in compliance with the Helsinki Declaration of 1975, as revised in 2013.⁴ Regarding the ethics of the procedure, the participant gave her written informed consent after verbal and written information. The substances for the skin topical treatments were purchased from the certified Pharmacy at the Faculty Hospital Bulovka, Budínova 67/2, Prague, 180 81, Czechia, according to European Pharmacopoeia. Before measurement, the hand was washed with antibacterial unscented soap and water. We have not observed any effect of this washing treatment on BAL signals. After this procedure, the hand was placed into a light-tight chamber for 30 minutes to prevent delayed luminescence. BAL was measured from the dorsal side of the right hand in each experiment: 20 minutes for BAL kinetics detection using PMT and 30 minutes for BAL imaging using an EMCCD camera.

1.4 Chemical model system of skin

The proposed minimal chemical model of the skin is composed of linoleic acid (Sigma-Aldrich, L1376) that here serves as a model lipid, melanin (Sigma-Aldrich, M8631) as a model pigment that plays an important role in the oxidation reactions and Fe^{2+} ($\text{FeSO}_4 \cdot 7\text{H}_2\text{O}$, P-LAB, R.P015.1) as an initiator of the Fenton reaction. The model sample was prepared without mixing and the total volume was 3 mL (fractions: 0.3 mL H_2O or Asc^+ , 2 mL lipid stock solution, 0.2 mL melanin stock solution, 0.2 mL iron stock solution, 0.3 mL H_2O_2 stock solution). The final concentrations of the chemicals are provided in Table S1.

The linoleic acid stock was a homogenous emulsion of linoleic acid. In the final sample, the fraction of linoleic acid still forms an emulsion. The degree of turbidity increases with the amount of the linoleic acid. Although microstructurally far from identical to the biological tissue, our model system carries a certain resemblance to some of the main structural and optical features of biological tissue: the linoleic acid emulsion microparticles are

light-scattering objects similar to the cellular and subcellular structures in the tissue, and the thin lipid layer on the surface of the sample is reminiscent of the lipid-rich skin sebum and stratum corneum. To have a better idea of the state and appearance of the model system, we made photographs of the samples with varied concentrations of linoleic acid and melanin, see Figure S2.

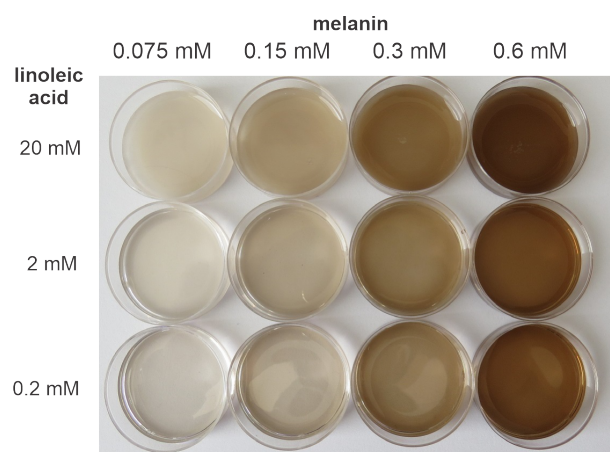


Figure S2: Photo of the samples with varying concentrations of linoleic acid and melanin

Linoleic acid was dissolved in physiological saline - 0.9 % NaCl (sodium chloride, Penta, 16610-31000) together with 0.7 μ M DMSO (dimethyl sulfoxide, P-LAB, 12630-11000). Linoleic acid provides a substrate for the lipid peroxidation process in a model system. Melanin was dissolved in DMSO. Melanin is one of the major cutaneous pigments. Micromolar to millimolar concentrations of iron cations are present in biological systems.⁵⁻⁷ The reactions of Fe^{2+} and other transition metals with hydrogen peroxide (H_2O_2) lead to the Fenton and Fenton-like reactions, which initiate radical oxidation of organic molecules either via the generated hydroxyl radicals ($\text{HO}\cdot$) or other pathways.⁸

1.5 Chemical treatment

Two different studies were conducted, the first on varying degrees of oxidative stress (by varying the concentration of hydrogen peroxide) and the second on the antioxidant effects

Table S1: Final concentration of chemicals in experiments with the model system

	PMT/EMCCD	EPR ^a	HPLC
linoleic acid	10 mM	10 mM	10 mM
melanin	0.15 mM	0.15 mM	-
Fe ²⁺	2 mM	2 mM	2 mM
H ₂ O ₂	3/0.9/0.3 % ~ 880/264/88 mM	0.3/0.09/0.03 % ~ 88/26.4/8.8 mM	0.09 % ~ 26.4 mM
Asc ⁺	5 mM	5 mM	-

^a 25 mM TMPD (spin trap) added

in samples. For the first study, we used hydrogen peroxide (Penta, 23980-11000) with three different final concentrations ($c_1=3$ %, $c_2=0.9$ %, $c_3=0.3$ %), where 0.3 mL stock solution was injected. For testing the protective effect of antioxidants on skin, we used 0.3 mL of a stock solution of ascorbic acid (AA, Penta, 18650-30500) with a concentration of 5 mM. For the antioxidant experiment, oxidative stress of the skin was induced with 3 % hydrogen peroxide, which increased BAL. The chemical model system was in a plastic Petri dish (35 mm diameter, Thermo Scientific, Nunc cell culture/Petri dishes) without a lid for the experiments.

For imaging experiments on the skin, three rectangular spots were defined by a mask from transparent adhesive tape and black dots. Each substance of volume 5 μL was applied by micropipette and the drop was uniformly distributed by gloves in each rectangular spot. After these procedures, the tape mask was removed before measurement. The gray scale image of the hand was taken after each luminescence imaging experiment. For the antioxidant experiment, we first applied the ascorbic acid and then the H₂O₂. For the BAL measurement with PMT, experiments with each concentration were carried out consecutively. There, in experiments with a skin, a given substance (10 μL) was applied on the whole area of the dorsal side of the hand, in contrast to the imaging experiments, where only smaller limited areas were treated.

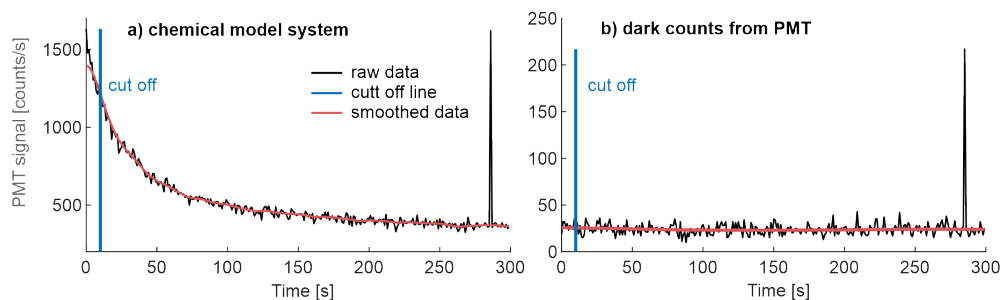


Figure S3: Preprocessing of PMT signals was composed from smoothing the signal (red line) and their shortening from the blue cut-off line. The red shortened smoothed signals were used for subsequent analyses. a) a typical BAL signal of the chemical model system (black line) and b) dark count of the PMT (black line).

1.6 Data processing

Raw PMT signals were fitted by function `smoothn.m`^{9,10} designed by D.Garcia with parameter 'robust', which minimizes the influence of outlying data (see in Figure S3). This smoothing method is based on discretized spline with the minimization of the generalized cross-validation score. Due to estimation error in the beginning of signal (see in Figure S3a) the first 10 values were removed (blue vertical line). These smoothed shortened lines were used for further data analysis.

Imaging data were recorded by Andor Solis software in SIF format. Original images have 256×256 pixels due to software binning 4×4 and grey scale from 0 to 65535 intensity levels. The image was converted to .dat format for analysis by Matlab software.¹¹ Data included noise which distorted the results of the analysis. The preprocessing method was based on thresholding. We calculated a cumulative sum from the histogram of image and empirically determined the threshold of 99.6 % for hand and 99.8 % for model system. The values equal to or higher than the threshold were replaced by NaN values, which were not included in the further analysis. Figure S4 shows the whole image processing procedure and figure S5 effect thresholds on the image.

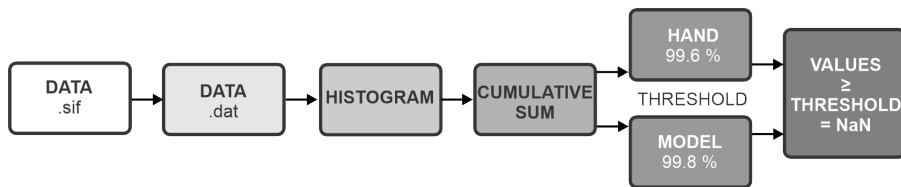


Figure S4: Scheme of preprocessing procedure for quantitative image data analysis. The thresholding was used to remove the outliers and excessive noise; see the text for a detailed description.

2 Additional data

To test whether BAL imaging can be used to quantify the spatially heterogeneous distribution of oxidative stress, we performed a parallel topical skin treatment with H_2O_2 concentration row ($c_1=3\%$, $c_2=0.9\%$, $c_3=0.3\%$) on the selected sites on the dorsal side of the right hand of the test subject (Figure S6a). The BAL from the skin (Figure S6b) was imaged for 30 min using a cooled EMCCD camera (Andor iXon3 888) mounted to our custom-built light-tight chamber. Although the endogenous BAL signal from the skin is only weakly above the dark count, the BAL image following the shape of the hand is clearly discernable.

A representative image of BAL from the human hand with three topical H_2O_2 treatments is shown in Figure 1a. Apart from endogenous BAL, which follows the morphology of the hand, it can be seen that the higher the concentration of H_2O_2 (higher oxidative stress) the higher the BAL intensity from the topically treated skin areas. In addition to the three major areas of interest, where the H_2O_2 was applied, other patches of increased BAL intensity are also noticeable. The most prominent one in Figure 1a is at the root of the thumb and several other smaller ones scattered on the hand. It cannot be excluded that the small patches are just due to instrumental noise. However, the larger patch likely corresponds to light emitted from the skin and is of unknown origin. Patches of comparable size or even larger are not uncommon in the imaging of BAL from the human hand,¹² even if great care is taken to avoid skin treatments. They might indicate local skin irritation due to various factors and subclinical skin conditions that are not visible by visual observation by the naked eye. A

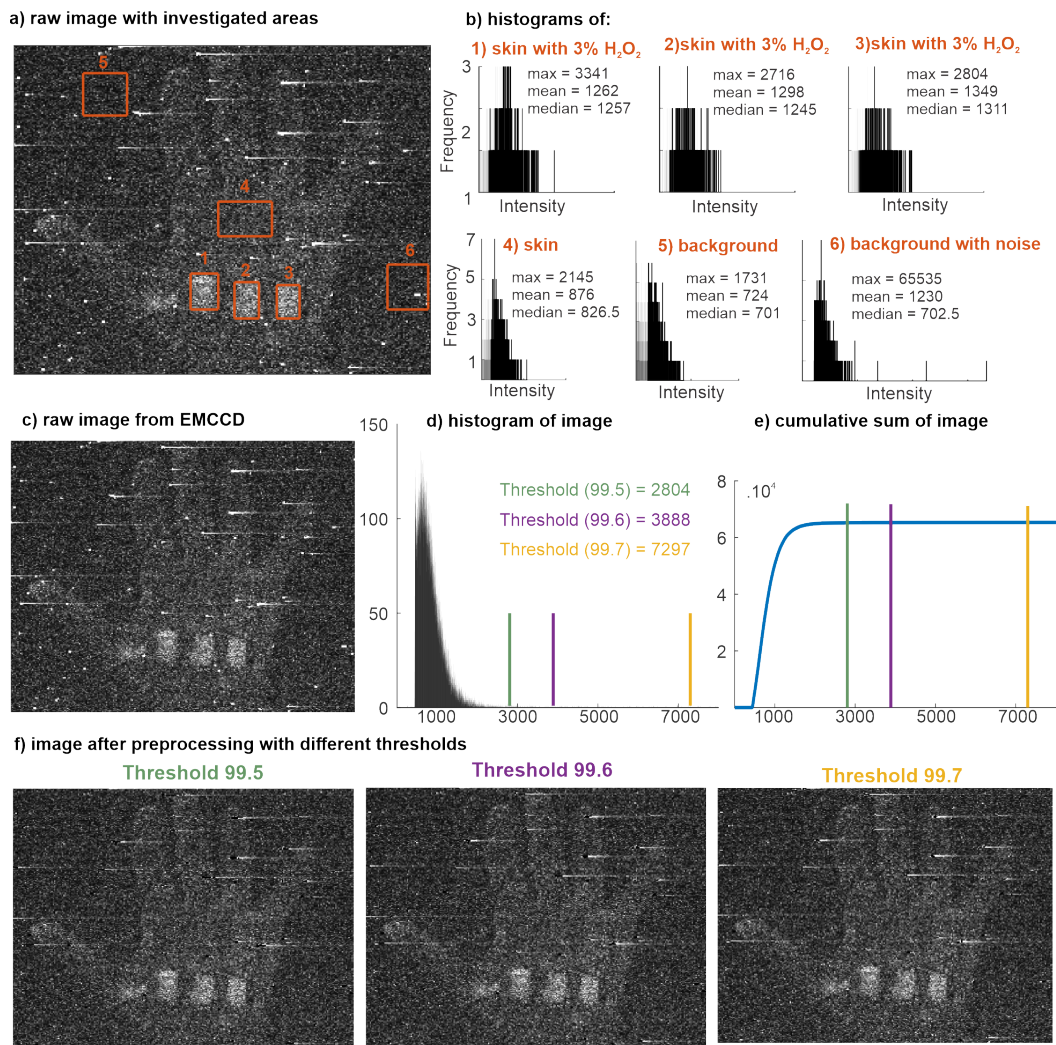


Figure S5: Effect of the histogram-based thresholding on the image. a) Raw image with five investigated areas(1-3:treated areas with the same concentration of H₂O₂, 4:skin none-treated area, and two background areas 5:without and 6:with noise. b) shows histogram analysis with basic parameters such as max, mean, and median values. Contrast for mean values of background without b)5 and with noise b)6 proves the necessity of removing of noise from images. c) Raw image of skin, and their histogram d) and cumulative sum e) with different thresholds. According to the result after preprocessing f), the threshold was empirically set to 99.6 for the skin. The same procedure was done for the model system.

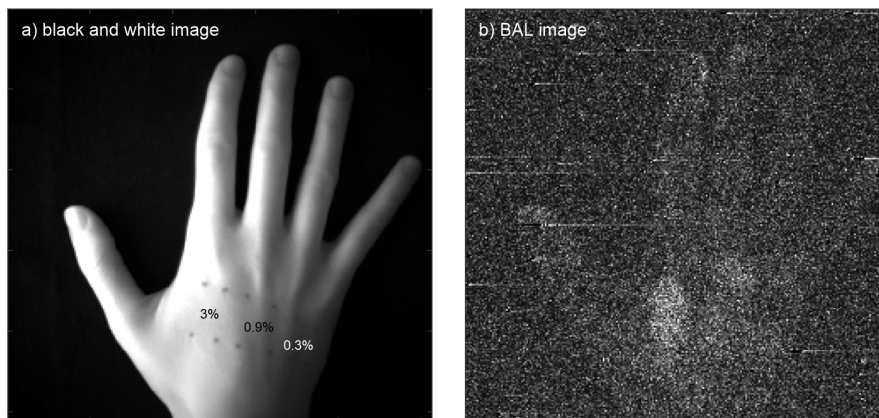


Figure S6: A typical a) greyscale image of a hand and the corresponding b) BAL image from EMCCD camera. The four dots mark the corners of rectangular sites where the $c_1=3\%$, $c_2=0.9\%$, $c_3=0.3\%$ concentration of hydrogen peroxide was applied on the skin.

systematic study would be required to find a causal relationship of the origins of the patches.

We provide here also a different representation of the data from Figure 1c,f and Figure 2c,f: instead of the absolute values of the detected counts, we display the data as the ratios of the treated/non-treated area, see Figure S7, S8.

Stability of the data The data presented in the main text of the paper was collected to be consistent in concentrations across all the methods we used as much as the experimental limitations allowed. However, this final selection of concentrations was preceded by tens of types of experiments, each with multiple repetitions, that were already optimized for sample handling and measurement stability and which showed a very high degree of stability even between the experimental days. These hundreds of experiments support the paper's overall results and conclusions. Here we provide further selected results from this huge batch of experiments on chemical model systems with varying concentrations of linoleic acid, and melanin to show that the results from chemical model system are indeed very stable, see Figure S9, S10.

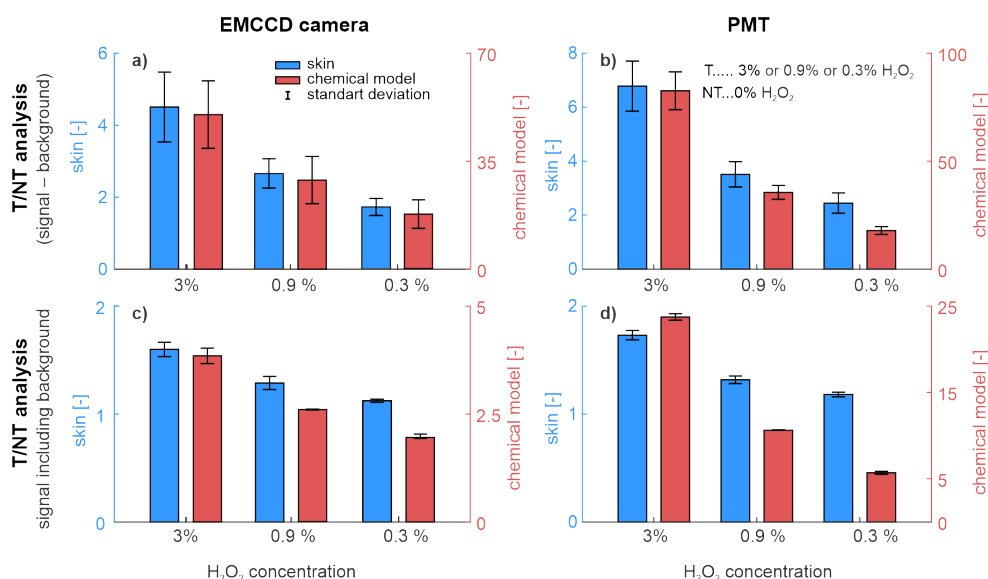


Figure S7: The ratios (T/NT, i.e. treated with H₂O₂/non-treated) BAL signals from samples for a variety of H₂O₂ concentrations. There are two versions of the analysis: a) and b) display ratios of the signals without background (dark count) and c),d) display ratios of the signals which included background.

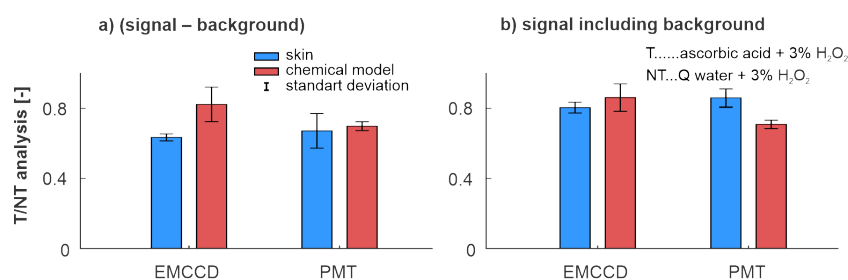


Figure S8: The ratios (T/NT, i.e. with ascorbate/without ascorbate) BAL signals from samples. There are two versions of the analysis: a) display ratios of the signals without background (dark count) and b) display ratios of the signals which included background.

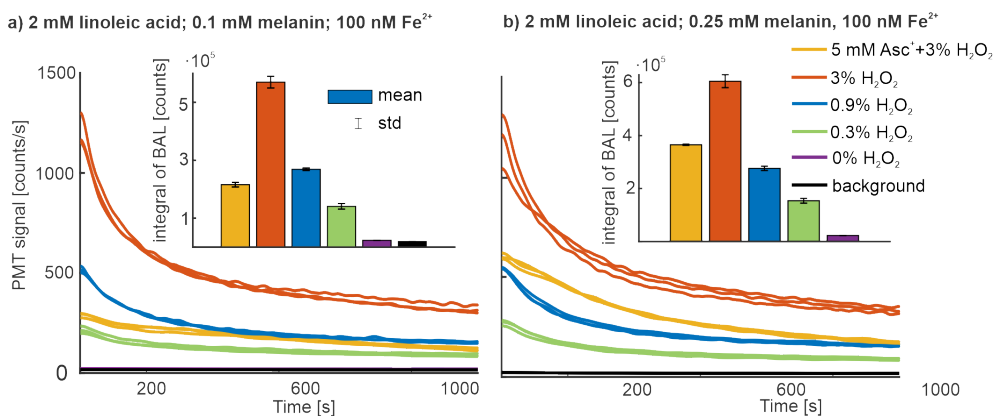


Figure S9: BAL signals measured from the chemical model system with two different concentrations of melanin 0.1mM a) and 0.25 mM b) using photomultiplier showing that the reproducibility is very high and the results are very stable. The results include both different concentrations of H₂O₂ and the presence or absence of antioxidant - ascorbic acid.

3 Antioxidants in skin

What are the main substances, for which there is evidence of protective capabilities against oxidation in skin? Antioxidants, such as ascorbic acid (vitamin C - on which we focused in this paper), tocopherols (vitamin E), carotenoids, Coenzyme Q10, ergothioneine, and polyphenols, have been shown to have diverse effects on the skin,¹³ see these representative examples. Ascorbic acid acts as an antioxidant and promotes epidermal differentiation,¹⁴ collagen synthesis, and inhibits melanin production.¹⁵ Tocopherols also prevent oxidative stress from various sources and suppress matrix metalloproteinase-1 (MMP-1) expression.¹⁶ Carotenoids are pigments possessing the ability to quench ¹O₂¹⁷ making them particularly effective in protecting against UV damage. Natural substances like Coenzyme Q10 have antioxidative and anti-aging effects¹⁸ via reduction of MMP-1 expression,¹⁹ similarly to tocopherols. Polyphenols, including epigallocatechin gallate (EGCG) and resveratrol, strengthen skin tolerance to UV stress and reduce MMP production.¹³ Overall, these antioxidants neutralize reactive oxygen species (ROS), promote collagen synthesis, inhibit melanin production, and protect against UV-induced damage.

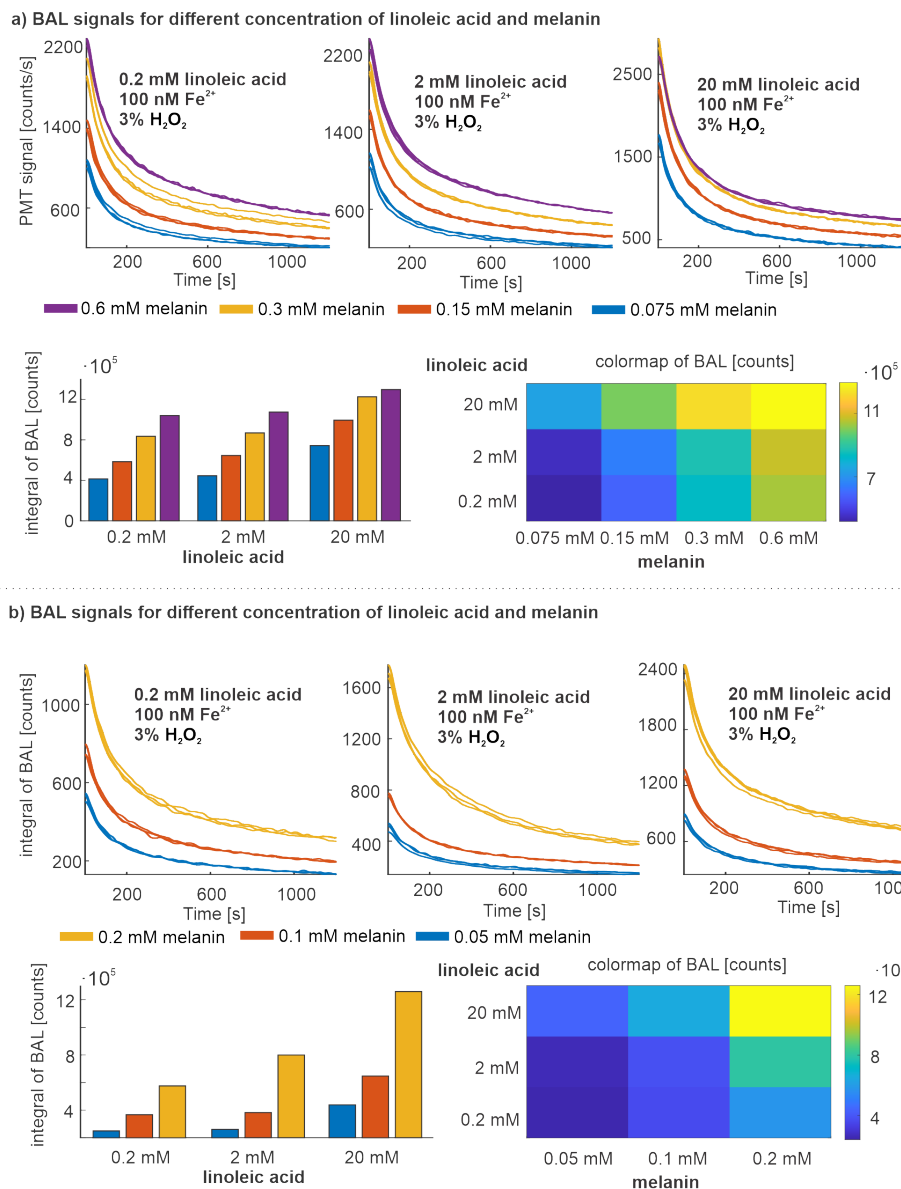


Figure S10: BAL signals measured from chemical model system using photomultiplier where we systematically changed the concentration of linoleic acid and melanin for two experiments. a) Linoleic acid concentration was set to 0.2, 2, 20 mM, and for melanin 0.6, 0.3, 0.15, 0.075 mM. Second experiment b) had the same concentration of linoleic acid as the previous one but different concentrations of melanin 0.2, 0.1 0.05 mM. The total "Counts" are per 1200 s.

References

- (1) Ondrušová, B. Measurement Optimization and Analysis of Selected Physical and Chemical Effects on the Ultra-Weak Proton Emission from a Human Hand. M.Sc. thesis, CZECH TECHNICAL UNIVERSITY IN PRAGUE, Faculty of Electrical Engineering, Department of Circuit Theory, 2016.
- (2) Van Wijk, E. P.; Van Wijk, R. Multi-Site Recording and Spectral Analysis of Spontaneous Photon Emission from Human Body. *Complement. Med. Res.* **2005**, *12*, 96–106.
- (3) Kobayashi, M.; Iwasa, T.; Tada, M. Polychromatic spectral pattern analysis of ultra-weak photon emissions from a human body. *J. Photochem. Photobiol. B: Biol.* **2016**, *159*, 186–190.
- (4) Emanuel, E. J. Reconsidering the Declaration of Helsinki. *The Lancet* **2013**, *381*, 1532–1533.
- (5) Martínez-Garay, C. A.; de Llanos, R.; Romero, A. M.; Martínez-Pastor, M. T.; Puig, S. Responses of *Saccharomyces cerevisiae* Strains from Different Origins to Elevated Iron Concentrations. *AEM* **2016**, *82*, 1906–1916.
- (6) Olivieri, N. F. Progression of iron overload in sickle cell disease. *Semin. Hematol.* **2001**, *38*, 57–62.
- (7) Wood, J. C. Estimating Tissue Iron Burden: Current Status and Future Prospects. *Br. J. Haematol.* **2015**, *170*, 15–28.
- (8) Meyerstein, D. What Are the Oxidizing Intermediates in the Fenton and Fenton-like Reactions? A Perspective. *Antioxidants* **2022**, *11*, 1368.
- (9) Garcia, D. A fast all-in-one method for automated post-processing of PIV data. *Experiments in Fluids* **2010**, *50*, 1247–1259.

- (10) Garcia, D. Robust smoothing of gridded data in one and higher dimensions with missing values. *Comput. Stat. Dat. Anal.* **2010**, *54*, 1167–1178.
- (11) *MATLAB version 9.10.0.1602886 (R2021a)*; The Mathworks, Inc.: Natick, Massachusetts, 2021.
- (12) Scholkmann, F.; van de Kraats, E.; van Wijk, R.; van Wijk, E.; van der Greef, J. Spatio-temporal dynamics of spontaneous ultra-weak photon emission (autoluminescence) from human hands measured with an EMCCD camera: Dependence on time of day, date and individual subject. *Matters* **2018**,
- (13) Masaki, H. Role of antioxidants in the skin: Anti-aging effects. *Journal of Dermatological Science* **2010**, *58*, 85–90.
- (14) Boyce, S. T.; Supp, A. P.; Swope, V. B.; Warden, G. D. Vitamin C Regulates Keratinocyte Viability, Epidermal Barrier, and Basement Membrane In Vitro, and Reduces Wound Contraction After Grafting of Cultured Skin Substitutes. *J. Invest. Dermatol.* **2002**, *118*, 565–572.
- (15) Ohshima, H.; Mizukoshi, K.; Oyobikawa, M.; Matsumoto, K.; Takiwaki, H.; Kanto, H.; Itoh, M. Effects of vitamin C on dark circles of the lower eyelids: quantitative evaluation using image analysis and echogram. *Skin Res. Technol.* **2009**, *15*, 214–217.
- (16) Polte, T.; Tyrrell, R. M. Involvement of lipid peroxidation and organic peroxides in UVA-induced Matrix Metalloproteinase-1 expression. *Free Radic. Biol. Med.* **2004**, *36*, 1566–1574.
- (17) Camera, E.; Mastrofrancesco, A.; Fabbri, C.; Daubrawa, F.; Picardo, M.; Sies, H.; Stahl, W. Astaxanthin, canthaxanthin and β -carotene differently affect UVA-induced oxidative damage and expression of oxidative stress-responsive enzymes. *Exp. Dermatol.* **2009**, *18*, 222–231.

- (18) Muta-Takada, K.; Terada, T.; Yamanishi, H.; Ashida, Y.; Inomata, S.; Nishiyama, T.; Amano, S. Coenzyme Q10 protects against oxidative stress-induced cell death and enhances the synthesis of basement membrane components in dermal and epidermal cells. *BioFactors* **2009**, *35*, 435–441.
- (19) Inui, M.; Ooe, M.; Fujii, K.; Matsunaka, H.; Yoshida, M.; Ichihashi, M. Mechanisms of inhibitory effects of CoQ10 on UVB-induced wrinkle formation in vitro and in vivo. *BioFactors* **2008**, *32*, 237–243.

The results of the research presented in this thesis have been published in scientific journals and conference proceedings, as indicated in the author's list of publications [10]. Chapters based on papers include their full bibliographic citation, the candidate's contribution, and acknowledgments at the beginning. The dissertation is structured into two main parts: (1) The state of the art section, which covers the historical introduction of Biological autochemiluminescence, its generation mechanism, applications with representative experiments, and its detection systems.(2) The experimental part, which consists of 7 chapters.

Chapter 4 and 5 deal with the methodology of BAL measurements. The outcome includes the development of light-tight chambers, system configuration, testing, and identifying suitable detectors for BAL. As a result, handling procedures and protocols for cells, seeds and human skin were established. Preliminary results indicate that non-adherent cells such as yeast cells or HL-60 cells, seeds and human skin are suitable materials for investigating BAL due to their sufficiently high intensity.

In chapter 6, two main aspects were investigated:(1) the photocounts statistic of BAL from germinating mung beans over six days and (2) a minor hypothesis exploring whether the presence of 1% sucrose can affect BAL parameters. (1) It was observed that BAL intensity increased with the number of growth days. The distribution of BAL was fitted with a negative binomial distribution for each day. It was found that as the signal-to-noise ratio increased, the distribution approached a Poisson distribution, which is the theoretically assumed distribution for BAL. This can be explained by considering that the measured BAL signals include both naturally occurring BAL and dark counts from detectors. With a higher signal-to-noise ratio, measured BAL is less affected by the distribution of dark counts, which follows a negative binomial distribution. (2) The presence of 1% sucrose during seed handling resulted in a slight yet statistically significant decrease in BAL compared to the control group that used ultra-pure water for seed handling. Interestingly, the total length and weight gain of mung bean seedlings remained unaffected by the presence of sucrose.

Chapter 7 describes a novel pre-processing method for non-stationary Poisson signal, assuming non-negative integers samples with equal mean and variance. Our method makes the signal stationary, preserving the mean-variance relationship. Additionally, the pre-processed signal retains its original rectangular structure in the phase space, making our pre-processing method potentially useful for preparing signals for further complexity and chaos theory-based analyses. When applied to non-Poisson non-stationary signals, it never transforms them into a Poisson distribution. It also does not alter the distribution of stationary integer data, causing only minor changes due to rounding when applied to non-integer data, such as those originating from a normal distribution. Using our method can prevent artificial findings and enable the analysis of non-stationary photonic signals that might have otherwise been unusable and discarded due to the baseline drifts.

In chapter 8, the spectral analysis of two biological samples using long-pass optical filters is presented. The preliminary results indicate: (i) The possibility of measuring BAL optical spectra from living systems with very low intensities. (ii) The demonstration of stability in results obtained from three repetitions of one sample, yeast cells. (iii) The observation of repeatability in measurements from three different concentrations of HL60 cells. (iv) Clear differences in the spectra between two distinct types of cell cultures. The spectra were corrected based on the spectral quantum efficiency of PMT and filter transmission while disregarding the reflectance at interfaces and the angular dependence of the filters.

Chapter 9 focuses on the optical propagation model of BAL within human skin across various wavelengths. The discrete model comprises six distinct skin layers defined by their thickness, blood volume, and melanin content. This model represents the attenuation of photons within the skin layers based on calculations of absorption and scattering parameters. The outcome is an estimation of the light intensity generated by the skin's surface at the selected wavelength. The model reveals that the majority of photons originate from the uppermost, thin skin layer (0.03 cm), and photons are more attenuated at shorter wavelengths. The model was employed to estimate the number of photons generated within the skin based on data measured by PMT R2256. The estimation demonstrates that detected photons experience approximately 1000-fold attenuation within the skin, including reflectance at the interfaces encountered on their path to the detector.

Chapter 10 demonstrates (i) the capability to quantitatively differentiate between several degrees of oxidation level on human skin *in vivo* induced by the application of H₂O₂ and (ii) the possibility of monitoring the protective effect of antioxidants. BAL images depict local oxidative changes on human skin under controlled conditions. Data were confirmed by BAL results from PMTs, where one measurement corresponds to one level of oxidative stress on human skin without spatial information. Ascorbic acid, as an antioxidant, reduced the effects of oxidant treatment. Our minimal chemical model of skin, composed of linoleic acid, melanin, and trace amounts of iron, produces singlet oxygen ¹O₂, which is a potential emitter of BAL and ROS itself. The oxidation of the chemical model system was confirmed by the detection of MDA (malondialdehyde) - a lipid peroxidation product.

12.1 CONTRIBUTION OF THE DISSERTATION

This dissertation has contributed to the understanding of the natural light phenomenon in the visible spectral range termed biological autoluminescence from a historical view, over the generation mechanisms, and measurement principles (Chapter 2). To preserve appropriate measuring conditions of BAL, light-tight chambers were designed (Chapter 4). The preliminary studies on various (i) types of living systems, and (ii) measuring devices established handling procedures and protocols for BAL (Chapter 5). The content of this work involved the investigation of (i) photocount statistic and analysis of stationary BAL signals (Chapter 6) and (ii) proposing a solution for non-stationary BAL signal resolved by designing a novel preprocessing method for signals with a Poisson distribution in Chapter 7. The performed method for the detection of BAL spectra was used for the verification of the theoretical generation mechanism of BAL (Chapter 8). The optical propagation model within human skin estimates light intensity across various wavelengths, highlighting the role of different skin layers, and is utilized for comparison with measured data (Chapter 9). The experiment in Chapter 10 showed the possibility of distinguishing local oxidative changes in human skin, which could lead to applicability in medicine. This research enhances understanding of BAL in diverse biological contexts, providing valuable insights and methodologies for further studies in this field. In conclusion, the goals of the thesis summarized in Chapter 3 were fulfilled in Chapters 4-10.

12.2 FUTURE DIRECTIONS

The results presented in this thesis provide an overview based on theoretical and experimental evidence. BAL appears to be a useful, indirect, non-invasive, label-free and irradiation-free tool for monitoring oxidative processes within living systems. The next steps might involve the following directions: (i) Using BAL to monitor oxidative changes during and after applying a pulsed electric field to the biological samples and proteins. (ii) Utilizing BAL to measure oxidative metabolism of cancer cells on surface tissues. (iii) Developing a polychromatic spectroscope for our research. (iv) There is also recent increased interest in the biological role of biologically generated electron-excited states within a quantum biology research community.

BIBLIOGRAPHY

- [1] A. G. Gurwitsch and L. D. Gurwitsch, "Twenty Years of Mitogenetic Radiation: Emergence, Development, and Perspectives," *21st Century Science and Technology*, p. 13, 1999.
- [2] D. Balasigamani, M. Usa, and H. Inaba, "Biophotons: ultraweak light emission from living systems," *Current Opinion in Solid State and Materials Science*, vol. 2, no. 2, pp. 188–193, 1997.
- [3] F. Popp, "Emission of visible and ultraviolet radiation by active biological system," *Collective Phenomena*, vol. 3, pp. 187–214, 1981.
- [4] E. Cadenas, "Biological chemiluminescence," *Photochemistry and photobiology*, vol. 40, no. 6, pp. 823–830, 1984.
- [5] A. A. Alfadda and R. M. Sallam, "Reactive Oxygen Species in Health and Disease," *Journal of Biomedicine and Biotechnology*, vol. 2012, 2012.
- [6] Y. A. Vladimirov and E. V. Proskurnina, "Free radicals and cell chemiluminescence," *Biochemistry (Moscow)*, vol. 74, no. 13, pp. 1545–1566, Dec. 2009.
- [7] P. Pospíšil, A. Prasad, and M. Rác, "Mechanism of the Formation of Electronically Excited Species by Oxidative Metabolic Processes: Role of Reactive Oxygen Species," *Biomolecules*, vol. 9, no. 7, p. 258, Jul. 2019.
- [8] P. Vahalová and M. Cifra, "Biological autoluminescence as a perturbation-free method for monitoring oxidation in biosystems," *Progress in Biophysics and Molecular Biology*, vol. 177, pp. 80–108, 2023.
- [9] K. Brieger, S. Schiavone, J. Miller, and K. Krause, "Reactive oxygen species: from health to disease," *Swiss Medical Weekly*, Aug. 2012.
- [10] C. Wilson and C. González-Billault, "Regulation of cytoskeletal dynamics by redox signaling and oxidative stress: implications for neuronal development and trafficking," *Frontiers in Cellular Neuroscience*, vol. 9, Sep. 2015.
- [11] K. Das and A. Roychoudhury, "Reactive oxygen species (ROS) and response of antioxidants as ROS-scavengers during environmental stress in plants," *Frontiers in Environmental Science*, vol. 2, pp. 53–65, Dec. 2014.
- [12] F. Cristiana and A. Elena, *Reactive Oxygen Species (ROS) in Living Cells*. BoD – Books on Demand, May 2018, google-Books-ID: hnCQDwAAQBAJ.
- [13] R. S. Balaban, S. Nemoto, and T. Finkel, "Mitochondria, Oxidants, and Aging," *Cell*, vol. 120, no. 4, pp. 483–495, Feb. 2005.
- [14] A. Rastogi and P. Pospíšil, "Effect of exogenous hydrogen peroxide on biophoton emission from radish root cells," *Plant Physiology and Biochemistry*, vol. 48, no. 2-3, pp. 117–123, Feb. 2010.
- [15] K. Nakamura and M. Hiramatsu, "Ultra-weak photon emission from human hand: Influence of temperature and oxygen concentration on emission," *Journal of Photochemistry and Photobiology B: Biology*, vol. 80, no. 2, pp. 156–160, Aug. 2005.
- [16] M. Kobayashi, K. Sasaki, M. Enomoto, and Y. Ehara, "Highly sensitive determination of transient generation of biophotons during hypersensitive response to cucumber mosaic virus in cowpea," *Journal of Experimental Botany*, vol. 58, no. 3, pp. 465–472, Dec. 2006.

- [17] J. W. Mansfield, "Biophoton distress flares signal the onset of the hypersensitive reaction," *Trends in Plant Science*, vol. 10, no. 7, pp. 307–309, Jul. 2005.
- [18] A. Rastogi and P. Pospíšil, "Production of hydrogen peroxide and hydroxyl radical in potato tuber during the necrotrophic phase of hemibiotrophic pathogen *Phytophthora infestans* infection," *Journal of Photochemistry and Photobiology B: Biology*, vol. 117, pp. 202–206, Dec. 2012.
- [19] M. Cifra and P. Pospíšil, "Ultra-weak photon emission from biological samples: Definition, mechanisms, properties, detection and applications," *Journal of Photochemistry and Photobiology B: Biology*, vol. 139, pp. 2–10, Oct. 2014.
- [20] G. W. Taylor and E. N. Harvey, "The theory of mitogenetic radiation," *The Biological Bulletin*, vol. 61, no. 3, pp. 280–293, 1931.
- [21] N. Choucrun, "On the hypothesis of mitogenetic radiation," *Journal of the Marine Biological Association of the United Kingdom*, vol. 17, no. 1, pp. 65–74, 1930.
- [22] F. A. Popp, W. Nagl, K. Li, W. Scholz, O. Weingärtner, and R. Wolf, "Biophoton emission: New evidence for coherence and DNA as source," *Cell Biochemistry and Biophysics*, vol. 6, no. 1, pp. 33–52, 1984.
- [23] K. Li and F. Popp, "Dynamics of DNA excited states," *Molecular and Biological Physics of Living Systems*, pp. 31–52, 1990.
- [24] C. Brouder and M. Cifra, "Coherence and statistical properties of ultra-weak photon emission," *Fields of The Cell*, pp. 163–188, 2015.
- [25] E. J. Bechara and T. Wilson, "Alkyl substituent effects on dioxetane properties. Tetraethyl-, dicyclohexylidene-, and 3, 4-dimethyl-3, 4-di-n-butyl-dioxetanes. A discussion of decomposition mechanisms," *The Journal of Organic Chemistry*, vol. 45, no. 26, pp. 5261–5268, 1980.
- [26] E. L. Bastos, P. Farahani, E. J. Bechara, and W. J. Baader, "Four-membered cyclic peroxides: Carriers of chemical energy," *Journal of Physical Organic Chemistry*, vol. 30, no. 9, p. e3725, Sep. 2017.
- [27] W. Adam and W. J. Baader, "Effects of methylation on the thermal stability and chemiluminescence properties of 1, 2-dioxetanes," *Journal of the American Chemical Society*, vol. 107, no. 2, pp. 410–416, 1985.
- [28] A. Rastogi and P. Pospíšil, "Spontaneous ultraweak photon emission imaging of oxidative metabolic processes in human skin: effect of molecular oxygen and antioxidant defense system," *Journal of Biomedical Optics*, vol. 16, no. 9, p. 096005, 2011.
- [29] R. Van Wijk and E. P. Van Wijk, "Free radicals and low-level photon emission in human pathogenesis: State of the art," *Indian Journal of Experimental Biology*, p. 37, 2008.
- [30] A. Boveris, E. Cadenas, R. Reiter, M. Filipowski, Nasake, and B. Chance, "Organ chemiluminescence: Noninvasive assay for oxidative radical reaction," *Proceedings of the National Academy of Sciences*, vol. 77, pp. 347–351, 1980.
- [31] M. Havaux, C. Triantaphylides, and B. Genty, "Autoluminescence imaging: a non-invasive tool for mapping oxidative stress," *Trends in plant science*, vol. 11, no. 10, pp. 480–484, 2006.
- [32] M. Cifra, J. Z. Fields, and A. Farhadi, "Electromagnetic cellular interactions," *Progress in Biophysics and Molecular Biology*, vol. 105, no. 3, pp. 223–246, May 2011.
- [33] M. Freitas, G. Porto, J. L. Lima, and E. Fernandes, "Optimization of experimental settings for the analysis of human neutrophils oxidative burst in vitro," *Talanta*, vol. 78, no. 4-5, pp. 1476–1483, Jun. 2009.

- [34] C. L. Hawkins and M. J. Davies, "Detection, identification, and quantification of oxidative protein modifications," *The Journal of Biological Chemistry*, vol. 294, no. 51, pp. 19 683–19 708, Dec. 2019.
- [35] H. Sies and D. P. Jones, "Reactive oxygen species (ROS) as pleiotropic physiological signalling agents," *Nature Reviews Molecular Cell Biology*, Mar. 2020.
- [36] A. A. Starkov, "The Role of Mitochondria in Reactive Oxygen Species Metabolism and Signaling," *Annals of the New York Academy of Sciences*, vol. 1147, pp. 37–52, Dec. 2008.
- [37] V. B. O'Donnell and A. Azzi, "High rates of extracellular superoxide generation by cultured human fibroblasts: involvement of a lipid-metabolizing enzyme." *Biochemical Journal*, vol. 318, no. Pt 3, pp. 805–812, Sep. 1996.
- [38] E. Gross, C. S. Sevier, N. Heldman, E. Vitu, M. Bentzur, C. A. Kaiser, C. Thorpe, and D. Fass, "Generating disulfides enzymatically: Reaction products and electron acceptors of the endoplasmic reticulum thiol oxidase Ero1p," *Proceedings of the National Academy of Sciences*, vol. 103, no. 2, pp. 299–304, Jan. 2006.
- [39] J. S. McNally, M. E. Davis, D. P. Giddens, A. Saha, J. Hwang, S. Dikalov, H. Jo, and D. G. Harrison, "Role of xanthine oxidoreductase and NAD(P)H oxidase in endothelial superoxide production in response to oscillatory shear stress," *American Journal of Physiology-Heart and Circulatory Physiology*, vol. 285, no. 6, pp. H2290–H2297, Dec. 2003.
- [40] A. San Martín and K. K. Griendling, "Redox Control of Vascular Smooth Muscle Migration," *Antioxidants & Redox Signaling*, vol. 12, no. 5, pp. 625–640, Mar. 2010.
- [41] J. Yun, P. Rocic, Y. F. Pung, S. Belmadani, A. C. R. Carrao, V. Ohanyan, and W. M. Chilian, "Redox-Dependent Mechanisms in Coronary Collateral Growth: The "Redox Window" Hypothesis," *Antioxidants & Redox Signaling*, vol. 11, no. 8, pp. 1961–1974, Aug. 2009.
- [42] P. Jamnik and P. Raspor, "Methods for monitoring oxidative stress response in yeasts," *Journal of Biochemical and Molecular Toxicology*, vol. 19, no. 4, pp. 195–203, Sep. 2005.
- [43] M. Percival, "Antioxidants," *Clin. Nutr. Ins.*, vol. 1, pp. 1–6, 1996.
- [44] P. M. Abuja and R. Albertini, "Methods for monitoring oxidative stress, lipid peroxidation and oxidation resistance of lipoproteins," *Clinica Chimica Acta*, vol. 306, no. 1-2, pp. 1–17, Apr. 2001.
- [45] E. Cabiscol Català, J. Tamarit Sumalla, and J. Ros Salvador, "Oxidative stress in bacteria and protein damage by reactive oxygen species," *International Microbiology, 2000*, vol. 3, núm. 1, p. 3-8, 2000.
- [46] M. J. Davies, "Protein oxidation and peroxidation," *Biochemical Journal*, vol. 473, no. 7, pp. 805–825, Apr. 2016.
- [47] W. Adam, D. V. Kazakov, and V. P. Kazakov, "Singlet-Oxygen Chemiluminescence in Peroxide Reactions," *Chemical Reviews*, vol. 105, no. 9, pp. 3371–3387, Sep. 2005.
- [48] A. Prasad and P. Pospíšil, "Linoleic Acid-Induced Ultra-Weak Photon Emission from *Chlamydomonas reinhardtii* as a Tool for Monitoring of Lipid Peroxidation in the Cell Membranes," *PLoS ONE*, vol. 6, no. 7, p. e22345, Jul. 2011.
- [49] G. Cilento, R. C. de Baptista, and I. L. Brunetti, "Triplet carbonyls: from photophysics to biochemistry," *Journal of molecular structure*, vol. 324, no. 1-2, pp. 45–48, 1994.
- [50] G. F. Fedorova, A. V. Trofimov, R. F. Vasil'ev, and T. L. Veprintsev, "Peroxy-radical-mediated chemiluminescence: mechanistic diversity and fundamentals for antioxidant assay," *Arkivoc*, vol. 8, pp. 163–215, 2007.

- [51] J. M. Gallas and M. Eisner, "Fluorescence of melanin-dependence upon excitation wavelength and concentration," *Photochemistry and photobiology*, vol. 45, no. 5, pp. 595–600, 1987.
- [52] P. Kayatz, G. Thumann, T. T. Luther, J. F. Jordan, K. U. Bartz, P. J. Esser, and U. Schraermeyer, "Oxidation Causes Melanin Fluorescence," *Investigative ophthalmology & visual science*, vol. 42, no. 1, 2001.
- [53] H. M. Kalaji, V. Goltsev, K. Bosa, S. I. Allakhverdiev, R. J. Strasser, and Govindjee, "Experimental in vivo measurements of light emission in plants: a perspective dedicated to David Walker," *Photosynthesis Research*, vol. 114, no. 2, pp. 69–96, Dec. 2012.
- [54] E. Cadenas, A. Boveris, and B. Chance, "Low-level chemiluminescence of bovine heart submitochondrial particles," *Biochemical Journal*, vol. 186, no. 3, pp. 659–667, 1980.
- [55] F. Scholkmann, M. Cifra, T. A. Moraes, and C. de Mello Gallep, "Using multifractal analysis of ultra-weak photon emission from germinating wheat seedlings to differentiate between two grades of intoxication with potassium dichromate," *Journal of Physics: Conference Series*, vol. 329, p. 012020, Dec. 2011.
- [56] H. Iyozumi, K. Kato, C. Kageyama, H. Inagaki, A. Yamaguchi, K. Furuse, K. Baba, and H. Tsuchiya, "Plant defense activators potentiate the generation of elicitor-responsive photon emission in rice," *Physiological and Molecular Plant Pathology*, vol. 66, no. 1-2, pp. 68–74, Jan. 2005.
- [57] H. Inagaki, Y. Ishida, A. Uchino, K. Kato, C. Kageyama, H. Iyozumi, and H. Nukui, "Difference in ultraweak photon emissions between sulfonylurea-resistant and sulfonylurea-susceptible biotypes of *Scirpus juncooides* following the application of a sulfonylurea herbicide," *Weed Biology and Management*, vol. 8, no. 2, pp. 78–84, Jun. 2008.
- [58] H. Inagaki, T. Imaizumi, G.-X. Wang, T. Tominaga, K. Kato, H. Iyozumi, and H. Nukui, "Spontaneous ultraweak photon emission from rice (*Oryza sativa* L.) and paddy weeds treated with a sulfonylurea herbicide," *Pesticide Biochemistry and Physiology*, vol. 89, no. 2, pp. 158–162, Oct. 2007.
- [59] D. Slawinska, K. Polewski, and J. Slawinski, "The stress-induced electromagnetic emission from biosystems: chemiluminescence response of plants to mechanical and chemical damage," *Journal of Electroanalytical Chemistry*, vol. 343, no. 3, pp. 483–488, 1992.
- [60] A. Prasad, U. Ferretti, M. Sedlářová, and P. Pospíšil, "Singlet oxygen production in *Chlamydomonas reinhardtii* under heat stress," *Scientific Reports*, vol. 6, p. 20094, Feb. 2016.
- [61] L. V. Belousov, "Ultraweak Photon Emission as a Tool For Analysing Collective Processes in Cells and Developing Embryos," in *Biophotonics and Coherent Systems in Biology*, Boston, MA, 2005, pp. 139–157.
- [62] J. Kim, J. Lim, H. Kim, S. Ahn, S.-B. Sim, and K.-S. Soh, "Scanning Spontaneous Photon Emission From Transplanted Ovarian Tumor of Mice Using a Photomultiplier Tube," *Electromagnetic Biology and Medicine*, vol. 25, no. 2, pp. 97–102, Jan. 2006.
- [63] M. Takeda, M. Kobayashi, M. Takayama, S. Suzuki, T. Ishida, K. Ohnuki, T. Moriya, and N. Ohuchi, "Biophoton detection as a novel technique for cancer imaging," *Cancer Science*, vol. 95, no. 8, pp. 656–661, Aug. 2004.
- [64] F. Licastro, M. C. Morini, L. J. Davis, P. Malpassi, D. Cucinotta, R. Parente, C. Melotti, and G. Savorani, "Increased chemiluminescence response of neutrophils from the peripheral blood of patients with senile dementia of the Alzheimer's type," *Journal of Neuroimmunology*, vol. 51, no. 1, pp. 21–26, Apr. 1994.
- [65] Repetto, Reides, Evelson, Kohan, De Lustig, and Llesuy, "Peripheral markers of oxidative stress in probable Alzheimer patients: Oxidative stress in Alzheimer's disease," *European Journal of Clinical Investigation*, vol. 29, no. 7, pp. 643–649, Jul. 1999.

- [66] H. Inaba, A. Yamagishi, C. Takyu, B. Yoda, Y. Goto, T. Miyazawa, T. Kaneda, and A. Saeki, "Development of an ultra-high sensitive photon counting system and its application to biomedical measurements," *Optics and Lasers in Engineering*, vol. 3, no. 2, pp. 125–130, 1982.
- [67] J. Kim, Y.-u. Kim, Y. J. Lee, M. Kobayashi, Y. Tsutsumi, R. Kondo, S. K. Lee, and K.-S. Soh, "Spontaneous ultraweak photon emission during the growth of the cell population of cultured HeLa cell line," *Journal of health science*, vol. 53, no. 4, pp. 481–485, 2007.
- [68] R. Van Wijk, F. Wiegant, F. A. Popp, and G. Storms, "Biophoton emission from blood serum of diabetic patients," in *International Symposium on Biomedical Optics Europe'94*. International Society for Optics and Photonics, 1994, pp. 212–223.
- [69] W. Baader, C. Bohne, G. Cilento, and H. Dunford, "Peroxidase-catalyzed formation of triplet acetone and chemiluminescence from isobutyraldehyde and molecular oxygen." *Journal of Biological Chemistry*, vol. 260, no. 18, pp. 10 217–10 225, 1985.
- [70] F. H. Bartoloni, M. A. d. Oliveira, F. A. Augusto, L. F. M. Ciscato, E. L. Bastos, and W. J. Baader, "Synthesis of unstable cyclic peroxides for chemiluminescence studies," *Journal of the Brazilian Chemical Society*, vol. 23, no. 11, pp. 2093–2103, 2012.
- [71] R. C. Allen, D. C. Dale, and F. B. Taylor, "Blood phagocyte luminescence: gauging systemic immune activation," *Methods in enzymology*, vol. 305, pp. 591–629, 2000.
- [72] R. C. Allen, "Chemiluminescence from Eukaryotic and Prokaryotic Cells: Reducing Potential and Oxygen Requirements*," *Photochemistry and Photobiology*, vol. 30, no. 1, pp. 157–163, 1979.
- [73] R. Bajpai, "Squeezed state description of spectral decompositions of a biophoton signal," *Physics Letters A*, vol. 337, no. 4-6, pp. 265–273, Apr. 2005.
- [74] —, "Biophoton emission in a squeezed state from a sample of *Parmelia tinctorum*," *Physics Letters A*, vol. 322, no. 1-2, pp. 131–136, Feb. 2004.
- [75] M. H. de Medeiros and E. J. Bechara, "Chemiluminescent aerobic oxidation of protein adducts with glycolaldehyde catalyzed by horseradish peroxidase," *Archives of Biochemistry and Biophysics*, vol. 248, no. 1, pp. 435–439, Jul. 1986.
- [76] G. S. Timmins, R. E. dos Santos, A. C. Whitwood, L. H. Catalani, P. Di Mascio, B. C. Gilbert, and E. J. H. Bechara, "Lipid Peroxidation-Dependent Chemiluminescence from the Cyclization of Alkylperoxyl Radicals to Dioxetane Radical Intermediates," *Chemical Research in Toxicology*, vol. 10, no. 10, pp. 1090–1096, Oct. 1997.
- [77] L. V. Belousov, A. B. Burlakov, and N. N. Luchinskaya, "Statistical and frequency-amplitude characteristics of ultraweak emissions of the loach eggs and embryos under the normal conditions and during their optic interactions. 1. Characteristics of ultraweak emission in normal development and the optic role of egg envelopes," *Russian Journal of Developmental Biology*, vol. 33, no. 3, pp. 174–181, 2002.
- [78] —, "Statistical and Frequency-Amplitude Characteristics of Ultraweak Emissions of the Loach Eggs and Embryos under the Normal Conditions and upon Their Optic Interactions. 2. Changes in Characteristics of Ultraweak Emissions upon Optic Interaction of Groups of Embryos of Different Ages," *Russian Journal of Developmental Biology*, vol. 34, no. 6, pp. 379–388, 2003.
- [79] A. B. Burlakov, O. V. Burlakova, and V. A. Golichenkov, "Distant wave-mediated interactions in early embryonic development of the loach *Misgurnus fossilis* L." *Russian Journal of Developmental Biology*, vol. 31, no. 5, pp. 287–292, 2000.
- [80] I. V. Volodyaev and L. V. Belousov, "Ultraweak emissions of developing *Xenopus laevis* eggs and embryos," *Russian Journal of Developmental Biology*, vol. 38, no. 5, pp. 322–328, Sep. 2007.

- [81] A. V. Budagovsky, "On the ability of cells to distinguish the coherence of optical radiation," *Quantum Electronics*, vol. 35, no. 4, pp. 369–374, Apr. 2005.
- [82] I. F. Borodin, A. V. Budagovskii, O. N. Budagovskaya, I. A. Budagovskii, and Y. A. Sudnik, "Using the effect of photoinduced variability of optical properties of chlorophyll-containing tissues for diagnosing the functional state of plants," *Russian Agricultural Sciences*, vol. 34, no. 5, pp. 357–359, Oct. 2008.
- [83] E. Cadenas, H. Wefers, and H. Sies, "Low-Level Chemiluminescence of Isolated Hepatocytes," *European Journal of Biochemistry*, vol. 119, no. 3, pp. 531–536, 1981.
- [84] G. Cilento and W. Adam, "From free radicals to electronically excited species," *Free Radical Biology and Medicine*, vol. 19, no. 1, pp. 103–114, 1995.
- [85] T. A. Moraes, P. W. Barlow, E. Klingel , and C. M. Gallep, "Spontaneous ultra-weak light emissions from wheat seedlings are rhythmic and synchronized with the time profile of the local gravimetric tide," *Naturwissenschaften*, vol. 99, no. 6, pp. 465–472, Jun. 2012.
- [86] C. M. Gallep and S. R. Dos Santos, "Photon-counts during germination of wheat (*Triticum aestivum*) in wastewater sediment solutions correlated with seedling growth," *Seed Science and Technology*, vol. 35, no. 3, pp. 607–614, 2007.
- [87] C. Gallep, E. Conforti, M. Braghini, M. Maluf, Y. Yan, and F. Popp, "Ultra-weak delayed luminescence in coffee seeds (*Coffea arabica* and *C. canephora*) and their germination potential: some indications for a photonic approach in seed viability," in *Proceeding of 11th Brazilian Symposium of Microwave and Optoelectronics*, 2004.
- [88] C. de Mello Gallep, "Ultraweak, spontaneous photon emission in seedlings: toxicological and chronobiological applications: UPE in seedlings - applications," *Luminescence*, vol. 29, no. 8, pp. 963–968, Dec. 2014.
- [89] C. M. Gallep, D. C. Batista, C. A. Pereira, V. M. Oliveira, and N. A. Siqueira, "Ultra-weak light emission of *Daphnia similis* stressed by $K_2Cr_2O_7$ solutions," in *Microwave and Optoelectronics Conference, 2007. IMOC 2007. SBMO/IEEE MTT-S International*. IEEE, 2007, pp. 241–244.
- [90] A. Gurvich, G. Kufal', A. Bat'yanov, and N. Lazurkina, "Physicochemical processes in a photoexcited glycine solution," *Bulletin of Experimental Biology and Medicine*, vol. 104, no. 6, pp. 1684–1686, 1987.
- [91] A. Gurvich and T. Livanova, "Dependence of mitogenetic radiation and unbalanced molecular organization of liver cells on vagus nerve stimulation," *Bulletin of Experimental Biology and Medicine*, vol. 89, no. 2, pp. 156–158, 1980.
- [92] A. Gurvich, "Mitogenetic radiation spectra of muscles as an indicator of the dynamic molecular organization of the sarcoplasm," *Bulletin of Experimental Biology and Medicine*, vol. 62, no. 2, pp. 894–896, 1966.
- [93] A. Gurwitsch, L. Gurwitsch, "Ultra-violet chemi-luminescence," *Nature*, vol. 143, no. 3633, pp. 1022–1023, 1939.
- [94] A. Gurwitsch, V. Eremeyev, and Y. A. Karabchievsky, "Ultra-Weak Emission in the Visible and Ultra-Violet Regions in Oxidation of Solutions of Glycine by Hydrogen Peroxide," *Nature*, vol. 206, no. 4979, pp. 20–22, 1965.
- [95]  . Hideg, M. Kobayashi, and H. Inaba, "Spontaneous ultraweak light emission from respiring spinach leaf mitochondria," *Biochimica et Biophysica Acta (BBA)-Bioenergetics*, vol. 1098, no. 1, pp. 27–31, 1991.
- [96]  . Hideg, "On the spontaneous ultraweak light emission of plants," *Journal of Photochemistry and Photobiology B: Biology*, vol. 18, no. 2, pp. 239–244, 1993.

- [97] É. Hideg, M. Kobayashi, and H. Inaba, “Delayed fluorescence and ultraweak light emission from isolated chloroplasts (comparison of emission spectra and concentration dependence),” *Plant and cell physiology*, vol. 33, no. 6, pp. 689–693, 1992.
- [98] H. Inaba, “Measurement of biophoton from human body,” *Journal of International Society of Life Information Science*, vol. 18, pp. 448–452, 2000.
- [99] R. Scott, M. Usa, and H. Inaba, “Ultraweak emission imagery of mitosing soybeans,” *Applied Physics B: Lasers and Optics*, vol. 48, no. 2, pp. 183–185, 1989.
- [100] M. Kobayashi, D. Kikuchi, and H. Okamura, “Imaging of Ultraweak Spontaneous Photon Emission from Human Body Displaying Diurnal Rhythm,” *PLoS ONE*, vol. 4, no. 7, p. e6256, Jul. 2009.
- [101] M. Kobayashi, T. Iwasa, and M. Tada, “Polychromatic spectral pattern analysis of ultra-weak photon emissions from a human body,” *Journal of Photochemistry and Photobiology B: Biology*, vol. 159, pp. 186–190, Jun. 2016.
- [102] M. Kobayashi, M. Takeda, T. Sato, Y. Yamazaki, K. Kaneko, K.-I. Ito, H. Kato, and H. Inaba, “In vivo imaging of spontaneous ultraweak photon emission from a rat’s brain correlated with cerebral energy metabolism and oxidative stress,” *Neuroscience research*, vol. 34, no. 2, pp. 103–113, 1999.
- [103] M. Kobayashi, B. Devaraj, M. Usa, Y. Tanno, M. Takeda, and H. Inaba, “Two-dimensional Imaging of Ultraweak Photon Emission from Germinating Soybean Seedlings with a Highly Sensitive CCD Camera,” *Photochemistry and Photobiology*, vol. 65, no. 3, pp. 535–537, Mar. 1997.
- [104] S. Miyamoto, G. R. Martinez, D. Rettori, O. Augusto, M. H. Medeiros, and P. Di Mascio, “Linoleic acid hydroperoxide reacts with hypochlorous acid, generating peroxy radical intermediates and singlet molecular oxygen,” *Proceedings of the National Academy of Sciences of the United States of America*, vol. 103, no. 2, pp. 293–298, 2006.
- [105] S. Miyamoto, G. E. Ronsein, T. C. Corrêa, G. R. Martinez, M. H. G. Medeiros, and P. Di Mascio, “Direct evidence of singlet molecular oxygen generation from peroxyxynitrate, a decomposition product of peroxyxynitrite,” *Dalton Transactions*, no. 29, p. 5720, 2009.
- [106] P. Di Mascio, G. R. Martinez, S. Miyamoto, G. E. Ronsein, M. H. G. Medeiros, and J. Cadet, “Singlet Molecular Oxygen Reactions with Nucleic Acids, Lipids, and Proteins,” *Chemical Reviews*, vol. 119, no. 3, pp. 2043–2086, Feb. 2019.
- [107] F.-A. Popp, “On the Coherence of Ultraweak Photonemission from Living Tissues,” in *Disequilibrium and Self-Organisation*, ser. Mathematics and Its Applications, C. W. Kilmister, Ed. Dordrecht: Springer Netherlands, 1986, pp. 207–230.
- [108] S. Cohen and F. Popp, “Biophoton emission of the human body,” *Journal of Photochemistry and Photobiology B: Biology*, vol. 40, no. 2, pp. 187–189, 1997.
- [109] A. Rastogi and P. Pospíšil, “Ultra-weak photon emission as a non-invasive tool for the measurement of oxidative stress induced by UVA radiation in *Arabidopsis thaliana*,” *Journal of Photochemistry and Photobiology B: Biology*, vol. 123, pp. 59–64, Jun. 2013.
- [110] A. Prasad, P. Gouripeddi, H. R. N. Devireddy, A. Ovsii, D. P. Rachakonda, R. V. Wijk, and P. Pospíšil, “Spectral Distribution of Ultra-Weak Photon Emission as A Response to Wounding in Plants: An In Vivo Study,” *Biology*, vol. 9, no. 6, p. 139, Jun. 2020.
- [111] A. Prasad, M. Sedlářová, A. Balukova, M. Rác, and P. Pospíšil, “Reactive Oxygen Species as a Response to Wounding: In Vivo Imaging in *Arabidopsis thaliana*,” *Frontiers in Plant Science*, vol. 10, p. 1660, Jan. 2020.

- [112] A. Prasad and P. Pospíšil, "Two-dimensional imaging of spontaneous ultra-weak photon emission from the human skin: role of reactive oxygen species," *Journal of Biophotonics*, vol. 4, no. 11-12, pp. 840–849, Nov. 2011.
- [113] A. Prasad, A. Balukova, and P. Pospíšil, "Triplet Excited Carbonyls and Singlet Oxygen Formation During Oxidative Radical Reaction in Skin," *Frontiers in Physiology*, vol. 9, p. 9, 2018.
- [114] A. Prasad, H. Duchová, R. R. Manoharan, D. Rathi, and P. Pospíšil, "Imaging and Characterization of Oxidative Protein Modifications in Skin," *International Journal of Molecular Sciences*, vol. 24, no. 4, p. 3981, Jan. 2023.
- [115] T. Quickenden, A. Matich, S. Pung, and R. Tilbury, "An attempt to stimulate cell division in *Saccharomyces cerevisiae* with weak ultraviolet light," *Radiation research*, vol. 117, no. 1, pp. 145–157, 1989.
- [116] T. I. Quickenden and R. N. Tilbury, "Luminescence spectra of exponential and stationary phase cultures of respiratory deficient *Saccharomyces cerevisiae*," *Journal of Photochemistry and Photobiology B: Biology*, vol. 8, no. 2, pp. 169–174, 1991.
- [117] R. Tilbury and T. Quickenden, "Luminescence from the yeast *Candida utilis* and comparisons across three genera," *Luminescence*, vol. 7, no. 4, pp. 245–253, 1992.
- [118] H. Sies, "Physiological society symposium: Impaired endothelial and smooth muscle cell function in oxidative stress," *Exp. Physiol*, vol. 82, pp. 291–295, 1997.
- [119] H. Sies, C. Berndt, and D. P. Jones, "Oxidative Stress," *Annual Review of Biochemistry*, vol. 86, no. 1, pp. 715–748, 2017.
- [120] A. Ezzahir, M. Godlewski, M. Krol, T. Kwiecinska, Z. Rajfur, D. Sitko, and J. Slawinski, "The influence of environmental factors on the ultraweak luminescence from yeast *Saccharomyces cerevisiae*," *Journal of Electroanalytical Chemistry*, vol. 342, no. 1, pp. 57–61, 1992.
- [121] D. Slawinska and J. Slawinski, "Chemiluminescence of cereal products I. Kinetics, activation energy and effect of solvents," *Journal of bioluminescence and chemiluminescence*, vol. 12, no. 5, pp. 249–259, 1997.
- [122] D. Sławinska and J. Sławinski, "Chemiluminescence of cereal products. II. Chemiluminescence spectra," *Journal of bioluminescence and chemiluminescence*, vol. 13, no. 1, pp. 13–19, 1998.
- [123] W. Gorączko and J. slawiński, "SECONDARY ULTRAWEAK LUMINESCENCE FROM HUMIC ACIDS INDUCED BY γ -RADIATION," *Nonlinearity in Biology, Toxicology, and Medicine*, vol. 2, no. 3, pp. 245–258, Jul. 2004.
- [124] P. Pluciński, Z. Górski, and J. Sławiński, "Resistance of model humic acids to ultraviolet-c radiation," *Acta Agrophysica*, vol. 9, no. 1, pp. 191–202, 2007.
- [125] J. Stauff and P. Bartolmes, "Chemiluminescence on Oxidative Formation of Triplet States of Anthrasemiquinone-and Anthraquinone-2-sulfonate," *Angewandte Chemie International Edition in English*, vol. 9, no. 4, pp. 307–308, 1970.
- [126] G. F. Fedorova, V. D. Kancheva, V. A. Menshov, V. V. Naumov, R. F. Vasil'ev, T. L. Veprintsev, A. V. Trofimov, Y. B. Tsaplev, and O. I. Yablonskaya, "Exogenous and Endogenous Mediators of Oxygen Metabolism: Alternatives for Chemical and Biological Activity," in *Studies in Natural Products Chemistry*. Elsevier, 2016, vol. 47, pp. 357–385.
- [127] R. F. Vasil'ev and G. F. Fedorova, "Asymmetric $\text{PhCH}(\text{CH}_3)\text{CH}_2\text{OOOC}(\text{CH}_3)_2\text{Ph}$ Tetroxide as an Intermediate in Chain-Termination Processes and Chemiluminescence Excitation in the Oxidation of Cumene," *Kinetics and Catalysis*, vol. 45, no. 5, pp. 655–661, Sep. 2004.

- [128] R. F. Vasil'ev, A. V. Trofimov, and Y. B. Tsaplev, "Chemiluminescence of indole and its derivatives," *Russian Chemical Reviews*, vol. 79, no. 2, pp. 77–88, Feb. 2010.
- [129] R. F. Vasil'ev, V. D. Kancheva, V. V. Naumov, A. K. Slavova-Kazakova, A. V. Trofimov, G. F. Fedorova, and O. I. Yablonskaya, "Extreme Kinetics of Chemiluminescence in the Initiated Oxidation of Vegetable Lipids," *Russian Journal of Physical Chemistry B*, vol. 14, no. 3, pp. 479–482, May 2020.
- [130] Y. A. Vladimirov, E. V. Proskurnina, and D. Y. Izmailov, "Chemiluminescence as a method for detection and study of free radicals in biological systems," *Bulletin of experimental biology and medicine*, vol. 144, no. 3, pp. 390–396, 2007.
- [131] I. P. Ivanova, S. V. Trofimova, I. M. Piskarev, N. A. Aristova, O. E. Burhina, and O. O. Soshnikova, "Mechanism of chemiluminescence in Fenton reaction," *Journal of Biophysical Chemistry*, vol. 03, no. 01, pp. 88–100, 2012.
- [132] E. van Wijk, M. Kobayashi, R. van Wijk, and J. van der Greef, "Imaging of Ultra-Weak Photon Emission in a Rheumatoid Arthritis Mouse Model," *PLoS ONE*, vol. 8, no. 12, p. e84579, Dec. 2013.
- [133] R. Van Wijk, M. Kobayashi, and E. P. Van Wijk, "Anatomic characterization of human ultra-weak photon emission with a moveable photomultiplier and CCD imaging," *Journal of Photochemistry and Photobiology B: Biology*, vol. 83, no. 1, pp. 69–76, Apr. 2006.
- [134] E. P. Van Wijk and R. Van Wijk, "Multi-Site Recording and Spectral Analysis of Spontaneous Photon Emission from Human Body," *Forschende Komplementärmedizin / Research in Complementary Medicine*, vol. 12, no. 2, pp. 96–106, Apr. 2005.
- [135] E. P. Van Wijk, R. V. Wijk, R. P. Bajpai, and J. van der Greef, "Statistical analysis of the spontaneously emitted photon signals from palm and dorsal sides of both hands in human subjects," *Journal of Photochemistry and Photobiology B: Biology*, vol. 99, no. 3, pp. 133–143, Jun. 2010.
- [136] R. van Wijk, J. van der Greef, and E. van Wijk, "Human ultraweak photon emission and the yin yang concept of Chinese medicine," *Journal of acupuncture and meridian studies*, vol. 3, no. 4, pp. 221–231, 2010.
- [137] R. Van Wijk, K.-S. Soh, and E. P. Van Wijk, "Anatomic characterization of acupuncture system and ultra-weak photon emission," *Asian J Phys*, vol. 16, no. 4, pp. 443–474, 2007.
- [138] E. P. Van Wijk, H. Koch, S. Bosman, and R. Van Wijk, "Anatomic characterization of human ultra-weak photon emission in practitioners of Transcendental Meditation and control subjects," *The Journal of Alternative and Complementary Medicine*, vol. 12, no. 1, pp. 31–38, 2006.
- [139] A. Rastogi and P. Pospíšil, "Ultra-weak photon emission as a non-invasive tool for monitoring of oxidative processes in the epidermal cells of human skin: comparative study on the dorsal and the palm side of the hand," *Skin Research and Technology*, vol. 16, pp. 365–370, Mar. 2010.
- [140] R. Van Wijk, E. P. Van Wijk, H. A. van Wietmarschen, and J. v. d. Greef, "Towards whole-body ultra-weak photon counting and imaging with a focus on human beings: A review," *Journal of Photochemistry and Photobiology B: Biology*, vol. 139, pp. 39–46, Oct. 2014.
- [141] M. Calcerrada and C. Garcia-Ruiz, "Human Ultraweak Photon Emission: Key Analytical Aspects, Results and Future Trends – A Review," *Critical Reviews in Analytical Chemistry*, vol. 49, no. 4, pp. 368–381, Jul. 2019.
- [142] M. He, M. Sun, E. van Wijk, H. van Wietmarschen, R. van Wijk, Z. Wang, M. Wang, T. Hankemeier, and J. van der Greef, "A Chinese literature overview on ultra-weak photon emission as promising technology for studying system-based diagnostics," *Complementary Therapies in Medicine*, vol. 25, pp. 20–26, Apr. 2016.

- [143] D.-I. Seo, F. M. Laager, K. Young, H. Chang, W.-Y. So, H.-T. Kim, K.-S. Soh, and W. Song, "Ultra-weak photon emission during wrist curl and cycling exercises in trained healthy men," *Electromagnetic Biology and Medicine*, vol. 31, no. 2, pp. 122–131, Jun. 2012.
- [144] F. Laager, S.-H. Park, J.-M. Yang, W. Song, and K.-S. Soh, "Effects of exercises on biophoton emission of the wrist," *European journal of applied physiology*, vol. 102, no. 4, pp. 463–469, 2008.
- [145] R. Van Wijk and E. P. Wijk, "An Introduction to Human Biophoton Emission," *Forschende Komplementärmedizin / Research in Complementary Medicine*, vol. 12, no. 2, pp. 77–83, Apr. 2005.
- [146] M. Cifra, E. Van Wijk, H. Koch, S. Bosman, and R. Van Wijk, "Spontaneous ultra-weak photon emission from human hands is time dependent," *Radioengineering*, vol. 16, no. 2, p. 15, 2007.
- [147] S. Cohen and F. Popp, "Low-level luminescence of the human skin," *Skin Research and Technology*, vol. 3, no. 3, pp. 177–180, 1997.
- [148] F. Scholkmann, E. van de Kraats, R. van Wijk, E. van Wijk, and J. van der Greef, "Spatio-temporal dynamics of spontaneous ultra-weak photon emission (autoluminescence) from human hands measured with an EMCCD camera: Dependence on time of day, date and individual subject," *Matters*, Mar. 2018.
- [149] X. Zhao, E. van Wijk, Y. Yan, R. van Wijk, H. Yang, Y. Zhang, and J. Wang, "Ultra-weak photon emission of hands in aging prediction," *Journal of Photochemistry and Photobiology B: Biology*, vol. 162, pp. 529–534, Sep. 2016.
- [150] F. Zapata, V. Pastor-Ruiz, F. Ortega-Ojeda, G. Montalvo, A. V. Ruiz-Zolle, and C. García-Ruiz, "Human ultra-weak photon emission as non-invasive spectroscopic tool for diagnosis of internal states – A review," *Journal of Photochemistry and Photobiology B: Biology*, vol. 216, p. 112141, Mar. 2021.
- [151] H. Ou-Yang, "The application of ultra-weak photon emission in dermatology," *Journal of Photochemistry and Photobiology B: Biology*, vol. 139, pp. 63–70, Oct. 2014.
- [152] Y. Gabe, K. Takeda, M. Tobiishi, S. Kikuchi, K. Tsuda, Y. Haryuu, Y. Nakajima, Y. Inomata, S. Nakamura, D. Murase, S. Tokunaga, M. Miyaki, and Y. Takahashi, "Evaluation of subclinical chronic sun damage in the skin via the detection of long-lasting ultraweak photon emission," *Skin Research and Technology*, vol. 27, no. 6, pp. 1064–1071, 2021, [_eprint: https://onlinelibrary.wiley.com/doi/pdf/10.1111/srt.13059](https://onlinelibrary.wiley.com/doi/pdf/10.1111/srt.13059).
- [153] K. Tsuchida and M. Kobayashi, "Ultraviolet A irradiation induces ultraweak photon emission with characteristic spectral patterns from biomolecules present in human skin," *Scientific Reports*, vol. 10, no. 1, p. 21667, Dec. 2020.
- [154] K. Tsuchida, N. Sakiyama, Y. Ogura, and M. Kobayashi, "Skin lightness affects ultraviolet A-induced oxidative stress: evaluation using ultraweak photon emission measurement," *Experimental Dermatology*, vol. 32, no. 2, pp. 146–53, 2023, [_eprint: https://onlinelibrary.wiley.com/doi/pdf/10.1111/exd.14690](https://onlinelibrary.wiley.com/doi/pdf/10.1111/exd.14690).
- [155] F. Musumeci, L. A. Applegate, G. Privitera, A. Scordino, S. Tudisco, and H. J. Niggli, "Spectral analysis of laser-induced ultraweak delayed luminescence in cultured normal and tumor human cells: temperature dependence," *Journal of Photochemistry and Photobiology B: Biology*, vol. 79, no. 2, pp. 93–99, May 2005.
- [156] R. Hagens, F. Khabiri, V. Schreiner, H. Wenck, K.-P. Wittern, H.-J. Duchstein, and W. Mei, "Non-invasive monitoring of oxidative skin stress by ultraweak photon emission measurement. II: biological validation on ultraviolet A-stressed skin," *Skin Research and Technology*, vol. 14, pp. 112–20, 2008.
- [157] M. Kobayashi, "Highly sensitive imaging for ultra-weak photon emission from living organisms," *Journal of Photochemistry and Photobiology B: Biology*, vol. 139, pp. 34–38, Oct. 2014.

- [158] Hamamatsu Photonics K.K., “Electron Multiplying Charge-Coupled Devices (EMCCDs).”
- [159] H. P. K.K., “Photomultiplier tubes, basics and applications, Fourth edition,” 2017.
- [160] ———, “Photomultiplier tubes, construction and operating characteristics connections to external circuits.”
- [161] S. R. S. Company, “Signal recovery with PMTs.”
- [162] Oxford Instruments Andor, “Electron Multiplying CCD Cameras.”
- [163] O. I. Andor, “What is an EMCCD Camera?” 2021.
- [164] Teledyne Princeton Instruments, “EMCCD Sensors:the basics.”
- [165] ———, “Silicon-based CCDs: The basics.”
- [166] M. Fox, *Quantum optics: an introduction*, ser. Oxford master series in physics. Oxford ; New York: Oxford University Press, 2006, no. 15.
- [167] S. Anders and W. Huber, “Differential expression analysis for sequence count data,” *Genome Biology*, vol. 11, no. 10, p. R106, Oct. 2010.
- [168] T. D. Ahle, “Sharp and simple bounds for the raw moments of the binomial and Poisson distributions,” *Statistics & Probability Letters*, vol. 182, p. 109306, Mar. 2022.
- [169] I. R. Epstein, K. Kustin, P. De Kepper, and M. Orbán, “Oscillating chemical reactions,” *Scientific American*, vol. 248, no. 3, pp. 112–123, 1983.
- [170] I. R. Epstein and K. Showalter, “Nonlinear chemical dynamics: oscillations, patterns, and chaos,” *The Journal of Physical Chemistry*, vol. 100, no. 31, pp. 13 132–13 147, 1996.
- [171] D. Lloyd, “Systems dynamics of biology,” *J Appl Biomed*, vol. 3, no. 1.12, 2005.
- [172] R. Kopelman, “Fractal reaction kinetics,” *Science*, vol. 241, no. 4873, pp. 1620–1626, 1988.
- [173] J. Prasad and R. Kopelman, “Fractal-like molecular reaction kinetics: solute photochemistry in porous membranes,” *Journal of Physical Chemistry*, vol. 91, no. 2, pp. 265–266, 1987.
- [174] M. C. Teich, “Fractal character of the auditory neural spike train,” *IEEE Transactions on Biomedical Engineering*, vol. 36, no. 1, pp. 150–160, 1989.
- [175] R. Van Wijk, E. P. Van Wijk, and R. P. Bajpai, “Photocount distribution of photons emitted from three sites of a human body,” *Journal of Photochemistry and Photobiology B: Biology*, vol. 84, no. 1, pp. 46–55, Jul. 2006.
- [176] E. v. Wijk, J. v. d. Greef, and R. v. Wijk, “Photon Counts Statistics in Leukocyte Cell Dynamics,” *Journal of Physics: Conference Series*, vol. 329, p. 012021, Dec. 2011.
- [177] H. E. Stanley, L. N. Amaral, A. L. Goldberger, S. Havlin, P. C. Ivanov, and C.-K. Peng, “Statistical physics and physiology: monofractal and multifractal approaches,” *Physica A: Statistical Mechanics and its Applications*, vol. 270, no. 1, pp. 309–324, 1999.
- [178] F. Scholkmann, O. Schraa, R. van Wijk, and M. Wolf, “The effect of venous and arterial occlusion of the arm on changes in tissue hemodynamics, oxygenation, and ultra-weak photon emission,” in *Oxygen Transport to Tissue XXXIV*. Springer, 2013, pp. 257–264.
- [179] B. Cheson, R. Christensen, R. Sperling, B. Kohler, and B. Babior, “The origin of the chemiluminescence of phagocytosing granulocytes.” *Journal of Clinical Investigation*, vol. 58, no. 4, p. 789, 1976.

- [180] J. Slawinski, E. Grabikowski, and L. Ciesla, “Spectral distribution of the ultraweak luminescence from germinating plants,” *Journal of Luminescence*, vol. 24, pp. 791–794, 1981.
- [181] T. I. Quickenden and S. S. Q. Hee, “The spectral distribution of the luminescence emitted during growth of the yeast *Saccharomyces cerevisiae* and its relationship to mitogenetic radiation,” *Photochemistry and photobiology*, vol. 23, no. 3, pp. 201–204, 1976.
- [182] R. N. Tilbury and T. I. Quickenden, “Spectral and time dependence studies of the ultra weak bioluminescence emitted by the bacterium *Escherichia coli*,” *Photochemistry and Photobiology*, vol. 47, no. 1, pp. 145–150, 1988.
- [183] H. Iyozumi, K. Kato, and T. Makino, “Spectral Shift of Ultraweak Photon Emission from Sweet Potato During a Defense Response,” *Photochemistry and Photobiology*, vol. 75, no. 3, pp. 322–325, May 2007.
- [184] M. Havaux and B. Ksas, “Imaging of Lipid Peroxidation-Associated Chemiluminescence in Plants: Spectral Features, Regulation and Origin of the Signal in Leaves and Roots,” *Antioxidants*, vol. 11, no. 7, p. 1333, Jul. 2022.
- [185] X. Zhao, M. Yang, Y. Wang, J. Pang, E. V. Wijk, Y. Liu, H. Fan, L. Zhang, and J. Han, “Spectrum of spontaneous photon emission as a promising biophysical indicator for breast cancer research,” *Scientific Reports*, vol. 7, no. 1, Dec. 2017.
- [186] M. Yang, J. Pang, J. Liu, Y. Liu, H. Fan, and J. Han, “Spectral discrimination between healthy people and cold patients using spontaneous photon emission,” *Biomedical Optics Express*, vol. 6, no. 4, p. 1331, Apr. 2015.
- [187] T. Iwasa and M. Kobayashi, “Imaging and Spectral Analysis of Ultra-weak Biophoton Emission and Delayed Luminescence from Human Skin,” in *CLEO Pacific Rim Conference*. Hong Kong: OSA, 2018, p. W3A.131.
- [188] R. Q. Scott and H. Inaba, “Single photon counting imagery,” *Journal of Bioluminescence and Chemiluminescence*, vol. 4, no. 1, pp. 507–511, Jul. 1989.
- [189] I. Volodyaev, E. Van Wijk, M. Cifra, and Y. A. Vladimirov, Eds., *Ultra-Weak Photon Emission from Biological Systems: Endogenous Biophotonics and Intrinsic Bioluminescence*. Cham: Springer International Publishing, 2023. [Online]. Available: <https://link.springer.com/10.1007/978-3-031-39078-4>
- [190] T. Nagoshi, N. Watanabe, S. Suzuki, M. Usa, H. Watanabe, T. Ichimura, and H. Inaba, “SPECTRAL ANALYSES OF LOW LEVEL CHEMILUMINESCENCE OF A SHORT LIFETIME USING A HIGHLY SENSITIVE POLYCHROMATIC SPECTROMETER INCORPORATING A TWO DIMENSIONAL PHOTON-COUNTING TYPE DETECTOR,” *Photochemistry and Photobiology*, vol. 56, no. 1, pp. 89–94, Jul. 1992.
- [191] Z. Wang, Z. Xu, Y. Luo, S. Peng, H. Song, T. Li, J. Zheng, N. Liu, S. Wu, J. Zhang, L. Zhang, Y. Hu, Y. Liu, D. Lu, J. Dai, and J. Zhang, “Reduced biophotonic activities and spectral blueshift in Alzheimer’s disease and vascular dementia models with cognitive impairment,” *Frontiers in Aging Neuroscience*, vol. 15, 2023.
- [192] S. Rihova, “Measurement of ultra weak photon emission from biological samples,” Ph.D. dissertation, Czech Technical University in Prague, Faculty of Electrical Engineering, Department of Circuit Theory, Jan. 2012.
- [193] B. Ondrušová, “Measurement Optimization and Analysis of Selected Physical and Chemical Effects on the Ultra-Weak Proton Emission from a Human Hand,” Master’s thesis, CZECH TECHNICAL UNIVERSITY IN PRAGUE, Faculty of Electrical Engineering, Department of Circuit Theory, 2016.

- [194] H. P. K.K., “Photomultiplier tubes and related products,” 2020.
- [195] K. Červinková, M. Nerudová, M. Cifra, J. Hašek, and J. Vrba, “Ultra Weak Photon Emission from *Saccharomyces Cerevisiae*.” in *PIERS Proceedings*, 2013.
- [196] K. Červinková and M. Nerudová, “Effects of diverse experimental conditions on the ultra- weak photon emission from yeast cells *Saccharomyces cerevisiae*,” 2014.
- [197] K. Červinková, M. Nerudová, J. Hašek, and M. Cifra, “Chemical modulation of the ultra-weak photon emission from *Saccharomyces cerevisiae* and differentiated HL-60 cells,” in *Photonics, Devices, and Systems VI*, P. Tománek, D. Senderáková, and P. Páta, Eds., vol. 9450. SPIE, 2015, pp. 169 – 175.
- [198] K. Cervinkova, M. Nerudova, M. Cifra, J. Hasek, and J. Vrba, “Two-channel measurement of the ultra-weak photon emission from a yeast culture during its growth,” in *2014 24th International Conference Radioelektronika*. Bratislava, Slovakia: IEEE, Apr. 2014, pp. 1–3.
- [199] M. Cifra, C. Brouder, M. Nerudová, and O. Kučera, “Biophotons, coherence and photocount statistics: A critical review,” *Journal of Luminescence*, vol. 164, pp. 38–51, Aug. 2015.
- [200] I. V. Meglinski and S. J. Matcher, “Quantitative assessment of skin layers absorption and skin reflectance spectra simulation in the visible and near-infrared spectral regions,” *Physiological Measurement*, vol. 23, no. 4, pp. 741–753, Nov. 2002.
- [201] R. R. Anderson and A. Parrish, “Optical Properties of Human Skin,” *The science of photomedicine*, pp. 147–194, 1982.
- [202] K. P. Nielsen, L. Zhao, J. J. Stamnes, K. Stamnes, and J. Moan, “The optics of human skin: Aspects important for human health,” *Solar radiation and human health*, vol. 1, no. 01, 2008.
- [203] M. Hulsbusch, D. Holscher, and V. Blazek, “Spectral Monte-Carlo Simulations of Photon Penetration in Biotissue in Visible and Near Infrared,” *Progress In Electromagnetics Research Symposium*, 2007.
- [204] Markus Hülbusch, “Ein bildgestütztes , funktionelles Verfahren zur optoelektronischen Erfassung der Hautperfusion,” Ph.D. dissertation, Fakultät für Elektrotechnik und Informationstechnik der Rheinisch-Westfälischen Technischen Hochschule Aachen, Germany, 2008.

LIST OF PUBLICATIONS RELATED TO THE DOCTORAL THESIS

All authors approved the quantitative contributions.

PAPERS IN PEER-REVIEWED JOURNALS WITH IMPACT FACTOR

- [A1] M. Poplová, A. Prasad, E. V. Wijk, P. Pospíšil and M. Cifra, "Biological Auto(chemi)luminescence Imaging of Oxidative Processes in Human Skin", *Analytical Chemistry*, vol. 95, issue 40, pages 14853–14860, 2023.
| Candidate's contribution: 55%
| Impact factor / Quartile (2022): 7.6 / Q1*
- [A2] M. Poplová, P. Sovka and M. Cifra, "Poisson pre-processing of nonstationary photonic signals: Signals with equality between mean and variance", *Plos one*, vol. 12, issue 12, pages e0188622, 2017.
| Candidate's contribution: 50%
| Impact factor / Quartile (2022): 2.766 / Q1
- [A3] N. Rafieiolhosseini*, M. Poplová*, P. Sasanpour, H. Rafii-Tabar, M. R. Alhossaini, Cifra, "Photocount statistics of ultra-weak photon emission from germinating mung bean", *Journal of Photochemistry and Photobiology B: Biology*, vol. 162, pages 50–55, 2016.
| Candidate's contribution: 30% (* equal contribution)
| Impact factor / Quartile (2016): 2.763 / Q3
- [A4] M. Dlask, J. Kukul, M. Poplová, P. Sovka, and M. Cifra, "Short-time fractal analysis of biological autoluminescence", *PLoS One*, vol. 14 (7), pages e0214427, 2019.
| Candidate's contribution: 10%
| Impact factor / Quartile (2019): 2.74 / Q2
- [A5] M. Cifra, C. Brouder, M. Nerudová (Poplová), O. Kučera, "Biophotons, coherence and photocount statistics: A critical review", *Journal of Luminescence*, vol. 164, pages 38–51, 2015.
| Candidate's contribution: 10%
| Impact factor / Quartile (2015): 2.693 / Q1
- [A6] O. Kučera, K. Červinková, M. Nerudová (Poplová), M. Cifra, "Spectral Perspective on the Electromagnetic Activity of Cells", *Current topics in medicinal chemistry*, vol. 15 (6), pages 513–522, 2015.
| Candidate's contribution: 10%
| Impact factor / Quartile (2015): 2.9 / Q2

PAPERS AND ABSTRACTS IN CONFERENCE PROCEEDINGS LISTED IN THE WEB OF KNOWLEDGE

- [C1] M. Nerudová (Poplová), K. Červinková, J. Hašek and M. Cifra, "Optical spectral analysis of ultra-weak photon emission from tissue culture and yeast cells", *Photonics, Devices, and Systems VI. SPIE*, pages 162-168, 2015.
| Candidate's contribution: 60 %
| Impact factor (2015): 0.533
- [C2] K. Červinková, M. Nerudová (Poplová), J. Hašek, M. Cifra, "Chemical modulation of the ultra-weak photon emission from *Saccharomyces cerevisiae* and differentiated HL-60 cells", *Photonics, Devices, and Systems VI. SPIE*, pages 169-175, 2015.
| Candidate's contribution: 15%
| Impact factor (2015): 0.533
- [C3] K. Červinková, M. Nerudová (Poplová), M. Cifra, J. Hašek, J. Vrba, "Two-channel measurement of the ultra-weak photon emission from a yeast culture during its growth", *24th International Conference Radioelektronika, IEEE*, pages 1-3, 2014.
- [C4] K. Červinková, M. Nerudová (Poplová), "Effects of diverse experimental conditions on the ultra-weak photon emission from yeast cells *Saccharomyces cerevisiae*", *POSTER 2014 - 18th International Student Conference on Electrical Engineering. Prague: Czech Technical University*, pages 1-5, 2014.
- [C5] K. Červinková, M. Nerudová (Poplová), . Cifra, J. Hašek, J. Vrba, "Ultra Weak Photon Emission from *Saccharomyces Cerevisiae*", *Proceedings of PIERS 2013 in Stockholm. Cambridge: Electromagnetics Academy*, pages 114-117, 2013.

UTILITY MODELS

- [U1] Michaela Nerudová (Poplová), Light-tight chamber for measuring photon emission from biological samples, registration number: 26119, application number: 2013-28492, owner: Institute of Photonics and Electronics of Academy of Sciences CR
- [U2] Michaela Nerudová (Poplová), Pointing light-tight chamber for parallel measurement of photon emission, registration number: 26574, application number: 2013-28829, owner: Institute of Photonics and Electronics of Academy of Sciences CR

CITATIONS IN WEB OF SCIENCE

H-index = 5

Times cites (without self-citations) = 44

RESEARCH PROJECTS AND CONTRACTS

- [P1] SubTHz on-chip devices for controlling protein nanomachines, GX20-06873X, Czech Science Foundation GA CR.
Member of the team
- [P2] Novel integrated approaches for research of biomedical effects of pulsed electric fields, No. SAV-15-22, Bilateral project between Czech and Slovak Academy of Sciences. *Member of the team*
- [P3] Biological Signals Analysis and Processing, No. SGS15/198/OHK3/3T/13, Student GA of CTU in Prague.
Member of the team
- [P4] Zkoumání fyzikálních základů interakce elektromagnetického pole s biomolekulami, buňkami a tkání, No. SAV-15-22, Bilateral project between Czech and Slovak Academy of Sciences. *Member of the team*
- [P5] Photonic biosignals: measurement and characterization, No. GP13-29294S, Czech Science Foundation.
Member of the team
- [P6] Biological Signals Analysis and Processing, No. SGS13/138/OHK3/2T/13, Student GA of CTU in Prague.
Member of the team
- [P7] (1) Měření ultraslabé emise fotonů z tkáňových kultur; (2) Měření ultraslabé emise fotonů z lidské kůže, SmartBrain s.r.o, 2012-2014.
Member of the team
- [P8] Research and Measurement of Signals Generated by Nanostructures, No. P102/11/0649, Czech Science Foundation GA CR.
Member of the team
- [P9] Development and production of a light-tight chamber for an EMCCD camera, Leiden University, The Netherlands.
Project manager

Experience

- 2012 – present
| photonic laboratory manager
| photonics systems - mentoring
| graduate student
Institute of Photonics and Electronics,
CAS, Prague, Czechia
- 02.2017–09.2022
| parental leave, Jan*2017, Jakub*2019
- 10.2015–01.2016
| Internship, Netherlands
Investigation of BAL from human skin
Leiden Academic Centre for Drug,
Faculty of Science, Leiden University
- 03.2014
| Internship, Germany
*Optical model of BAL propagation
in human skin*
MedIT, Helmholtz-Institute for Biomedical
Engineering, RWTH Aachen University

Education

- 2012 – present
| Ph.D. in Electrical Engineering Theory
CTU in Prague, Czechia
- 2010 – 2012
| MSc. in Biomedical Engineering
CTU in Prague, Czechia
- 2007 – 2010
| BSc. in Biomedical Technician
CTU in Prague, Czechia

Technical Skills

Experimental and Laboratory skills

- | photonics detectors systems
- | handling of cells
- | biochemical analysis

Software and analysis skills

- | Programming in MATLAB
- | drawing in PRO/ENGINEER
- | signals and statistics analysis

Training

- 2023
EBTT winter school, Slovenia
| Electroporation-based technologies
and treatments, University of Ljubljana
- 2016
Microscopy methods in biomedicine
| Institute of Molecular Genetics, CAS

Mentoring and Teaching

- 2017
supervisor of student science internship
| Melicharová, Otevřená věda, CAS
- 2015–2016
consultant for experimental part
| Ondrušová, Diploma thesis, CTU in Prague
- 2012–2013
Signal analysis-seminar
| Faculty of Electrical Engineering
CTU in Prague
- 2012–2013
Signal theory-seminar
| Faculty of Electrical Engineering
CTU in Prague

Achievements

- 2018
| 4th student poster's prize, Prague
CSNRS, URSI in Czechia and Slovakia
- 2015
| Invited talk
AMPER international trade fair
Brno, Czechia
- 2015
| International internship scholarship
Mobilit-Akce 200, CTU in Prague
- 2012
| Dean's Prize for the outstanding
diploma thesis

APPENDIX

THIS CHAPTER INCLUDES:

I) utility model: 26119

Light-tight chamber for measuring photon emission from biological samples

originator: M. Nerudová (**Poplová**); contribution: 100%

owner: Institute of Photonics and Electronics of the Czech Academy of Sciences

II) utility model: 26574

Positioning light-tight chamber for parallel measurement of photon emission samples

originator: M. Nerudová (**Poplová**); contribution: 100%

owner: Institute of Photonics and Electronics of the Czech Academy of Sciences

III) journal paper: [A6]

Biophotons, coherence and photocount statistics: A critical review

M. Cifra, C. Brouder, M. Nerudová (**Poplová**), O. Kučera

Journal of Luminescence, vol. 164, pages 38-51, 2015.

candidate's contribution: 10% (performed the calculations and analyzed the data)

Impact factor / Quartile (2015): 2.693 / Q1

UŽITNÝ VZOR

(19)
ČESKÁ
REPUBLIKA



ÚŘAD
PRŮMYSLOVÉHO
VLASTNICTVÍ

(21) Číslo přihlášky: **2013 - 28492**
(22) Přihlášeno: **19.09.2013**
(47) Zapsáno: **18.11.2013**

(11) Číslo dokumentu:

26119

(13) Druh dokumentu: **U1**

(51) Int. Cl.:
G01N 21/76 (2006.01)
G01N 21/01 (2006.01)

(73) Majitel:
Ústav fotoniky a elektroniky AV ČR, v.v.i., Praha, CZ

(72) Původce:
Nerudová Michaela Ing., Most, CZ

(54) Název užitého vzoru:
Světlotěsná komora pro měření fotonové emise z biologických vzorků

CZ 26119 U1

Úřad průmyslového vlastnictví v zápisném řízení nezjišťuje, zda předmět užitého vzoru splňuje podmínky způsobilosti k ochraně podle § 1 zák. č. 478/1992 Sb.

Světlotěsná komora pro měření fotonové emise z biologických vzorků

Oblast techniky

Technické řešení se týká světlotěsné komory pro měření ultra slabé fotonové emise z biologických vzorků, specializované pro měření lidských končetin či přístupem do vnitřku komory během měření.

Dosavadní stav techniky

Na trhu existují tři výrobci světlotěsných komor pro měření fotonové emise. Všechny tři komory jsou určeny pro měření s CCD kamerami. Na trhu není průmyslově vyráběna komora pro měření fotonásobičem. Rozdíl mezi senzory spočívá v typu získané informace. CCD kamery zaznamenávají prostorovou informaci o záření fotonů, zatímco fotonásobič zaznamenává časovou řadu bez prostorové informace. Výhodou fotonásobiče je okamžitá informace o počtu vyzářených fotonů, zatímco výsledek z CCD kamer se získává i několik hodin. Fotonásobič by právě proto, mohl být vhodnějším nástrojem pro diagnostiku v lékařství, potravinářství či zemědělství. První problém u průmyslově vyráběných komor je spojení fotonásobiče s komorou, protože každá komora je kompatibilní pouze s určitým typem CCD kamery. Druhou nevýhodou je nepřístupnost do vnitřku komory během měření, například z důvodu aplikace chemické látky do měřeného vzorku či pro měření fotonové emise z lidských končetin např. ruky.

Podstata technického řešení

Výše uvedené nevýhody řeší světlotěsná komora podle tohoto technického řešení. Komora obsahuje komponenty: víko, dno, stěnu pro rukáv, stěnu pro dveře, stěnu pro konektory a zadní stěnu. K víku je připojena příruba pro fotonásobič, ke stěně pro rukáv je připojena příruba pro rukáv, ke stěně pro dveře jsou připojeny dveře a k přírubě pro rukáv je připojen rukáv. Dále je ke dveřím připevněno madlo pro dveře, ke stěně pro dveře je připevněno madlo pro stěnu a ke stěně pro rukáv a zadní stěně je připevněno široké madlo.

Vnější rozměry komory mohou být v rozsahu od 20 do 120 cm, a to v jakémkoliv poměru stran. Vhodným materiálem pro výrobu komory jsou slitiny hliníku, které jsou pevné, lehké a dají se povrchově upravit. Pro světlotěsnou komoru byla použita povrchová úprava černý elox, který zlepšuje pevnostní vlastnosti materiálu a díky černé barvě je zajištěno vhodné prostředí pro měření fotonové emise.

Boky komory jsou spojeny za použití zámkového a šroubového spoje. Zámkový spoj zajistí neprůchodnost světla díky vytvořeným záhybům a šroubový spoj je slepý, tudíž se světlo nešíří ani podél šroubů. Víko a dno jsou spojeny s boky komory pomocí schodového přechodu a šroubového spoje, který je také slepý. Dveře a stěna komory obsahuje dvě drážky, které při zavření dveří tvoří zámkový spoj, který zajišťuje neprůchodnost světla kolem dveří. K dotěsnění dveří je ještě použito gumové těsnění, které vyplňuje drážky stěny pro dveře a kompresní klička, která je umístěna v madlu pro dveře. Ke stěně pro dveře je připojeno madlo pro stěnu, které slouží k zapření kompresní kličky a tím se zajišťuje dostatečné přitlačení dveří.

Světlotěsná komora má na víku připravené neprůchozí závity na dvě velikosti přírub pro různé typy fotonásobičů. CCD kamer či jejich chlazení. Pro jakýkoliv typ senzoru se dá vyrobit příruba na míru bez zásahu do sestavené komory. Výhodou tohoto řešení je možnost přizpůsobit měřicí komoru všem typům používaných senzorů za krátkou dobu a nízkou cenu.

Měření končetin či přístup do komory během měření je vyřešen pomocí příruby a rukávu. Do stěny komory je vyříznuta kruhová díra o průměru 14 až 20 cm, velikostí vhodná pro lidské končetiny. K této stěně je připevněna kruhová příruba, na kterou se připevňuje rukáv. Tento rukáv, musí být také světlotěsný, a proto je vyroben ze dvou vrstev. Rozměr rukávu může mít průměr od 14 do 20 cm a jeho délka od 35 do 60 cm. Vnitřní vrstva je tvořena zatemňovací černou látkou,

5 která se používá např. na výrobu závěsů ve fotografických ateliérech. Vnější vrstvu tvoří černá koženka. K zamezení šíření světla podél rukávu slouží tři tunýlky po jeho obvodu, ve kterých je gumička s brzdíčkou, která při stažení vytvoří rozčlenění rukávu. Příruba pro rukáv a rukáv tvoří dohromady řešení pro neprůchodnost světla i o velmi nízkých intenzitách dovnitř komory při používání rukávu při měření. Další výhodou je použití volně dostupných materiálů pro rukáv, což zajišťuje nízkou cenu nákladů na výrobu.

Přehled obrázků na výkresech

Na obrázku obr. 1 je zobrazena světlotěsná komora z pravého horního pohledu.

Na obrázku obr. 2 je zobrazena světlotěsná komora z levého spodního pohledu.

10 Na obrázku obr. 3a je znázorněn zámkový spoj použitý u stěn komory a na obr. 3b je znázorněn schodovitý přechod spoje víka a dna se stěnami komory.

Na obrázku obr. 4 je znázorněn zámkový spoj dveří se stěnou komory.

Na obrázku obr. 5 rukáv s třemi tunýlky pro gumičky a brzdíčky.

Příklady provedení

15 Příklad 1

Bylo vyrobeno zařízení, které je znázorněné na obr. 1 a obr. 2. Opěrná část zařízení, se skládá ze čtyř stěn (stěna 3 pro rukáv, stěna 5 pro dveře, stěna 7 pro konektory, zadní stěna 8), víka 1 a dna 9. Stěny jsou spojeny pomocí zámkového a šroubového spoje viz obr. 3a. Ke spojení víka 1 a dna 9 se stěnami (stěna pro rukáv 3, stěna pro dveře 5, stěna pro konektory 7, zadní stěna 8) je použito schodového přechodu se šroubovým spojem, který je znázorněn na obr. 3b.

20 Světlotěsná komora je vyrobena z duralu typ ENA W6082T651. Víko 1, dno 9, stěna 5 pro dveře a zadní stěna 8 mají rozměr 10x250x250 mm. Stěna 7 pro konektory a stěna 3 pro rukáv má rozměr 10x243, 8x250 mm. Dveře 6 mají rozměr 10x193x223 mm a příruba 2 pro fotonásobič má rozměr 5x140x176 mm. Příruba 4 pro rukáv je vyrobena z tyčoviny o průměru 190 mm a výšce 35 mm. Rukáv má průměr 158 mm a je dlouhý 45 cm.

25 Ve víku 1 se nachází vstupní otvor pro senzor a dvě série neprůchozích děr se závity, které slouží k upevnění přírub. Jako senzor byl použit fotonásobič od firmy Hamamatsu (R4220). Příruba 2 pro fotonásobič má ve spodní straně drážku na o-kroužek o rozměru 62x3 mm, který zajišťuje neprostupnost světla mezi víkem 1 a přírubou 2 pro fotonásobič. Horní strana příruby 2 pro fotonásobič obsahuje také drážku pro o-kroužek o rozměru 35x2 mm, který dosedá na chladič systému fotonásobiče od firmy Hamamatsu (typ C9143).

30 Na vnitřní straně stěny 3 pro rukáv se nacházejí neprůchozí díry se závity, které slouží k připevnění příruby 4 pro rukáv. Na přírubě 4 pro rukáv je drážka pro o-kroužek o rozměru 165x4 mm, který eliminuje průchod světla do komory. Ke stěně 3 pro rukáv je ještě připevněno široké madlo 10, umožňující manipulaci s komorou.

35 Ke stěně 5 pro dveře jsou pomocí pantů od firmy Else+Ganter (GN 238-42-42-EJ-SW) připojeny dveře 6. Jelikož nejsou dveře 6 v úrovni stěny 5 pro dveře, musí se vyrovnat výškový rozdíl pomocí podložek o výšce 9 mm. Na dveřích 6 se nachází madlo 12 pro dveře, které má díru pro uchycení kompresní kličky od firmy Southco (Handle Style, Miniature), sloužící k přitlačení dveří 6. Ve stěně 5 pro dveře se nacházejí 2 drážky kolem otvoru pro vstup, které se vyplní těsněním od firmy Ruml Těsnění s.r.o. (na míru). Tyto drážky spolu se dvěma drážkami ve dveřích 6 tvoří zámkový spoj. Tento zámkový spoj je vyobrazen na obr. 4. Ke stěně 5 je dále připevněno madlo 11 pro stěnu, sloužící k zapření kompresní kličky.

Ve stěně 7 pro konektory se nacházejí čtyři průchozí závity pro namontování elektrických konektorů (MIC 334 a MIC 324), umožňující dodání elektřiny dovnitř komory. K této stěně 7 pro konektory je připevněno široké madlo 10.

Rukáv 13 obr. 5 se navléká na přírubu 4 pro rukáv. Na přírubě 4 pro rukáv se nachází drážka, do které může být nasazen jisticí prvek rukávu např. hadicová spona o průměru 140-160 mm. Rukáv 13 je opatřen třemi tunýlky, ve kterých je navléknuta kulatá gumička 14 s brzdíčkou se dvěma dírkami 15.

Průmyslová využitelnost

Potravinářství, zemědělství, diagnostika v lékařství.

10

N Á R O K Y N A O C H R A N U

1. Světlotěsná komora pro měření fotonové emise z biologických vzorků, **vyznačující se tím**, že je složena z víka (1), dna (9), stěny (3) pro rukáv, stěny (5) pro dveře, stěny (7) pro konektory a zadní stěny (8), přičemž je k víku (1) připojena příruba (2) pro fotonásobič, ke stěně (3) pro rukáv je připojena příruba (4) pro rukáv, ke stěně (5) pro dveře jsou připojeny dveře (6), k přírubě (4) pro rukáv je připojen rukáv (13).

15

2. Světlotěsná komora podle nároku 1, **vyznačující se tím**, že ke dveřím (6) je připojeno madlo (12) pro dveře, ke stěně (5) pro dveře je připojeno madlo (11) pro stěnu a ke stěně (3) pro rukáv a stěně (7) pro konektory je připojeno široké madlo (10).

3. Světlotěsná komora podle nároků 1 a 2, **vyznačující se tím**, že rukáv (13) je opatřen minimálně jednou gumičkou (14) umístěnou v tunýlku a zajištěnou brzdíčkou (15), přičemž je rukáv výhodně vyroben ze dvou vrstev látek, kdy vnitřní vrstva je z černé zatemňovací látky a vnější vrstva je z černé koženky.

20

4. Světlotěsná komora podle nároků 1 a 2, **vyznačující se tím**, že víko (1) obsahuje dvě série neprůchozích děr se závity, které umožňují výrobu dvou velikostí přírub, které jsou opatřeny drážkou na horní a spodní straně pro o-kroužek.

25

5. Světlotěsná komora podle nároku 1, **vyznačující se tím**, že jedna stěna (3) komory obsahuje kruhový otvor pro přírubu (4) pro rukáv, kde jsou na vnitřní straně neprůchozí díry se závitem a kruhovou přírubou (4) pro rukáv, která je opatřena drážkou pro těsnící o-kroužek.

6. Světlotěsná komora podle nároků 1 až 3, **vyznačující se tím**, že všechny části komory jsou vyrobeny ze slitin hliníku a dále jsou povrchově upraveny černým eloxem.

30

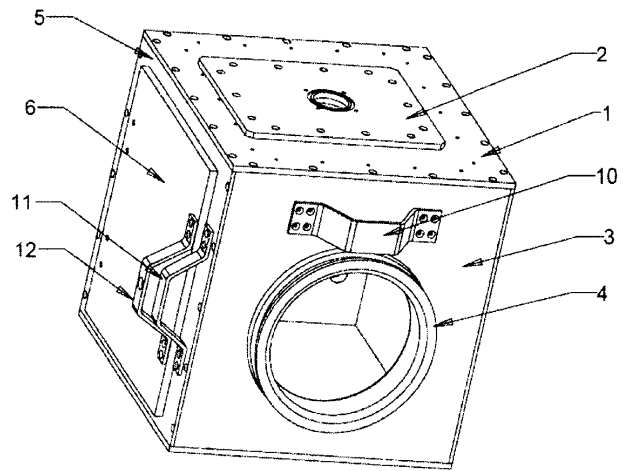
7. Světlotěsná komora podle nároků 1 až 4, **vyznačující se tím**, že je rukáv (13) navléknut na přírubu (4) ve které je drážka pro jisticí prvek, která umožňuje pevné přichycení rukávu k přírubě.

35

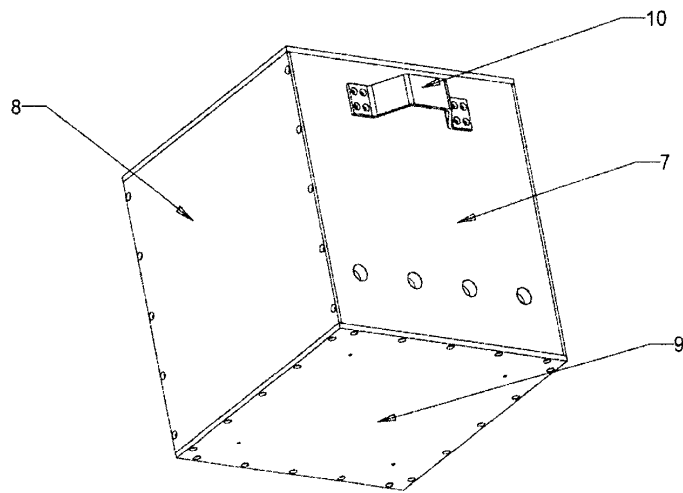
2 výkresy

Seznam vztahových značek:

- 1 - víko
- 2 - příruba pro fotonásobič
- 3 - stěna pro rukáv
- 5 4 - příruba pro rukáv
- 5 - stěna pro dveře
- 6 - dveře
- 7 - stěna pro konektory
- 8 - zadní stěna
- 10 9 - dno
- 10 - široké madlo
- 11 - madlo pro stěnu
- 12 - madlo pro dveře
- 13 - rukáv
- 15 14 - gumička
- 15 - brzdička.



Obr. 1




Obr. 2

UŽITNÝ VZOR

(11) Číslo dokumentu:

26 574

<p>(19) ČESKÁ REPUBLIKA</p>  <p>ÚŘAD PRŮMYSLOVEHO VLASTNICTVÍ</p>	<p>(21) Číslo přihlášky: 2013-28829 (22) Přihlášeno: 26.11.2013 (47) Zapsáno: 06.03.2014</p>	<p>(13) Druh dokumentu: U1 (51) Int. Cl.: G01N 21/76 (2006.01) G01N 21/01 (2006.01)</p>
--	---	--

(73) Majitel:
Ústav fotoniky a elektroniky AV ČR, v.v.i., Praha,
CZ

(72) Původce:
Ing. Michaela Nerudová, Most, CZ

(54) Název užitého vzoru:
Polohovací světlotěsná komora pro paralelní měření fotonové emise

CZ 26574 U1

Polohovací světlotěsná komora pro paralelní měření fotonové emise

Oblast techniky

Technické řešení se týká polohovací světlotěsné komory pro paralelní měření ultra slabé fotonové emise z biologických vzorků, které umožňuje nastavení vertikální nebo horizontální polohy komory související s typem měření. Součástí komory je zásuvná kazeta sloužící k uchycení a k snadné manipulaci nádoby se vzorkem.

Dosavadní stav techniky

Na trhu existují tři výrobci světlotěsných komor pro měření fotonové emise. Všechny tři komory jsou určeny pro měření s jednou CCD kamerou. Na trhu není průmyslově vyráběna komora pro paralelní měření s fotonásobiči. Rozdíl mezi senzory spočívá v typu získané informace a časové náročnosti měření. Získání prostorové informace o záření fotonů pomocí CCD kamery trvá i několik hodin, zatímco fotonásobiče měří okamžitou hodnotu počtu vyzářených fotonů za zvolený časový interval, ale chybí jim prostorová informace. Právě pro rychlost měření by mohl být fotonásobič vhodnějším nástrojem pro diagnostiku v lékařství, potravinářství či zemědělství. Výhodou paralelního měření od klasického jednosenzorového spočívá v ověřování či porovnávání naměřených signálů z jednoho vzorku. Jestliže budou dva stejné senzory směřovat do stejného místa vzorku, informace o fotonové emisi by měla být shodná. Druhou možností paralelního měření je zapojení dvou různých senzorů lišících se například ve spektrální citlivosti a porovnávat výsledky. Nevýhodou vyráběných komor je tedy jeden vstup pro senzor do vnitřku komory, který je umístěn v horní desce komory. Druhá nevýhoda spočívá právě v konfiguraci měřicí komory, kdy je možné měřit pouze ze shora. Měření ze shora je vhodné pouze pro určitý typ laboratorního nádobí např. Petriho misky s malými objemy vzorků. Pro měření větších objemů by bylo vhodnější senzor umístit z boku měřicí nádoby.

Podstata technického řešení

Výše uvedené nevýhody řeší polohovací světlotěsná komora pro paralelní měření podle tohoto technického řešení. Polohovací světlotěsná komora se skládá ze třech hlavních částí, jmenovitě z otočné komory, stojanu a zásuvného šuplíku pro nádobu se vzorkem. Otočná komora obsahuje komponenty: přední horní stěnu, zadní horní stěnu, levý horní bok, pravý horní bok, horní víko, spodní víko, přední spodní stěnu, zadní spodní stěnu, levý spodní bok, pravý spodní bok a dno. K hornímu víku je připevněno madlo pro horní víko, k přední horní stěně zevnitř jsou připevněny dva vymežovače pro šuplík a zarážka pro šuplík, k levému a pravému hornímu boku je zvenku připevněna posunovací podložka a válec pro otáčení, k přední a zadní horní stěně zvenku je připevněna příruba pro fotonásobič. Ve dně se nachází otvory pro připevnění termoregulační jednotky.

Stojan obsahuje komponenty: stěnu stojanu, čep s dírou pro závlačku a podpěru stojanu. Celý stojan se upevňuje k levému a pravému hornímu boku komory pomocí čepu se závlačkou, který zapadá do válce pro otáčení.

Šuplík pro laboratorní nádobu se vzorkem obsahuje komponenty: víko šuplíku, dno šuplíku a dva boky šuplíku. K víku šuplíku je připevněno madlo pro šuplík a ke dnu šuplíku jsou připevněny čtyři vymežovací kolíky šuplíku.

Vnější rozměry otočné komory mohou být v rozsahu od 20 do 80 cm, a to v jakémkoliv poměru stran. Vhodným materiálem pro výrobu komory jsou slitiny hliníku, které jsou pevné, lehké a dají se povrchově upravit. Pro světlotěsnou komoru byla použita povrchová úprava černý elox, který zlepšuje pevnostní vlastnosti materiálu a díky černé barvě je zajištěno vhodné prostředí pro měření fotonové emise.

Horní a spodní boky komory jsou spojeny za použití zámkového a šroubového spoje. Zámkový spoj zajistí neprůchodnost světla díky vytvořeným záhybům a šroubový spoj je slepý, tudíž se světlo nešíří ani podél šroubů. Spodní víko a dno jsou spojeny se spodními boky stěn komory pomocí schodového přechodu a šroubového spoje, který je také slepý. Horní víko má schodovitý přechod s vystupující drážkou, která dosedá na gumové těsnění, přilepené k hornímu okraji horních boků a stěn. Pomocí pákového uzávěru připevněnému k posouvací podložce, která je připevněna k levému a pravému hornímu boku, a víku dojde k dostatečnému přitlaku víka čímž se zajistí světlotěsnost spoje. Mezi spodní víko a horní boky stěny je vloženo gumové těsnění, které vyrovná nerovnosti povrchů, tudíž nedochází k šíření světla do vnitřku komory.

Otočná komora má na přední a zadní horní stěně připravené neprůchozí závity na dvě velikosti přírub pro různé typy fotonásobičů. CCD kamer či jejich chlazení. Pro jakýkoliv typ senzoru se dá vyrobit příruba na míru bez zásahu do sestavené komory. Výhodou tohoto řešení je možnost přizpůsobit měřicí komoru všem typům používaných senzorů za krátkou dobu a nízkou cenu.

Výměnný šuplík slouží k uchycení laboratorní nádoby s biologickým vzorkem, k rychlé manipulaci a možnosti výměny šuplíku přizpůsobený pro jiný typ nádoby. Další výhodou použití zásuvného šuplíku je přesné umístění vzorku do měřícího prostoru.

Stojan je navržen pro vertikální a horizontální měření, vhodné pro měření v Petriho miskách a květech. Systém se polohuje otáčením komory kolem čepu, který je pevně spojen s válcem pro otáčení pomocí závlačky, nastavení polohy se zajišťuje kolíky, které procházejí stojanem až do válce pro otáčení.

Polohovací světlotěsná komora umožňuje paralelní měření fotonové emise pomocí dvou senzorů s výběrem horizontální nebo vertikální polohy otočné komory a díky vymezovacímu systému pro šuplík a zásuvný šuplík umožňuje přesné, duplikovatelné umístění měřeného vzorku a jeho rychlou výměnu.

25 Přehled obrázků na výkresech

Na obr. 1 je zobrazena otočná komora zepředu z pravého spodního pohledu.

Na obr. 2 je zobrazena otočná komora zezadu z pravého horního pohledu.

Na obr. 3 je zobrazen vymezovací systém pro výměnný šuplík pro nádobu se vzorkem.

Na obr. 4 je zobrazen stojan s otočnou komorou.

30 Na obr. 5 je zobrazen šuplík pro nádobu se vzorkem.

Na obr. 6a je znázorněn zámkový spoj použitý u stěn komory a na obr. 6b je znázorněn schodovitý přechod spoje víka a dna se stěnami komory.

Příklady provedení

Příklad 1

35 Bylo vyrobeno zařízení, které se skládá ze tří částí, a to otočné komory, stojanu a zásuvného šuplíku. Vnější část otočné komory je znázorněna na obr. 1 a obr. 2. Hlavní kostra otočné komory se skládá z osmi stěn (přední horní stěna 1, zadní horní stěna 2, levý horní bok 3, pravý horní bok 4, přední spodní stěna 8, zadní spodní stěna 9, levý spodní bok 10, pravý spodní bok 11), horního víka 5, spodního víka 7 a dna 12. Stěny jsou spojeny pomocí zámkového a šroubového spoje viz obr. 6a. Ke spojení spodního víka 7 a dna 12 se spodními stěnami (přední spodní stěna 8, zadní spodní stěna 9, levý spodní bok 10, pravý spodní bok 11) je použit schodový přechod se šroubovým spojením, který je znázorněn na obr. 6. Horní víko 5 slouží jako vstup do komory, a proto je zde použit schodovitý přechod s horními stěnami (přední horní stěna 1, zadní horní stěna 2, levý horní bok 3, pravý horní bok 4) bez použití šroubových spojů pro rychlou manipulaci.

45

Horní víko 5 má na schodovitém přechodu vystupující drážku a na horních hranách horních stěn komory (přední horní stěna 1, zadní horní stěna 2, levý horní bok 3, pravý horní bok 4) je nalepeno gumové těsnění, které dohromady tvoří členění prostoru. Na horní víko 5 a posunovací podložku 13, která je připevněna k horním bokům (levý horní bok 3, pravý horní bok 4), je upevněn pákový uzávěr, který zajišťuje dostatečný přítlak horního víka 5 k horním hranám horních stěn komor (přední horní stěna 1, zadní horní stěna 2, levý horní bok 3, pravý horní bok 4), a tím je zabezpečena neprůchodnost světla na tomto přechodu.

V přední horní stěně 1 se nachází vstupní otvor pro senzor a dvě série neprůchozích děr se závity, které slouží k upevnění přírub. Jako senzor byl použit fotonásobič od firmy Hamamatsu (R4220). K přední horní stěně 1 je připevněna malá příruba 16 pro fotonásobič, která má ve spodní straně drážku na o-kroužek o rozměru 62x3 mm, který zajišťuje neprostupnost světla mezi přední horní stěnou 1 a malou přírubou 16 pro fotonásobič. Horní strana malé příruby 16 pro fotonásobič obsahuje také drážku pro o-kroužek o rozměru 35x2 mm, který dosedá na chladicí systém fotonásobiče od firmy Hamamatsu (typ C9143).

V zadní horní stěně 2 se nachází vstupní otvor pro senzor a také dvě série neprůchozích děr se závity, které slouží k upevnění přírub. Jako senzor byl použit fotonásobič od firmy Hamamatsu (H2256-02). K přední horní stěně 2 je připevněna velká příruba 17 pro fotonásobič, která má ve spodní straně drážku na o-kroužek o rozměru 76x3 mm, který zajišťuje neprostupnost světla mezi zadní horní stěnou 2 a velkou přírubou 17 pro fotonásobič.

V přední spodní stěně 8 a zadní spodní stěně 9 se nacházejí dva průchozí závity pro namontování elektrických konektorů (MIC 334 a MIC 324), umožňující dodání elektřiny dovnitř komory.

Ve dně komory 12 se nachází vstupní otvor pro termoregulační jednotku od firmy UWE electronic (typ A2A 50W), která zajišťuje konstantní teplotu uvnitř komory. Celá spodní část komory slouží právě pro namontování termoregulační jednotky, zatímco horní část komory funguje jako prostor pro měření. Tento typ konstrukce umožňuje mít biologický vzorek co nejbližší u senzorů což je výhodné, protože intenzita signálu je závislá na vzdálenosti mezi vzorkem a senzorem.

V obou horních bokách (levý horní bok 3, pravý horní bok 4) se nachází průchozí závit pro hadicovou průchodku, která umožňuje dodání plynu do komory či měřeného vzorku. Dále je k těmto stěnám připevněn válec pro otáčení 18. Na straně válce pro otáčení 18, které je ve styku s horními boky (levý horní bok 3, pravý horní bok 4) je drážka pro o-kroužek o rozměru 33x3 mm, který zajišťuje nepropustnost světla.

Stojan komory je znázorněn na obrázku obr. 4 a je složen ze stěny stojanu 19, čepu s dírou pro závlačku 20 a podpěry stojanu 21. Polohovací komora je se stojanem spojena pomocí válce pro otáčení 18. Mezi válcem pro otáčení 18 a stěnou stojanu 19 je vložena distanční podložka, která zabraňuje tření a umožňuje snazší polohování komory. Skrz stěnu stojanu 19, podložku a válec pro otáčení 18 je veden čep s dírou pro závlačku 20, který se pevně spojí s válcem pro otáčení 18 pomocí závlačky typu DIN 94-A4 s rozměrem 4x63 mm. Poloha komory se nastavuje pomocí čtyř až osmi nerezových kolíků typu h8 (DIN7-A1) s rozměrem 4x50 mm, které procházejí stěnou stojanu 19 do válce pro otáčení 18. Podpěry stojanu 21 slouží k zamezení deformace stěn komor a udržení stability. Stojan je poté možno namontovat k pevné podložce či stolu díky připraveným závitům na spodní hraně stěny stojanu 19.

Vnitřní část otočné komory je znázorněna na obrázku obr. 3. Na vnitřní straně přední horní stěny 1 jsou připevněny dva vymezořovače pro šuplík 14 a zarážka pro šuplík 15. Tyto tři opěrné prvky slouží ke správnému nastavení šuplíku pro nádobu se vzorkem.

Šuplík pro nádobu se vzorkem je znázorněn na obrázku obr. 5 a jeho hlavní kostra se skládá z víka šuplíku 22, dvou boků šuplíku 23 a dna šuplíku 22. Na víko šuplíku 22 je připevněno madlo pro šuplík 25 a ke dni šuplíku 23 jsou připevněny čtyři vymeřovací kolíky šuplíku, které vymezují prostor a udržují stabilitu nádoby se vzorkem. Šuplík je navržen pro měřicí kyvety o rozměru 20x70x70 mm. Bok šuplíku 23 je opatřen průchozím závitěm pro hadicovou průchodku zajišťující dodání plynu do vzorku.

Všechny části otočné komory, stojanu a šuplíku pro nádobu se vzorkem jsou vyrobeny z duralu typu ENA W6082T651, kromě válce pro otáčení, který je z nerezové oceli a všech madel (madlo pro horní víko 6, madlo pro šuplík 25), které jsou z plechu. Horní víko 5 má rozměr 10x50x240 mm, horní boky (levý horní bok 3, pravý horní bok 4) 10x50x260 mm, spodní víko 7 a dno 12 10x12x280 mm a spodní boky (levý spodní bok 10, pravý spodní bok 11) 10x75x280 mm. Válec pro otáčení 18 je vyroben z tyčoviny o průměru 40 mm a délce 30 mm. Stěna stojanu 19 má rozměr 20x200x500 mm, podpěra stojanu 21 20x110x190 mm a čep s dírou pro závlačku 20 je vyroben z tyčoviny o průměru 18 mm a délce 46 mm. Dno šuplíku 23 a víko šuplíku 22 mají rozměr 5x29, 8x83 mm, bok šuplíku 24 5x29, 8x125 mm a vymežovací kolík šuplíku 26 4x6x20 mm.

Průmyslová využitelnost

Potravinářství, zemědělství, diagnostika v lékařství

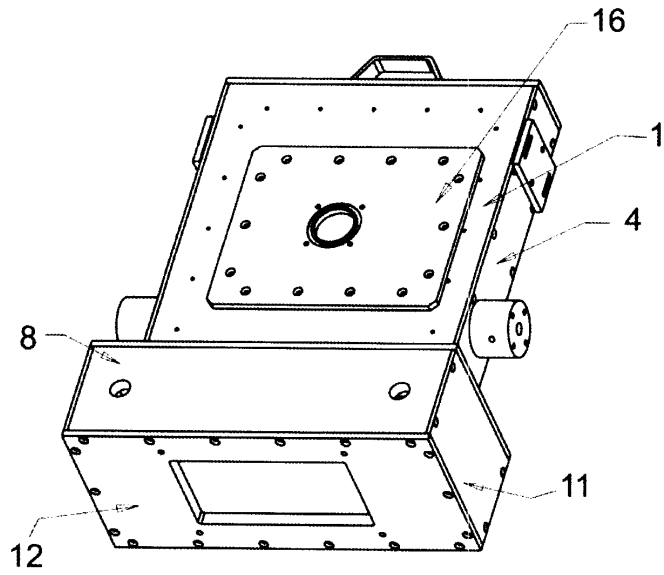
NÁROKY NA OCHRANU

1. Polohovací světlotěsná komora pro paralelní měření fotonové emise **vyznačující se tím**, že obsahuje tři hlavní části: otočnou komoru, stojan a zásuvný šuplík, přičemž jsou k otočné komoře paralelně připojeny dva senzory, výhodně ve formě fotonásobiče.
2. Zařízení podle nároku 1, **vyznačující se tím**, že otočná komora obsahuje horní víko (5), dno (12), přední horní stěnu (1), zadní horní stěnu (2), levý horní bok (3), pravý horní bok (4), spodní víko (7), přední spodní stěnu (8), zadní spodní stěnu (9), levý spodní bok (10) a pravý spodní bok (11).
3. Zařízení podle nároku 1, **vyznačující se tím**, že stojan obsahuje stěnu stojanu (19), čep s dírou pro závlačku (20) a podpěry stojanu (21).
4. Zařízení podle nároku 1, **vyznačující se tím**, že zásuvný šuplík pro nádobu se vzorkem obsahuje víko šuplíku (22), dno šuplíku (23) a dva boky šuplíku (24), přičemž je k víku šuplíku (22) připevněno madlo (25) pro šuplík a ke dnu šuplíku (23) jsou připevněny čtyři vymežovací kolíky šuplíku (26).
5. Zařízení podle nároku 2, **vyznačující se tím**, že k hornímu víku (5) je připojeno madlo (6) pro horní víko, k přední horní stěně (1) je připojena malá příruba (16) pro fotonásobič, k zadní horní stěně (2) je připojena velká příruba (17) pro fotonásobič, k levému hornímu boku (3) a k pravému hornímu boku (4) je připojen válec pro otáčení (18) a posunovací podložka (13) a z vnitřní strany přední horní stěny (1) jsou připojeny dva vymežovače pro šuplík (14) a zarážka šuplíku (15).
6. Zařízení podle nároku 2, **vyznačující se tím**, že přední horní stěna (1) a zadní horní stěna (2) obsahují dvě série neprůchozích děr se závity, které umožňují výrobu dvou velikostí přírub, které jsou opatřeny drážkou pro o-kroužek na horní, spodní či obou stranách příruby.

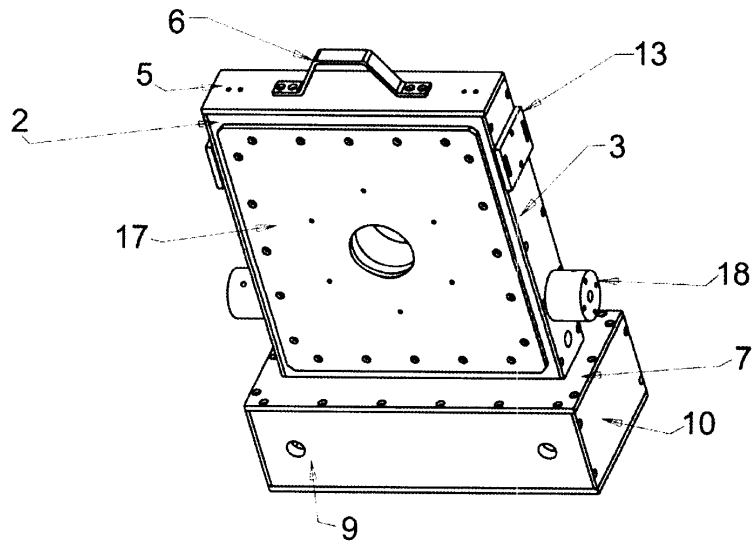
3 výkresy

Seznam vztahových značek:

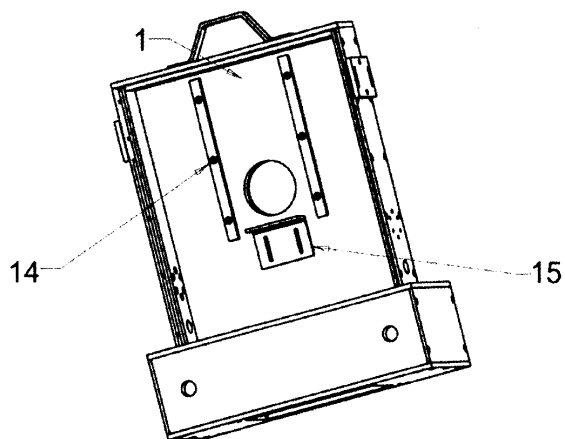
- | | |
|----|------------------------------------|
| | 1- přední horní stěna |
| | 2- zadní horní stěna |
| 5 | 3- levý horní bok |
| | 4- pravý horní bok |
| | 5- horní víko |
| | 6- madlo pro horní víko |
| | 7- spodní víko |
| 10 | 8- přední spodní stěna |
| | 9- zadní spodní stěna |
| | 10- levý spodní bok |
| | 11- pravý spodní bok |
| | 12- dno |
| 15 | 13- posunovací podložka |
| | 14- vymežovač pro šuplík |
| | 15- zarážka šuplíku |
| | 16- malá příruba pro fotonásobič |
| | 17 - velká příruba pro fotonásobič |
| 20 | 18- válec pro otáčení |
| | 19- stěna stojanu |
| | 20- čep s dírou pro závlačku |
| | 21- podpěra stojanu |
| | 22- víko šuplíku |
| 25 | 23- dno šuplíku |
| | 24- bok šuplíku |
| | 25- madlo pro šuplík |
| | 26- vymežovací kolík šuplíku. |



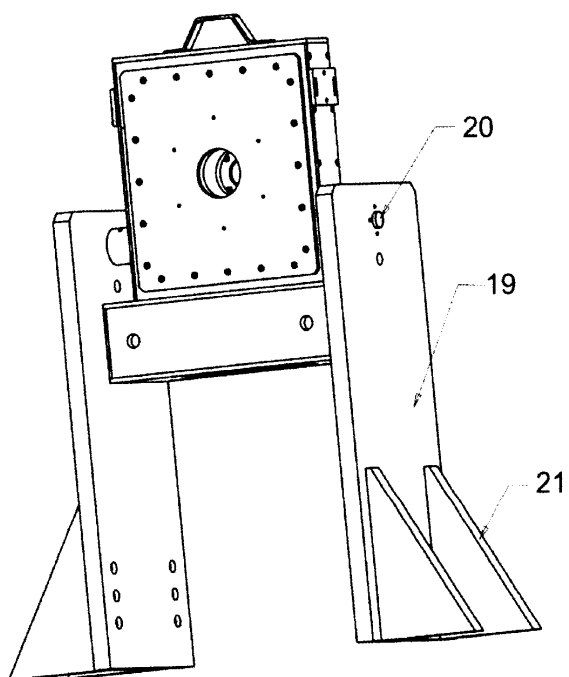
Obr. 1



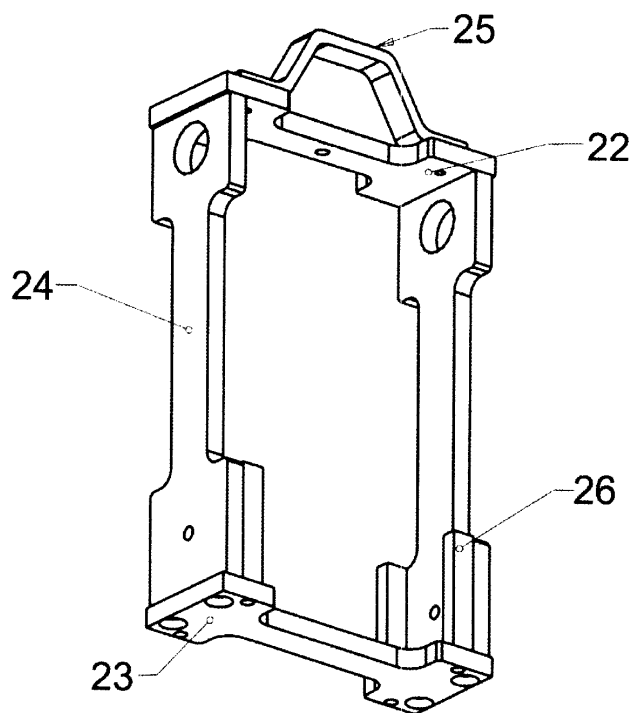
Obr. 2



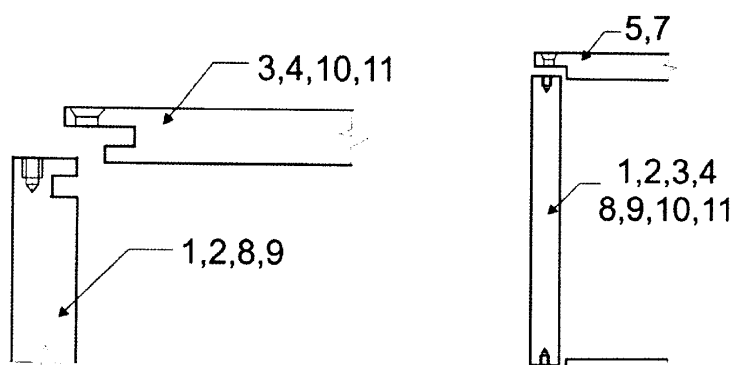
Obr. 3



Obr. 4



Obr. 5



Obr. 6a

Obr. 6b

Konec dokumentu



Contents lists available at ScienceDirect

Journal of Luminescence

journal homepage: www.elsevier.com/locate/jlumin

Review

Biophotons, coherence and photocount statistics: A critical review

Michal Cifra^{a,*}, Christian Brouder^b, Michaela Nerudová^{a,c}, Ondřej Kučera^a^a Institute of Photonics and Electronics, The Czech Academy of Sciences, Prague, Czech Republic^b Institut de Minéralogie, de Physique des Matériaux et de Cosmochimie, Université Pierre et Marie Curie, Paris 6, CNRS UMR7590, Paris, France^c Department of Circuit Theory, Faculty of Electrical Engineering, Czech Technical University in Prague, Prague, Czech Republic

ARTICLE INFO

Article history:

Received 1 December 2014

Received in revised form

23 February 2015

Accepted 16 March 2015

Available online 24 March 2015

Keywords:

Ultra-weak photon emission

Chemiluminescence

Photocount statistics

Coherence

Squeezed states

ABSTRACT

Biological samples continuously emit ultra-weak photon emission (UPE, or “biophotons”) which stems from electronic excited states generated chemically during oxidative metabolism and stress. Thus, UPE can potentially serve as a method for non-invasive diagnostics of oxidative processes or, if discovered, also of other processes capable of electron excitation. While the fundamental generating mechanisms of UPE are fairly elucidated together with their approximate ranges of intensities and spectra, the statistical properties of UPE are still a highly challenging topic. Here, we review claims about nontrivial statistical properties of UPE, such as coherence and squeezed states of light. After the introduction to the necessary theory, we categorize the experimental works of all authors to those with solid, conventional interpretation and those with unconventional and even speculative interpretation. The conclusion of our review is twofold; while the phenomenon of UPE from biological systems can be considered experimentally well established, no reliable evidence for the coherence or nonclassicality of UPE has actually been achieved up to now. Furthermore, we propose perspective avenues for the research of statistical properties of biological UPE.

© 2015 Elsevier B.V. All rights reserved.

Contents

1. Introduction	39
2. Statistical properties of light	39
2.1. Theory of photocount measurement	39
2.1.1. Classical theory	39
2.1.2. Quantum theory	39
2.1.3. Conditional probability	39
2.2. States of the light and their photocount statistics	40
2.2.1. Coherence and coherent states	40
2.2.2. Classical coherence	40
2.2.3. Quantum coherence	40
2.2.4. Coherent states	41
2.2.5. Squeezed states	41
2.2.6. Thermal states	43
2.2.7. Superposition of coherent and thermal states	43
2.2.8. Super-radiance	43
3. Experimental works on the photocount statistics of UPE	44
3.1. Works with conventional data interpretation	44
3.2. Works with speculative data interpretation	44
3.2.1. Coherence of ultra-weak photon emission?	44
3.2.2. Squeezed states of ultra-weak photon emission?	46
4. Conclusion and perspectives	46
Acknowledgment	48

* Corresponding author.

E-mail address: cifra@ufe.cz (M. Cifra).

Appendix A. Other works on statistical properties of UPE with speculative interpretations.....	48
Appendix B. Table of UPE photocount statistics experiments.....	49
References.....	49

1. Introduction

Ultra-weak photon emission (UPE, or “biophotons”) from biological systems is a luminescent phenomenon which is present without any direct external stimulation nor additionally applied external luminophores [1]. While there is some consensus about the intensity and spectrum of UPE [1,2], claims about statistical properties of UPE are very controversial. We aim to explain and settle this controversy in this critical review.

Electronic excited states giving rise to UPE are generated chemically in the course of oxidative metabolic and stress processes [1] in biological samples and living organisms. Several other terms synonymous to ultra-weak photon emission occur in the literature: autoluminescence [3], weak luminescence [4], low level chemiluminescence [5], biophotons/biophoton emission [6,7], etc. The spectral range of UPE is known to lie at least in the range from 350 nm to 700 nm [2] and its intensity is up to several hundreds to one thousand photons per square centimeter per second in the entire mentioned spectral range.¹

There have been many claims about nontrivial statistical properties of UPE since 1980s, such as coherence and even squeezed states of light [8–14]. Such properties of UPE would be of great physical and biological importance. Firstly, if the claims of UPE coherence were proved to be true, a novel mechanism of chemically powered ultra-low power lasing would be very likely discovered. Secondly, there would also be great implications in biology since coherence or squeezed states of UPE would bring an evolutionary advantage for organisms in terms of ultra-fast optical communication [15] for the purposes of intracellular and intercellular interactions and organization [16].

Optical biocommunication has been targeted by several reviews [15,17–21]. The intensity and spectral properties of UPE have also been recently reviewed [1,2]. However, there is no critical review which covers the detailed technical aspects of the statistical properties of photon emission from biological systems. Here, we present the development and current state of the literature on the statistical properties of UPE, we especially focus on coherent and squeezed states of light and provide a critical reflection of these works.

We start with the presentation of the necessary theory about photocount measurement coherence and quantum optics in Section 2 and then we review the models which are used to analyze experimental distributions of UPE photocount statistics. In Section 3, we review the experiments of statistical properties of UPE and assess them from the point of view of the current understanding of physics and biophysics. We found that although there are quite numerous papers which contain unsubstantiated claims about statistical properties of UPE, several high quality works can also be found. Based on reliable works, we propose future avenues in the research of the statistical properties of biological UPE in our conclusion.

2. Statistical properties of light

2.1. Theory of photocount measurement

The statistical properties of UPE were mostly investigated experimentally by measuring the distribution of counts produced by UPE in a photodetector. Therefore, we briefly introduce the classical and quantum approach to photocount distributions (*photocount statistics* is another term often used in the literature).

2.1.1. Classical theory

The intensity of the light field averaged over a cycle of the oscillation is given by the expression [22, p. 86]

$$\bar{I}(t) = \frac{1}{2} \epsilon_0 c |E(t)|^2, \quad (1)$$

where $\bar{I}(t)$ is the intensity (irradiance) averaged over a cycle of oscillation with units W/m^2 , ϵ_0 is the permittivity of the vacuum, c is the velocity of light in the vacuum and $E(t)$ is the intensity of the electric field. The intensity can also be obtained as the time average of the Poynting vector perpendicular to the surface of the detector.

Let the efficiency of the detector be denoted by η . According to the semi-classical theory of optical detection [22, p. 120], there is such a probability distribution $P(W)$ that the probability $p_h(t, T)$ of detecting n photoelectric emissions in a finite time interval from t to $t+T$ is

$$p_h(t, T) = \frac{1}{n!} \langle W^n e^{-W} \rangle = \frac{1}{n!} \int_0^\infty W^n e^{-W} P(W) dW, \quad (2)$$

where $W = \eta \int_t^{t+T} I(\tau) d\tau$ is the integrated light intensity and η is a coefficient containing dimensional factors and describing the efficiency of the detector, so that W is dimensionless.

2.1.2. Quantum theory

The quantum expression for the probability that n photocounts occur between time t and $t+T$ is [23; 22, p. 276; 24, p. 725]

$$p_h(t, T) = \left\langle : \frac{\hat{W}^n}{n!} e^{-\hat{W}} : \right\rangle, \quad (3)$$

where

$$\hat{W} = \eta \epsilon_0 c \int_t^{t+T} |\hat{E}(t)|^2, \quad (4)$$

in the Heisenberg representation.

All the phenomena are basically of a quantum nature, but we say that a distribution of photocounts is classical if there exists a classical density distribution (i.e. a non-negative $P(W)$) such that the (quantum) probability given by Eq. (3) is equal to the classical one given by Eq. (2). The characterization of non-classical light was investigated in detail [24,25]. The probability of photocount detection is purely quantum if no such $P(W)$ exists.

2.1.3. Conditional probability

Some experiments are carried out with two photomultipliers [26, p. 87; 27, Chapter by X. Shen, p. 287]. When a photon is detected by photomultiplier 1, the photons in photomultiplier 2 are registered during the time interval Δt . Bayes' theorem tells us that the conditional

¹ The intensity of UPE within the visible region of the spectrum is many orders of magnitude higher than the intensity of thermal radiation (described by Planck's law) for other parameters (sample area, temperature, etc.) being the same, see [1, Fig. 2].

probability for A given B is given by $P(A|B) = P(A \cap B)/P(B)$. The conditional probability of photocounts is calculated in [28, p. 79; 29]. The waiting-time distribution for coherent, squeezed and thermal states was investigated in [30].

2.2. States of the light and their photocount statistics

2.2.1. Coherence and coherent states

Coherence is a quite subtle property of light. In a nutshell, coherence is the ability of light to build interference which is, according to Grimaldi, the fact that darkness can be obtained by adding light to light.² Broadly speaking, light beams are coherent if they combine like waves (by adding the amplitudes of the beams) while they are incoherent if they combine like particles (by adding the intensities, *i.e.* the square of the amplitudes, of the beams).

It took a long time to clarify the meaning of coherence [32,33] and the coherence properties of even the most classical double-slit interference experiment are still a matter of active current research [34–36]. For example, the influence of coherence on the interference of light beams (*i.e.* the Fresnel–Arago laws) was fully understood only in 2004 [37] and the conditions for a light beam to be considered as a sum of a fully polarized and a fully unpolarized beams are still controversial [38].³ The coherence of a light beam is modified by its propagation, the degree of coherence of a beam can influence its spectrum (this is known as the Wolf effect).

As a consequence of all these subtle effects, the literature on coherence is often very cautious and each statement is carefully supported by solid proof. Many papers from the period 1980–2010 which aimed to study coherence of UPE often contain highly speculative statements. Therefore, one of the main purposes of the current work is to assess the solidity of the conclusions drawn by the authors based on the data they presented and on the currently accepted physical viewpoints. We would also like to warn readers, especially those outside of the field of statistical properties of the electromagnetic field, that some authors of the original UPE literature use the term “coherence” rather vaguely. Terminology from quantum mechanics and quantum field theory often occurs in the UPE literature, where the term coherence may refer either to (i) the wave function from the Schrödinger equation or to (ii) light, which is, strictly speaking, not the same (although related) and often creates confusion. In quantum mechanics, coherence is an intrinsic property of the wave function and once decoherence occurs (*i.e.* loss of the wave function coherence or collapse of the wave function), the system then behaves classically. Therefore, quantum behavior is considered synonymous to coherence by some authors, but this is reasonable only when speaking about the wave function. We refer to coherence of light in this paper and one cannot directly equate the terms *non-classical (quantum)* with *coherent* light, neither *classical* with *incoherent* light. Generally, the quantum optical framework can explain all states of light. The classical framework can explain only some of them and those can be called classical. The states which can be explained in the quantum framework only are usually called quantum states. Coherence of light can be both of a classical and quantum character, thermal states of light (see further down) can be described in the classical and the quantum framework, while certain states can be described only in the quantum framework (*e.g.* squeezed states).

² *obscuratio, facta per solam additionem luminis* [31, p. 189]. In fact, Grimaldi did not really observe interference [32, p. 135], but his happy turn of phrase was remembered.

³ The last example must be considered with a grain of salt because the concepts of polarization and coherence are not identical [39].

2.2.2. Classical coherence

If $\mathbf{E}_1(\mathbf{r}, t)$ and $\mathbf{E}_2(\mathbf{r}, t)$ are the electric fields of two light waves (*i.e.* two solutions of the Maxwell equations), then the linearity of the Maxwell equations implies that the two waves add to form a new light wave: $\mathbf{E}(\mathbf{r}, t) = \mathbf{E}_1(\mathbf{r}, t) + \mathbf{E}_2(\mathbf{r}, t)$. In particular, if $\mathbf{E}_1(\mathbf{r}, t) = -\mathbf{E}_2(\mathbf{r}, t)$, then $\mathbf{E}(\mathbf{r}, t) = 0$. In other words, as Gabor put it when he received his Nobel prize in physics for the invention of holography: “light added to light can produce darkness”. It may not be completely out of place to recall that Gabor and Reiter devoted a book to the radiations emitted by plants and their influence on cell division, where they observed diffraction [40, p. 20] and reflection [40, p. 21] of UPE (but they did not investigate coherence). In 1928, they stated: “die Existenz der Strahlung bestimmter biologischer Objekte und die Wirkung dieser Strahlung auf die Zellteilung steht nach unseren Versuchen außer allem Zweifel.” (translation: *the existence of the radiation of certain biological objects and the effect of the radiation on the cell division is beyond any doubts according to our experiments*) [40, p. 6]. Much later (in 1956), he wrote: “The results ... seemed to support... the hypothesis of some radiating agency; on the other hand all experiments for proving the radiation by physical means have failed. To this day (1956) nobody knows what these experiments really mean.” [41].

Light detectors do not resolve the time-dependence of electromagnetic fields and measure something which is proportional to an average of the intensity over a duration Δt : $I(\mathbf{r}, t) = (1/\Delta t) \int_t^{t+\Delta t} |\mathbf{E}(\mathbf{r}, \tau)|^2 d\tau$. The light beam is coherent if the total intensity of the two beams is obtained by adding the amplitudes: $I(\mathbf{r}, t) = (1/\Delta t) \int_t^{t+\Delta t} |\mathbf{E}_1(\mathbf{r}, \tau) + \mathbf{E}_2(\mathbf{r}, \tau)|^2 d\tau$. It is incoherent if the total intensity of the two beams is obtained by adding the intensities $I(\mathbf{r}, t) = (1/\Delta t) \int_t^{t+\Delta t} |\mathbf{E}_1(\mathbf{r}, \tau)|^2 + |\mathbf{E}_2(\mathbf{r}, \tau)|^2 d\tau = I_1(\mathbf{r}, t) + I_2(\mathbf{r}, t)$. The reason why intensities should be added is not entirely clear in classical optics.⁴

Coherence is not a yes-or-no attribute but a continuum-like one. Strictly speaking, any electromagnetic (light) field is coherent to certain extent. Coherence time T_c or coherence length L_c is often used to describe the extent of coherence [43, Section 7.5.8]. In practice, we say that the light is coherent if it displays very large coherence time (*i.e.* much larger than the period of the oscillation) or very large coherence length (*i.e.* much larger than the wavelength), such that interference effects can be observed. The relation between coherence length and coherence time is $L_c = cT_c \approx c/\Delta f = \lambda_0^2/\Delta\lambda$, where c is the velocity of light, λ_0 is the mean wavelength, Δf and $\Delta\lambda$ are the spectral bandwidth of the light in Hz and nm, respectively. The broader the spectral range emitted from the source, the shorter the coherence time and coherence length: $T_c \cdot \Delta f \geq 1/4\pi$ [43, p. 319].

2.2.3. Quantum coherence

We follow the discussion of coherence described by Mandel [24, Chapter 12]. If $\hat{\mathbf{E}}^{(+)}(\mathbf{r}, t)$ and $\hat{\mathbf{E}}^{(-)}(\mathbf{r}, t)$ are the annihilation and creation operator of the electric field, respectively [24, p. 574], then the intensity of light at a point is proportional to $\langle \hat{\mathbf{E}}^{(-)}(\mathbf{r}, t) \hat{\mathbf{E}}^{(+)}(\mathbf{r}, t) \rangle$, where the sign $\langle \cdot \rangle$ represents the expectation value over a quantum state, which can be a mixed state. More generally, a quantity such as $\langle \hat{\mathbf{E}}^{(-)}(\mathbf{r}_1, t_1) \dots \hat{\mathbf{E}}^{(-)}(\mathbf{r}_N, t_N) \hat{\mathbf{E}}^{(+)}(\mathbf{r}_M, t_M) \dots \hat{\mathbf{E}}^{(+)}(\mathbf{r}_1, t_1) \rangle$ is called a *correlation function* [24, p. 585]. A state for which there is a vector function $\mathbf{e}(\mathbf{r}, t)$

⁴ As noticed by Biedenharn and Louck for the related problem of unpolarized radiation: “Every solution of the Maxwell equations, which propagates spatially as a plane wave, is necessarily completely polarized transversally; every additive superposition of two completely polarized solutions yields another completely polarized solution. An unpolarized wave cannot be a solution to the Maxwell equations! Thus, the concept of an unpolarized wave goes beyond Maxwell electrodynamics and involves quantal considerations.” [42, p. 453].

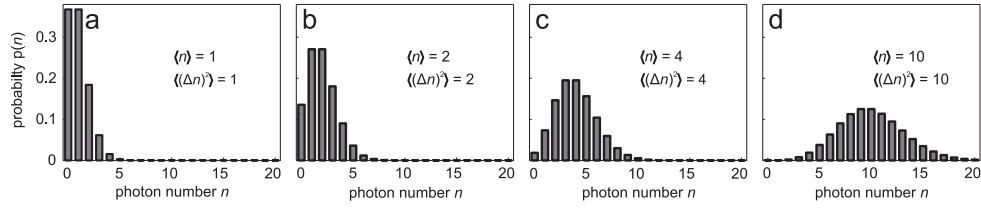


Fig. 1. Poisson photocount distribution is asymmetric for low intensities of light flux. Here we show Poisson distribution for four different average values of photon counts (n).

such that

$$\langle \hat{\mathbf{E}}^{(-)}(\mathbf{r}_1, t_1) \dots \hat{\mathbf{E}}^{(-)}(\mathbf{r}_N, t_N) \hat{\mathbf{E}}^{(+)}(\mathbf{r}_M, t_M) \dots \hat{\mathbf{E}}^{(+)}(\mathbf{r}_1, t_1) \rangle = \mathbf{e}^*(\mathbf{r}_1, t_1) \dots \mathbf{e}^*(\mathbf{r}_N, t_N) \mathbf{e}(\mathbf{r}_M, t_M) \dots \mathbf{e}(\mathbf{r}_1, t_1)$$

is said to *factorize*.

Such a state corresponds to full coherence in the classical case. As we shall see, all correlation functions factorize if the system is in a *coherent state*. The reciprocal question (i.e. the determination of all the states that lead to factorized correlation functions) was studied by Honegger and Rieckers [44,45]. They found out that there are states for which all correlation functions factorize and which are not coherent states in the usual sense. Very general coherent states were defined in the mathematical literature [46], but they have not yet been used in the present context.

2.2.4. Coherent states

Coherent states were discovered by Schrödinger [47], rediscovered by Schwinger [48], then called *coherent states* and further studied by Glauber [49]. Coherent states are now a standard tool of quantum optics [24]. From a mathematical point of view, a coherent state $|\alpha\rangle$ is an eigenstate of the annihilation operator: $\hat{a}|\alpha\rangle = \alpha|\alpha\rangle$, where α is a complex number [24, p. 523]. From the conceptual point of view, coherent states are the quantum states that correspond to classical electromagnetic waves. For instance, a classical current (for instance, a piece of electric wire carrying a macroscopic current) gives rise to a coherent state of the photon field [50].

The photocount statistics of a system in a coherent state is a Poisson distribution (see Fig. 1)

$$p_n(t, T) = \frac{\langle n \rangle^n}{n!} e^{-\langle n \rangle},$$

where $\langle n \rangle = T\langle \dot{n} \rangle$ is the average number of photons measured between time t and time $t + T$. A Poisson distribution is a sign of a classical light field. Its variance is equal to its mean: $\langle (\Delta n)^2 \rangle = \langle n \rangle$. The departure from a Poisson distribution is measured by the Fano factor F such that $\langle (\Delta n)^2 \rangle = \langle n \rangle F$ or by the Mandel parameter $Q = F - 1$. A photocount statistics is super-Poissonian if $F > 1$ and $Q > 0$, it is sub-Poissonian (and therefore non-classical) if $F < 1$ and $Q < 0$. The departure from Poisson distribution is a sign of a non-classical (quantum) nature of light.

Note that laser light is not in a coherent state [51], although it has a very large coherence length and a pronounced phase coherence [52]. Moreover, its probability distribution can be far from Poissonian [24, p. 940].

2.2.5. Squeezed states

Squeezed states have the characteristic that the dispersion (uncertainty) of one variable is reduced at the cost of an increase in the dispersion of the other canonical variable, for instance position vs. momentum or amplitude vs. phase.⁵ Following Loudon [53], this can be easily visualized when we write the equation for the electric field operator of a single mode of the photon field as

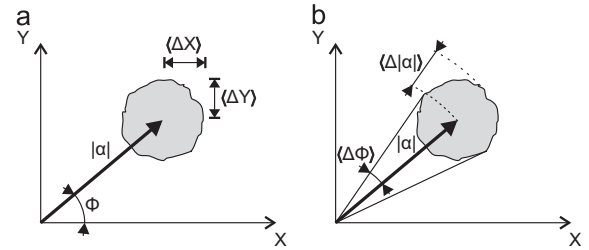


Fig. 2. The uncertainty region (in grey color) in phase space. The uncertainty region actually corresponds to the contour of the Wigner function given by ca. 1 standard deviation from its center. (a) The uncertainty of the canonical variables, here quadrature components X and Y , is expressed as their standard deviations $\langle \Delta X \rangle$ and $\langle \Delta Y \rangle$, respectively. (b) The uncertainties in the phase and amplitude of the field can be expressed through their standard deviations $\langle \Delta \phi \rangle$ and $\langle \Delta |\alpha| \rangle$, respectively. It is useful to note that the photon number standard deviation (i.e. standard deviation of the photocount distribution) is related to the standard deviation of a field amplitude approximately as $\langle \Delta n \rangle \approx 2\langle n \rangle^{1/2} \langle \Delta |\alpha| \rangle$ [54, Eq. (9)] for the measurement of the photocount statistics.

$$\hat{\mathbf{E}}(\mathbf{r}, t) = \mathbf{E}_0 \left[\hat{X} \sin(\omega t - \mathbf{k}\mathbf{r}) - \hat{Y} \cos(\omega t - \mathbf{k}\mathbf{r}) \right] \quad (5)$$

where \mathbf{E}_0 is the amplitude of the vectorial electric field, \hat{X} and \hat{Y} are Hermitian operators related to annihilation and creation operators of the photon field as $\hat{X} = (\hat{a} + \hat{a}^\dagger)/2$ and $\hat{Y} = (\hat{a} - \hat{a}^\dagger)/2i$. \hat{X} and \hat{Y} , the real and imaginary parts of the complex amplitude, give dimensionless amplitudes for the two quadrature phases. They obey the commutation relation $[\hat{X}, \hat{Y}] = i/2$. The electric field can be then depicted in a complex plane, see Fig. 2.

Various squeezed states were used in the UPE literature, but the most general ones are called two-photon coherent states and were proposed in 1976 by Yuen [55]. They have become the standard states of quantum optics [24, p. 1046]. They are simply defined as the solution $|\alpha, \xi\rangle$ to the eigenvalue equation $\hat{A}|\alpha, \xi\rangle = \beta|\alpha, \xi\rangle$. We follow the notation from Orszag [56, Chapter 5]:

$$\hat{A} = \mu \hat{a} + \nu \hat{a}^\dagger \quad (6)$$

$$\beta = \mu \alpha + \nu \alpha^* \quad (7)$$

$$\nu = e^{i\theta} \sinh r \quad (8)$$

⁵ It turns out that it is impossible to generate the phase operator which would be Hermitian [24, p. 492]. Note that the property of being “Hermitian” is necessary for the operators used in quantum mechanical calculations. Instead of a phase operator, cosine and sine operators, which can be generated as Hermitian, are used to work with the phase properties of the field.

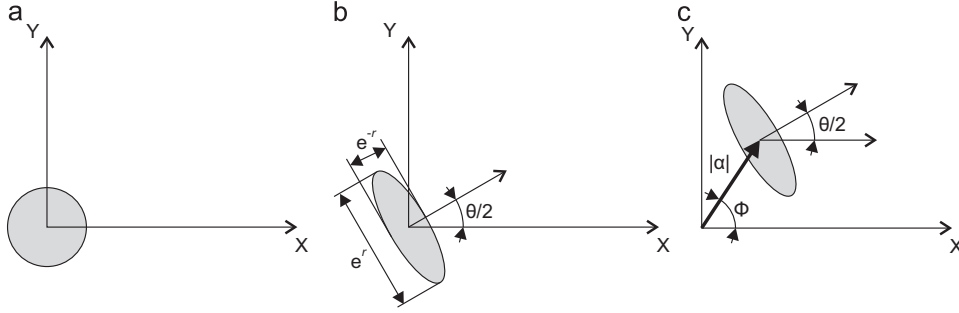


Fig. 3. Generation of a coherent squeezed state $|\alpha, \xi\rangle$ from a vacuum state $|0\rangle$. (a) Region of uncertainty of the canonical variables of the vacuum state is represented by a circle at the origin of the phase space. (b) Application of the squeezing operator on the vacuum state leads to squeezing of the uncertainty region into an ellipse and the rotation of it by $\theta/2$. (c) The application of the displacement operator simply shifts the uncertainty region by $|\alpha|$ in the direction given by the angle ϕ .

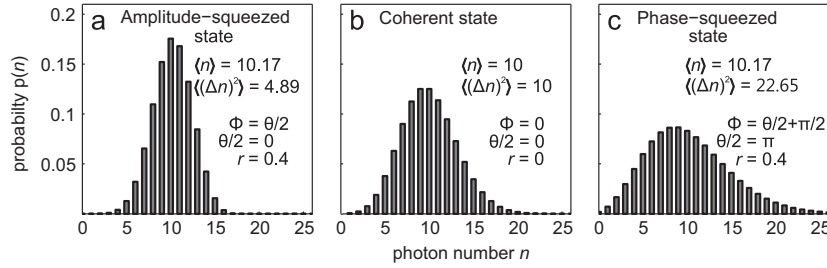


Fig. 4. The shape of the photocount distribution of the squeezed state depends on the squeezing parameters r and rotation angles ϕ, θ , see their meaning explained in Fig. 3. Here, we show quadrature-squeezed coherent state photocount distribution for (a) amplitude-squeezed light, where the fluctuations of the amplitude (i.e. number of photon counts) are reduced – the distribution is narrower than that of Poisson distribution, (b) coherent light (Poisson distribution) for comparison, (c) phase-squeezed light, where the phase fluctuations are reduced (not possible to depict in photocount distribution), which inevitably leads to an increase of the amplitude fluctuations – the photocount distribution is broader.

$$\mu = \cosh r \quad (9)$$

$$\alpha = |\alpha|e^{i\phi} \quad (10)$$

$$\xi = r e^{i\theta} \quad (11)$$

Squeezed states, as originally defined by Yuen [55], were produced by squeezing the coherent state. It means that at first, the displacement operator $\hat{D}(\alpha)$ is used to create a coherent state $|\alpha\rangle$ from a vacuum state $|0\rangle$ and then the squeezing operator $\hat{S}(\xi)$ is used, see [24, Fig 21.3.b, p. 1043]. Mathematically: $\hat{S}(\xi)\hat{D}(\alpha)|0\rangle = \hat{S}(\xi)|\alpha\rangle = |\xi, \alpha\rangle$. However, it is more convenient, and also often used in modern literature, to apply first the squeezing operator on the vacuum state and then the displacement operator: $\hat{D}(\alpha)\hat{S}(\xi)|0\rangle = \hat{D}(\alpha)|\xi\rangle = |\alpha, \xi\rangle$. Such procedure which gives the so-called ideal squeezed state (see [24, Fig. 21.3.a, p. 1043] and Fig. 3 in this paper), was introduced in Reference [57] and we use it also in this paper.

The photocount statistics of a light field in a coherent squeezed state is given in terms of Hermite polynomials [58, p. 21]

$$P_n(t, T) = (n! \cosh r)^{-1} \left[\frac{1}{2} \tanh r \right]^n e^{(-|a|^2 - (1/2)\tanh r (|a^*|^2 e^{i\theta} + a^2 e^{-i\theta}))} |H_n(z)|^2, \quad (12)$$

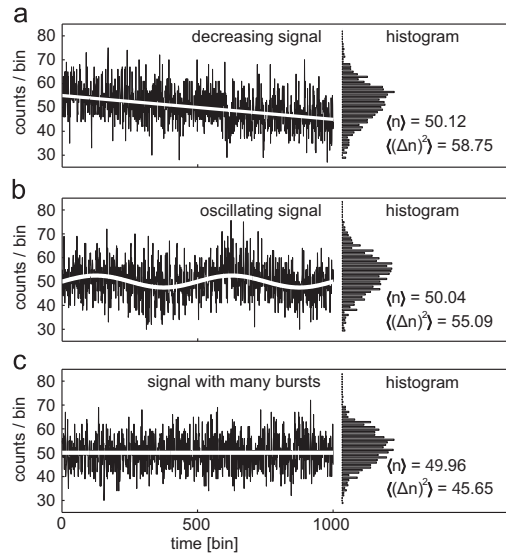


Fig. 5. Non-stationary signals can generate super- and sub-Poisson distributions from Poissonian signals. Random signals with Poisson distribution have been generated by a computer (Matlab, function *poissrnd*) and combined with other signals to simulate specific experimental artifacts. (a) Poisson signal superposed to a decreasing trend, (b) Poisson signal superposed to an oscillating trend, (c) Poisson signal with 200 random (uniform distribution) bursts with values from the interval from 20 to 40. Bursts were placed in random positions in the signal and their values substituted the original values at these positions.

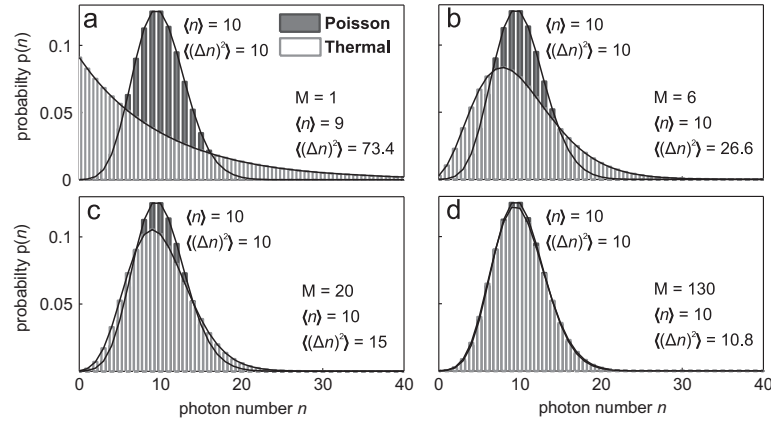


Fig. 6. Thermal field photocount distribution (light grey) approaches Poisson distribution (dark grey) for a large number of modes M , i.e. for a large number of independently radiating sources (molecules, atoms) or from single source with very short coherence time compared to the time interval of the measurement. The average value of intensity of the photon signal ($\langle n \rangle$) is the same for all displayed distributions.

where

$$z = \frac{\alpha + \alpha^* e^{i\theta} \tanh r}{\sqrt{2e^{i\theta} \tanh r}},$$

Squeezed states are interesting because they can manifest lower intrinsic noise (fluctuations around the mean of a canonical variable) than coherent light [59], a feature which classical light with Poisson distribution cannot achieve. See Fig. 4 for manifestation of squeezing in the photocount distributions. The lower the intrinsic noise (related to uncertainty of a canonical variable), the higher the capability of such states to transmit information [60], but there are natural limits [59]. However, squeezed states are fragile. They can be “destroyed” by the interaction with their environment, such as attenuation, beam splitter or a mirror, as those admit the vacuum fluctuations, which exceed the squeezed fluctuations, to enter from the outside.

One has to be careful to avoid experimental and instrumental artifacts before interpreting the photocount statistics data. Non-Poisson distribution of photocounts can be also generated by a classical and thermal light which would otherwise lead to a Poisson distribution if the measurement had been performed correctly. Trivial manifestation of non-Poisson distribution can be caused by non-stationarity of the light source such as modulation of the intensity of the photon signal due to the (i) slow drifting (Fig. 5a) or periodic (Fig. 5b) trends, (ii) random small bursts caused by electronic noise or by photon emission caused by other intensity limited stochastic processes (Fig. 5c) and added to the Poisson signal, (iii) thresholding the pulses from the photodetector, etc. Non-Poisson distribution caused by such non-stationarities and photon signal deformation has nothing to do with the squeezed state of light (Fig. 6).

2.2.6. Thermal states

A thermal state of light can be physically obtained by filtering thermal radiation. The photocount statistics of a thermal source with M modes (degrees of freedom) is well approximated by the expression [24, p. 680]

$$p_n(t, T, M) = \frac{(n + M - 1)!}{n!(M - 1)!} \left(1 + \frac{M}{\langle n \rangle}\right)^{-n} \left(1 + \frac{\langle n \rangle}{M}\right)^{-M}, \quad (13)$$

where $\langle n \rangle$ is the average number of photons and M is the number of field modes (see also [24, p. 731]). The number of degrees of

freedom M can be estimated by the product of time degeneracy M_t and space degeneracy M_s . Time degeneracy is the ratio of the measurement time (bin time) over the coherence time [22, p. 97]. Thermal states are classical. An important characteristic of these states is the relation between the variance and the mean:

$$\langle (\Delta n)^2 \rangle = \langle n \rangle + \frac{\langle n \rangle^2}{M}. \quad (14)$$

The coefficient M is generally very large for chaotic sources [61], so that the relation between the variance and the mean is close to that of a coherent state. Another interpretation says that, for reasonable intensities, the expectation value of the number operator n is very small and the expectation value of n^2 is therefore negligible with respect to that of n [62, p. 19]. As a matter of fact, for large M , $p_n(t, T, M)$ tends to a Poisson distribution of parameter $\langle n \rangle$.

Since the question whether the field which gives rise to UPE is in a coherent or a thermal state is recurrent in the UPE literature, it is important to know whether photocount statistics can distinguish between them. Since photocount statistics of thermal light becomes equal to that of a coherent state when the number of modes M is large, photocount statistics are not able to discriminate between a coherent and a thermal state with many modes. This can be seen in particular in the relation between variance and mean in a thermal state, see Eq. (14) (Fig. 6).

2.2.7. Superposition of coherent and thermal states

If UPE contained a mixture of coherent and thermal states, a corresponding description of such superposed fields should be used. This has not been done in the UPE literature up to our knowledge, although photocount statistics of superpositions of coherent and thermal states was already investigated by Perina [63,64].

2.2.8. Super-radiance

Super-radiance is the coherent emission of light by several sources. It was first proposed by Dicke [65] and is now a thoroughly investigated subject [66–69]. Its main characteristic is the fact that the intensity of the emitted light can vary with the square of the number of sources because they can emit in phase.

The photocount statistics of super-radiant emission was investigated in detail by Trifonov [70], who found cases where the statistics are sub-Poissonian (see also [68,68], Sections 1.3 and 11.6).

Nagashima [71] observed that the photon state of a super-radiant system is generally not a coherent state.⁶

3. Experimental works on the photocount statistics of UPE

Photoelectric measurements of UPE have been attempted already since the early 1930s (see [73,74,74], and references therein), but reliable measurements could be obtained only in the early 1950s [75,76]. The very delicate instrumental aspects of UPE photocount measurements were discussed in several papers [77–82].

First, it is instructive to refer to several relevant works dealing with statistical properties of luminescence from non-biological sources. The photocount statistics of weak luminescent sources was measured for solid-state ZnS:Cu luminophores [83], luminescent glass [83] and single molecules in microdroplets [84]. All these experiments can be analyzed in terms of thermal source or Poisson statistics. The photocount statistics of light emitting diodes was found to be Poissonian [85] or super-Poissonian in case of avalanche photodiodes operated above its breakdown voltage and used as a light source [86]. Chemiluminescence of a 9,10-diphenylanthracene radical ions in acetonitrile solution shows Poisson statistics [87].

For the following discussion, it is important to stress that Poisson statistics are not a proof of the existence of a coherent state of light. According to the Palm–Khintchine theorem, the superposition of a large number of independent equilibrium renewal processes, each with a small intensity, behaves asymptotically like a Poisson process. For example this is true for the limit $X(t) = \sum_{i=1}^n x_i(nt)$, where the processes x_i are independent [88]. However, this result depends on the way the limit is taken [89,88]. We suggest that the superposition of random nonstationary emissions, which was investigated by [90,91], seems to be the most reasonable first approach for modelling biological chemiluminescence.

3.1. Works with conventional data interpretation

There are several works on the UPE photocount statistics that are at the qualitative level of the quantum optics literature, without over-interpretation of the results. Papers of Kobayashi and Inaba belong to this category. They performed [85] an interesting and useful investigation of the photocount statistics of a time-dependent system. The influence of cosmic rays and microdischarges is taken into account to get reliable data. For a light emitting diode they found a Fano factor close to one, for the photoluminescent bacterium *Photobacterium phosphoreum* they measured a Fano factor significantly greater than one, indicating a super-Poissonian statistics. More precisely: “During the primary stage of cell proliferation, the photon statistics show super-Poisson behavior, which changes to Poisson statistics according to the increase in the number of cells”. The Fano factor is analyzed in terms of a chaotic source (using Eq. (41) of Ref. [91]) and denotes a “clustering of excitation and emission”.

In another paper [78], they describe the experimental setup in great detail. The long-term stability of the dark counts is checked as well as their power spectrum, their statistics as a function of counting time, their auto-correlation function and the dependence of it on the photomultiplier. The regenerative effects, cosmic rays and microdischarges are also taken into account. The authors measured the temperature-dependence of the dark counts and made a careful analysis of how the dark counts should be subtracted. They compare the corrected $g^{(2)}(\tau)$ (second order correlation function) with an experiment for randomized laser light of various intensities. They discuss the measurement of the Fano

factor in the presence of a dark current and for a time-dependent source. Finally, they measure the photon statistics of *Dictyostelium discoideum*. Variation of the Fano factor during the early stage of development and after starvation is observed. Further, they found super-Poisson statistics (i.e. photocount distribution with a width greater than a Poissonian distribution and a Fano factor >1), which they interpreted, as in their previous work, to be caused by the clustering of excitation and emission processes where the optical field is composed of a sequence of independent flashes initiated by Poisson random time events. No relation to the squeezed states, which can also manifest super-Poisson statistics, was mentioned. This article [78] represents a quality benchmark for all UPE photocount measurements in terms of careful verification of the experimental setup and rigorous interpretation of the data.

Kobayashi et al. also discussed the measurement of photocount statistics with 2D-photomultipliers [92,79,93]. Note that Inaba et al. measured UPE images already in 1988 ([94], see also Refs. [95–97]).

Another remarkable publication on this subject is the PhD thesis by Erich Schirmacher [82]. He made very careful experiments and a thorough theoretical analysis. He measured photon statistics from samples of lichen (*Parmelia physodes*) covering a tree bark, a leaf from a dark plum tree (*Prunus cerasifera* ‘Nigra’), leaves on a twig from a silver fir (*Abies alba*), a leaf from a banyan tree (*Ficus microcarpa*), a leaf of a stinging nettle (*Urtica dioica*) and a leaf from an oak (*Quercus robur*) that he compared to the light beam of a He–Ne laser. He observed only super-Poissonian statistics and did not find conclusive evidence of a non-classical (quantum) behavior of light.

There are several other works which provided UPE photocount statistics without speculative interpretation. Williams et al. measured UPE from human breath and observed a photocount distribution with two peaks [98,99]. This interesting experiment should certainly be reproduced. This is not really UPE from a living organism, but this effect could create an artifact in the measurement of UPE from human beings. Shen et al. [100] measured the photocount statistics of cucumber seedlings, mungbean seedlings and rhizobium bacteroids. They concluded that: “Experimental evidence accumulated so far leaves no doubt as to the validity of the biochemical interpretation of the chemi-excitation and its association with metabolism in biological systems.” Similarly, Gallep measured many different samples and analyzed his results in a rational way [101,102]. Van Wijk et al. made use of Bajpai’s coherent states to fit experimental photocount statistics. This enabled them to distinguish UPE from various parts of a human body [103–105]. These papers already contain unjustified speculations about squeezed states of UPE.

3.2. Works with speculative data interpretation

There are several researchers who pursued unconventional and speculative interpretation of the UPE experiments and photocount statistics, mainly based on the hypothesis of coherent processes in biological systems. We analyze the evolution of two main streams of ideas of coherent states and squeezed states of biological light chronologically. See Appendix A for the reference and selected comments on the works of other authors in the category of speculative data interpretation.

3.2.1. Coherence of ultra-weak photon emission?

Work on statistical properties of biological ultra-weak photon emission focused on coherence was pioneered by Fritz-Albert Popp. Activities of F.-A. Popp attracted many scientists and also public interest to the topic of biophotons. However, his interpretation of the experimental results of UPE photocount statistics in terms of coherent states is controversial and therefore is not generally accepted within the scientific community.

⁶ This contradicts a previous paper by Bonifacio [72], who overlooked the contribution of non-diagonal terms.

Table 1

Chronologically ordered assessment of publications of F.A. Popp and the statements contained within it which are the most controversial and deviate most strongly from currently accepted knowledge.

Statements, issues	Main references
UPE statistics of variously stressed cucumber seedlings were measured and analyzed in terms of chaotic light. The photocount distribution was far from Poissonian in many cases. The body of the paper brings plenty of data. The part of the conclusion involves a statement which is not substantiated by the data in the paper. For instance, the authors state that DNA is the origin of UPE: "DNA may represent active photon stores which are governed by Bose condensation" [117, p. 312]	[117]
Further unfounded statements. For instance, often a statement that erythrocytes (red blood cells) do not emit UPE because they do not contain DNA appears in the text. This argument is used to support the hypothesis of UPE generation by DNA. Although this statement is important, no reference to the source of experimental data is found. It should be noted that erythrocytes have also many other differences in their structure compared to other cell types than the presence of a nucleus. Only mammalian erythrocytes, compared to vertebrates, do not contain nuclei as well as other organelles such as mitochondria, Golgi apparatus and endoplasmic reticulum	[118–120,8,121,122]
"Measurements of photocount statistics show that the probability of registering n photons within a given time interval Δt is significantly different from a purely chaotic distribution, even for a multimode system with the highest possible degree of freedom" [123, p. 119]. Although they do not show any comparison with an experiment, they add: "On the other hand, the consistency of the results with a Poisson distribution, which accounts for a coherent radiation field, cannot be refused" [123, p. 119]. As we mentioned earlier, a Poisson distribution is indeed compatible with a coherent state but also similar to other states of light	[123]
Papers where the authors were trying to prove that the hyperbolic decay of delayed luminescence is a "sufficient condition for coherence". They start from a harmonic oscillator [123,120]. There have been several conceptual and mathematical mistakes identified in these papers, see Ref. [124] for a detailed investigation of one of these papers. Further, it needs to be stressed that the state of stationary UPE (autoluminescence), where light is generated by some biochemical reaction, cannot be fully determined by the state of delayed luminescence, which is a relaxation from an excited state and is not stationary by definition. In other words, the state of light met in delayed luminescence is different from the state of light of autoluminescence because the former is time-dependent and the latter is not. Therefore, conclusions from the study of physical parameters of delayed luminescence cannot be directly used to prove the parameters of autoluminescence	[123,120]
Delayed luminescence in plants is usually interpreted as a consequence of the complex reactions involved in photosystem II [125]. Experimental delayed luminescence can then be reproduced using reasonable reaction constants [126]. Popp and Li used a different approach. They postulated that the intricate behavior of the photosynthetic chain could be modelled by a simple one-dimensional harmonic oscillator with a time-dependent force: $\ddot{x}(t) + 2\mu(t)\dot{x}(t) + \omega_0^2 x(t) = 0$. They remove the term in \dot{x} by writing $x(t) = \exp\left(-\int_0^t \mu(\tau) d\tau\right) y(t)$, where y satisfies the equation $\ddot{y} + (\omega_0^2 - \mu^2 - \dot{\mu})y = 0$. Without any reasonable justification, they further postulate that the oscillating part $y(t)$ should have a constant frequency. This gives us the equation $\mu^2 + \dot{\mu} = \omega^2$, so that y oscillates with a constant frequency of $\sqrt{\omega_0^2 - \omega^2}$. The basic solutions of this equation are $\mu(t) = \omega \tanh(\omega t + \mu_0)$, so that $x(t) = e^{\pm i\omega t} \cosh \mu_0 / \cosh(\mu_0 + \omega t)$. Without any justification, Popp and Li completely dismiss these general solutions and choose the very special $\mu(t) = -\omega \tan(\omega t + \mu_0)$, which corresponds to $\omega = 0$	[123,120,127,128]
Popp and Yan use the above-mentioned special solution and try to get a coherent-state model of delayed luminescence. The solution of the problem does not satisfy them (it is not compatible with experiments) and the desired solution is achieved in the procedure which unfortunately includes several mathematical errors – see [124] for the detailed critical analysis	[129,130]
Numerous evidences are provided for a Poisson distribution of biological UPE by showing two examples where $\langle n \rangle \approx \langle (\Delta n)^2 \rangle$ for cucumber seedlings with and without acetone poisoning. However, the non-poisoned case is not compatible with the value previously reported [117]. Other measurements of the previous reference [117], which are not compatible with Poisson distribution, are not mentioned. He admits that a chaotic field would also have $\langle n \rangle \approx \langle (\Delta n)^2 \rangle$ for a large number of degrees of freedom M . However, this point of view is dismissed because "we found an extremely strong mode-coupling indicating that M is of order 1." As a reference, Ref. [117] is cited where this statement or similar ones supporting it cannot be found	[8]
The <i>Coherence hypothesis</i> is stated, which claims in very general terms that "biophotons are released from a fully coherent electromagnetic field which serves as a basis for communication in living tissues" [131, p. 577]. They show the measurement of cucumber seedlings with smaller (but variable) values of δ . They argue that the statistics alone do not prove coherence, but that the temperature dependence, the transparency of biological materials and the hyperbolic decay of luminescence do [131, p. 581]. These statements are not supported by any rigorously convincing proof. They set up a simple model to describe the emission of coherent light by DNA	[131]
Several strong (but largely unfounded) statements are made in this reference. For example, it is written that the phase is completely determined in a coherent state [132, p. 147], whereas in fact the variance of the phase is $1/(2\sqrt{\langle n \rangle})$ [22, p. 196], which can be very large for the low intensity of UPE	[132]
Further examples of statements which seem to be of conclusive nature but are unfounded: "While spontaneous chemiluminescence cannot sensitively depend on biological and physiological processes, like the cell-cycle, growth phases, differentiation, enzymatic activity, conformational changes of DNA, the external temperature, and weak external perturbations, the opposite behavior is expected for a coherent field, since it is modulated by any small change of the boundary conditions, including all the environmental and internal factors." [132, p. 148] and "As far as results are available, there is no indication for the validity of hypothesis 1, the chaos theory, but complete support of hypothesis 2, namely the coherence theory of biophotons" [132, p. 148]. The equation $(\dot{x}\dot{x}) = (1 + \kappa)(\dot{x}^2)$ [132, p. 160] is solved as if it was the equation $\dot{x}\dot{x} = (1 + \kappa)\dot{x}^2$. This is not correct in general	[132]
Several novelties are introduced in the review paper [133]. Factorial moments [28, p. 71] are used to describe photocount statistics, new experimental photocount distributions are presented and an optical biocommunication experiment between <i>Gonyaulax polyedra</i> is described without giving closer details on experimental protocols. In the same book, Popp makes several speculative statements about "evolution as the expansion of coherent states" [134], Popp and Li see "hyperbolic relaxation as a sufficient condition of a fully coherent Ergodic field" [127]. [135] postulates super-radiance in DNA and mentions squeezed states	[116]
The optical biocommunication experiment between <i>Gonyaulax polyedra</i> is ascribed to super-radiance	[9]
Results of coincidence counting of UPE from mungbean seedlings and an elder bush leaflet are published [26]. When a photon is registered in channel 1, the photons in channel 2 are registered during the time interval Δt . A coincidence occurs when at least one photon is detected in channel 2. For a non-stationary process, the number of random coincidences Z_j in the j -th time interval Δt_j is $Z_j = n_{1j}(1 - P_2(\Delta t, 0))$, where $P_2(\Delta t, 0)$ is the probability of counting no photon in the time interval Δt and n_{1j} is the number of counts in channel 1 in the Δt_j . For a Poissonian distribution we have $P_2(\Delta t, 0) = e^{-a\Delta t}$, where a is determined by $\langle n \rangle = a\Delta t$. Therefore, $Z_j = n_{1j}(1 - e^{-a\Delta t})$. Experimental results for mungbean (<i>Vigna radiata</i>) seedlings and elder bush (<i>Sambucus nigra</i>) leaflets are given. Photocount statistics agree with the Poissonian distribution. Similar experiments were done on soybeans ([136], see also Ref. [137]). Poissonian distribution is interpreted there in terms of super-radiance, although super-radiance does not generally generate Poissonian photocount statistics (see Section 2.2.8)	[26,136,137]
Squeezed states were used instead of super-radiance as an attempt to describe UPE photocount statistics [12]. The squeezed states they used are not as general as the ones of [138]. They are of the form $ \alpha, r\rangle = D(\alpha)S(r) 0\rangle$. If we compare them with Eq. (21.3-1) of [24, p. 1038] we see that	[12]

Table 1 (continued)

Statements, issues	Main references
<p>$z = re^{i\theta}$ is real, so that $\theta = 0$, $\alpha = r$ [24, p. 1042] and $\alpha, r\rangle = (\nu, z)\rangle$ is an ideal squeezed state (21.4-2) of [24, p. 1042]. For Mandel and Wolf $\mu = \cosh r$ and $\nu = e^{i\theta} \sinh r$ in Eq. (21.3-3) of [24, p. 1039]. The values of $p(n)$ and $p(0)$ are not correct. For example, the value of $p(n)$ given in the paper is not real when α is not real. But the formula is wrong even if α is real. The correct form for real α is</p> $p(n) = \frac{1}{n! \cosh r} \left(\frac{\tanh r}{2} \right)^n e^{-\alpha^2(1+\tanh r)} H_n^2 \left(\frac{\alpha e^r}{\sqrt{\sinh 2r}} \right).$ <p>Thus,</p> $p(0) = \frac{1}{\cosh r} e^{-\alpha^2(1+\tanh r)}.$ <p>By using $(n) = \alpha^2 + \sinh^2 r$ we obtain</p> $p(0) = \frac{1}{\cosh r} e^{-(n-\sinh^2 r)(1+\tanh r)},$ <p>which does not reduce to the expression for $p(0)$ given in [12]. Unfortunately, this incorrect formula is repeated in [139,140] Review articles with no new results and similar issues as those mentioned above</p>	[141,11,10]

Bernhard Ruth, supervised by Popp, built an efficient photo-multiplier-based measurement system of UPE. Within his thesis [77] he showed that many biological samples are a source of ultra-weak photon emission. The most controversial result of this thesis is a series of UPE spectra [106,77] that are completely different from UPE spectra measured later [107,79]. Care needs to be taken because it is possible that the artifact leading to these strange spectra is the luminescence of the filters [108].

In this period, the following working hypothesis was introduced: biological UPE originates from a biological coherent photon field [109] which regulates biological processes. This hypothesis was inspired mainly by the following points:

- Several polycyclic hydrocarbons have been investigated. Correlations between their electronic properties and carcinogenic activity have been found [110]. Popp proposed that the mechanism of the action of the cancerogenic substances is the disturbance of the excitation cellular photon field at certain energy which is related to DNA repair [110; 111, p. 117].
- Coherent electrically polar vibration states within the GHz–THz region in metabolically active cells have been postulated by Fröhlich [112–115]. Popp embraced the general idea of coherent processes in biology and assumed, based on the model of Li [116, Chapter 5], that the DNA in cells behaves as a low level excimer laser generating a coherent photon field.

From that time on, experimental data obtained in Popp's group and their followers have been attempted to fit the coherence theory of biological ultra-weak photon emission. In Table 1, we highlight several specific points from these works which are the most controversial and deviate most strongly from currently accepted knowledge in order to inform readers where caution should be exercised.

The research work described in this section was led by the working hypothesis that coherence is a fundamental principle responsible for functioning of biological systems. Fine experimental setups were built, clever experiments with very interesting results performed, but there are several methodological drawbacks: (i) experiments are not described in detail, (ii) surprising experimental results (for example the concentration dependence of UPE in *Daphnia*) are not repeated with many other samples or other experimental setups, (iii) data that do not agree with the coherence interpretation are dismissed, (iv) alternative interpretations are not seriously considered, (v) oversimplified models are used instead of realistic biophysical ones, (vi) mathematical

errors in the articles. While the ideas presented inspired many researchers, incorrect and controversial interpretations of the data brought the subject of “biophotons” into disrepute.

3.2.2. Squeezed states of ultra-weak photon emission?

The squeezed state of light provides a flexible shape to fit the UPE photocount statistics because this state is based on four independent parameters ($|\alpha|, \phi, r, \theta$), see Fig. 3. This interesting model was first introduced by Bajpai et al. [138]. See the review of his work in (Table 2). However, the fact that this model fits the experimental data does not mean that UPE is in a squeezed state. We saw that a Poisson distribution can be obtained from a coherent state but also from many other (classical or quantum) states of light. The same is true for the distribution given by a squeezed state. For example, Mandel and Wolf notice that for certain values of the squeezed-state parameters, the Mandel parameter has positive (i.e. classical) values [24, p. 1051]. Even if restricted to Fock space, the number of states of light is immensely larger than the number of photocount distributions. Thus, it is generally impossible to deduce a state of light from a photocount distribution. Higher order correlation functions must be measured. As in the case of the previous section, interesting experimental results are somewhat spoiled by speculative interpretations [14,142].

4. Conclusion and perspectives

We reviewed practically all the available literature on the statistical properties of UPE. There are several high quality works on the level of standard quantum optics literature that provide an analysis of UPE in terms of a chaotic light field. In contrast, there are numerous papers which contain claims about coherent and squeezed states of UPE. However, only incorrect argumentation and data interpretation or indirect anecdotal evidence is presented to support these claims.

The conclusion of our review is that while the phenomenon of UPE from biological systems can be considered experimentally well established, no reliable evidence for the coherence or non-classicality of UPE has been actually achieved up to now. The presence of coherence seems to follow from straightforward reasoning: a living organism must be in some coherent state because it is obviously not in thermal equilibrium [154]. However, the actual situation is subtle. On the one hand, a thermal source can emit partially coherent light, even close to the source [155], and independent thermal sources can produce two-photon

Table 2

Chronologically ordered assessment and brief description of publications focused on squeezed states.

Statements, issues	Main references
<p>Paper [138] presents an analysis of UPE photocount distribution with squeezed states $\beta, \mu, \nu\rangle$ (or more precisely, Yuen's two-photon coherent states [24, p. 1046]) instead of standard coherent states. The relation with Mandel and Wolf is $\mu = \mu, \nu = \nu, w = \beta$. The authors impose a hyperbolic decay $\lambda(t) = \lambda_0/(1 + \lambda_0 t)$ and they find a time-dependent pseudo-annihilation operator $b(t) = \mu \hat{a} + \nu \hat{a}^\dagger$, with μ and ν being explicitly given. From this, they compute $n(t)$ and remove the oscillatory terms. They get an expression $B_0 + B_1/(1 + \lambda_0 t) + B_2/(1 + \lambda_0 t)^2$ but they find that $B_1 = 0$. They also calculate the Mandel factor $Q = \langle \Delta(\Delta n)^2 \rangle - \langle n \rangle$. They find it non-zero but small. They consider earlier experiments on flowers of <i>Tagetes patula</i>. They had fitted the fluorescence decay with a sum of two exponentials, but they say that using their new formula gives also a good fit</p> <p>In [13], coincidence measurements made with Popp's experimental setup [9] using two photomultipliers are presented. Experiments were carried out on "leaves of different sizes from different plants". Some experimental results are given but the author does not specify for which sample. The paper ends with the idea that, from the evolutionary point of view, "the advantages of using squeezed light were too overwhelming"</p> <p>Bajpai [143] argues that the "inadequacy of the conventional framework to describe a biophoton signal is easy to demonstrate". Then, the "separate identity of sub-units and the independence of de-excitations give rise to the thermal nature of photons and exponential decay character of the signal". This is generally not correct. The statement in the conclusion "The signal was, therefore, coherent for 5 h" does not seem to be substantiated</p> <p>Here [144], Bajpai accepts another definition of coherent states and the real r is replaced by the complex number ξ, which is the same as $z = re^{i\theta}$ in Eq. (21.3-1) of [24, p. 1038]. From this paper on, this definition of squeezed coherent states is kept. However, his value of $p_0(\langle n \rangle)$ is wrong in this paper, since it would be complex when α is complex. The denominator is also wrong. The correct result is</p> $p_0(\langle n \rangle) = \frac{e^{- \alpha ^2} e^{-\Re(\alpha^2 e^{-i\theta}) \tanh r}}{\cosh r} = e^{-\langle n \rangle} \frac{e^{\sinh^2 r - \Re(\alpha^2 e^{-i\theta}) \tanh r}}{\cosh r}$ <p>where we used $\langle n \rangle = \alpha ^2 + \alpha ^2 = \alpha ^2 + \sinh^2 r$ from Eq. (21.4-10) of [24, p. 1044]. The value of $p(n)$ is obtained from Eq. (21.5-25) of [24, p. 1050] and the value of $\langle n \alpha \xi \rangle$ is obtained from $\langle n \mu, \nu; w \rangle$ of Eq. (21.5-24) of [24, p. 1050] by the substitution of $\mu = \cosh r, \nu = e^{i\theta} \sinh r$ and $w = \alpha \cosh r + \alpha^* e^{i\theta} \sinh r$. This is explained in Eq. (21.4-5) of [24, p. 1042]</p> <p>Lichen <i>Parmelia tinctorum</i> is measured in [145,146] since "Lichen, because of its very slow growth or decay, is a suitable system for making repeated experiments". The results are analyzed using squeezed state distributions. In these and the following works by Bajpai, the formulas for the photocount distribution of squeezed states are correct. It is stated that "Since a photon signal of quantum nature emanates from a quantum state the biophoton emitting parts of a living system must remain in a pure quantum state". This is not true in general. The fact is that a classical source generates a coherent state of the photon field, although the source is not quantum at all. Even squeezed states can be generated by classical currents in the non-linear regime. The only requirement is the presence of a quadratic term (in the photon creation and annihilation operators) in the interaction Hamiltonian [147]</p> <p>Photocount statistics of <i>Parmelinella wallichiana</i> is measured and fitted by squeezed state statistics [148]</p> <p>Time-dependent squeezed states with a time dependence giving the density $n(t) = \sum_{i=0}^2 B_i (t_0 + t)^{-i}$ are considered. Then, for $t \rightarrow \infty$, $p(n)$ is the distribution coming from a squeezed state: [150]</p> $\hat{H} = f(t)\hat{p}^2 + g(t)\omega^2\hat{q}^2.$ <p>We write $q = \beta\hat{a} + \beta^*\hat{a}^\dagger$ and $p = \alpha\hat{a} + \alpha^*\hat{a}^\dagger$, where \hat{a}^\dagger and \hat{a} are creation and annihilation operators. The Hamiltonian becomes</p> $\hat{H} = 2f_1\hat{a}^\dagger\hat{a} + f_2(\hat{a}^\dagger)^2 + f_2\hat{a}^2 + f_1,$ <p>where</p> $f_1 = \alpha ^2 f + \beta ^2 \omega^2 g,$ $f_2 = \alpha^2 f + \beta^2 \omega^2 g.$ <p>This type of Hamiltonian was investigated in detail also elsewhere [55,149]. Delayed luminescence from <i>Parmelinella wallichiana</i> is measured. One of the fits is displayed, the noise is very large</p> <p>An interesting and critical survey of previous measurements. Additionally, new measurements of <i>Xanthoria parietina</i> and a rather good fit of the data using squeezed-state distributions are presented. Speculative statements: "A holistic property is correctly described only in the quantum framework", "The photon signal remained in its squeezed state at least for 5 h", "emission of photon signal in a squeezed state is a characteristic property of living systems" [151]</p> <p>In [152], authors introduced a second order correlation function at zero time lag $g^{(2)}(\tau = 0)$ to estimate the non-classicality of UPE. By varying the detector response time (or bin size) around the period of expected coherence time one can estimate the coherence time and $g^{(2)}(0)$ [153]. $g^{(2)}(0) < 1$ is a signature of non-classical (quantum nature) of the light [22, Fig. 5.21, pp. 229, 249–250]. Racine and Bajpai [152] estimated $g^{(2)}(0)$ from the Fano factor of the measured UPE signal and compensated for the detector background. In Fig. 2 in [152], $g^{(2)}(0) = 1$ and shows no variation across different bin sizes for hydrogen peroxide induced UPE signal from a human hand. The authors claim there that there are hints to quantum behavior of UPE ($g^{(2)}(0) < 1$) but the data provided do not fully justify that. The fluctuation of the Fano factor sometimes falls under the value of 1 (again a signature of quantum states of light) for certain bin sizes, but considering the shape of the Fano factor curve as a whole [152, Fig. 2], this could be also attributed to fluctuation and error of the measurement. Nevertheless, these interesting data should be reproduced and thoroughly verified [152]</p>	

interference [156].⁷ On the other hand, the organization required to maintain life has no *a priori* reason to imply that UPE is in a coherent state. Moreover, thermal states and coherent states are two extremes of a very broad range of the possible states of light. What we would need is to actually *measure* the coherence length

and time of UPE. The extremely long UPE coherence times (10 days,⁸ 5 h⁹) proposed by some authors seem to be completely off the mark. It is remarkable that, except for a few exceptions

⁷ Note that two-photon interference is not the interference of two photons [157].

⁸ "A reasonable coherence time is the lifetime of cell organelles (for instance, mitotic figures) of about ten days" [10, p. 59].

⁹ "The signal was, therefore, coherent for 5 hr" [143].

[158,124], the physical community did not provide any critique of these extraordinary claims.

Although the role of coherent processes in biology, in particular quantum coherence, cannot be dismissed in general [159–162], it needs to be emphasized that the research work published until now does not provide any generally accepted proof for coherence of biological ultra-weak photon emission according to the physical definitions (see Section 2.2.1).

Perspectively, standard methods in quantum optics can deliver more reliable information on coherence and statistical properties of UPE of living systems. Coherence parameters (coherence time, coherence length) could be quantified by measuring light interference or light correlation functions [24,163]. A non-classical, *i.e.* quantum nature, could be assessed by using a Hanbury Brown–Twiss interferometer and measuring higher order correlation functions. However, the extremely low intensity of UPE and inherent nonstationarity of biological signals make these experiments highly challenging.

We believe that the development of new types of photon detectors which will have properties closer to that of the ideal detectors [1, Section 5] may bring at least partial answers to the open questions about UPE statistical properties. Such new developments include light (200–3000 nm) sensors based on the cryogenically cooled microwave kinetic inductance detectors [164,165]. Further futuristic possibilities of light detection could include nondestructive detection of the presence of photons, *i.e.* without absorbing them, by detecting the change of the phase they incur on a pre-prepared quantum state of the atom in cavity, as was recently experimentally demonstrated [166]. A promising technological direction to explore is to couple the UPE into optical fibers. Once in a fiber, the light can be easily manipulated, spectrally and spatially filtered and small low noise avalanche

photodiode (APD) detectors can be used. This manipulation allows control of the number of modes which can enter the detector. It has been demonstrated already 20 years ago, that in spite of its low intensity UPE can be coupled to an optical fiber and detected by a liquid nitrogen cooled Si-APD [167]. Actually, fiber optics and APD detectors based setups are standard in quantum optics experiments.

Apart from the quantum statistical properties, there are indications that other signal properties of biological UPE stemming from dynamics underlying chemical reactions [168–172] may also be of interest. Biological processes are naturally oscillatory, complex (chaotic) and fractal. Thus, suitable methods adapted from statistical physics and very carefully used for other biological signals to uncover “hidden information” [173] may also be used to analyze the UPE signals.

Acknowledgment

Ch.B. would like to thank Reinhard Honegger for his kind explanation of the relation between coherent states and factorizing correlations. M.C. acknowledges F.-A. Popp for introducing him to the field of biological ultra-weak photon emission and R.P. Bajpai for extensive discussions and inspiration. M.C. and M.N. are financially supported by the Czech Science Foundation, Grant no. GP13-29294S.

Authors' contribution: M.C. and Ch.B. conceived the research. M. N. and M.C. performed the calculations and analyzed the data. M.C., Ch.B. and O.K. wrote the paper. All authors read and approved the final manuscript.

Appendix A. Other works on statistical properties of UPE with speculative interpretations

Several more authors indulged themselves in the speculations about the nature of the light emitted from biosystems. We list their relevant publications here for the sake of completeness. Gu has strong theoretical background in quantum optics. In [174], he describes a three-level system as the emitter of UPE. Super-radiance and a model involving the sum of two coherent states is introduced by He in [175]. In [176], Gu discusses non-classical light and asks the question “are there nonclassical effects in biological systems?” (p. 301). He recalls the non-classical aspect of sub-Poissonian photon distribution from *Gonyaulax polyedra* [133] and higher order coherence in mungbean seedlings [9, p. 1272]. Further, he states that biophotons may be emitted by standing vibrational waves in DNA. Gu considers the interaction of a single mode of the biophoton field with a phonon reservoir. He considers a Schrödinger cat initial state (healthy or ill, yin or yang). These theoretical considerations are apparently not used in the paper. Photon statistics of a piece of leaf of a banyan tree (probably *Ficus elastica*) is reported. The photon distribution, its variance and entropy are given for the leaf and a radiator. Gu further compares the variance and entropy observed during the delayed luminescence and autoluminescence phases, and observes that they are similar. The normalized variance for the leaf and the radiator are 1.26 and 2.20, respectively. He compares the value for the leaf (1.26) to the value $g^{(2)}(0) = 1.2$ obtained in [174, p. 83]. Other measurements give values much closer to 1. An important point is that the author does not measure $\langle n^2 \rangle$, he calculates it from the distribution $p(n)$. Thus, he cannot observe non-classical effects because $p(n)$ is always positive. Finally, Gu compares the variance and entropy for traditional and genetically modified soybeans. Extensive theoretical work of Gu is covered in his book [177].

Kun et al. [178] considers the single-mode coherent states corresponding to parameters α and $-\alpha$. They make the same mistake as Popp [129] and consider that $\omega(t)$ and $\beta(t)$ can be chosen independently. This is wrong because the time dependence of $n(t)$ is determined by ω and f [124].

Chang [139] describes coincidence counting experiments. Distributions were measured for Dinoflagellates, chicken embryos, fireflies *Lampyridae*. She discusses Popp's hypothesis that biophotons come from DNA: “DNA excimer radiation is based on the same principle as laser radiation”. She pushes this hypothesis very far: “During gene transcription the long distance regulative functions may be performed by biophotons.” “Presumably one of the neurofilament's functions is to act as transmission channels for photon signals.” “The biophoton fields are in coherent and squeezed states suggesting that over a long period of life evolution livings learned how to use quantum mechanism to regulate themselves.” Another published paper [140] is of a similar nature as the previous one. Reference [179] is another speculative paper, see for instance one statement: “The emission of biophotons becomes coherent when the minuscule electric double layers start their moving state at the same moment.”

Appendix B. Table of UPE photocount statistics experiments

Sample from		References
Chemicals		
Luminol	$C_8H_7N_3O_2$	[100]
Polystyrene	$(C_8H_8)_n$	[133]
9,10-Diphenylanthracene	$C_{26}H_{18}$	[87]
Prokaryotes		
Symbiotic bacteria	<i>Photobacterium phosphoreum</i>	[85]
Nitrogen-fixating symbiont	<i>Bradyrhizobium japonicum</i>	[100]
Eukaryotes, unicellular		
“Umbrella” or cap algae	<i>Acetabularia acetabulum</i>	[133]
Dinoflagellate	<i>Prorocentrum elegans</i>	[133]
Dinoflagellate	<i>Gonyaulax polyedra</i>	[133,175,139]
Slime mold (also multicellular)	<i>Dictyostelium discoideum</i>	[78]
Algae-mushroom symbiont		
Lichen	<i>Parmelia physodes</i>	[82]
Lichen	<i>Parmelia tinctorum</i>	[145,146]
Lichen	<i>Parmelinella wallichiana</i>	[148,150]
Lichen on a tree bark	<i>Xanthoria parietina</i>	[151]
Plants		
Silver fir twig	<i>Abies alba</i>	[82]
Arabica coffee grains	<i>Coffea arabica</i>	[101]
Robusta coffee grains	<i>Coffea canephora</i>	[101]
Cucumber seedlings	<i>Cucumis sativus</i>	[117,100]
Cucumber	<i>Cucumis sativus</i>	[175]
Elder bush leaflet	<i>Sambucus sp.</i>	[26]
Banyan tree leaf	<i>Ficus microcarpa</i>	[82]
Gum tree leaf	<i>Ficus elastica</i>	[176]
Mungbean seedlings	<i>Phaseolus aureus</i>	[100,9,26]
Purple plum leaf	<i>Prunus cerasifera</i> ‘Nigra’	[82]
Oak leaf	<i>Quercus robur</i>	[82]
Soybean seedlings	<i>Glycine max</i>	[133,9]
Soybeans	<i>Glycine max</i>	[136]
Stinging nettle leaf	<i>Urtica dioica</i>	[82]
Animal		
Waterfleas (Crustacean)	<i>Daphnia sp.</i>	[134,175,102]
Fireflies (Insects)	<i>Lampyridae</i>	[139]
Thailand firefly (Insects)	<i>Lampyridae</i>	[133]
Chicken embryo, brain	<i>Gallus gallus domesticus</i>	[139]
Man		
Body	<i>Homo sapiens sapiens</i>	[103,105]
Body of meditating subjects	<i>Homo sapiens sapiens</i>	[180]
Hand of a multiple sclerosis patient	<i>Homo sapiens sapiens</i>	[181]
Hands	<i>Homo sapiens sapiens</i>	[104,152]

References

- [1] M. Cifra, P. Pospíšil, J. Photochem. Photobiol. B: Biol. 139 (2014) 2–10.
- [2] P. Pospíšil, A. Prasad, M. Rác, J. Photochem. Photobiol. B: Biol. 139 (2014) 11–23.
- [3] M. Havaux, C. Triantaphyllidis, B. Genty, Trends Plant Sci. 11 (2006) 480–484.
- [4] T. Quickenden, S.S. Que Hee, Biochem. Biophys. Res. Commun. 60 (1974) 764–770.
- [5] E. Cadenas, A. Boveris, B. Chance, Biochem. J. 186 (1980) 659–667.
- [6] S. Cohen, F.-A. Popp, J. Photochem. Photobiol. B: Biol. 40 (1997) 187–189.
- [7] B. Devaraj, M. Usa, H. Inaba, Curr. Opin. Solid State Mater. Sci. 2 (1997) 188–193.
- [8] F.-A. Popp, in: C.W. Kilmister (Ed.), Disequilibrium and Self-Organization, Reidel Publishing Company, Dordrecht, 1986, pp. 207–230.
- [9] F.-A. Popp, Q. Gu, K.-H. Li, Mod. Phys. Lett. B 8 (1994) 1269–1296.
- [10] F.-A. Popp, Electromagn. Biol. Med. 28 (2009) 53–60.
- [11] F.-A. Popp, Indian J. Exp. Biol. 41 (2003) 391–402.
- [12] F.-A. Popp, J.J. Chang, A. Herzog, Z. Yan, Y. Yan, Phys. Lett. A 293 (2002) 98–102.
- [13] R.P. Bajpai, in: J.-J. Chang, J. Fisch, F.-A. Popp (Eds.), Biophotons, Kluwer Academic Publishers, Dordrecht, 1998, pp. 323–339.
- [14] R.P. Bajpai, in: L.V. Belousov, F.-A. Popp, V.L. Voeikov, R. van Wijk (Eds.), Biophotonics and Coherent Systems, University Press, Moscow, 2007, pp. 135–140.
- [15] O. Kučera, M. Cifra, Cell Commun. Signal. 11 (2013) 871–878.
- [16] J. Pokorný, T.-M. Wu, Biophysical Aspects of Coherence and Biological Order, Academia, Praha, Czech Republic, Springer, Berlin, Heidelberg, New York, 1998.
- [17] A. Prasad, C. Rossi, S. Lamponi, P. Pospíšil, A. Foletti, J. Photochem. Photobiol. B: Biol. 139 (2014) 47–53.
- [18] F. Scholkmann, D. Fels, M. Cifra, Am. J. Transl. Res. 5 (2013) 586.
- [19] M. Cifra, A. Farhadi, J.Z. Fields, Progr. Biophys. Mol. Biol. 105 (2011) 223–246.
- [20] M. Trushin, Microbiol. Res. 159 (2004) 1–10.
- [21] Y.A. Nikolaev, Microbiology (Translated from Mikrobiologiya) 69 (2000) 597–605.
- [22] R. Loudon, The Quantum Theory of Light, third ed. Clarendon Press, Oxford, 2000.
- [23] P.L. Kelly, W.H. Kleiner, Phys. Rev. 136 (1964) A316–A334.
- [24] L. Mandel, E. Wolf, Optical Coherence and Quantum Optics, Cambridge University Press, Cambridge, 1995.

- [25] B. Picinbono, C. Bendjaballah, *Phys. Rev. A* 71 (2005) 013812.
- [26] F.-A. Popp, X. Shen, in: J.-J. Chang, J. Fisch, F.-A. Popp (Eds.), *Biophotons*, Kluwer Academic Publishers, Dordrecht, 1998, pp. 87–92.
- [27] F.-A. Popp, L.V. Belousov (Eds.), *Integrative Biophysics—Biophotonics*, Kluwer Academic Publishers, Dordrecht, Boston, London, 2003.
- [28] F.T. Arecchi, in: R.J. Glauber (Ed.), *Quantum Optics. International School of Physics Enrico Fermi*, Academic Press, New York, 1969, pp. 57–110.
- [29] Z.Y. Ou, H.J. Kimble, *Phys. Rev. A* 52 (1995) 3126–3146.
- [30] R. Vyas, S. Singh, *Phys. Rev. A* 38 (1988) 2423–2430.
- [31] F.M. Grimaldi, *Physico-mathesis de lumine, coloribus, et iride, aliisque annexis libri duo*, Vittorio Bonati, Bologna, 1665.
- [32] N. Kipnis, *History of the Principle of Interference of Light*, Birkhäuser, Basel, 1991.
- [33] C. Brosseau, in: E. Wolf (Ed.), *Progress in Optics*, vol. 54, North-Holland, Amsterdam, 2009, pp. 149–208.
- [34] T.D. Visser, R.W. Schoonover, *Opt. Commun.* 281 (2008) 1–6.
- [35] B.K. Yadav, S.A.M. Rizvi, H.C. Kandpal, *J. Opt. A: Pure Appl. Opt.* 8 (2006) 72–76.
- [36] G.S. Agarwal, A. Dogariu, T.D. Visser, E. Wolf, *Opt. Lett.* 30 (2005) 120–122.
- [37] M. Mujat, A. Dogariu, E. Wolf, *J. Opt. Soc. Am. A* 21 (2004) 2414–2417.
- [38] J. Tervo, J. Turunen, *Opt. Lett.* 34 (2009) 1001.
- [39] A.G. Jones, *J. Geophys.* 45 (1979) 223–229.
- [40] T. Reiter, D. Gabor, *Zellteilung und Strahlung*, Springer, Berlin, 1928.
- [41] T.E. Allibone, *Biograph. Mem. Fell. R. Soc.* 26 (1980) 106–147.
- [42] L. Biedenharn, J. Louck, *Angular Momentum in Quantum Physics*, Encyclopedia of Mathematics and its Applications, vol. 8, Addison-Wesley, Reading, 1981.
- [43] M. Born, E. Wolf, *Principles of Optics*, 6th ed., Cambridge University Press, Cambridge, 1985.
- [44] R. Honegger, A. Rieckers, *Ann. Phys.* 289 (2001) 213–231.
- [45] R. Honegger, A. Rieckers, *Physica A* 335 (2004) 487–510.
- [46] Z. Skoda, *Lett. Math. Phys.* 81 (2007) 1–17.
- [47] E. Schrödinger, *Naturwissenschaften* 14 (1926) 664–666.
- [48] J. Schwinger, *Phys. Rev.* 91 (1953) 728–740.
- [49] R.J. Glauber, *Phys. Rev.* 131 (1963) 2766–2788.
- [50] C. Itzykson, J.-B. Zuber, *Quantum Field Theory*, McGraw-Hill, New York, 1980.
- [51] D.T. Pegg, J. Jeffers, *J. Mod. Opt.* 52 (2005) 1835–1856.
- [52] D.T. Pegg, *Phys. Rev. A* 79 (2009) 053837.
- [53] R. Loudon, P.L. Knight, *J. Mod. Opt.* 34 (1987) 709–759.
- [54] M. Teich, *IEEE Trans. Biomed. Eng.* 36 (1989) 150–160.
- [55] H.P. Yuen, *Phys. Rev. A* 13 (1976) 2226–2243.
- [56] M. Orszag, *Quantum Optics: Including Noise Reduction, Trapped Ions, Quantum Trajectories, and Decoherence*, Springer, Berlin Heidelberg New York, 2008.
- [57] C.M. Caves, *Phys. Rev. D* 23 (1981) 1693–1708. <http://dx.doi.org/10.1103/PhysRevD.23.1693>, URL <http://link.aps.org/doi/10.1103/PhysRevD.23.1693>.
- [58] D.F. Walls, G.J. Milburn, *Quantum Optics*, Springer, Berlin Heidelberg, 2008.
- [59] H.P. Yuen, in: *Quantum Squeezing*, Springer, Berlin Heidelberg, 2004, pp. 227–261.
- [60] B. Saleh, M. Teich, *Phys. Rev. Lett.* 58 (1987) 2656.
- [61] Y. Jiang, O. Jedrkiewicz, S. Minardi, P.D. Trapani, A. Mosset, E. Lantz, F. Devaux, *Eur. Phys. J. D* 22 (2003) 521–526.
- [62] A. Mosset, *Etude expérimentale des fluctuations spatiales d'origine quantique en amplification paramétrique d'images* (Ph.D. thesis), University of Franche Comté, 2004.
- [63] J. Perina, *Phys. Lett. A* 24 (1967) 333–334.
- [64] J. Perina, *J. Eur. Opt. Soc.* 5 (2010) 10048s.
- [65] R.H. Dicke, *Phys. Rev.* 93 (1954) 99–110.
- [66] K. Hepp, E.H. Lieb, *Ann. Phys.* 76 (1973) 360–404.
- [67] M. Gross, S. Haroche, *Phys. Rep.* 93 (1982) 301–396.
- [68] M.G. Benedict, A.M. Ermolaev, V.A. Malyshev, I.V. Sokolov, E.D. Trifonov, *Super-radiance Multiatomic Coherent Emission*, Institute of Physics Publishing, Bristol, 1996.
- [69] C. Emary, T. Brandes, *Phys. Rev. E* 67 (2003) 066203.
- [70] E.D. Trifonov, in: V.V. Tuchin, V.P. Ryubakho, D.A. Zimnyakov (Eds.), *Light Scattering Technologies for Mechanics, Biomedicine, and Material Science*, Proceedings of SPIE, vol. 3726, SPIE, 1999, pp. 125–137.
- [71] M. Nagashima, *J. Phys. Soc. Japan* 44 (1978) 1647–1655.
- [72] R. Bonifacio, G. Preparata, *Phys. Rev. A* 2 (1970) 336–347.
- [73] E. Lorenz, *J. Gen. Physiol.* 17 (1934) 843–862.
- [74] J. Gray, C. Ouellet, *Proc. R. Soc. Lond. B* 114 (1933) 1–9.
- [75] B.L. Strehler, W. Arnold, *J. Gen. Physiol.* 34 (1951) 809–820.
- [76] L. Colli, U. Facchini, *Il Nuovo Cimento* 12 (1954) 150–153.
- [77] B. Ruth, *Experimenteller Nachweis ultraschwacher Photonemission aus biologischen Systemen* (Ph.D. thesis), University of Marburg, 1977.
- [78] M. Kobayashi, H. Inaba, *Appl. Opt.* 39 (2000) 183–192.
- [79] M. Kobayashi, *Trends Photochem. Photobiol.* 10 (2003) 111–135.
- [80] M. Kobayashi, in: F. Musumeci, L.S. Brizhik, M. Ho (Eds.), *Energy and Information Transfer in Biological Systems*, World Scientific, Singapore, 2003, pp. 157–187.
- [81] X. Shen, in: F.-A. Popp, L.V. Belousov (Eds.), *Integrative Biophysics—Biophotonics*, Kluwer Academic Publishers, Dordrecht, 2003, pp. 287–305.
- [82] E. Schirmacher, *Untersuchung des Lichts biologischer Proben hinsichtlich nichtklassischer Zustände* (Ph.D. thesis), University of Mainz, 2008.
- [83] C. Konak, P. Stepanek, L. Dvorak, Z. Kupka, J. Krepelka, J. Perina, *Opt. Acta* 29 (1982) 1105–1116.
- [84] S.C. Hill, M.D. Barnes, N. Lermer, W.B. Whitten, J.M. Ramsey, *Anal. Chem.* 70 (1998) 2964–2971.
- [85] M. Kobayashi, B. Deveraj, H. Inaba, *Phys. Rev. E* 57 (1998) 2129–2133.
- [86] T. Huang, J. Shao, X. Wang, L. Xiao, S. Tia, *Opt. Eng.* 44 (2005) 074001.
- [87] M.M. Collinson, R.M. Wightman, *Science* 268 (1995) 1883–1885.
- [88] B. Lindner, *Phys. Rev. E* 73 (2006) 022901.
- [89] H. Câteau, A.D. Reyes, *Phys. Rev. Lett.* 96 (2006) 058101.
- [90] R. Banys, *Lith. Math. J.* 17 (1977) 11–16.
- [91] B.E.A. Saleh, D. Stoler, M.C. Teich, *Phys. Rev. A* 27 (1983) 360–374.
- [92] M. Kobayashi, M. Takeda, K.-I. Ito, H. Kato, H. Inaba, *J. Neurosci. Methods* 93 (1999) 163–168.
- [93] M. Kobayashi, in: X. Shen, R. van Wijk (Eds.), *Biophotonics—Optical Science and Engineering for the 21st Century*, Springer, New York, 2005, pp. 155–171.
- [94] R.Q. Scott, M. Usa, H. Inaba, *Appl. Phys. B* 48 (1989) 183–185.
- [95] H. Inaba, in: J.B. Andersen (Ed.), *Modern Radio Science 1990*, Oxford University Press, Oxford, 1990, pp. 163–184.
- [96] M. Kobayashi, B. Deveraj, M. Usa, Y. Tanno, M. Takeda, H. Inaba, *Front. Med. Biol. Eng.* 7 (1996) 299–309.
- [97] M. Kobayashi, B. Deveraj, M. Usa, Y. Tanno, M. Takeda, H. Inaba, *Photochem. Photobiol.* 65 (1997) 535–537.
- [98] M.D. Williams, J.S. Leigh, Jr., B. Chance, *Ann. New York Acad. Sci.* 386 (1982) 478–483.
- [99] M.D. Williams, B. Chance, *Journal of Biological Chemistry* 258 (1983) 3628–3631.
- [100] X. Shen, F. Liu, X.Y. Li, *Experientia* 49 (1993) 291–295.
- [101] C.M. Gallep, E. Conforti, M.T. Braghini, M.P. Maluf, Y. Yan, F.-A. Popp, in: 11th Brazilian Symposium on Microwaves and Optoelectronics, São Paulo.
- [102] C.M. Gallep, D.C. Batista, C.A. Pereira, V.M. Oliveira, N.A. Siqueira, in: *Proceedings of 2007 SBMO/IEEE MTT-S International Microwave and Optoelectronics Conference*, Salvador, Brazil, pp. 241–244.
- [103] R. van Wijk, E.P.A. van Wijk, R.P. Bajpai, *J. Photochem. Photobiol. B* 84 (2006) 46–55.
- [104] E.P.A. van Wijk, R. van Wijk, R.P. Bajpai, J. van der Greef, *J. Photochem. Photobiol. B* 99 (2010) 133–143.
- [105] R.P. Bajpai, E. van Wijk, R. van Wijk, J. van der Greef, *J. Photochem. Photobiol. B: Biol.* 129 (2013) 6–16.
- [106] B. Ruth, F.-A. Popp, *Z. Natur. C* 31 (1976) 741–745.
- [107] E. Hideg, M. Kobayashi, H. Inaba, *FEBS Lett.* 275 (1990) 121–124.
- [108] W. Schmidt, *Photochem. Photobiol.* 45 (1987) 555–556.
- [109] F.-A. Popp, B. Ruth, *Arzneimittel-Forschung/Drug Res.* 27 (1977) 933–939.
- [110] F.-A. Popp, *Biophotonen. Ein neuer Weg zur Lösung des Krebsproblems*, Verlag f. Medizin Ewald Fischer, Heidelberg, 1976.
- [111] L. Belousov, F.-A. Popp, V. Voeikov, R.V. Wijk (Eds.), *Biophotonics and Coherent Systems*, Moscow University Press, Moscow, 2000.
- [112] H. Fröhlich, *Riv. Nuovo Cimento* 7 (1977) 399–418.
- [113] H. Fröhlich, *Int. J. Quantum Chem.* 2 (1968) 641–649.
- [114] H. Fröhlich, *Nature* 228 (1970) 1093.
- [115] H. Fröhlich, *IEEE Trans. Microw. Theory Techn.* 26 (1978) 613–618.
- [116] F.-A. Popp, K.H. Li, Q. Gu (Eds.), *Recent Advances in Biophoton research and its Applications*, World Scientific, Singapore, London, New York, Hong Kong, 1992.
- [117] F.-A. Popp, B. Ruth, W. Bahr, J. Böhm, P. Graß, G. Grolig, M. Rattemeyer, H.G. Schmidt, P. Wulle, *Collective Phenom.* 3 (1981) 187–213.
- [118] F.-A. Popp, in: K. Theurer, G.F. Domagk, H. Kraft (Eds.), *Wiederherstellung und Erneuerung als Prinzipien der Organo- und Immunotherapie*, Enke, Stuttgart, 1981, pp. 48–67.
- [119] F.-A. Popp, *Ärztz. Naturheilverfahren* 24 (1983) 361–366.
- [120] F.-A. Popp, W. Nagl, K.H. Li, W. Scholz, O. Weingärtner, R. Wolf, *Cell Biophys.* 6 (1984) 33–52.
- [121] F.-A. Popp, in: Louis Pasteur, *Source d'une Nouvelle Renaissance*, Fondation pour l'Energie de la Fusion, Paris, 1986, pp. 169–177.
- [122] F.-A. Popp, in: L.V. Belousov, F.-A. Popp (Eds.), *Biophotonics—Non-equilibrium and Coherent Systems in Biology, Biophysics and Biotechnology*, Bioinform Services Co, Moscow, 1995, pp. 85–98.
- [123] K.H. Li, F.-A. Popp, W. Nagl, H. Klima, in: H. Fröhlich, F. Kremer (Eds.), *Coherent Excitations in Biological Systems*, Springer, Berlin, 1983, pp. 117–127.
- [124] V. Salari, C. Brouder, *Phys. Lett. A* 375 (2011) 2531–2532.
- [125] V. Goltsev, I. Zaharieva, P. Chernev, R.J. Strasser, *Photosynth. Res.* 101 (2009) 217–232.
- [126] Y. Guo, J.-L. Tan, *BioSystems* 95 (2009) 98–103.
- [127] F.-A. Popp, K.H. Li, in: F.-A. Popp, K.H. Li, Q. Gu (Eds.), *Recent Advances in Biophoton Research and its Applications*, World Scientific, Singapore, 1992, pp. 47–58.
- [128] F.-A. Popp, K.-H. Li, *Int. J. Theor. Phys.* 32 (1993) 1573–1583.
- [129] F.-A. Popp, Y. Yan, *Phys. Lett. A* 293 (2002) 93–97.
- [130] Y. Yan, F.-A. Popp, S. Sigrist, D. Schlesinger, A. Dolf, Z. Yan, S. Cohen, A. Chotia, *J. Photochem. Photobiol. B* 78 (2005) 235–244.
- [131] F.-A. Popp, K.H. Li, W.P. Mei, M. Galle, R. Neurohr, *Experientia* 44 (1988) 576–585.
- [132] F.-A. Popp, in: F.-A. Popp, U. Warnke, H.L. König, W. Peschka (Eds.), *Electromagnetic Bio-Information*, Urban & Schwarzenberg, Munich, 1989, pp. 144–167.
- [133] F.-A. Popp, in: F.-A. Popp, K.H. Li, Q. Gu (Eds.), *Recent Advances in Biophoton Research and its Applications*, World Scientific, Singapore, 1992, pp. 1–46.

- [134] F.-A. Popp, in: F.-A. Popp, K.H. Li, Q. Gu (Eds.), *Recent Advances in Biophoton Research and its Applications*, World Scientific, Singapore, 1992, pp. 357–373.
- [135] K.-H. Li, in: F.-A. Popp, K.H. Li, Q. Gu (Eds.), *Recent Advances in Biophoton Research and its Applications*, World Scientific, Singapore, 1992, pp. 113–155.
- [136] J.J. Chang, F.-A. Popp, in: J.-J. Chang, J. Fisch, F.-A. Popp (Eds.), *Biophotons*, Kluwer Academic Publishers, Dordrecht, 1998, pp. 217–227.
- [137] F.-A. Popp, J.-J. Chang, *Sci. China C* 43 (2000) 507–518.
- [138] R.P. Bajpai, S. Kumar, V.A. Sivadasan, *Appl. Math. Comput.* 93 (1998) 277–288.
- [139] J.-J. Chang, *Indian J. Exp. Biol.* 46 (2008) 371–377.
- [140] J.-J. Chang, *NeuroQuantology* 6 (2008) 420–430.
- [141] F.-A. Popp, in: F.-A. Popp, L.V. Belousov (Eds.), *Integrative Biophysics—Biophotonics*, Kluwer Academic Publishers, Dordrecht, 2003, pp. 387–438.
- [142] R.P. Bajpai, in: V.B. Meyer-Rochow (Ed.), *Bioluminescence in Focus—A Collection of Illuminating Essays*, Research Signpost, Trivandrum, 2009, pp. 357–385.
- [143] R.P. Bajpai, *J. Theor. Biol.* 198 (1999) 287–299.
- [144] R.P. Bajpai, *Indian J. Exp. Biol.* 41 (2003) 514–527.
- [145] R.P. Bajpai, *Phys. Lett. A* 322 (2004) 131–136.
- [146] R.P. Bajpai, in: X. Shen, R. van Wijk (Eds.), *Biophotonics—Optical Science and Engineering for the 21st Century*, Springer, New York, 2005, pp. 125–140.
- [147] W. Zhang, in: A.N. Mira (Ed.), *Quantum Field Theory: A Twentieth Century Profile*, Hindustan Book Agency, Gurgaon, 2000, pp. 297–323.
- [148] R.P. Bajpai, *Phys. Lett. A* 337 (2005) 265–273.
- [149] W.S. Liu, P. Tombesi, *Nuovo Cimento B* 107 (1992) 595–602.
- [150] R.P. Bajpai, in: L.V. Belousov, V.L. Voeikov, V.S. Martynuk (Eds.), *Biophotonics and Coherent Systems in Biology*, Springer, Berlin, 2007, pp. 33–46.
- [151] R.P. Bajpai, *Indian J. Exp. Biol.* 46 (2008) 420–432.
- [152] D. Racine, A. Rastogi, R.P. Bajpai, *Chin. Med.* 4 (2013) 72.
- [153] M. Assmann, M. Bayer, *Opt. Lett.* 37 (2012) 2811–2813.
- [154] E. del Giudice, A. de Ninno, M. Fleischmann, G. Mengoli, M. Milani, G. Talpo, G. Vitiello, *Electromag. Biol. Med.* 24 (2005) 199–210.
- [155] J.J. Greffet, R. Carminati, K. Joulain, J.P. Mulet, S. Mainguy, Y. Chen, *Nature* 416 (2002) 61–64.
- [156] Y.H. Zhai, X.H. Chen, L.A. Wu, *Phys. Rev. A* 74 (2006) 053807.
- [157] T.B. Pittman, D.V. Strelakov, A. Migdall, M.H. Rubin, A.V. Sergienko, Y.H. Shih, *Phys. Rev. Lett.* 77 (1996) 1917–1920.
- [158] V.S. Letokhov, A.L. Dobryakov, in: F. Musumeci, L.S. Brizhik, M. Ho (Eds.), *Energy and Information Transfer in Biological Systems*, World Scientific, Singapore, 2003, pp. 205–216.
- [159] W. Parson, *Science* 316 (2007) 1438–1439.
- [160] P. Wolynes, *Proc. Natl. Acad. Sci.* 106 (2009) 17247.
- [161] G.S. Engel, T.R. Calhoun, E.L. Read, T.-K. Ahn, T. Mančal, Y.-C. Cheng, R.E. Blankenship, G.R. Fleming, *Nature* 446 (2007) 782–786.
- [162] K.R. Shelly, E.C. Golovich, K.L. Dillman, W.F. Beck, *J. Phys. Chem. B* 112 (2008) 1299–1307.
- [163] E. Wolf, *Introduction to the Theory of Coherence and Polarization of Light*, Cambridge University Press, Cambridge, 2007.
- [164] B.A. Mazin, B. Bumble, S.R. Meeker, K. O'Brien, S. McHugh, E. Langman, *Opt. Express* 20 (2012) 1503–1511.
- [165] B. Mazin, S. Meeker, M. Strader, P. Szypryt, D. Marsden, J. van Eyken, G. Duggan, A. Walter, G. Ulbricht, M. Johnson, et al., *Publ. Astron. Soc. Pac.* 125 (2013) 1348–1361.
- [166] A. Reiserer, S. Ritter, G. Rempe, *Science* 342 (2013) 1349–1351.
- [167] T. Isoshima, Y. Isojima, K. Hakomori, K. Kikuchi, K. Nagai, H. Nakagawa, *Rev. Sci. Instrum.* 66 (1995) 2922–2926.
- [168] M. Iranifam, M.A. Segundo, J.L. Santos, J.L. Lima, M.H. Sorouraddin, *Luminescence* 25 (2010) 409–418.
- [169] V.L. Voeikov, V.V. Koldunov, D.S. Kononov, *Kinet. Catal.* 42 (2001) 606–608.
- [170] V.L. Voeikov, V.V. Koldunov, D.S. Kononov, *Russ. J. Phys. Chem.* 75 (2001) 1443–1448.
- [171] E. van Wijk, J. van der Greef, R. van Wijk, *J. Phys.: Conf. Ser.* 329, 2011, 012021.
- [172] F. Scholkmann, M. Cifra, T. Moraes, C. de Mello Gallep, *J. Phys.: Conf. Ser.* 329 (2011) 012020.
- [173] A. Goldberger, L. Amaral, J. Hausdorff, P. Ivanov, C. Peng, H. Stanley, *Proc. Natl. Acad. Sci. U.S.A.* 99 (2002) 2466–2472.
- [174] Q. Gu, in: F.-A. Popp, K.H. Li, Q. Gu (Eds.), *Recent Advances in Biophoton Research and its Applications*, World Scientific, Singapore, 1992, pp. 59–112.
- [175] Q. Gu, in: L.V. Belousov, F.-A. Popp (Eds.), *Biophotonics—Non-equilibrium and Coherent Systems in Biology*, Biophysics and Biotechnology, Bioinform Services Co, Moscow, 1995, pp. 116–135.
- [176] Q. Gu, in: J.-J. Chang, J. Fisch, F.-A. Popp (Eds.), *Biophotons*, Kluwer Academic Publishers, Dordrecht, 1998, pp. 299–321.
- [177] Q. Gu, *Radiation and Bioinformation*, Science Press, Beijing, New York, 2003.
- [178] S. Kun, C.-L. Liu, J. Hun-Yu, in: X. Shen, X.-L. Yang, X.-R. Zhang, Z.-J. Cui, L.J. Kricka, P.E. Stanley (Eds.), *Proceedings of the 15th International Symposium on Bioluminescence and Chemiluminescence*, World Scientific, Singapore, 2009, pp. 63–66.
- [179] E. Lozneanu, M. Sandulovicu, *Roman. Rep. Phys.* 60 (2008) 885–898.
- [180] E.P.A. van Wijk, R. van Wijk, R.P. Bajpai, *Indian J. Exp. Biol.* 46 (2008) 345–352.
- [181] R.P. Bajpai, M. Drexel, *J. Acupunct. Meridian Stud.* 1 (2008) 114–120.